STUDY OF THE HOT CORROSION OF SUPERALLOYS

J. J. Walters

FOREWORD

This report covers the work performed under Air Force Contract AF33(615)-5212, BPS Number 66(687381-738107-62405514), Project Number 7381, "Materials Applications", Task Number 738107, "Detection Control and Prevention of Corrosion", during the period 1 July 1966 through 30 June 1967.

This report is submitted in fulfillment of the contract which was initiated between Systems Engineering Group, Air Force Materials Laboratory, and AVCO/Lycoming Division for the Study of the Hot Corrosion of Superalloys. This report was released for publication September 1967.

Mr. J.J. Walters was project engineer of this study. Mr. W.A. Rentz, Manager of Materials Development Laboratory, had overall responsibility for project management. The study program is under the direction of Mr. W.R. Freeman, Jr., Director of the Materials Laboratories, who provided technical assistance.

This technical report has been reviewed and is approved.

W. P. Conrardy

W.P. CONRARDY, Chief
Systems Support Branch
Materials Applications Division
Air Force Materials Laboratory

ABSTRACT

The effect of operating environment and alloy composition on the nature and extent of sulfidation attack has been studied with the aid of the Lycoming environmental test rig. Sulfidation attack of 11 nickel-base and 1 cobalt-base alloys was produced by burning JP-4 or JP-4R fuel while ingesting synthetic sea water into the combustor discharge. In general, the nickel-base alloys showed an upper (terminal) and a lower (threshold) temperature between 1450°F and 1750°F where sulfidation attack occurred. Reduction of the fuel sulfur content from 0.16 weight percent (JP-4R fuel) to 0.02 weight percent (JP-4 fuel) significantly reduced the amount of corrosion at constant salt-to-air ratios of both 4 and 8 ppm. The temperature range over which sulfidation occurred and the maximum depth of attack increased with increasing salt-to-air ratios (4 to 8 ppm) and with increases in the time of exposure from 120 to 360 hours. In general, the high chromium content alloys possessed better resistance than the low chromium content alloys, but high chromium alone did not guarantee good resistance to attack. Microprobe and X-ray investigations showed that chromium-rich surface oxides provided good resistance to sulfidation, and that high Al/Ti ratios provided good oxidation resistance.

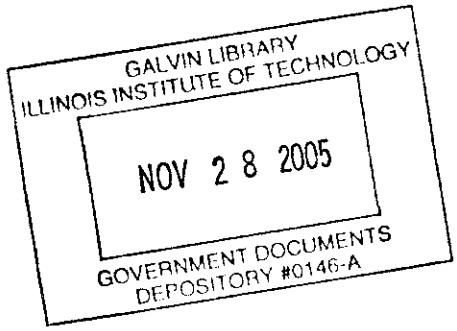

TABLE OF CONTENTS

LIST OF ILLUSTRATIONS

LIST OF ILLUSTRATIONS (Cont'd)

LIST OF ILLUSTRATIONS (Cont'd)

LIST OF ILLUSTRATIONS (Cont'd)

LIST OF ILLUSTRATIONS (Cont'd)

LIST OF ILLUSTRATIONS (Cont'd)

LIST OF ILLUSTRATIONS (Cont'd)

LIST OF ILLUSTRATIONS (Cont'd)

LIST OF ILLUSTRATIONS (Cont'd)

LIST OF TABLES

SECTION I

INTRODUCTION

BACKGROUND

Gas turbine engineering and its associated technology have made immense advances since their inception in the late 1930's, with the technology of materials development and its application being foremost. The initial requirements of materials for use in the turbine section were met by the relatively simple 80/20 nickel-chromium alloy, which has moderate high-temperature strength coupled with good, inherent corrosion and oxidation resistance. As the requirements became more and more stringent, modification of the basic 80/20 alloy took place, resulting in the addition of aluminum and titanium, known to increase strength by forming Ni_3 (Al, Ti), and a consequent decrease in chromium content. The first such modified 80/20 alloy was Nimonic 80, quickly followed by Waspaloy. Subsequently, many alloys from the same basic family became available. The major emphasis in continuing alloy development has been toward maintenance of strength at the higher operating temperatures required to develop greater turbine horsepower/weight ratios while retaining adequate resistance to oxidation. Concurrent with these improvements, the use of gas turbine engines spread to fields other than aircraft. Their use in marine applications subjected the high-temperature alloys to new environments and resulted in the appearance of catastrophic corrosion of turbine components manufactured from these sophisticated, high-temperature strength alloys. Because the attack was characterized by sulfur penetration into the base metal, the term sulfidation was used to describe it. Recurring cases reported by many sources using the high-temperature strength nickel-base alloys indicated that sulfidation was an industry-wide problem and not just an isolated phenomenon associated with local environments and/or fuels. At AVCO Lycoming, experience with the problem of sulfidation commenced with the discovery, at engine overhaul, of an unusual form of corrosion on uncoated T53 gas producer nozzle vanes of Inco 713C (Figure 1) after they had seen service in Viet Nam.[1] During this same period of time, the Navy returned a T53-L-11 engine to AVCO Lycoming from Patuxent River for investigation of a premature turbine failure. Subsequent analysis of damaged engine hardware revealed that the uncoated Inco 713C gas producer nozzle vanes exhibited the same type of attack as that observed on the nozzles which had seen service in Viet Nam. Concurrently, a similar attack was observed on uncoated Inco 713C hardware from AVCO Lycoming's marine engines (LVW, LVH) which were being developed during this period.

Early research into the causes of sulfidation, or hot corrosion as it is also called, revealed that at least four independent parameters play major roles:

1. Temperature of operation.
2. Presence of sulfur in the operating environment.
3. Presence of salt.
4. Alloy composition.

However, the variation of alloy performance due to changes in these parameters was not well understood, and in some cases, obviously conflicting results had been reported. The disagreements in tests results were largely caused by differences in the experimental procedure used to produce corrosion. Many of the testing approaches were much too severe and yielded only crude qualitative results. Other testing techniques ignored the importance of simulating certain basic characteristics of the gas turbine engine environment and were, therefore, incapable of reproducing the desired attack. Because of these inconsistencies, an environmental test rig was designed and built by AVCO Lycoming which can reasonably simulate engine operating conditions and produce characteristic corrosion in a reproducible and controlled manner. Alloy performance as measured by this environmental rig has shown excellent agreement with the performance as measured by T53-L-11 engine testing[1] (Figure 2). Based on this type of rig testing, an experimental program was designed to evaluate the effect of various operating parameters on the corrosion resistance of some current gas turbine materials.

RESEARCH PROGRAM

The program for the study of hot corrosion of superalloys emphasized the use of rig testing to determine the effects of operating environment (i.e., exposure, temperature, time of exposure, sea-salt concentration, fuel sulfur level, and fuel type), alloy composition and alloy structure (i.e., as-cast and heat treated) on the degree of sulfidation attack.

The alloys selected for evaluation were Inco 713C, Inco 713LC, TRW 1800, B1900, B1910, MAR-M-200, PDRL 161, PDRL 162, IN728X (formerly PDRL 165), U700, IN100, and X40. The cobalt-base alloy X40, which is widely used as a nozzle guide vane material, was chosen to provide a basis for comparison of the performance of a typical cobalt-base alloy with the higher strength, nickel-base alloys. Although all of the nickel-base alloys have sufficient creep-rupture strength for turbine blade applications, a wide range of compositions is represented; thus an opportunity is afforded to gain additional understanding of the effect of chemistry on hot corrosion.

The first phase of the program consisted of rig testing airfoil-shaped specimens for 120 hours at peak specimen metal temperatures of 1600°F and 1750°F with salt/combustor inlet air ratios of 4 and 8 ppm and fuel sulfur levels of 0.03 w/o (JP-4) and 0.16 w/o (JP-4R). An additional test was run with JP-5 fuel (0.16 w/o sulfur) to evaluate the effects of changes in the fuel burning characteristics, while a constant fuel sulfur level was maintained. A summary of the Phase I test parameters is shown in Table I.

The second phase of the program involved rig testing specimens for 120, 240, and 360 hour periods at peak specimen metal temperatures of 1600° and 1750°F with a salt/air ratio of 4 ppm and fuel sulfur content of 0.03 w/o (JP-4). The phase II test parameters are summarized in Table II.

SECTION II

EXPERIMENTAL PROCEDURE

ALLOY PREPARATION

Test specimens were prepared by vacuum induction remelting of ingot bars from previously vacuum induction-melted and refined master heats, and they were cast into shell molds prepared by the lost wax technique. The selection of processing parameters, such as mold temperatures, metal temperatures, cooling rates, etc., was left to the discretion of the investment foundry, Misco Division, Howmet Corporation. The geometry and dimensional characteristics of the airfoil-type specimen are shown in Figure 3.

DETERMINATION OF SPECIMEN TEMPERATURE DISTRIBUTION

The metal temperature distribution across the airfoil section of the specimens was determined by use of .030-inch diameter pins which were inserted into five (5) holes (0.035-inch diameter) running longitudinally through the airfoil of one specimen in a special set of control specimens (See sketch in Figure 4). Predetermined curves of hardness vs. temperature for the particular heats representing each pin material were used to determine the metal temperatures characteristic of different areas of the test specimen. Inco 718 pins were used for temperatures between 1450°F and 1650°F, and Waspaloy pins for temperatures between 1550°F and 1750°F.

THERMOCOUPLE TEMPERATURE MEASUREMENTS

Tests were conducted with instrumented test paddle specimens in order to check the validity of the temperature profiles obtained from hardness pins. The thermocouple readings were obtained by utilizing a slip ring assembly which enabled thermocouples to be mounted at nine locations on the test specimen airfoil during the testing. Testing was conducted at both 1600 and 1750° F peak specimen temperatures.

RIG TESTING PROCEDURE

The Lycoming environmental test rig was used to expose the airfoil-type specimens to conditions similar to those which exist in the gas turbine engine. The rig contains a combustor capable of generating high-velocity (approximately 700 feet per second) gases to which synthetic seawater is added in order to produce sulfidation attack. The high-temperature, high-velocity flame is impinged against the airfoil specimens as shown in Figure 5. The specimens were fixed in a holder which is mounted on a water-cooled shaft rotating at 1000 rpm. Rotation in the flame is required

to insure that each specimen is exposed to the same test environment. After 10 minutes at temperature, the specimens were cycled out of the combustion gas stream and allowed to air-cool, simulating the cyclic condition typical of gas turbine engine operation. This cycle was repeated until 120 hours of time were completed. Approximately 1 1/2 minutes were required to reach temperature in the 1750°F peak metal temperature test and about 1 minute was required in the 1600°F test. In both tests, cooling to below 1000°F was accomplished in approximately 1 minute. Temperature fluctuations at peak test temperature were estimated at plus or minus 10°F.

During Phase I of the program, three grades of fuel were burned in the combustor. Tests were carried out with referee grade JP-4 gas turbine fuel (MIL-J-5161F) and field grade JP-4 fuel (MIL-T-5624G), and in addition, a single test with a peak specimen metal temperature of 1750°F was conducted with JP-5 fuel (0.16 w/o sulfur). Synthetic seawater was added to the combustion gases to produce the corrosive environment. This synthetic seawater which was prepared according to Federal Specification 66-M-151A, Method 812, was added to the combustion gases to produce solid sea-salt to combustor inlet air ratios of 4 ppm and 8 ppm. The synthetic seawater was diluted with demineralized water so that the addition of the diluted mixture at a flow rate of 400 milliliters per hour was equivalent to the addition of 22 milliliters per hour of undiluted solution. This was done in order to permit more accurate control of the contaminant flow rate. The air/fuel ratio during testing was maintained on the oxidizing side of stoichiometry, varying between 25:1 and 34:1.

Duplicate test schedules for the two salt/air ratios at the two temperatures and for two fuels, JP-4 and JP-4R, were run in order to insure that any observed trends were reproducible. One specimen of each alloy was included in each test so that comparison of all twelve alloys was obtained after exposure to the identical test environment.

Also in Phase I of the program a single test was conducted with JP-5 and JP-4R fuels mixed to produce the same sulfur content as JP-4R.

Phase II of the program involved the testing of six (6) materials from Phase I for extended periods with JP-4 fuel and a salt/air ratio of 4 ppm at 1600° and 1750°F peak specimen metal temperatures. Duplicate tests for the two temperatures and for the three times of exposure (120, 240, and 360 hours) were conducted to check reproducibility. One specimen of each alloy was included in each test so that comparisons of all six materials was obtained after exposure to the identical test environment.

EVALUATION TECHNIQUE

Upon completion of each test, the specimens of the various alloys were visually examined for the extent, nature, and location of sulfidation. The specimens concave and convex airfoils were also photographed in order to provide a visual record of specimen appearance. Depth of attack measurements were made on sections, cut at 0.25, 1.0, and 1.5 inches from the tip of the specimens. After suitable metallographic preparation, photographs of the specimen cross sections (magnified 10X) were prepared. Comparisons were made between the photographs and tracings of the original cross section which were made on a New England Machine and Tool Co. Model Number 105 turbine blade contour plotting machine. The comparisons which give the depth of attack are made at the points where the sections intersect the temperature isotherms plotted at 25°F intervals.

In the evaluation of the 1600°F peak metal temperature tests, the 1/4-inch section intersects the 1450°, 1475°, and 1500°F isotherms, the 1-inch section crosses the 1525°, 1550°, 1575°, and 1600°F isotherms, and the 1 1/2-inch sections intersects the 1475°, 1500°, 1525°, and 1550°F isotherms. In the evaluation of the 1750°F peak metal temperatures, the 1/4-inch section crosses the 1700°, 1725°, and 1750°F isotherms while the 1 1/2-inch section intersects the 1675°, 1700°, 1725°, and 1750°F isotherms.

X-ray Diffraction Studies

X-ray diffraction studies were initiated to study the role of oxide formation on the surface of superalloys in the sulfidation process. Eleven alloys were investigated during this study; they include one cobalt-base material X40 and ten (10) nickel-base alloys: IN728X, TRW 1800, U700, Inco 713C, PDRL 162, PDRL 161, MAR-M-200, B1900, B1910 and IN100. Inco 713LC was not included in this study because its composition is almost identical to that of Inco 713C. Test paddles of the selected materials were exposed to a sulfidation test (S548) in the Lycoming Environmental Test Rig by using JP-4R fuel and a salt to air ratio of 8 ppm and a peak specimen metal temperature of 1750°F. The test was run in two stages; an initial 40 hours of testing was performed to study the products of the initial stages of corrosion. The oxides formed were subjected to "in-situ" X-ray diffraction analysis. The test was subsequently continued until a total of 120 hours had elapsed, and the paddles were again submitted for examination. After 120 hours, the paddles contained areas where normal oxidation had occurred and areas which were badly corroded from sulfidation attack. The oxidized areas were examined "in-situ", whereas the areas where sulfidation occurred were scraped to provide powdered products for X-ray analysis. All investigations where made by use of a Norelco Diffractometer equipped with a focusing monochromator. Copper radiation at 50 kv and 40 ma was utilized on all samples. Detection of diffracted intensities was accomplished with a scintillation counter and was recorded on a strip chart recorder. Complete instrumental parameters are listed in Table III.

Microprobe Studies

All ten of the nickel-base alloys which were subjected to X-ray diffraction analysis were also selected for microprobe analysis. Prior to microprobe analysis, segments of the paddles were metallographically prepared and examined in the optical microscope. From this examination it was decided to investigate several points within three district areas in each alloy. These three areas are illustrated in Figure 6 and are defined as follows:

1. Initial attack—In this area, oxidation has taken place, and a very narrow depleted zone containing only a few sulfides had been generated.

2. Mild attack—In this area, oxides, sulfides and a depleted zone have been formed, but the depth to which the attack has penetrated is shallow.

3. Gross attack—These areas are microstructurally similar to the mild attack region, however, the attack has penetrated to a much greater depth.

Three types of analysis were performed in these areas of each specimen. Spectral scans were made at various locations to determine the elements present. Scans were then made across the corroded regions by use of the spectrometer setting for one particular element, and finally, spot analyses were made at predetermined locations in the corroded areas. The apparatus used was able to record the intensities of the following characteristic X-ray lines: NiK_α, CuK_α, CoK_α, AlK_α, TiK_α, SK_α, MoL_α, WL_α, CbL_α and TaL_α.

SECTION III

RESULTS AND DISCUSSION

CHEMICAL ANALYSIS

The nominal compositions and chemical analysis of the alloys used in both phases of the program are shown in Tables IV, V and VI. The analytical results performed at Special Metals, Utica, New York, and Ledoux and Company, Teaneck, New Jersey, are in good agreement.

TEMPERATURE PROFILES

The temperature-versus-span length curves at the leading edge, trailing edge, and the specimen center line obtained from three different hardness pin runs at both 1600° and 1750°F peak metal temperature are shown in Figures 7 and 8. Isotherms characteristics of this testing are shown in Figures 9 and 10. Metal temperatures are maximum near the center of the trailing edges, and decrease a total of about 170°F at the tips of the leading edges.

The use of peak metal temperatures of 1600° and 1750°F provided continuous data over the temperature range of 1450° and 1750°F, which encompassed normal turbine blade operating temperatures. In addition, preliminary work had indicated that alloys were most susceptible to sulfidation in this region.

The temperature profiles produced by the thermocouples during testing were in good agreement with those produced by hardness pins techniques. The comparative results are shown in Figure 11. One thermocouple gave consistently high reading, and this is attributed to a defective instrument. This measure of agreement is a good confirmation of the temperature profiles which were previously used to obtain the corrosion/temperature relationship.

RIG TESTING

Figures 12 through 19 show the general appearance of the specimens after testing at the two test temperatures and two salt levels for the two fuels used in Phase I of the program. Figure 20 shows the specimens after testing at 1750°F with JP-5 fuel. Figures 21 through 26 show the specimens tested for 120, 240, and 360 hours with JP-4 fuel and a salt/air ratio of 4 ppm during Phase II of the program.

The depth of penetration data for the tests in Phase I of the program is shown in Figures 27 through 86. This data for the Phase II testing is presented in Figures 87 through 92. Each curve represents a composite of four tests (i.e., duplicate runs at peak metal temperature of both 1600 and 1750°F)

except for the Phase I test involving JP-5 fuel where the points represent an average of two measurements taken from different portions of the specimen airfoils.

EFFECT OF TEMPERATURE

Testing at a peak specimen metal temperature of 1600°F caused the corrosion to be located in the hotter portions of the airfoils while the cooler areas tended to be corrosion-free (Figures 12, 14, 16, and 18). Exposure to a 1750°F peak metal temperature results in corrosion-free areas in the hotter sections of the paddles while the cooler areas were susceptible to attack (Figures 13, 15, 17, and 19). Combining the 1600 and 1750°F tests, it is apparent that most alloys exhibit a temperature below which corrosion does not occur (threshold temperature) and a temperature above which sulfidation does not occur (terminal temperature).

From the various curves of alloy corrosion versus temperature, the threshold temperature, terminal temperatures, temperatures of maximum depths of attack, and total corrosion values were obtained.

These results are listed in Tables VII and VIII. Occasionally, the threshold or terminal temperatures do not fall within the temperature range studied. Since it is difficult to extrapolate the curves, the result must be listed as less than 1450°F or greater than 1750 F. The total corrosion, which is taken as the area under the depth of attack vs. temperature curve, is also affected, and is listed, as being greater than some value.

Apparently during the combustion process, the ingested salts are vaporized and presumably at least an appreciable portion of the halides are converted to sulfates. When the resultant mixture deposits as a liquid on the specimen, there will be a tendency for the protective oxide to be fluxed by the salt mixture allowing sulfur to penetrate into the base metal. As the temperature is reduced, the time required to destroy the film on a given alloy would presumably increase. Thus, for a fixed time of modest duration (e.g., 120 hours), a temperature below which sulfidation would not occur would be expected. This temperature would vary depending on the exposure time and the solubility of the protective oxide in the sulfate mixture — assuming that the environment remains constant. In the case of alloys having very poor sulfidation resistance, the threshold temperature would probably approach the solidus temperature of the salt mixture. Below the solidus temperature of the salt, the solubility of the protective oxide in the salt mixture is presumably nil.

Threshold temperatures varied according to the fuel type and salt level used in the testing.

Salt level	JP-4 Fuel	JP-4-R Fuel
4ppm	Less than 1450 up to 1650°F	Less than 1450 up to 1625°F
8ppm	Less than 1450 up to 1625°F	Less than 1450 up to 1650°F

The terminal temperature is probably associated with the vaporization temperature of the salt. If the metal temperature is above this value, condensation would not occur and the protective oxide could not be destroyed, although the possibility of accelerated oxidation due to the salt vapors does exist. When the samples were exposed to JP-4 fuel and a salt-to-air ratio of 8 ppm, eight of the twelve alloys exhibited terminal temperatures between 1700° and 1750°F. Two alloys, IN100 and U700, showed terminal temperatures in excess of 1750°F although the corrosion of U700 was so slight that a precise evaluation was difficult. The terminal temperature for PDRL 162 was estimated to be 1625°F. With a salt-to-air ratio of 4 ppm, three alloys showed terminal temperatures less than 1700°F; TRW 1800 at 1675°F, PDRL 162 at 1675°F and PDRL 161 at 1625°F. Five alloys had terminal temperatures between 1700° and 1750°F, and two alloys (IN728X and IN100) had terminal temperatures in excess of 1750°F. Under the conditions of the test, two alloys, X40 and U700 did not corrode.

The use of JP-4R fuel and a salt/air ratio of 8 ppm caused nine of the materials to show terminal temperatures between 1700 and 1750°F and two alloys (IN100 and U700) to show terminal temperatures in excess of 1750°F. With a salt-to-air ratio of 4 ppm; two materials exhibited terminal temperatures less than 1700°F; TRW 1800 at 1625°F and PDRL 161 at 1675°F. Seven alloys showed terminal temperatures between 1700 and 1750°F and two materials (IN728X and U700) had terminal temperatures above 1750°F. The cobalt-base material X40 did not corrode at either salt level when JP-4R fuel was used. Between the threshold and terminal temperatures, the depth of penetration rises to a maximum value. As temperature increases between the starting and end points, at least two opposing processes would be at work; increase attack resulting from more rapid film destruction and sulfur penetration; and decreased attack due to the presence on the specimen of less salt because of the increased vapor pressure of this phase.

EFFECT OF SALT-TO-AIR RATIO

The general appearance of specimens which were run at 1600 and 1750°F peak metal temperatures with a salt-to-air ratio of 4 ppm are shown in Figures 16 and 17 for JP-4 fuel and Figures 18 and 19 for JP-4R fuel. The specimens which were tested with a salt-to-air ratio of 8 ppm and JP-4 fuel

are shown in Figures 12 and 13, and those tested with JP-4R fuel are shown in Figures 14 and 15.

A comparison of the appearance of specimens tested at 1600°F with two salt-to-air ratios indicates that the degree of corrosion is greater at the higher salt level. Depth of penetration measurements showed that if the salt-to-air ratio was lowered from 8 ppm to 4 ppm while a constant fuel sulfur content was maintained, generally, the threshold temperature increased; the terminal temperature decreased; and the maximum attack decreased. The total corrosion of all alloys except TRW 1800 and IN728X was lowered when the salt-to-air ratio was reduced from 8 to 4 ppm. This can be seen in Figure 93 where the total corrosion of the various alloys is depicted at the two salt levels. In the case of TRW 1800 and IN728X, the total corrosion values at the two salt levels were essentially the same. However, the level of corrosion was so low that an accurate appraisal is not possible.

EFFECT OF FUEL SULFUR CONTENT

It is possible to compare the corrosion of the various alloys at sulfur levels of 0.02 percent (JP-4) and 0.16 percent (JP-4R) with constant salt-to-air ratios of both 4 and 8 ppm. At the 4 ppm salt-to-air level, lowering the fuel sulfur content from 0.16 to 0.02 percent reduced the total corrosion of all alloys except TRW 1800 which remained at about the same level. At the higher salt level of 8 ppm, the effect of reduction of the fuel sulfur content from .16 to .02 percent reduced the total corrosion of all the alloys including TRW 1800. The effect of sulfur content at the two salt levels for the various alloys is shown graphically in Figure 93.

The lower fuel sulfur content decreased the maximum depths of attack while the threshold temperatures generally remained about the same or increased slightly. Two of the high chromium alloys, IN728X and PDRL 161, showed an an appreciable increase in threshold temperature with the reduction in fuel sulfur content. There seemed to be little effect of sulfur (at the two levels studied) on the terminal temperatures.

During a 120 hour test at a salt-to-air ratio of 8 ppm, the following quantities of salts are ingested into the system.

a.	NaCl	96 grams
b.	Na_2SO_4	15 grams
c.	KCl	0.85 grams
d.	KBr	3.9 grams
e.	$MgCl_2$	21.9 grams
f.	$CaCl_2$	4.8 grams

If it is assumed that the halide salts would pass through the system as vapors rather than deposit on the specimens in liquid form, the role of sulfur in the corrosion process would presumably be to convert the halides to sulfates. This was substantiated by chemical analyses of unreacted salt deposits removed from the surface of an X40 specimen which confirmed that the deposit is sodium sulfate with a small amount of magnesium sulfate present. The choloride ion was not detected. The reaction of sodium and magnesium chlorides with sulfur dioxide should proceed according to the following equations:

$$2NaCl + SO_2 + 1/2\ O_2 + H_2O = Na_2SO_4 + 2HCl$$

$$MgCl_2 + SO_2 + 1/2\ O_2 + H_2O = MgSO_4 + 2HCl$$

With approximately 1200 pounds of JP-4 fuel containing 0.02 percent sulfur required for the 120 hour test, about 210 grams of SO_2 could be expected to form. At a salt-to-air ratio of 8 ppm, only about 53 grams of SO_2 would be required to convert the entire 96 grams of NaCl to Na_2SO_4 while the conversion of $MgCl_2$ would consume about 14 grams of SO_2. Thus, under conditions of minimum sulfur and maximum salt, there is over three times the required SO_2 for the conversion of sodium and magnesium chlorides to sodium and magnesium sulfates. Similarly the ratio of available sulfur dioxide to that required for stoichiometric reaction would be over 6 to 1 in the case of 0.02 percent sulfur with a 4 ppm salt-to-air ratio, over 24 to 1 with 0.16 percent sulfur and a salt-to-air ratio of 8 ppm, and over 48 to 1 with a 0.16 percent sulfur and a salt-to-air of 4 ppm. Consequently, it is difficult to explain why an increase in sulfur increased corrosion when sufficient SO_2 was available in all cases to convert the halides to sulfates. One possible explanation could be that the time for reaction is so brief that the conversion is only partial but the percent converted increases as the system is more saturated with SO_2.

EFFECT OF FUEL TYPE

The general appearance of the alloys after exposure to a peak metal temperature of 1750°F for 120 hours with JP-5 fuel (0.16 percent sulfur) and a salt-to-air ratio of 8 ppm is shown in Figure 20. The degree of corrosion appears to be similar to that observed on specimens tested under identical conditions but with JP-4R fuel containing 0.16 percent sulfur (See Figure 15). The depth of penetration measurements plotted as a function of temperature are shown in Figures 75 through 86 . The 1600 to 1750°F portion of the curves obtained by burning 0.16 percent sulfur JP-4R fuel are included for comparative purposes. In seven out of twelve cases, the depth of attack measurements for the JP-5 run are similar to or slightly less than the penetrations obtained with JP-4R fuel. While in the remaining five cases, the data appear to be

appreciably less. Since duplicate tests were not run, additional work would be required to substantiate this trend.

EFFECT OF COMPOSITION

The relative performance of the alloys tested under different combinations of fuel sulfur contents and salt-to-air ratios are listed in Table IX. Total corrosion, which was used as the basis for the ranking, is useful for comparative purposes but has certain limitations which should be taken under consideration. First, the errors in the measurement of depth of penetration become appreciable, on a percentage basis, when the amount of attack is small (e.g., penetrations less than 2 mils). This, combined with the precision of the planimeter when measuring small areas, can lead to a significant percentage of experimental error in the final answer which in turn could result in conclusions which are not necessarily valid. For example, under the conditions of 0.02 percent sulfur with a salt-to-air ratio of 4 ppm, the total corrosion of PDRL 162 is listed at 0.4 square inches and TRW 1800 is listed as 0.6 square inches, inferring that PDRL 162 is 50 percent better than TRW 1800. The only valid conclusion that can be made is that both alloys, under the test conditions used, show a small amount of corrosion and that the corrosion resistance of PDRL 162 is at least equivalent and probably superior to the corrosion resistance of TRW 1800. The second factor which must be considered when using total corrosion to judge alloys is that it does not reveal anything about the threshold temperature, the terminal temperature, or the maximum depth of attack. An alloy showing a moderate attack over a wide temperature range could have essentially the same total corrosion as an alloy having a severe attack over a narrow temperature range. Obviously the corrosion behavior of the two alloys is radically different and any ranking would have to be made in light of a specific application. With these limitations in mind, the relative performance of the alloys in Table IX can be discussed.

On the basis of data obtained with JP-4R fuel (0.16 percent sulfur) with salt-to-air ratios of 4 and 3 ppm, the alloys were ranked as follows:

a. B1900, B1910, MAR-M-200 and IN100 - very poor resistance to attack.
b. Inco 713C. Inco 713LC, PDRL 161 and PDRL 162 - poor resistance to attack.
c. U700, IN728X and TRW 1800 - relatively good resistance to attack.
d. X40 - excellent resistance (no attack).

Since the test conditions during the later portion of the investigation are probably more consistent with the environments which would be found in actual service, a ranking of the various alloys under these test conditions may be more meaningful. The low sulfur tests confirm that B1900, B1910,

MAR-M-200, and IN100 have the poorest resistance to sulfidation attack of the alloys investigated. Of this group, B1900 exhibits the greatest degree of hot corrosion while B1910 apparently has the best resistance to attack. At the other end of the spectrum, U700, IN728X, and TRW 1800 are only mildly attacked; this substantiates what was found at the higher sulfur content. Inco 713C and 713LC continue to fall between the alloys having poor resistance to sulfidation and the alloys having relatively good resistance to sulfidation. The fact that they did undergo appreciable attack at the low sulfur-low salt condition, justifies the poor rating which was previously given. The only significant shift in performance involves PDRL 161 and PDRL 162. Under the conditions of high fuel sulfur content, at both the 4 and 8 ppm salt-to-air ratios, there was no question that the corrosion resistance of U700, IN728X and TRW 1800 was superior to that of PDRL 161 and 162. However, at the low fuel sulfur content (0.02 percent) with the reduced salt-to-air ratio of 4 ppm, the performance of PDRL 161 and 162 appears to be comparable to that of the U700, IN728X, TRW 1800 group of alloys. Of course, long time testing at the low sulfur and salt conditions might restore the performance rankings to the levels obtained with the 120-hour test using high sulfur and high salt.

It is also interesting to note that in the case of the most severely attacked alloys (B1900, IN100, MAR-M-200), there was more corrosion at the high salt-low sulfur condition than at the low salt-high sulfur condition indicating that the change in salt is more influential than the change in sulfur (See Figure 93.). The reverse situation was observed with the remaining, less corroded alloys.

Figure 94 illustrates the effect of chromium on the total corrosion of the various alloys tested. As previously reported, there is a general trend of increasing corrosion resistance with increasing chromium content. The low side of the total corrosion vs. chromium content scatter band contains U700, TRW 1800, PDRL 162 and B1910 while the upper portion consists of PDRL 161, Inco 713C, Inco 713LC, IN100, MAR-M-200, and B1900. The good performance of PDRL 162 and TRW 1800 and the poor performance of PDRL 161, relative to their chromium contents was evident in tests conducted at both fuel sulfur contents. The effect of chromium content on the threshold temperature of alloys tested with JP-4 and JP-4R fuels and a salt-to-air ratio of 8 ppm is shown in Figure 95. Under the two test conditions, alloys containing less than 14 percent chromium had threshold temperatures of 1500°F or less. In 11 out of 16 cases, the threshold temperatures were 1450°F, or lower, while 15 out of 16 fell at or below 1475°F. The three higher chromium alloys, U700, IN728X, and PDRL 161 all exhibited threshold temperatures at or above 1500°F. The highest threshold temperatures were associated with U700 (15 percent chromium) while PDRL 161 (17 percent chromium) showed the lowest and those of IN728X (16.6 percent

chromium) were intermediate. Tests on other compositions containing 15 percent and higher chromium would be required to determine if the dropoff of threshold temperature of the alloys containing more than 15 percent chromium is really a function of the chromium content. It is, of course, quite possible that the lower threshold temperature of IN728X and PDRL 161 (relative to U700) are due to other compositional differences. Nevertheless, if threshold temperature is taken as the minimum temperature required for the salt mixture to penetrate the protective oxide, it is clear that the higher chromium alloys are forming more protective oxides.

EFFECT OF EXPOSURE TIME ON EXTENT OF SULFIDATION

The depth of attack data for the tests which exposed the specimens to temperatures between 1450 and 1750° F for periods of 120, 240 and 360 hours using JP-4 fuel (0.03 w/o sulfur) and a salt-to-air ratio of 4 ppm, is shown in Figures 87 through 92. The curve represents a composite of four tests, i.e., duplicated tests with peak metal temperatures of 1600 and 1750° F. Every point represents an average of the results from two points on the specimen airfoils in each of two tests. Figure 96 shows the total corrosion for the materials for the three exposure times.

Three of the alloys, B1910, Inco 713C and TRW 1800, showed severe sulfidation attack and the depth of corrosion for these materials increased with time. After 360 hours, the surface areas over which the attack had taken place had also increased. Figure 97 shows the variation of the depth of attack with time at 1550° F for these three materials. The results appear to show that the depth of attack increases approximately linearly with increased time of exposure to the corrosive environment. This would appear to indicate that the corrosion process is surface reaction rather than diffusion controlled. However, the presence of a distinct incubation period before the onset of rapid corrosion makes the significance of this observation questionable. The increase in the area which had corroded carried the attack into a location which was at a temperature slightly lower than the threshold temperature observed for 120-hour exposure. The threshold and terminal temperatures for 120 and 360 hours of exposure are shown in Table X. The change indicates the threshold temperature for these test conditions is not an absolute value but is still dependent on the time of exposure to the corrosive environment. The other three materials, IN728X, IN728X heat treated, and U700, showed corrosion at higher temperatures than those where corrosion occurred in the more sulfidation-prone materials. This corrosion was associated with oxidation rather than sulfidation and is illustrated in Figure 98. The specimens of IN728X, in the as-cast or heat treated condition, showed a needle-type phase which appeared after 360 hours of testing at above 1700° F. This needle phase is shown in Figure

99 together with aluminum and chromium X-ray images of the area which show that the needles are rich in aluminum compared to the surrounding material. Figure 99 also shows that the surface oxides are rich in chromium, and that the chromium concentration drops immediately below the surface, giving a chromium-depleted band just prior to the needle phase. Whether the needles are an aluminum oxide or nitride phase could not be established. However, they apparently form as a result of the oxidation process during long exposure times. Finally, a comparison of the heat treated and as-cast specimens of IN728X indicated the variation in the depth of attack which was observed (Figure 90 and 91) was very small. Consequently, the expected homogenization associated with the two hours solution heat treatment at 2050° F did not cause any significant variation in the alloy's corrosion resistance.

X-RAY DIFFRACTION ANALYSIS

The X-ray diffraction patterns obtained from these samples are complex patterns containing from 20 to 30 diffraction peaks. Tables XI, XII, and XIII summarize the corrosion products from the various areas for each alloy tested. As indicated, analyses were performed after 40 and 120 hours and the results are consequently discussed separately as follows:

After 40 Hours

Only slight evidence of sulfidation was noted at a few points on the leading edge of the paddles at this point in the test. At the trailing edges of all the paddles where the X-ray analysis was performed, only evidence of oxidation was noted. Table XI summarizes the oxidation products formed on the various alloy paddles. The X-ray intensity from the Ni_3Al in the base metal indicated that this initial oxide layer was quite thin on the nickel-base alloys, and the intensity from the alpha cobalt phase indicates the same condition for the X40 cobalt-base alloy. Since this initial oxide layer was quite thin, and was analyzed "in-situ", only the major constituents gave measurable X-ray intensities. Nickel oxide and the spinels are the major phases present in this initial oxide layer for all the nickel-base alloys. All except U700, IN100, and MAR-M-200 show evidence of trace amounts of Al_2O_3 or Cr_2O_3; TRW 1800 and MAR-M-200 show the presence of $NiWO_4$.

After 120 Hours

After 120 hours of testing, considerable corrosive attack was produced on the specimen airfoil surfaces in regions where the metal temperatures were less than approximately 1725° F. Figure 100 shows the condition of the paddles after testing. The most corrosion-resistant material is at the

upper left and the least corrosion-resistant at the lower right (this order was obtained from Figure 93). In the hotter regions of the specimens, there was generally no evidence of attack except for three alloys (U700, IN100, and MAR-M-200) which showed evidence of formation of a dark corrosion product in this area. Metallographic examination indicated the attack in these areas was apparently due to oxidation attack since no evidence of sulfide and/or depletion zone formation was evident. Table XII summarizes the oxidation products formed in the hotter area of the test specimens. The major phases observed after the 40-hour test are still present. However, the X-ray intensities are stronger, and the Ni_3Al peak in the nickel-base alloys is diminished indicating that the oxide film had grown in thickness during the additional time in the sulfidation rig. For the nickel-base material, nickel oxide was predominant phase with the spinels and other minor phases secondary, both after 40 hours and 120 hours in the test rig, as indicated in Table XII. Al_2O_3 was detected in the scale of all the nickel-base alloys in this high temperature area with the exception of U700, MAR-M-200 and IN100. These alloys, as already noted, were the only three showing evidence of attack due to oxidation at this location. The Al/Ti ratio of these three alloys is low (1.1 to 2.5) compared to the remaining alloys (6.0). It appears that the presence of the Al_2O_3 oxide film provides protection against oxidation (Reference 2 and 3), and those alloys with low Al/Ti ratios are susceptible to oxidation due to their inability to form a protective Al_2O_3 layer. This can not be associated with the aluminum concentration alone, since both IN100 and MAR-M-200 have relatively high aluminum contents. Instead, the poorer oxidation resistance of these alloys must also be associated at least partially with the relatively higher titanium concentration of these alloys.

The effect of tungsten in such alloys as TRW 1800 and MAR-M-200, which has been reported to be beneficial, is to form a $NiWO_4$ phase. This can be positively identified in both of these alloys as a major phase in addition to NiO and spinel. How this phase affects sulfidation resistance is not clear, as TRW 1800 is in the relatively good class while MAR-M-200 is in the very poor class. It may be a byproduct due to the corrosion of the matrix in general after the protective film has been destroyed and has no inhibitive character of its own.

The spinels (type AB_2O_4 oxides) can be identified by microprobe technique as probably $NiCr_2O_4$ depending on the alloy under study. Since the thin oxide layer was examined "in-situ", it is felt that the lack of precision in the determination of the lattice parameters prevents the placing of too much significance on the differences between the values obtained and the published ASTM data. Stresses and orientation effects present in oxide films grown on a metal surface can result in lattice parameters that differ somewhat from ASTM-reported values.

Table XIII summarizes the corrosion products formed in the cooler areas where sulfidation had taken place. Samples from these areas were removed from the alloy paddles and analyzed by X-ray diffraction. No attempt was made to remove corrosion products from selected areas. Instead, it was gathered in a random fashion from all of the surface that had corroded. It is interesting to note from this data that in every case the relative quantities are the same for NiO and spinel, from the "in-situ" film after oxidation, and from the corrosion product sampled after sulfidation. This seems to infer that if a spinel or NiO is formed as a major phase in the oxide film, the further formation of this same composition is continued during the process of sulfidation.

MICROPROBE ANALYSIS

Ten nickel-base alloys were evaluated by microprobe techniques using quantitative point analysis, element distribution and spectral scan techniques. The results of these analyses of the individual areas are described below as follows:

Matrix

Data was gathered at several points in the matrix ranging from 5 to 150 microns away from the depletion zone. Comparison of the results taken at these different matrix locations indicates that the effect of the corrosion process does not generally extend into the grains themselves beyond the depletion zone. That is, there is no significant variation in the matrix composition as we move toward the depletion zone (Figure 101). Occasionally, however, sharp decreases in the chromium level were noted in grains which were not in the depleted zone. These changes were always found to be associated with the presence of grain boundary sulfidation. A fine precipitate preceding the bulk corrosion front was detected in the matrix of some specimens adjacent to the depletion zone. In the areas where this fine precipitate existed, a small detectable rise in chromium content was observed. Although these precipitates were too small to be analyzed in a quantitative manner, they were found to be rich in sulfur and chromium, based on X-ray scans of these two elements. These results indicate essentially that the progression of attack is caused by the outward diffusion of some of the matrix elements through the depletion zone to the oxide layer and the movement of sulfur inward to eventually react with the alloy's chromium addition.

Depleted Zone

Microprobe data was collected at several points within the depleted zone of each alloy in order to determine the composition of this area. The results, shown in Table XIV, indicate that, in general, the depletion zones of all the alloys tend to be depleted of chromium and titanium compared with the original unattacked matrices. Aluminum appeared to decrease to less than one-half its original value. This was also observed in the element distribution scans, an example of which is shown in Figure 102 for alloy TRW 1800. The distribution of aluminum is uniform in the matrix and then drops off over a three-micron distance at the interface. At the outer surface, the high rise in the trace indicates a high concentration of aluminum in the oxide layer. When chromium was studied in the same manner (Figure 102), depletions observed were attributed to the formation of carbides. The sharp dropoff marks the interface area between the matrix and depleted zone. The sharp increases of chromium within the depletion zone are due to the presence presence of chromium-rich sulfides. In the oxide area on the outer surface, a significant rise in chromium content is observed for alloys which exhibit better performance during testing. Lower chromium contents were found in the oxide layer of the poorer alloy systems (i.e., B1900, IN100, MAR-M-200), apparently indicating that the ability to form chromium-rich oxides is important in determining alloy sulfidation corrosion resistance. This, of course, is in agreement with the generally accepted observation that chromium is beneficial in providing corrosion resistance.

It can be assumed that some of the chromium and the majority of the aluminum and titanium which are removed from the depletion zone go into the formation of oxides. However, the major portion of the chromium is depleted by the formation of chrome-rich sulfides. The heavy refractory elements (molybdenum, tungsten, columbium and tantalum) behave as a group, and are partially depleted from the respective alloy matrices by sulfide formation and oxidation. These changes in element concentration which occur at the interface between matrix and the depletion zone are shown in Figure 101.

It can be assumed that the rate of attack, following initial breakdown of the protective film and subsequent sulfide formation, is a function of the oxidation resistance of the depletion-zone alloy. Following this approach, the depletion-zone chemistry can be related to the overall alloy system corrosion rates. Pursuing this approach, the performance of the two medium chromium (13 percent) alloys, TRW 1800 and Inco 713, should be analyzed because of the similarity of their composition. They differ only in their tungsten and molybdenum concentrations. In addition, a similar comparison of the two high chromium alloys, PDRL161 and IN728X (17 and 16 weight percent chromium, respectively), can be made since the essential difference in the composition of these latter two alloys is that IN728X contains tungsten,

cobalt and columbium as additives. The PDRL161 alloy has a higher initial chromium content than the Inco 713C. However, after exposure to the corrosive media, the composition of the depleted zone in PDRL161 approaches that of Inco 713C, and as would be expected, the alloys exhibit similar corrosion rates, with Inco 713C having slightly poorer corrosion resistance. This slight difference may be due to the lower aluminum level of its depletion zone. Aluminum would be expected to be beneficial to the oxidation resistance of nickel due to the formation of the $NiAl_2O_4$ spinel.

On the other hand, comparing Inco 713C and TRW 1800, we have two alloys with similar nominal chromium contents (13 weight percent) which exhibit markedly different corrosion rates under the same testing conditions. The major differences in the depletion zone composition of these alloys are the higher tungsten (4.8 versus 0 weight percent) and aluminum (2.4 versus 0.1 weight percent) and the lower molybdenum (0 versus 2.3 weight percent) contents of TRW 1800 compared to Inco 713C. By inference, the significantly lower corrosion rate of TRW 1800 is due to the beneficial effect of both aluminum and tungsten and/or the detrimental effect of molybdenum (the undesirable effect of molybdenum on oxidation resistance is logical and can be used as a further explanation of the relative performance of Inco 713C and PDRL161 already discussed). In relation to IN728X several of the previous arguments could apply. However, the complete explanation for the exceptionally good corrosion resistance of the alloy cannot be justified, based on the above hypotheses. In addition, similar discussion of the other alloys does not yield significant relationships between corrosion resistance and depletion-zone chemistry, apparently due to the complexity of the differences in alloy composition and the resultant syngergistic effects.

Sulfides and Carbides

From the data gathered to date, the sulfides which were analyzed can be broken down into two general types. The first type is the one most commonly found, and is generally a mixture of Cr_3S_4 and Cr_2S_3. These are the typical sulfide phases found in the depleted zone (Figure 103). The second type of sulfide is apparently related to the carbides which previously existed in the grain boundaries. These sulfides (Figure 103) were found to contain varying amounts of columbium, tantalum, molybdenum, titanium, and tungsten, in addition to chromium. The amount of these elements depends upon composition of the original carbide phases of each alloy, and the degree to which the normally present carbide has been converted to a sulfide. Evidence of the carbide-to-sulfide transformation and grain boundary sulfidation was found in all of the alloys except IN100 and Inco 713C. In alloy PDRL161, quantitative data indicates that the carbides in the matrix grain boundaries are rich in columbium and titanium. As the depleted zone is approached, these carbides became richer in sulfur and chromium and depleted in columbium and titanium. It is interesting to note that as this process is taking place the grains

adjacent to the carbide phase become depleted in chromium, the chromium concentration dropping from 16 to 12.8 weight-percent while the columbium and titanium contents increase.

SECTION IV

CONCLUSIONS

Based on the results obtained during this study of the hot corrosion of superalloys, the following conclusions can be made:

a. Using the Lycoming-developed environmental test rig, it has been possible to quantitatively determine the sulfidation resistance of superalloys while simulating the environment of a gas turbine engine.

b. Corrosion was detected on all of the 11 nickel-base alloys tested, while the cobalt-base alloy (X40) was not attacked. Chromium additions in excess of about 12 percent appear necessary to develop some reasonable level of sulfidation resistance, but high chromium contents alone do not guarantee that this will occur.

c. Each of the 11 nickel-base alloys showed an upper (terminal) and lower (threshold) temperature between which sulfidation attack occurred. Between these two values, the depth of penetration varied appreciably with alloy composition.

d. Most of the alloys exhibited terminal temperatures between 1700 and 1750°F, suggesting that the characteristics of the salt are more important than the composition of the base metal in determining this value.

e. Reduction of the fuel sulfur content from 0.16 to 0.02 percent significantly reduced the amount of sulfidation at salt-to-air ratios of both 4 and 8 ppm. The threshold temperatures generally remained about the same or increased slightly while little effect was noted on the terminal temperatures.

f. At both fuel sulfur levels the amount of corrosion was reduced when the salt-to-air ratio was lowered from 8 ppm to 4 ppm. Reduction of the salt-to-air ratio generally increased the threshold temperatures, lowered the terminal temperatures, and reduced the maximum depth of attack.

g. The depth of attack and threshold temperatures varied appreciably with the alloy composition, with the chromium content having the greatest single effect. At the 8 ppm salt-to-air ratio, it was noted that all alloys having less than 14 percent chromium had threshold temperatures equal to or less than 1500°F, while the alloys containing 15 percent or more chromium, i.e., U700, IN728X, and PDRL 161, showed threshold temperatures equal to or greater than 1500°F.

h. The rate of sulfidation corrosion, as measured by changes in the depth of attack, appeared to approach a linear function with respect to time of exposure of the specimens to the corrosive environment.

i. The area of the specimen's surface over which corrosion occurred increased with exposure time, indicating that the threshold temperature is a function of time for the test conditions employed.

j. Homogenization of as-cast chemical segregation by heat treatment (solution and age) of IN728 had no significant effect on the material's resistance to sulfidation when tested using fuel containing 0.03 percent sulfur and salt-to-air ratio of 4 ppm.

k. Microprobe analysis of corroded specimens showed a sharp drop in the concentration of alloying elements had occurred at the matrix depleted zone interface. This, and the occurrence of grain boundary sulfidation, indicated that the matrix is being attacked by the inward movement of sulfur.

l. The presence of oxides with a high chromium content (25 to 35%) was found to be synonymous with those alloys which showed the best sulfidation corrosion resistance.

m. High Al/Ti ratios (> 6) were shown to be synonymous with the formation of an Al_2O_3 scale and good oxidation resistance.

REFERENCES

1. St. John, F. J., Rentz, W. A., and Freeman, W. R., Jr., Evaluation of Recently Developed Sulfidation-Resistant Alloys, paper presented at the Sixth Annual National Conference on Aircraft and Propulsion Systems, September, 1966.

2. W. A. Rentz, M. A. Donachie, Jr., Oxidation and Sulfidation Corrosion of Nickel-Base Superalloys, Amercian Society for Test Metals Technical Report No. C 6-18.5, 1966.

3. G. J. Danek, State-of the Art Survey on Hot Corrosion in Marine Gas Turbine Engines. U. S. Navy Marine Engineering Laboratory R & D Report 32/65, March 1965.

TABLE I

PHASE I TEST PARAMETERS

TEST NO.	PEAK TEST TEMP. (°F)	TEST TIME (Hrs.)	FUEL TYPE	FUEL SULFUR CONTENT (w/o)	SALT/AIR RATIO (ppm)
S527	1750	120	JP-4R	0.16	8
S528	1750	120	JP-4R	0.16	8
S530	1600	120	JP-4R	0.16	8
S531	1600	120	JP-4R	0.16	8
S532	1600	120	JP-4R	0.16	4
S533	1600	120	JP-4R	0.16	4
S534	1750	120	JP-4R	0.16	4
S535	1750	120	JP-4R	0.16	4
S536	1750	120	JP-4	0.02	4
S537	1750	120	JP-4	0.02	4
S538	1600	120	JP-4	0.02	4
S539	1600	120	JP-4	0.02	4
S540	1600	120	JP-4	0.02	8
S541	1600	120	JP-4	0.02	8
S542	1750	120	JP-4	0.02	8
S543	1750	120	JP-4	0.02	8
S544	1750	120	JP-5* + JP-5R	0.16	8

* JP-5 (.08% S) and JP-5R (.35%S) Mixed to Yield .16% S.

TABLE II

PHASE II TEST PARAMETERS

TEST NO.	PEAK TEST TEMP. °F	TEST TIME (HRS.)	FUEL TYPE	FUEL SULFUR CONTENT (W/O)	SALT/AIR RATIO (PPM)
S550	1600	120, 240 and 360	JP-4	0.03	4
S551	1750	120, 240 and 360	JP-4	0.03	4
S552	1600	120, 240 and 360	JP-4	0.03	4
S553	1750	120, 240 and 360	JP-4	0.03	4

TABLE III

OPERATING PARAMETERS

X-RAY GENERATOR:	Copper X-ray Tube 50K. V. 40 M.a.
DIFFRACTOMETER:	Equipped with focusing Monochromator. Divergence Slits - 1° Receiving Slit - 1° Scatter Slit - None
SCANNING SPEED:	1°/min.
CHART SPEED:	1/2 in./min.
DETECTOR:	Scintillation detector operated at 960 volts. Amplifier gain at 50 No pulse height discrimination Baseline at 12 volts
MONOCHROMATOR ALIGNMENT:	Aligned on Silicon (311) peak at 56.2°2θ
RATEMETER:	Set at 1x16x.8

TABLE IV

RESULTS OF CHEMICAL ANALYSES OF THE NICKEL AND COBALT BASE ALLOYS (USED IN PHASE I)

Alloy & Heat No.	Source of Analyses	COMPOSITION - WEIGHT PERCENT															
		Cr	Al	Ti	Mo	Cb	Ta	Co	W	C	Fe	Ni	Mn	Si	B	Zr	V
INCO713C (RW113)	N.C. (1)	13.00	5.75	0.75	4.50	2.30				0.14		Bal			.012	.10	
	S.M.C(2)	13.60	5.92	0.68	4.45	2.17				0.12	0.14	Bal	<.10	<.10	0.011	0.09	
	Ledoux	13.34	5.96	0.69	4.44	2.26					.07	Bal				.06	
INCO713LC (RW153)	N.C.	12.00	5.90	0.60	4.50	2.00				0.05		Bal			.010	.10	
	S.M.C.	12.50	5.70	0.70	4.45	2.08		<.10		0.06	0.17	Bal	<.10	<.10	0.010	0.08	
	Ledoux	12.17	5.54	0.69	4.62	2.08					.08	Bal				0.05	
TRW1800 (X2832)	N.C.	13.00	6.00	0.50		2.00			9.0	0.11		Bal			.02	.10	
	S.M.C.	12.90	6.15	0.53		2.03			9.1	0.12	<.30	Bal	<.10	<.10	.019	0.09	
	Ledoux	12.73	6.55	0.54		2.04			8.46		.07	Bal				.09	
PDRL161 (X2834)	N.C.	17.00	6.50	1.00	1.00	2.00				0.12		Bal			.02	.10	
	S.M.C.	17.00	6.45	1.03	1.05	1.97				0.13	0.10	Bal	<.10	<.10	0.02	.10	
	Ledoux	16.75	6.63	1.01	1.00	2.00					0.11	Bal				.04	
PDRL162 (UD698)	N.C.	10.00	6.50	1.00	4.00	1.00	2.00		2.00	0.18		Bal			.02	.10	
	S.M.C.	10.95	6.08	0.90	3.79	0.88	2.27		1.94	0.16	0.11	Bal	<.10	<.10	0.18	0.08	
	Ledoux	10.43	6.10	0.95	3.96	1.06	2.04		1.89		.06	Bal				.05	
IN728NX 21325	N.C.	17.00	6.25		1.50	1.00	2.00	10.00	2.00	0.05		Bal			0.020	0.10	
	S.M.C.																
	Ledoux	16.62	5.35	.01	1.53	1.18	2.24	10.10	1.74		.23	Bal				.08	

(1) N. C. - Nominal Composition

(2) S. M. C.- Special Metals Corp.

TABLE V

RESULTS OF CHEMICAL ANALYSES OF THE NICKEL AND COBALT BASE ALLOYS (USED IN PHASE I)

Alloy and Heat No.	Source of Analyses*	COMPOSITION - WEIGHT PERCENT															
		Cr	Al	Ti	Mo	Cb	Ta	Co	W	C	Fe	Ni	Mn	Si	B	Zr	V
B1900 (X2833)	N. C. (1)	8.00	6.00	1.00	6.00	-	4.00	10.00	-	0.10	-	Bal.	-	-	.015	.10	-
	S. M. C. (2)	8.10	5.95	1.04	6.00	-	4.05	9.80	-	0.11	0.10	Bal.	0.10	<0.10	.012	.10	-
	LeDoux	7.84	6.03	.98	6.11	-	3.95	9.93	-	-	.12	Bal.	-	-	-	.07	-
B1910 (84V4819)	N. C.	10.00	6.00	1.00	3.00	-	7.00	10.00	-	0.10	-	Bal.	-	-	.015	.10	-
	S. M. C.	10.01	6.15	1.00	3.00	-	6.85	10.25	-	0.14	0.15	Bal.	0.01	<0.10	.013	.10	-
	LeDoux	9.80	6.08	1.18	3.12	-	7.00	10.35	-	-	0.08	Bal.	-	-	-	.06	-
MAR-M-200 (RL088)	N. C.	9.00	5.00	2.00	-	1.00	-	10.0	12.5	0.15	-	Bal.	-	-	.015	.05	-
	S. M. C.	9.07	4.92	2.05	-	1.10	-	10.1	12.2	0.15	0.19	Bal.	<0.10	0.05	.016	0.042	-
	LeDoux	9.16	4.99	1.92	-	1.05	-	10.07	11.74	-	.35	Bal.	-	-	-	.04	-
IN100 (RV134)	N. C.	10.00	5.50	5.00	3.00	-	-	15.0	-	0.18	-	Bal.	-	-	0.014	.06	1.0
	S. M. C.	10.80	5.48	4.28	3.20	-	-	15.3	-	0.17	0.14	Bal.	0.10	0.10	0.013	.07	0.80
	LeDoux	10.24	5.41	4.21	3.12	-	-	15.24	-	-	0.06	Bal.	-	-	-	.03	-
U-700 (64156)	N. C.	15.00	4.50	3.50	5.25	-	-	17.0	-	0.10	-	Bal.	-	-	.03	-	-
	S. M. C.	14.95	4.34	3.39	4.20	-	-	15.10	-	0.08	0.17	Bal.	<.10	<.10	0.015	<0.01	-
	LeDoux	14.22	4.24	3.39	4.40	-	-	15.01	-	-	0.7	Bal.	-	-	-	ND	-
X-40 (M4460)	N. C.	25.50	-	-	0.30	-	-	Bal.	7.5	0.50	-	10.5	-	-	-	-	-
	S. M. C.	-	-	-	-	-	-	-	-	-	-	-	-	-	-	-	-
	LeDoux	24.78	-	-	-	-	-	Bal.	7.39	-	1.19	10.62	-	-	-	-	-

(1) N. C. - Nominal Composition

(2) S. M. C.- Special Metals Corp.

TABLE VI

RESULTS OF CHEMICAL AND X-RAY FLUORESCENCE ANALYSES OF PHASE II NICKEL BASE ALLOYS

ALLOY & HEAT NO.	Source of Analyses	Composition - Weight Percent															
		Cr	Al	Ti	Mo	Cb	Ta	Co	W	C	Fe	Ni	Mn	Si	B	Zr	V
INCO713C RW113	NC	13.00	5.75	0.75	4.50	2.30				0.14		72.0			.012	.10	
	SMC	13.6	5.92	0.68	4.45	2.17				0.12		BAL	<.10	<.10	.011	.09	
	LEDOUX	13.34	5.96	0.69	4.44	2.26											
IN728X 21324	NC	17.0	6.25		1.50	1.00	2.00	10.00	2.00	0.05		BAL			0.020	0.10	
	AL(X-RAY)	17.48	6.22		1.12	1.22	2.00	10.44	1.81								
U700 64156	NC	15.00	4.50	3.50	5.25			17.0		0.10		BAL			0.03		
	SMC	14.95	4.34	3.39				15.10		0.08	0.17	BAL	<0.10	<0.10	0.015	<.01	
	LEDOUX	14.22	4.24	3.39	4.40			15.01			0.07	BAL					
TRW1800 LYC008	NC	13.00	6.00	0.50		2.00			9.00	0.11		69.4				0.02	
	AL(X-RAY)	13.00	6.67	0.41		2.80			8.89								
	AL(CHEM)	12.69	6.44	0.63		2.6			9.13	0.12		BAL				0.017	.10
B1910 84V4819	NC	10.00	6.00	1.00	3.00		7.00	10.00		0.10		62.3			.015	.10	
	SMC	10.01	6.15	1.00	3.00		6.85	10.25		0.14	0.15	BAL	0.01	<.10	0.013	0.10	
	LEDOUX	9.80	6.08	1.18	3.12		7.00	10.35			0.08	61.93				0.06	

NC - Nominal Composition
SMC - Special Metals Corp.
AL - Avco Lycoming

TABLE VII

RESULTS OF TESTING AT 1600° AND 1750°F PEAK TEMPERATURES USING JP-4 and JP-4R FUEL WITH A 4 PPM SALT/AIR RATIO

ALLOY	HEAT NO.	FUEL TYPE	SULFUR (w/o)	THRESHOLD TEMP. (°F)	TERMINAL TEMP. (°F)	TEMP. OF MAX. ATTACK (°F)	MAX. DEPTH OF ATTACK (mils)	TOTAL ** CORROSION
Inco 713C	RW 113	JP4R	0.16	1475	1700	1575	13	4.8
Inco 713C	RW 113	JP4	0.02	1500	1725	1625	3	.9
Inco 713LC	RW 153	JP4R	0.16	1450	1700	1625	8	3.3
Inco 713LC	RW 153	JP4	0.02	1500	1700	1650	3	1.3
TRW 1800	X2832	JP4R	0.16	1525	1625	1600	3	.5
TRW 1800	X2832	JP4	0.02	1525	1675	1625	2	.6
B1900	X2833	JP4R	0.16	< 1450	1700	1575	18	> 7.2
B1900	X2833	JP4	0.02	< 1450	1700	1625	9	> 5.1
B1910	84V4819	JP4R	0.16	1440*	1700	1525	15	6.0
B1910	84V4819	JP4	0.02	1450	1700	1550	4	1.9
MAR-M200	RL088	JP4R	0.16	1475	1725	1550	19	5.5
MAR-M200	RL088	JP4	0.02	1450	1725	1525	11	2.5
PDRL-161	X2834	JP4R	0.16	1500	1675	1600	13	3.4
PDRL-161	X2834	JP4	0.02	1500	1625	1575	2	.3
PDRL-162	VD698	JP4R	0.16	1575	1700	1625	10	2.2
PDRL-162	VD698	JP4	0.02	1600	1675	1650	4	.4
IN728X	21325	JP4R	0.16	1600	1760	1700	2	.6
IN728X	21325	JP4	0.02	1650	> 1750	> 1750	2	> .4
X40	MA460	JP4R	0.16	NO VISIBLE CORROSION			0	0
X40	MA460	JP4	0.02	NO VISIBLE CORROSION			0	0
U700	64156	JP4R	0.16	1600	> 1750	> 1750	4	1.0
U700	64156	JP4	0.02	NO VISIBLE CORROSION			0	0
IN100	RV 134	JP4R	0.16	1550	1700	1625	11	2.8
IN100	RV 134	JP4	0.02	1600	> 1750	1650	8	> 1.7

*Extrapolated

**Area under the corrosion vs. temperature curve (square inches)

TABLE VIII

RESULTS OF TESTING AT 1600° AND 1750°F PEAK TEMPERATURES USING JP-4 and JP-4R FUEL WITH A 8 PPM SALT/AIR RATIO

ALLOY	HEAT NO.	FUEL TYPE	SULFUR (w/o)	THRESHOLD TEMP. (°F)	TERMINAL TEMP. (°F)	TEMP. OF MAX. ATTACK (°F)	MAX. DEPTH OF ATTACK (mils)	TOTAL ** CORROSION
Inco 713C	RW113	JP4R	0.16	1450	1725	1600	16.	7.8
Inco 713C	RW113	JP4	0.02	1450	1750	1600	4.	1.8
Inco 713LC	RW153	JP4R	0.16	1450	1725	1675	21.	7.7
Inco 713LC	RW153	JP4	0.02	1450	1725	1600	5.	2.4
TRW 1800	X2832	JP4R	0.16	1500	1725	1600	5.	1.6
TRW 1800	X2832	JP4	0.02	1450	1725	1550	2.	.8
B1900	X2833	JP4R	0.16	1430*	1750	1650	20.	11.3
B1900	X2833	JP4	0.02	< 1450	1750	1600	17.	> 9.8
B1910	84V4819	JP4R	0.16	< 1450	1750	1650	16.	> 8.4
B1910	84V4819	JP4	0.02	1475	1725	1550	.7.	2.4
MAR-M200	RL088	JP4R	0.16	1450	1750	1600	20.	9.7
MAR-M200	RL088	JP4	0.02	1450	1750	1575	12.	6.7
PDRL 161	X2834	JP4R	0.16	1500	1725	1600	20.	5.9
PDRL 161	X2834	JP4	0.02	1550	1725	1650	6.	1.6
PDRL 162	VD698	JP4R	0.16	1475	1725	1625	12.	4.5
PDRL 162	VD698	JP4	0.02	1475	1625	1550	3.	.7
IN728X	21325	JP4R	0.16	1550	1700	1650	7.	1.4
IN728X	21325	JP4	0.02	1625	1750	1700	2.	.4
X40	MA460	JP4R	0.16	No	Visible	Corrosion	0	0
X40	MA460	JP4	0.02	No	Visible	Corrosion	0	0
U700	64156	JP4R	0.16	1625	> 1750	1700	10	> 2.0
U700	64156	JP4	0.02	1600	> 1750	***	1	> .3
IN100	RV134	JP4R	0.16	1475	1770*	1625	22	10.8
IN100	RV134	JP4	0.02	1450	> 1750	1550	15.	> 6.2

*Extrapolated

**Area Under the Corrosion vs. Temperature Curve (Square Inches)

***Amount of Corrosion too Little to Determine Temperature of Maximum Attack

TABLE IX

RELATIVE PERFORMANCE OF ALLOYS TESTED UNDER VARIOUS TEST CONDITIONS

RANK	0.16% S/8 PPM SALT ALLOY	TOTAL CORR*.	0.16% S/4 PPM SALT ALLOY	TOTAL CORR.*	0.02% S/8 PPM SALT ALLOY	TOTAL CORR.*	0.02% S/4 PPM ALLOY	TOTAL CORR.*
1	X40	0	X40	0.	X40	0.	X40	0.
2	IN728X	1.4	TRW 1800	0.5	U700	> 0.3	U700	0.
3	TRW 1800	1.6	IN728X	0.6	IN728X	0.4	PDRL161	0.3
4	U700	> 2.0	U700	1.0	PDRL 162	0.7	PDRL 162	> 0.4
5	PDRL162	4.5	PDRL162	2.2	TRW 1800	0.8	IN728X	0.4
6	PDRL161	5.9	IN100	2.8	PDRL161	1.6	TRW1800	0.6
7	Inco713LC	7.7	Inco 713LC	3.3	Inco 713C	1.8	Inco 713C	0.9
8	Inco713C	7.8	PDRL161	3.4	Inco 713LC	2.4	Inco713LC	1.3
9	B1910	> 8.4	Inco713C	4.8	B1910	2.4	IN100	> 1.7
10	MAR-M200	9.7	MAR-M200	5.5	IN100	> 6.2	B1910	1.9
11	IN100	10.8	B1910	6.0	MAR-M200	6.7	MAR-M200	2.5
12	B1900	11.3	B1900	> 7.2	B1900	> 9.8	B1900	> 5.1

*Area Under Depth of Penetration vs. Temperature Curve

TABLE X

THRESHOLD AND TERMINAL TEMPERATURES AFTER 120 AND 360 HOURS TESTING USING JP-4 FUEL AND A SALT-TO-AIR RATIO OF 4 PPM

	THRESHOLD		TERMINAL	
	120 Hours °F	360 Hours °F	120 Hours °F	360 Hours °F
Inco 713C	1475	1450	1700	1750
TRW1800	1500	1475	1600	1635
B1910	1450	1450	1625	1650
IN728X	1675	1600	1750	1750
IN728X HT	1650	1575	1750	1750
U700	1625	1600	1750	1750

TABLE XI

SUMMARY OF CORROSION PRODUCTS FOUND ON THE TRAILING EDGE AFTER 40 HOURS OF RIG TESTING

ALLOY	CORROSION PRODUCTS
X40	Co Matrix (fcc) + CoO + $CoCr_2O_4$
IN 728	Ni_3Al[(b)] + Spinel (a_o = 8.27) + NiO + Cr_2O_3 + Unknown
TRW 1800	Ni_3Al[(b)] + Spinel (a_o = 8.24) + NiO + $NiWO_4$ (trace) + Al_2O_3 (trace)
U700	Ni_3Al[(b)] + NiO + Spinel (a_o = 8.32)
PDRL 162	Ni_3Al[(b)] + Spinel (a_o = 8.15) + NiO + Al_2O_3 (trace) + Unknown
PDRL 161	Ni_3Al[(b)] + NiO + Spinel (a_o = 8.24) + Al_2O_3 + Cr_2O_3 (trace)
INCO 713	Ni_3Al[(b)] + NiO + Spinel (a_o = 8.17) + Al_2O_3 (trace) + Cr_2O_3 (trace)
B1910	Ni_3Al[(b)] + Spinel (a_o = 8.27) + NiO + Unknown (a major phase d = 3.90, 3.30, 2.75) + Al_2O_3 (trace)
M200	Ni_3Al[(b)] + NiO + Spinel (a_o = 8.26) + $NiWO_4$ (trace)
IN 100	Ni_3Al[(b)] + NiO + Spinel (a_o = 8.34)
B1900	Ni_3Al[(b)] + Spinel (a_o = 8.17) + NiO + Al_2O_3

(a) Phases listed in order of decreasing quantities as indicated by X-ray intensities.

(b) This phase is the γ' phase from the base alloy and is used as a reference for the patterns.

TABLE XII

SUMMARY OF CORROSION PRODUCTS FOUND ON THE TRAILING EDGE AFTER 120 HOURS TESTING

ALLOY	CORROSION PRODUCTS
X 40	Co (Matrix) (fcc) + CoO + $CoCr_2O_4$
IN 738	$Ni_3Al^{(b)}$ + Spinel (a_o = 8.27) + NiO + Cr_2O_3 Unknown
TRW 1800	$Ni_3Al^{(b)}$ + Spinel (a_o = 8.24) + NiO + $NiWO_4$ (trace) Al_2O_3 (trace)
U700	$Ni_3Al^{(b)}$ + NiO + Spinel (a_o = 8.32)
PDRL 162	$Ni_3Al^{(b)}$ + Spinel (a_o = 8.15) + NiO + Al_2O_3 + Cr_2O_3 + Unknown
PDRL 161	$Ni_3Al^{(b)}$ + NiO + Spinel (a_o = 8.24) + Al_2O_3 + Cr_2O_3
INCO 713	$Ni_3Al^{(b)}$ + NiO + Spinel (a_o = 8.17) + Unknown + Al_2O_3 (trace + Cr_2O_3 (trace)
B1910	$Ni_3Al^{(b)}$ + Spinel (a_o = 8.27) + NiO + Unknown (a major phase d = 3.90, 3.30, 2.75)
M200	$Ni_3Al^{(b)}$ + NiO + Spinel (a_o = 8.26) + $NiWO_4$ Uknown (d = 2.11, 2.63, 1.93, 1.86)
IN 100	$Ni_3Al^{(b)}$ + NiO + Spinel (a_o = 8.34)
B1900	$Ni_3Al^{(b)}$ + Spinel (a_o = 8.17) + NiO + Al_2O_3 + Unknown (d = 3.88, 3.29, 2.74, 1.94, 1.67, 1.65, 1.38)

(a) Phases presented are listed in order of decreasing quantities as indicated by X-ray intensities.

(b) This phase is the γ' phase from the base alloy and is used as a reference for the pattern.

TABLE XIII

SUMMARY OF CORROSION PRODUCTS FOUND IN POWDERS REMOVED FROM AREA WHICH HAS UNDERGONE SULFIDATION CORROSION FOR 120 HOURS OF TESTING

ALLOY	CORROSION PRODUCTS
X 40	No oxides removed, too thin and adherent
IN 728	Spinel (a_o = 8.24) + NiO + Unknown
TRW 1800	Spinel (a_o = 8.20) + NiO + $NiWO_4$
U 700	NiO + Spinel (a_o = 8.32)
PDRL 162	Spinel (a_o = 8.20) + NiO + Unknown (d = 3.40, 2.34)
PDRL 161	NiO + Spinel (a_o = 8.20) + Unknown (d = 3.33, 1.76, 1.72)
INCO 713	NiO + Spinel (a_o 8.24) + Al_2O_3 (trace) + Cr_2O_3 (trace) + Unknown
B1910	Spinel (a_o = 8.27) + NiO + Al_2O_3 + Unknown (d = 3.34)
M200	NiO + Spinel (a_o 8.27) + $NiWO_4$
IN 100	NiO + Spinel (a_o = 8.27)
B1900	Spinel (a_o = 8.25) + NiO + Unknown (d = 3.33, 2.54, 1.73)

(a) Phases listed in order of decreasing quantities as indicated by X-ray intensities.

TABLE XIV

MICROPROBE ANALYSIS OF DEPLETION ZONE AREAS

ALLOY	Ni	Cr	Mo	Al	Ti	Cb	S	W	Co	Ta
INCO 713C	95.0	0.30	3.5	3.0	0.01	0.2	-	-	-	-
TRW 1800	90.5	0.5	-	2.8	0.08	1.0	-	4.6	-	-
IN 728	80.3	0.4	1.2	2.0	-	0.1	-	1.5	13.7	1.1
PDRL 161	95.5	0.8	0.7	2.8	0.02	0.1	-	-	-	-
PDRL 162	94.2	0.4	0.9	2.4	0	-	-	1.3	0	1.0
U700	76.2	0.9	3.6	2.3	0.12	-	-	-	19.0	-
B1900	84.2	0.5	4.0	2.7	0	-	-	-	5.9	1.5
IN100	94.0	0.4	1.0	1.4	0.03	-	-	-	3.0	-
M200	80.5	0.5	-	1.9	0	0	-	7.8	10.8	-
B1910	83.0	2.0	1.9	3.3	.05	-	-	-	8.2	4.3

0 Indicates complete depletion of element
- Indicates element not present in original alloy.

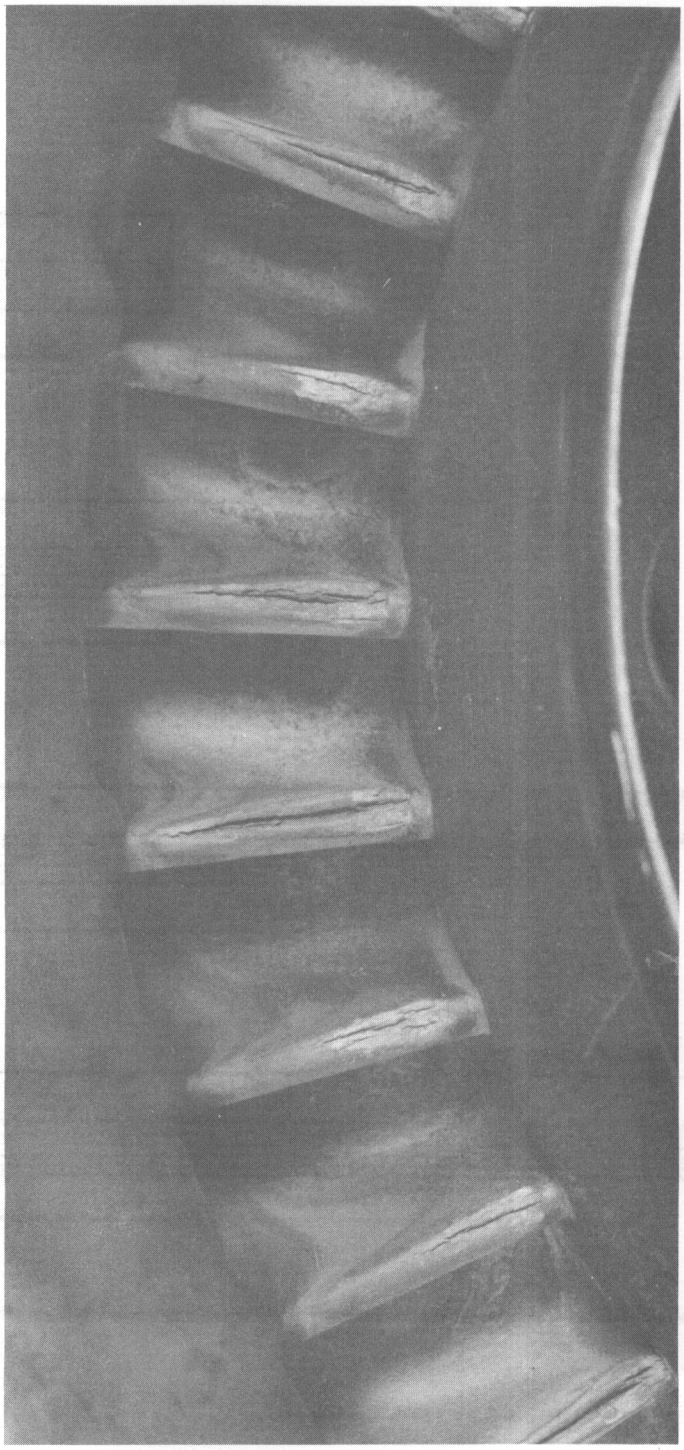

Figure 1. Leading Edges of T53 Gas Producer Nozzle Vanes After Engine Operation in Viet Nam, Showing Typical Sulfidation Attack.

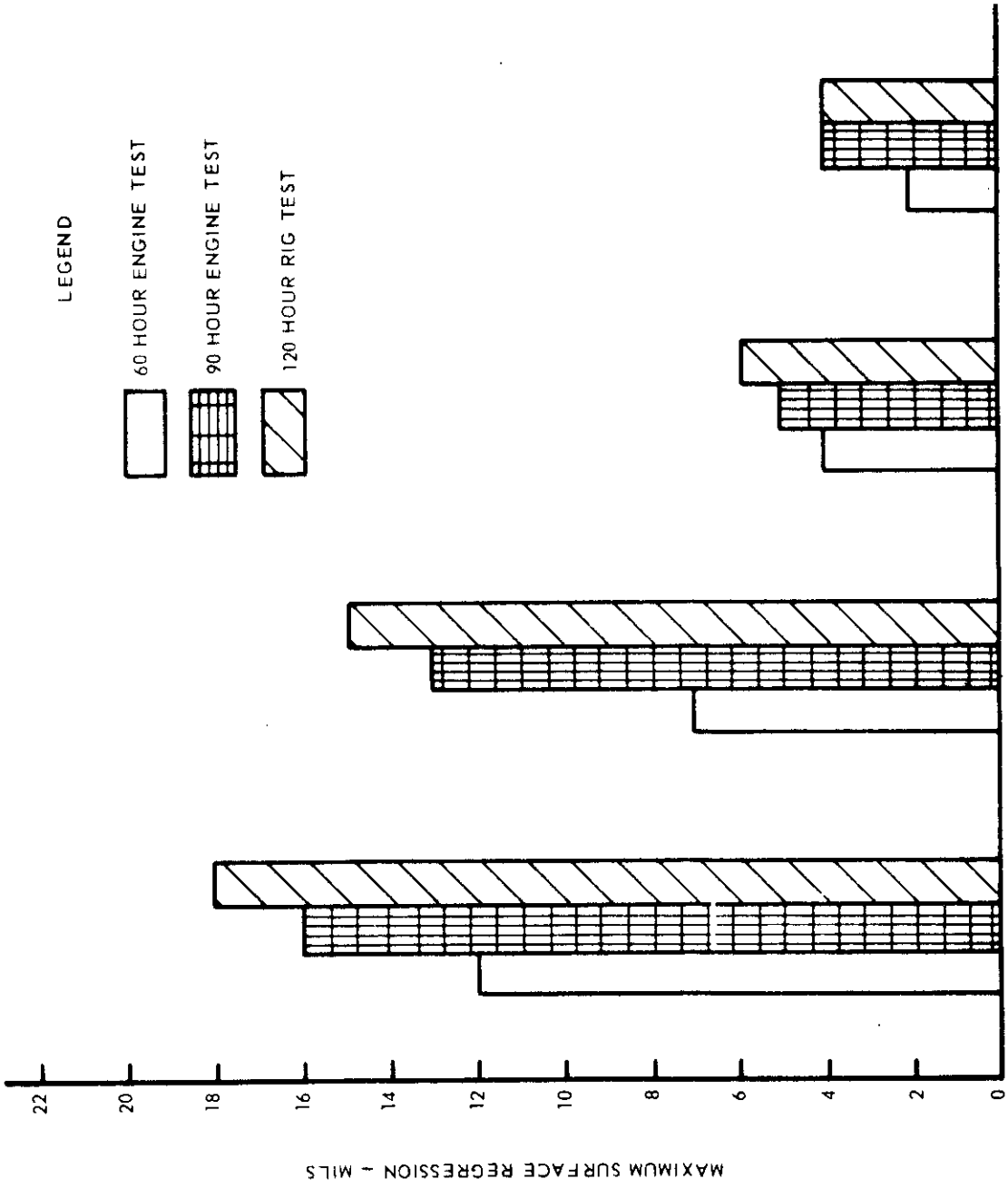

Figure 2. Relative Performance of Superalloys Investigated in Engine (Salt/Air Ratio: 1 ppm) and Rig (Salt/Air Ratio: 6 ppm) Tests. (From Bibliographical Reference 1.)

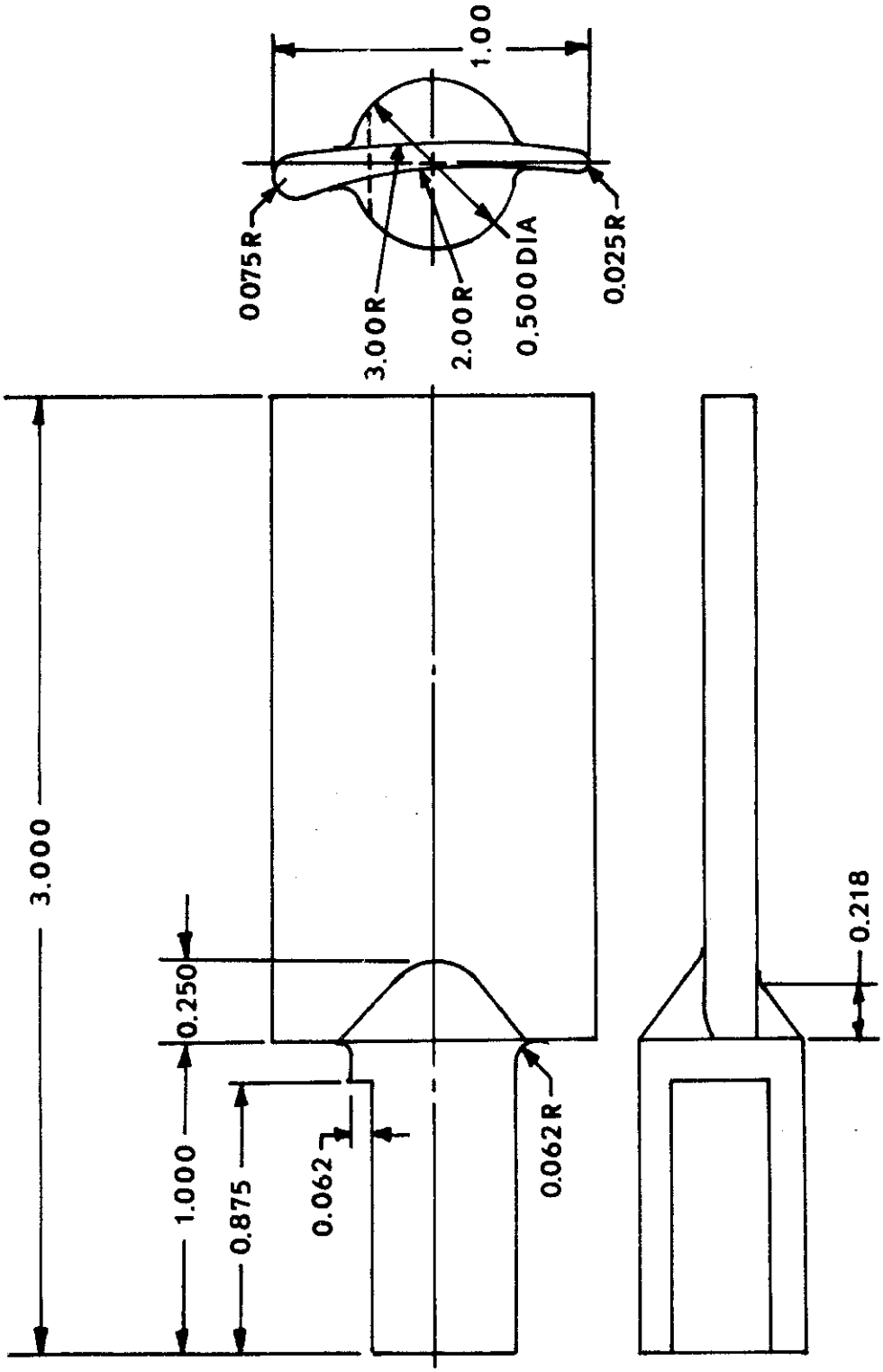

All dimensions are in inches unless otherwise specified.

Figure 3. Airfoil Test Specimen.

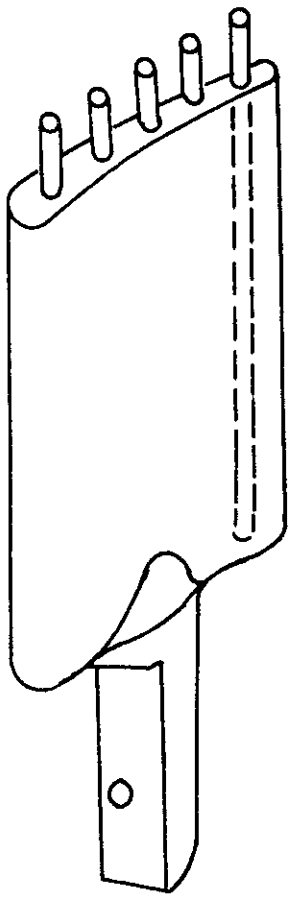

Figure 1. Schematic Illustration of Airfoil Test Specimen with Hardness Pins in Place.

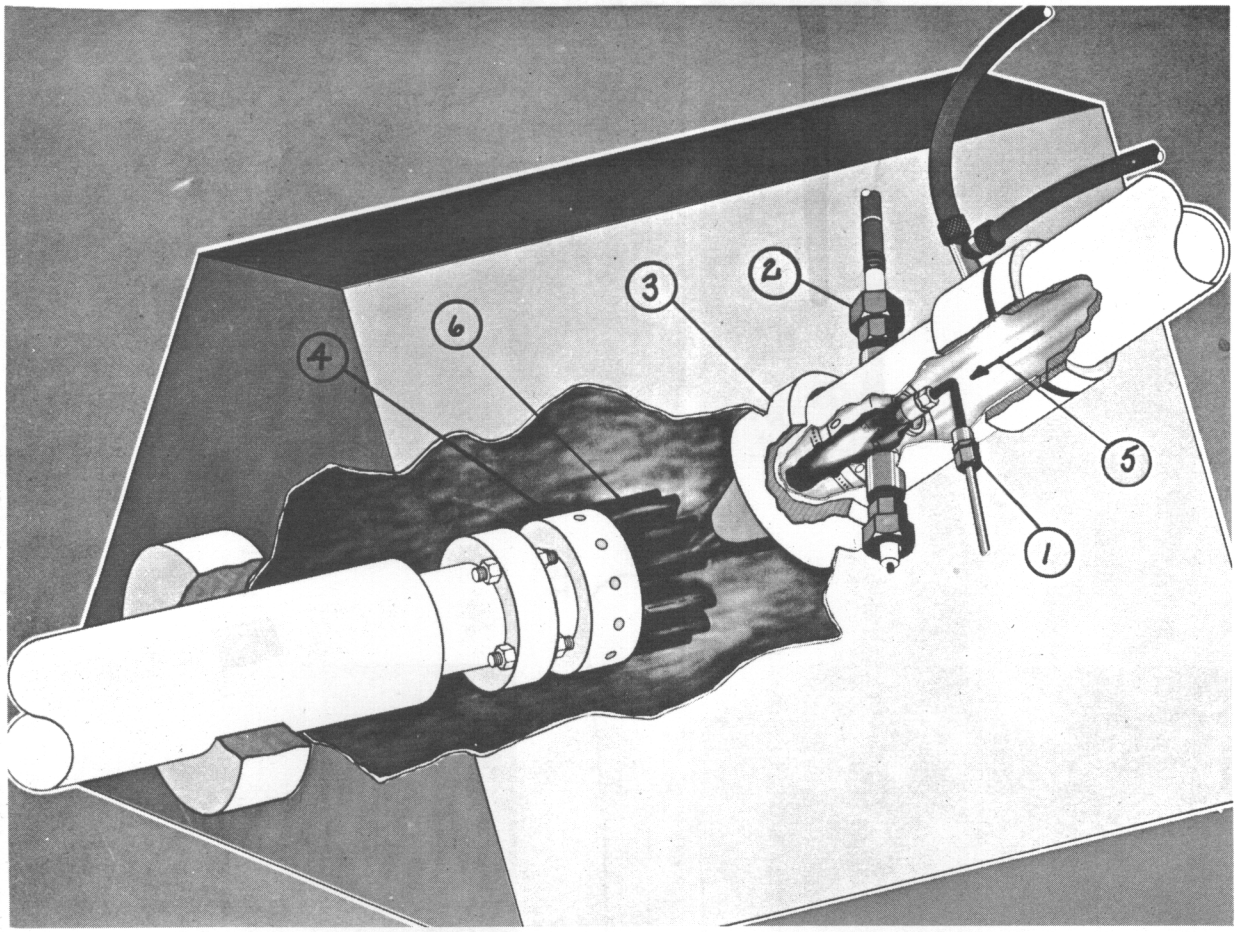

1. Fuel Line
2. Igniter
3. Synthetic Sea Water Injection System
4. Rotating Specimen Holder
5. Inlet Air
6. Test Specimens

Figure 5. Schematic Illustration of a Rig Heating Chamber Showing the Essential Components of the Combustor and Synthetic Sea Water Injection System.

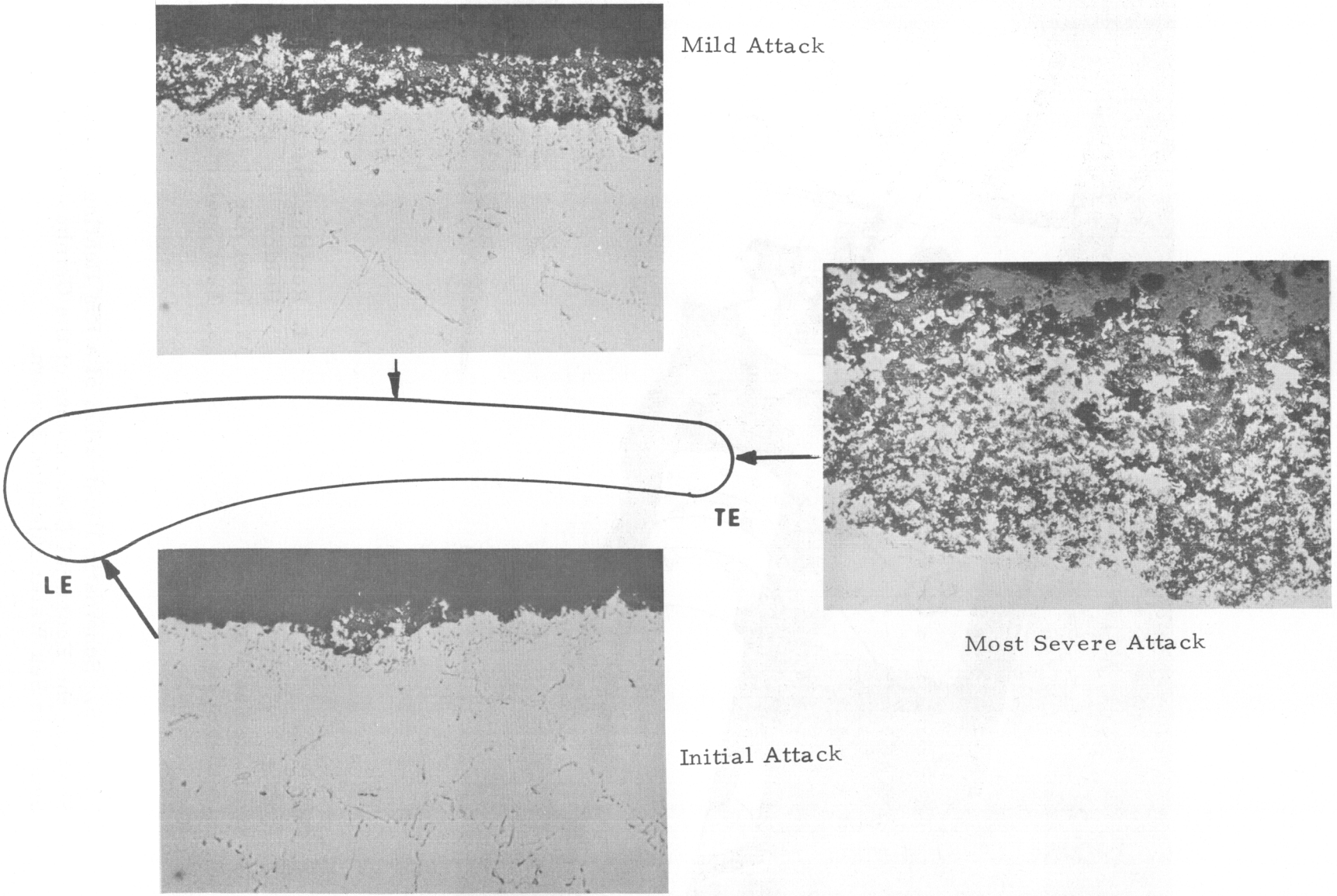

Figure 6. Photomicrographs Showing Various Stages of Corrosive Attack on a Cross Section of a Test Specimen.

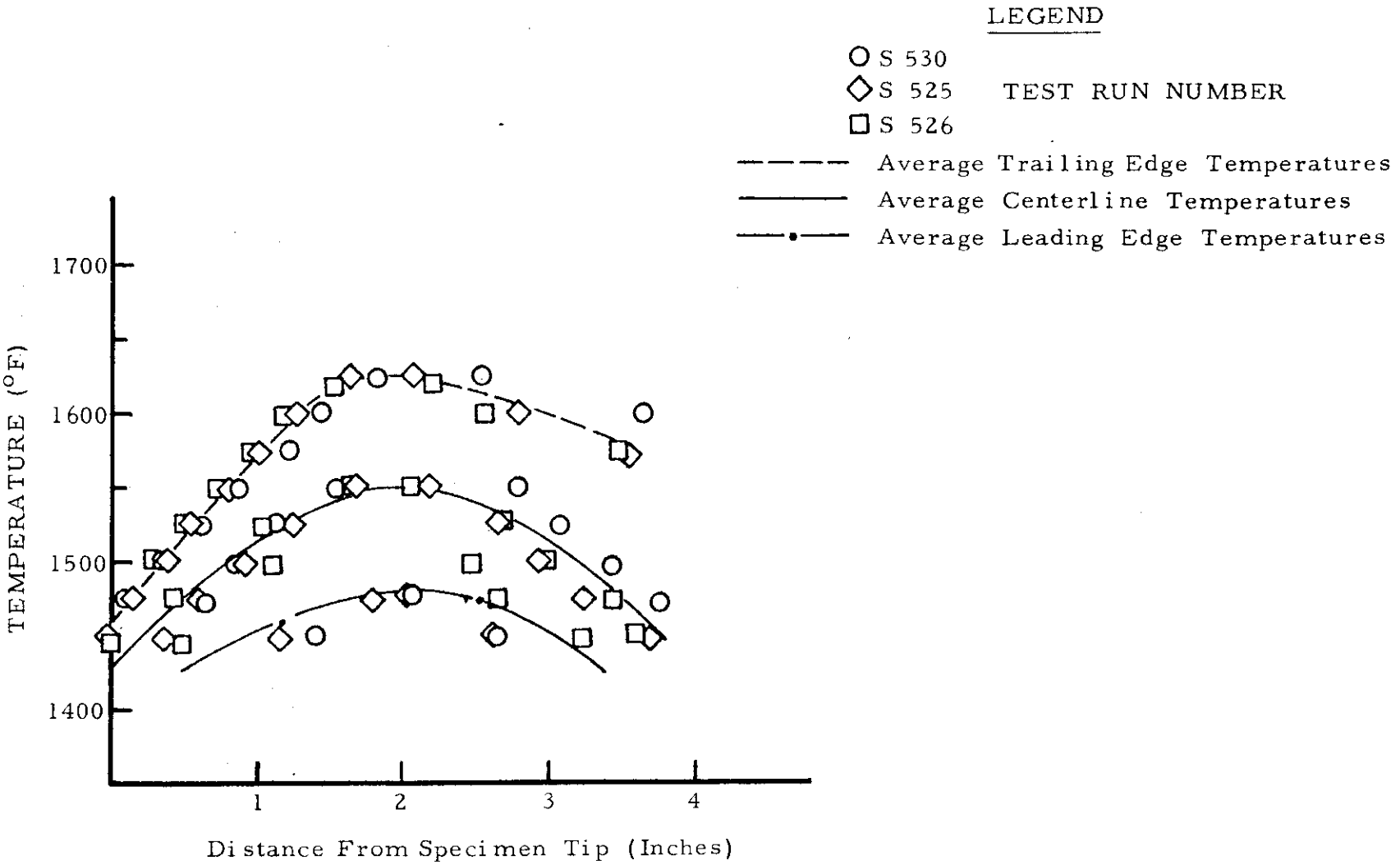

Figure 7. Metal Temperature vs. Span Length for 1600°F Peak Metal Temperature Test Obtained by Using Axial Hardness Pins Inserted Along the Specimen Leading and Trailing Edges and Mid-Chord Position.

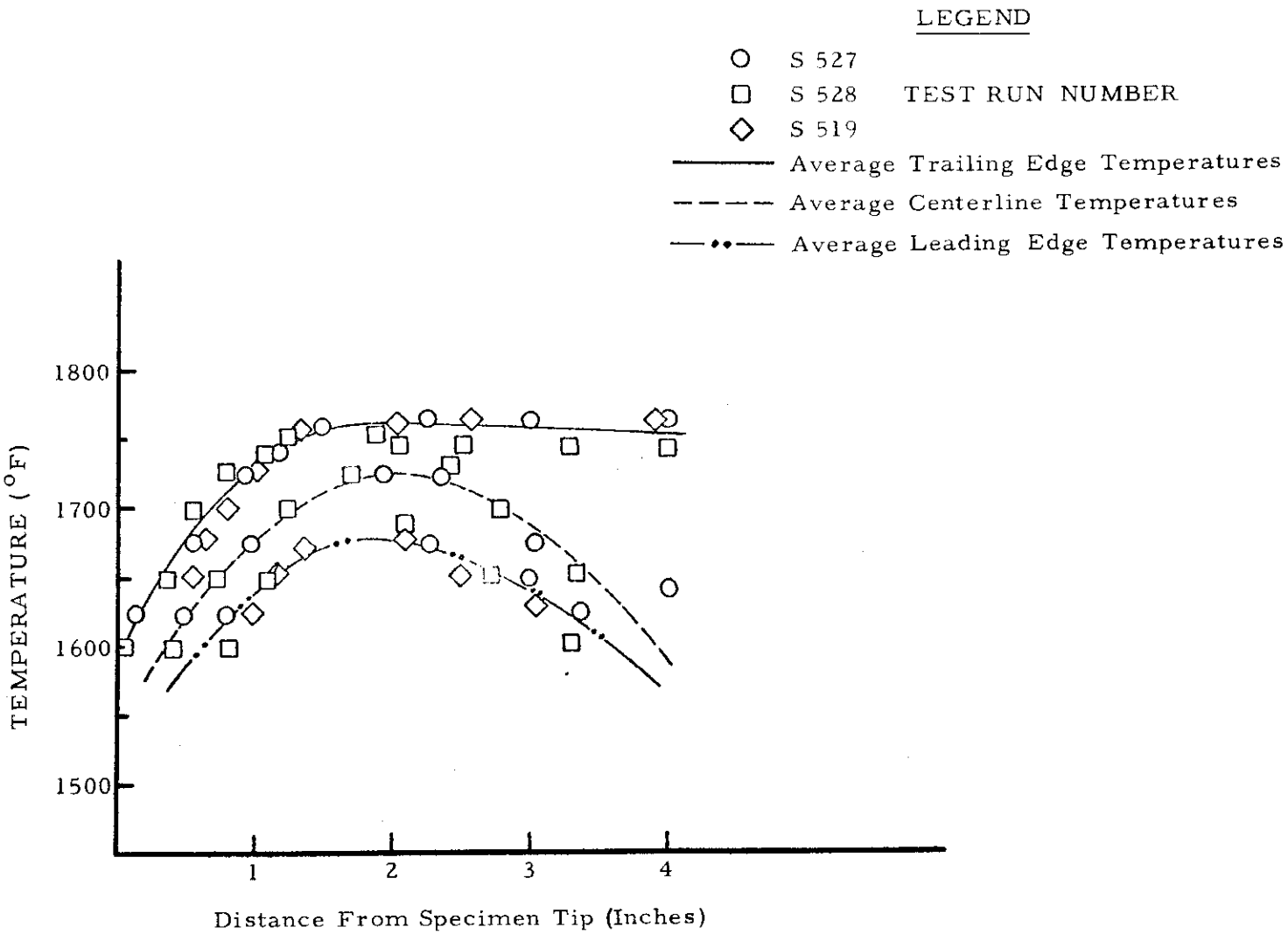

Figure 8. Metal Temperature vs. Span Length for 1750°F Peak Metal Temperature Test Obtained by Using Axial Hardness Pins Inserted Along the Specimen Leading and Trailing Edges and Mid-Chord Position.

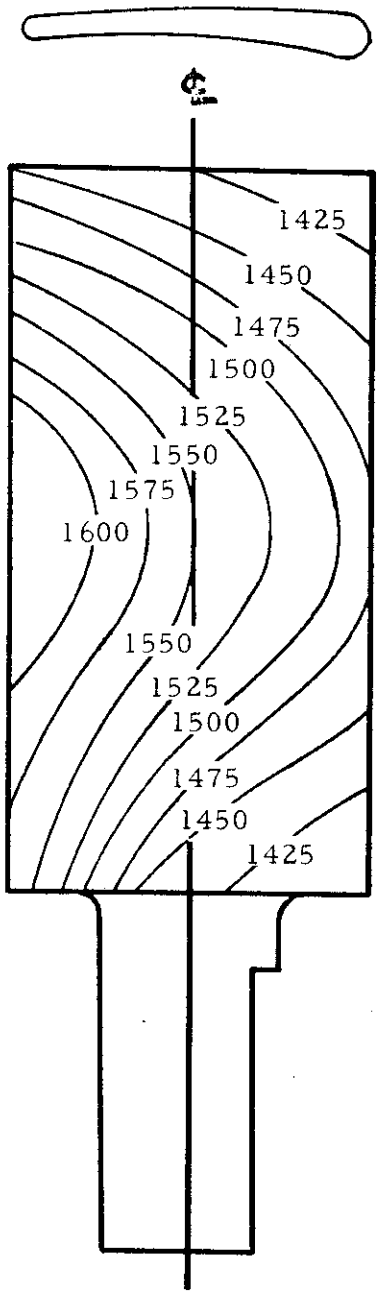

Figure 9. Specimen Temperature Distribution Characteristic of 1600°F Peak Test Temperature.

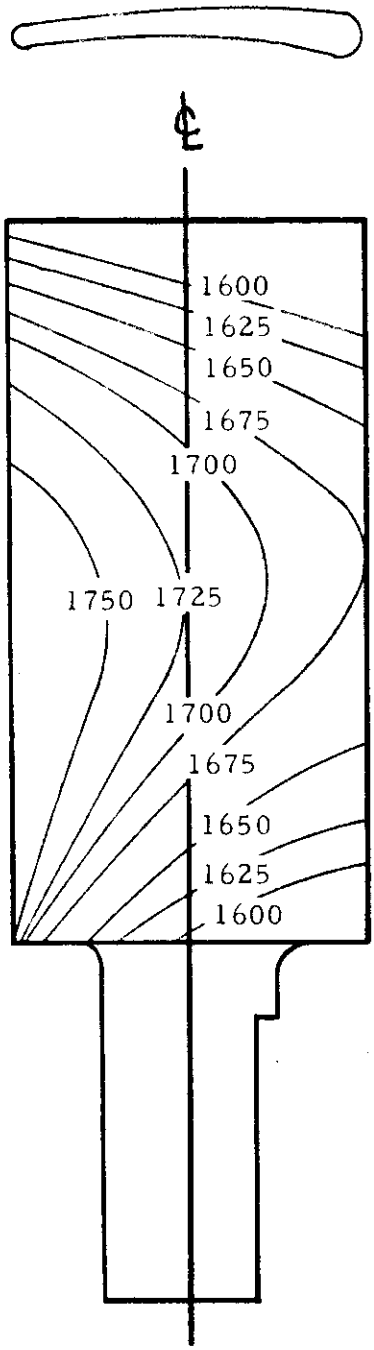

Figure 10. Specimen Temperature Distribution Characteristic of 1750°F Peak Test Temperature.

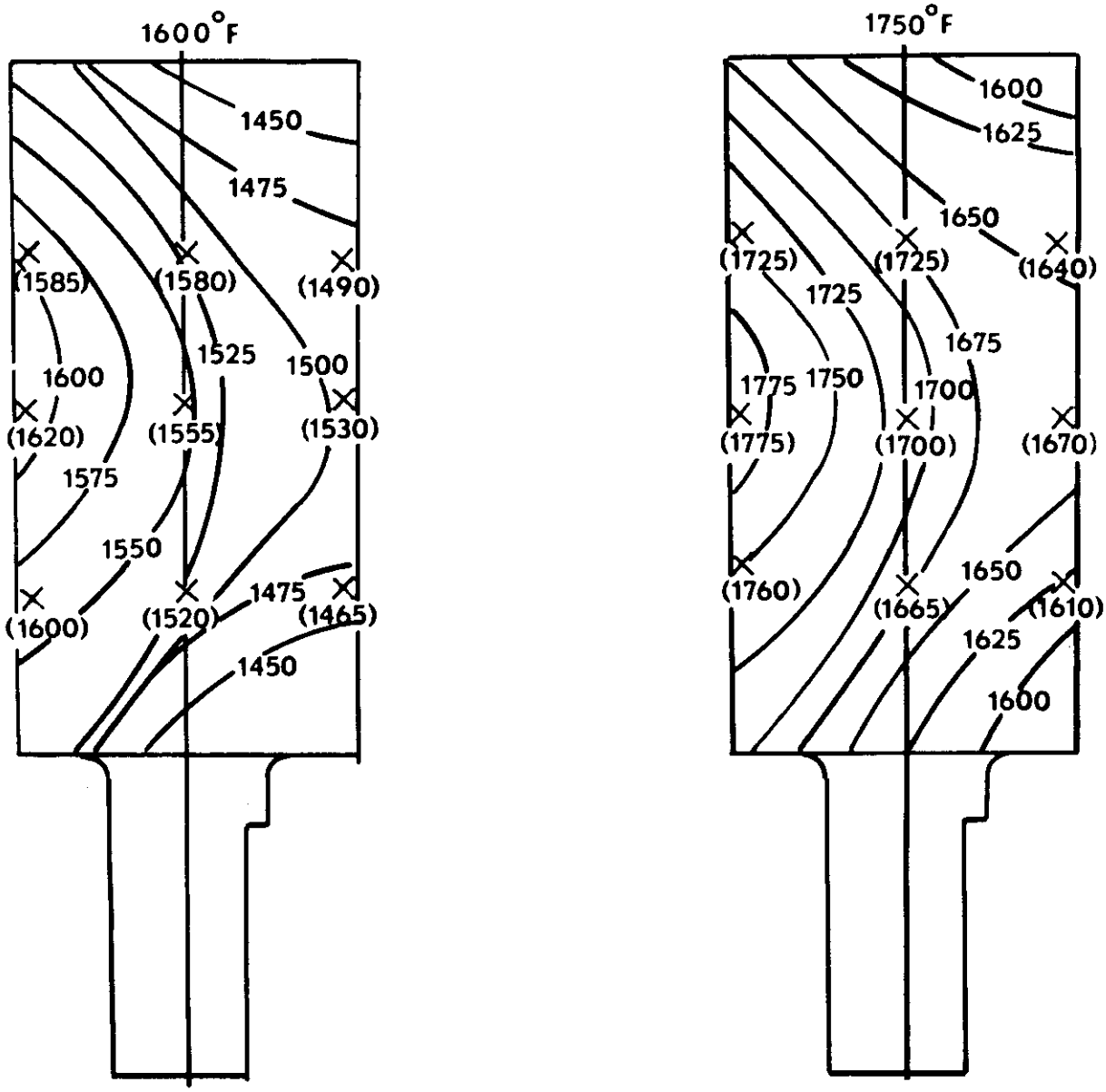

Figure 11. Comparison of Specimen Metal Temperatures Obtained by Using Thermocouple (Temperatures in Parentheses) and Hardness Pin Techniques.

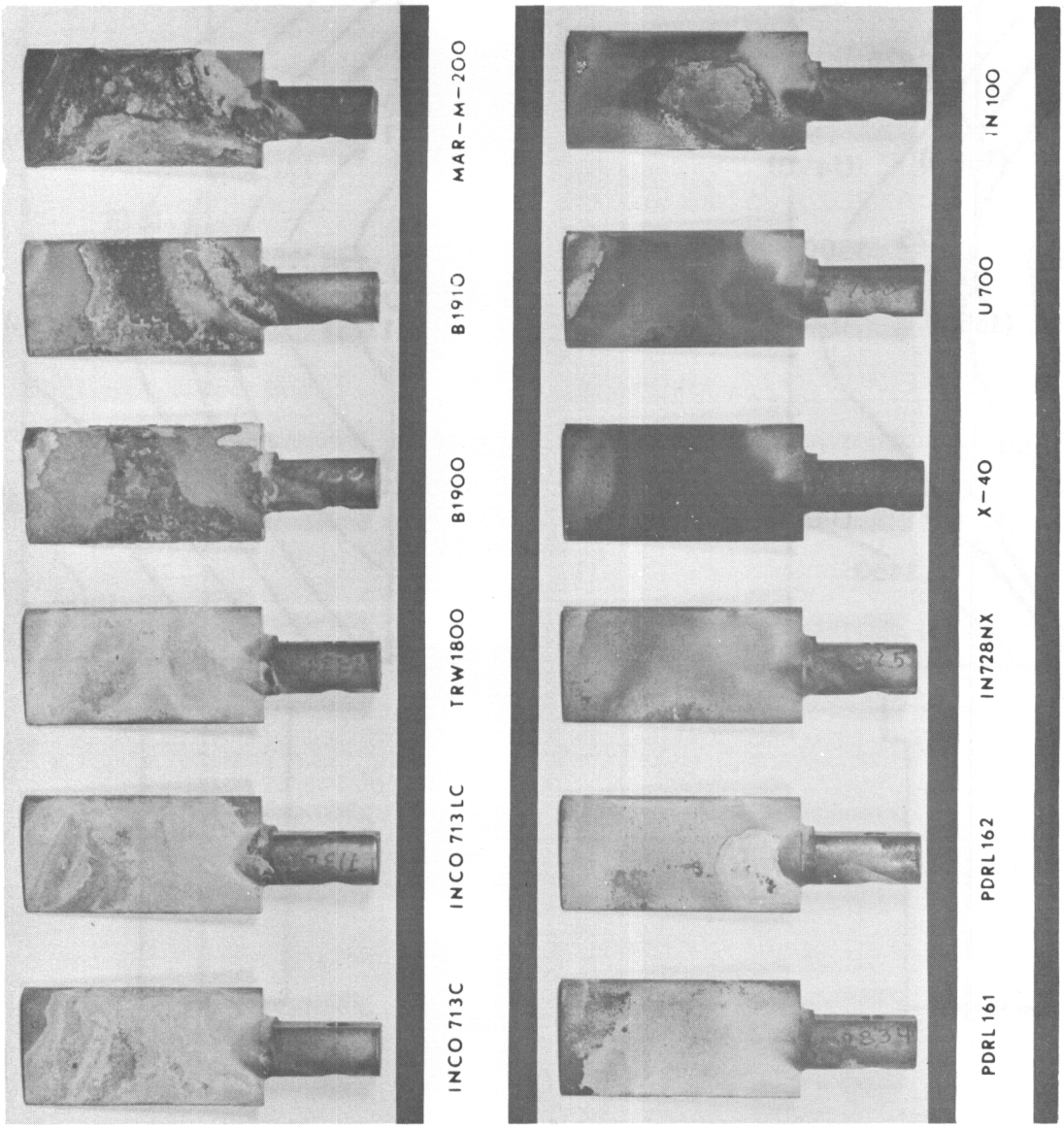

Figure 12. General Appearance of Specimens Tested 120 Hours at 1600°F (Peak) Using JP-4 Fuel and a Salt/Air Ratio of 8 ppm (S540).

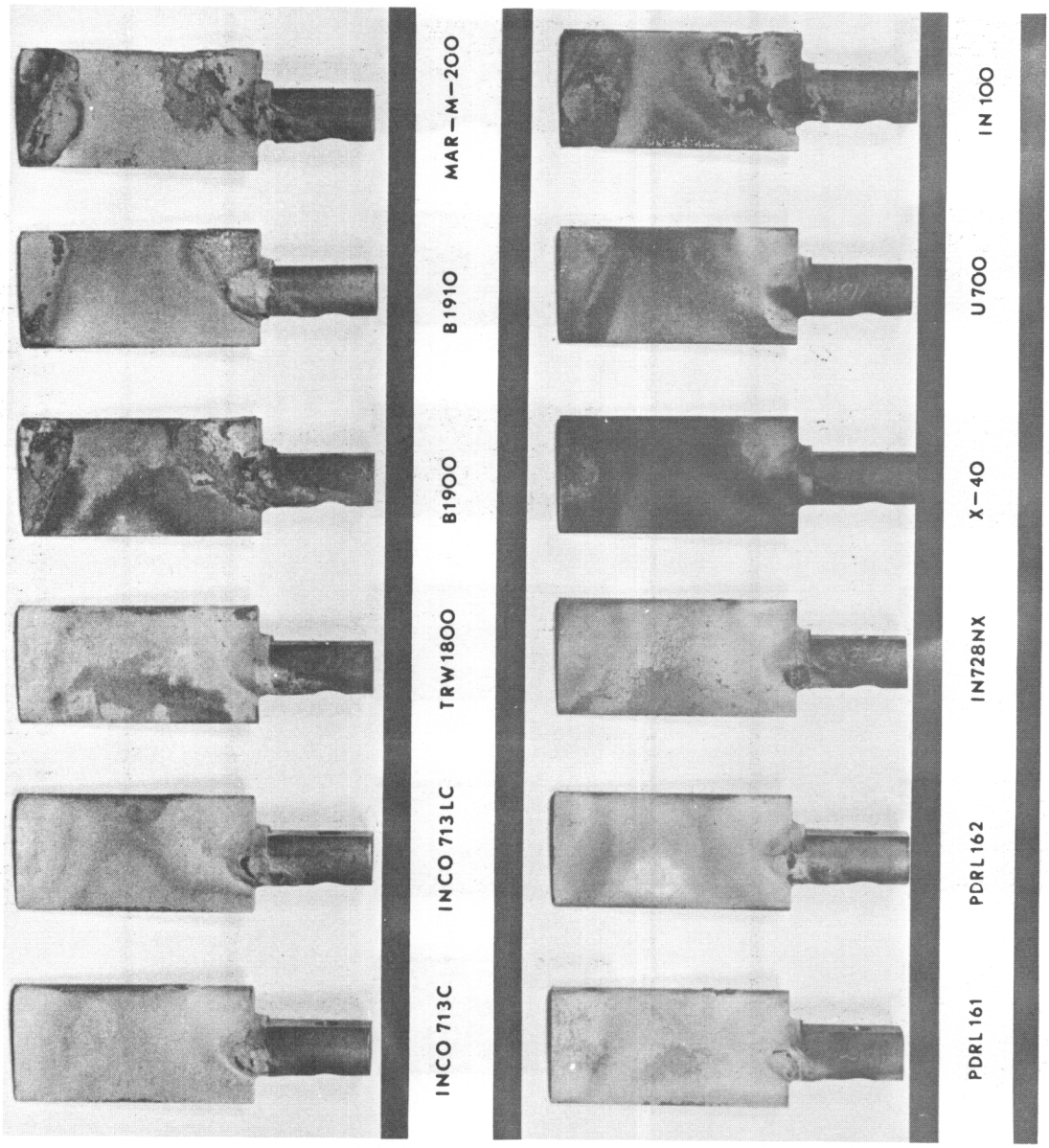

Figure 13. General Appearance of Specimens Tested 120 Hours at 1750°F (Peak) Using JP-4 Fuel and a Salt/Air Ratio of 8 ppm (S542).

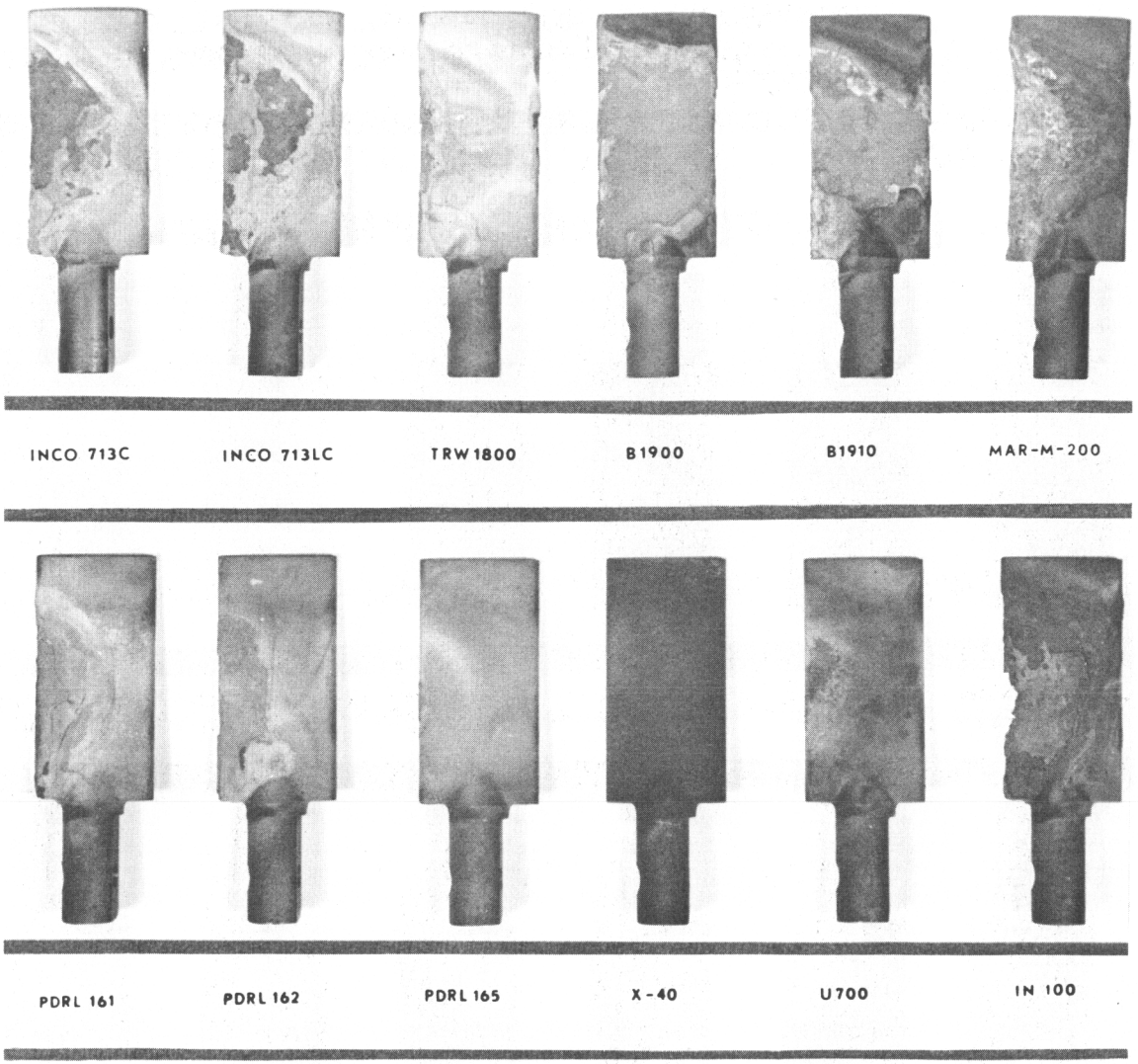

Figure 14. General Appearance of Specimens Tested 120 Hours at 1600°F Using JP-4R Fuel and an 8 ppm Salt/Air Ratio (Test S-530).

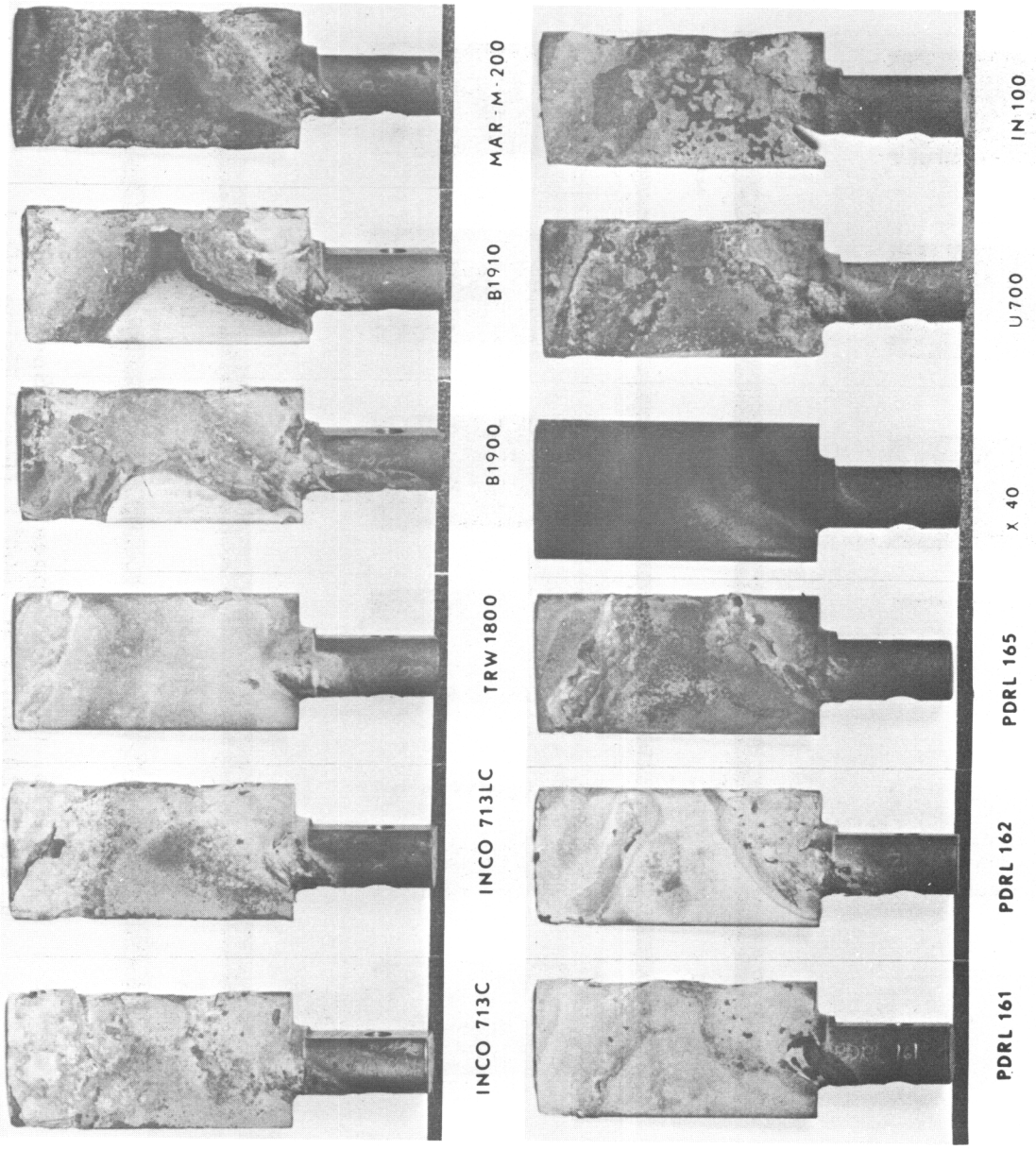

Figure 15. General Appearance of Specimens Tested 120 Hours at 1750°F Using JP-4R Fuel and an 8 ppm Salt/Air Ratio (Test S-527).

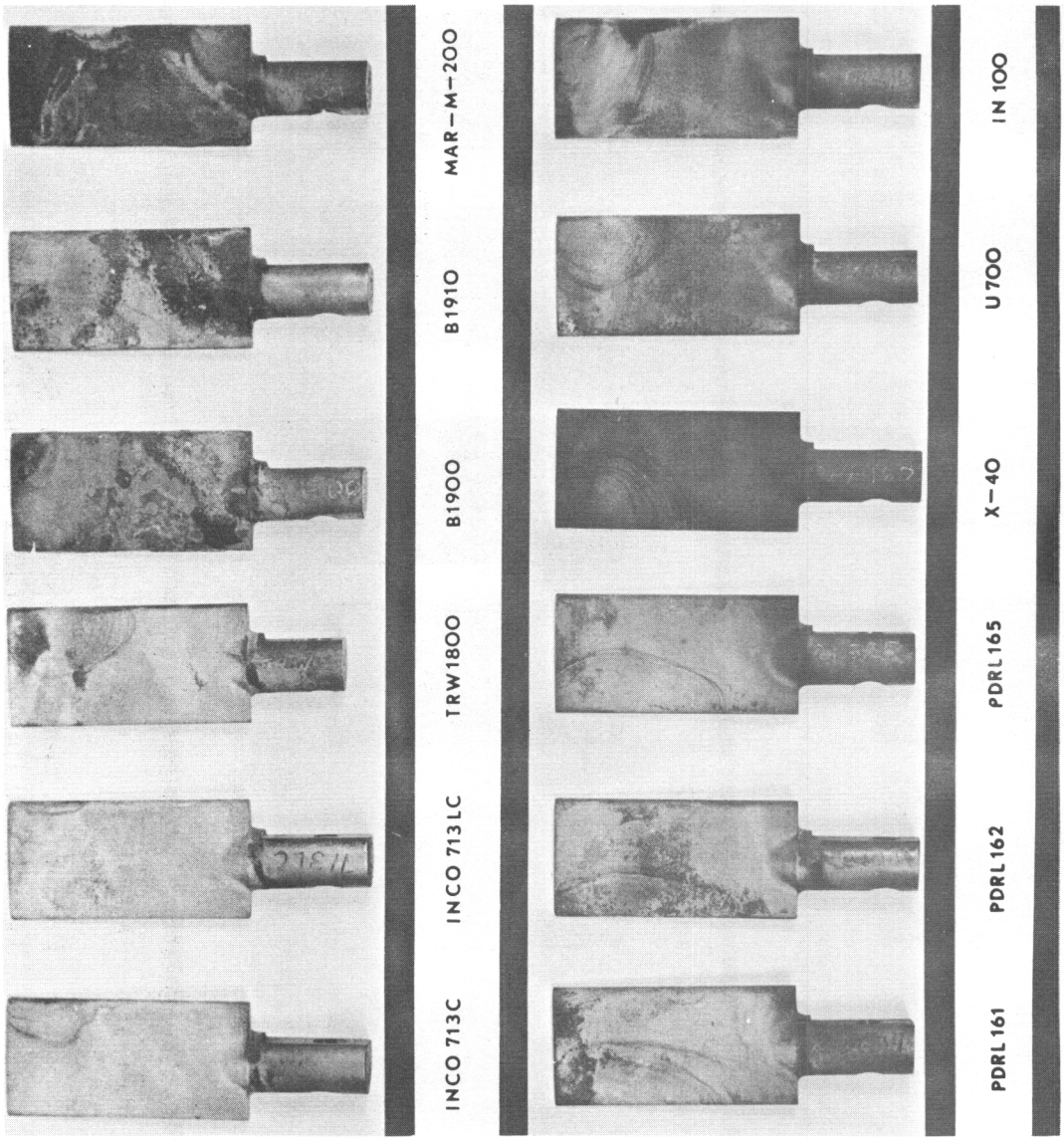

Figure 16. General Appearance of Specimens Tested 120 Hours at 1600°F (Peak) Using JP-4 Fuel and a Salt/Air Ratio of 4 ppm (S538).

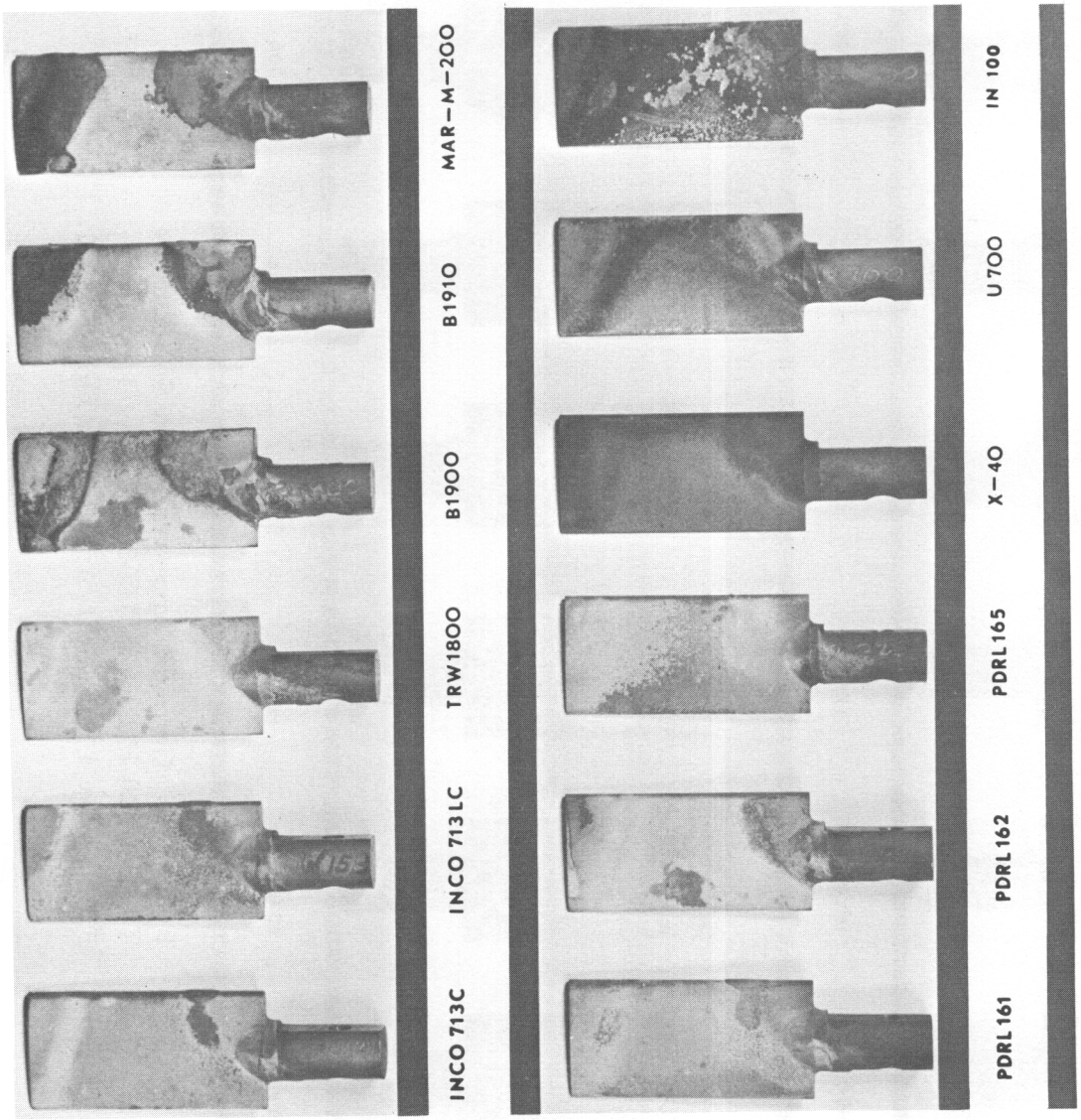

Figure 17. General Appearance of Specimens Tested 120 Hours at 1750°F (Peak) Using JP-4 Fuel and a Salt/Air Ratio of 4 ppm (S537).

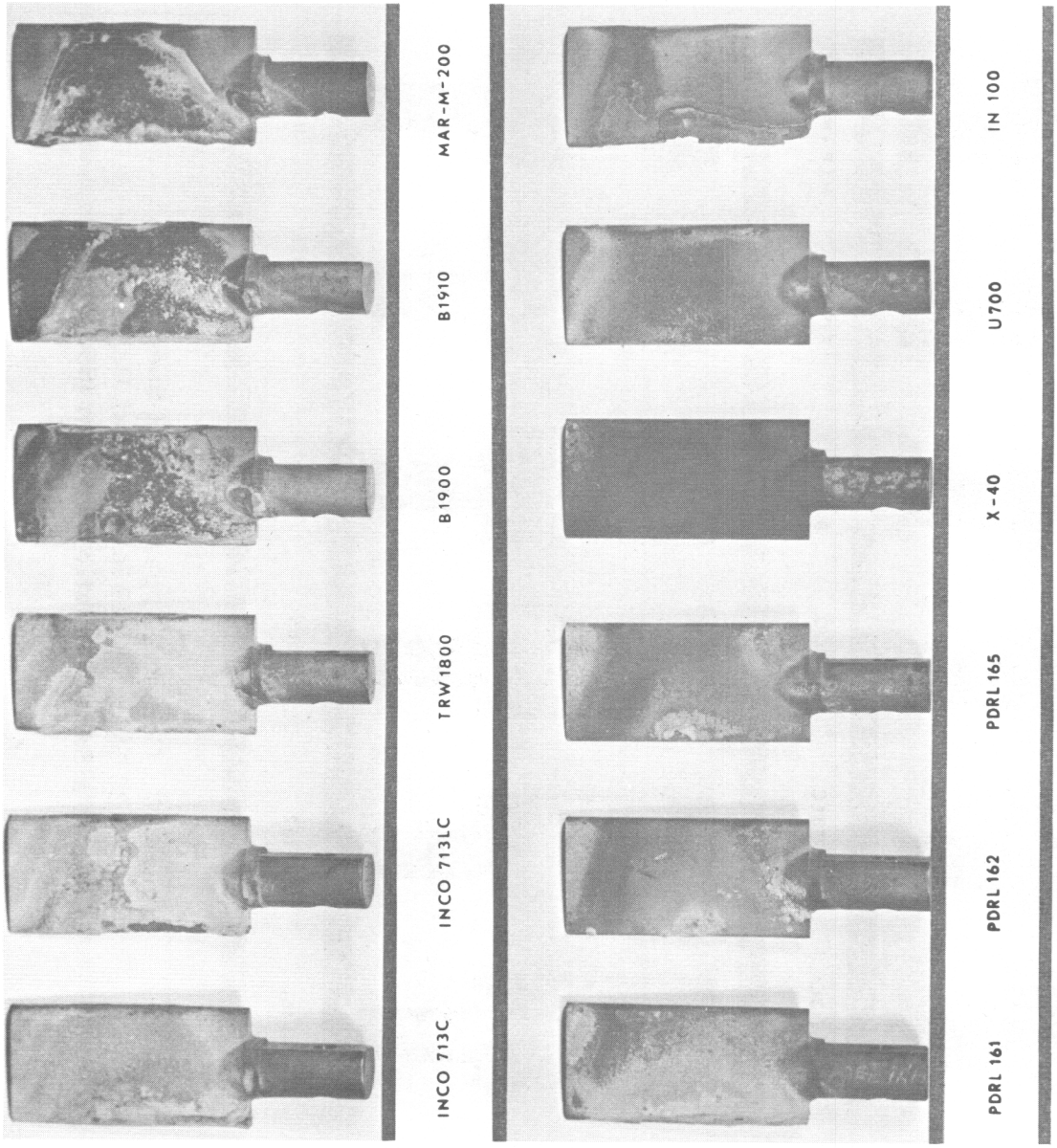

Figure 18. General Appearance of Specimens Tested 120 Hours at 1600°F Using JP-4R Fuel and a 4 ppm Salt/Air Ratio (Test S-532).

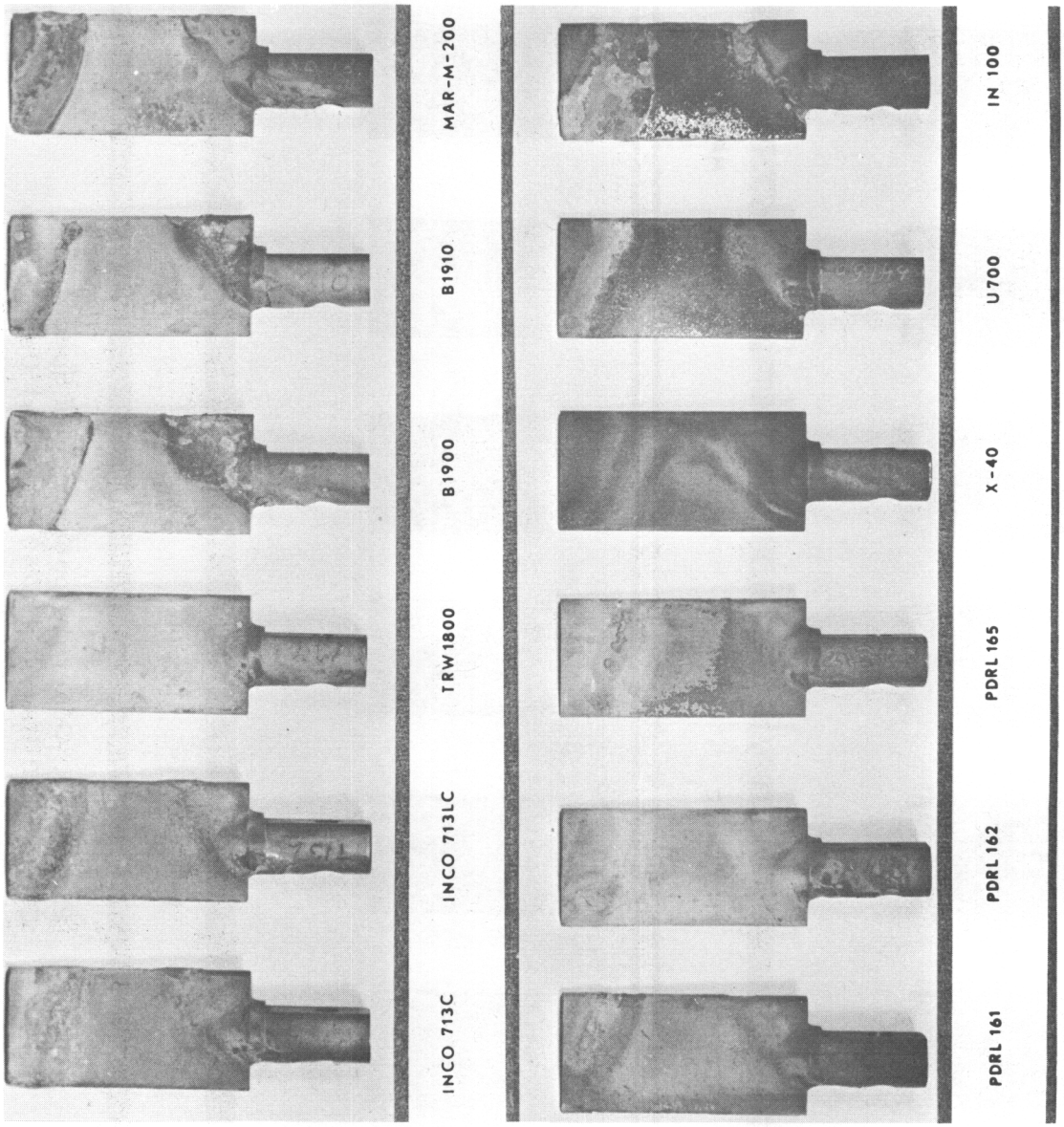

Figure 19. General Appearance of Specimens Tested 120 Hours at 1750°F Using JP-4R Fuel and a 4 ppm Salt/Air Ratio (Test S-534).

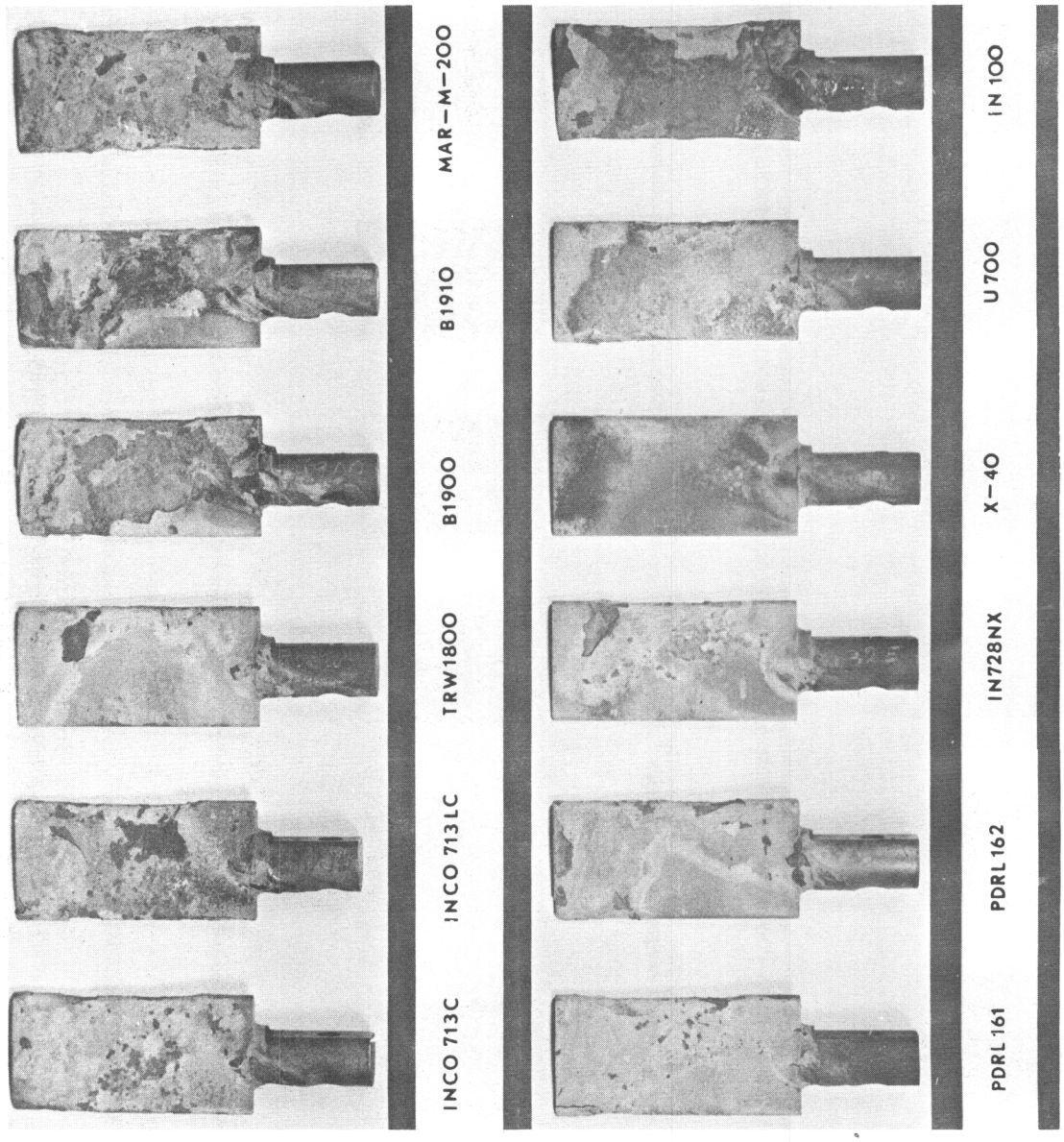

Figure 20. General Appearance of Specimens Tested 120 Hours at 1750°F (Peak) Using JP-5 Fuel and a Salt/Air Ratio of 8 ppm (S546).

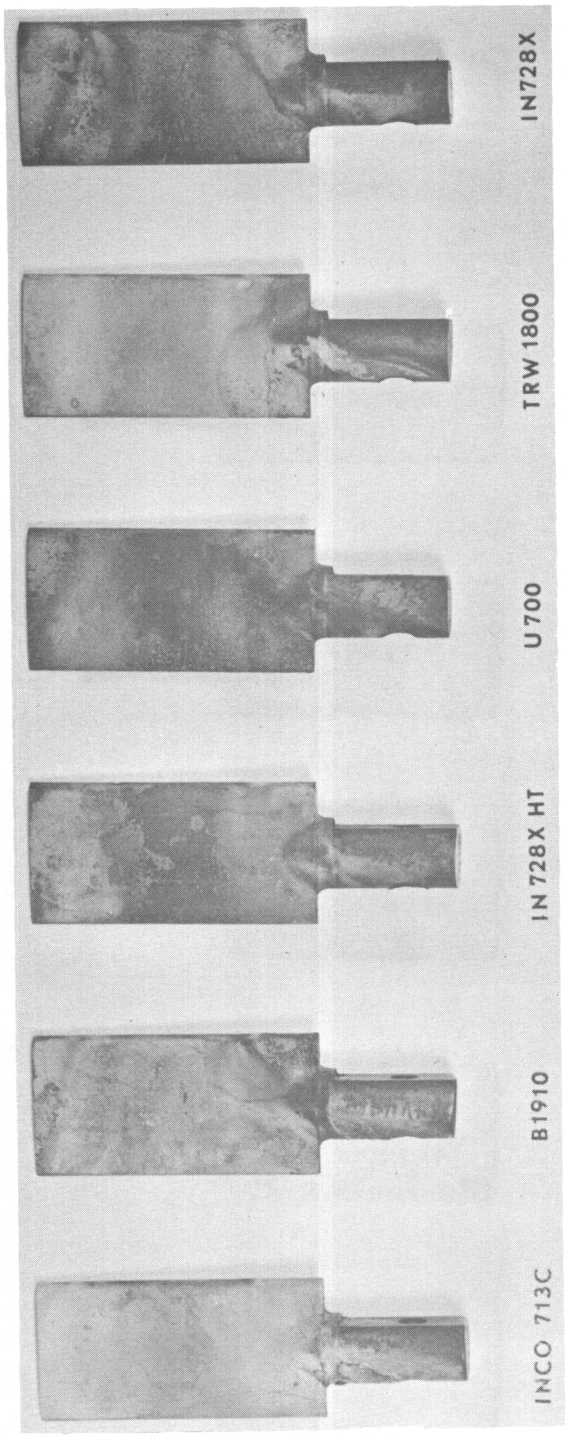

Figure 21. General Appearance of Specimens Tested 120 Hours at 1750°F (Peak) Using JP-4 Fuel and a Salt/Air Ratio of 4 ppm (Test S551).

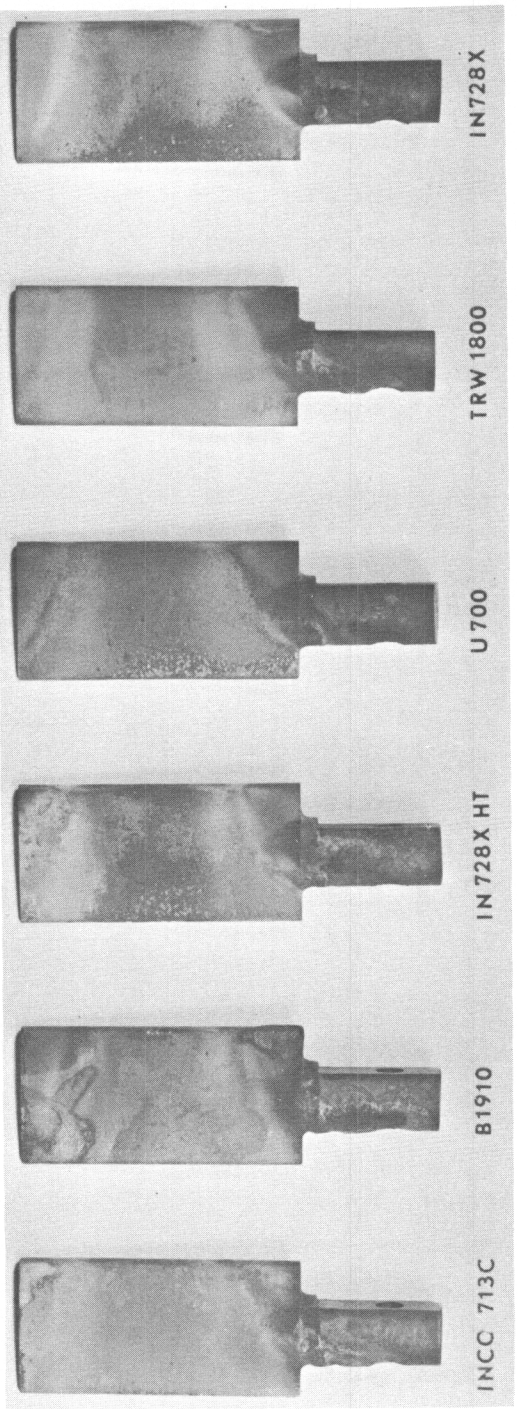

Figure 22. General Appearance of Specimens Tested 240 Hours at 1750°F (Peak) Using JP-4 Fuel and a Salt/Air Ratio of 4 ppm (Test S551).

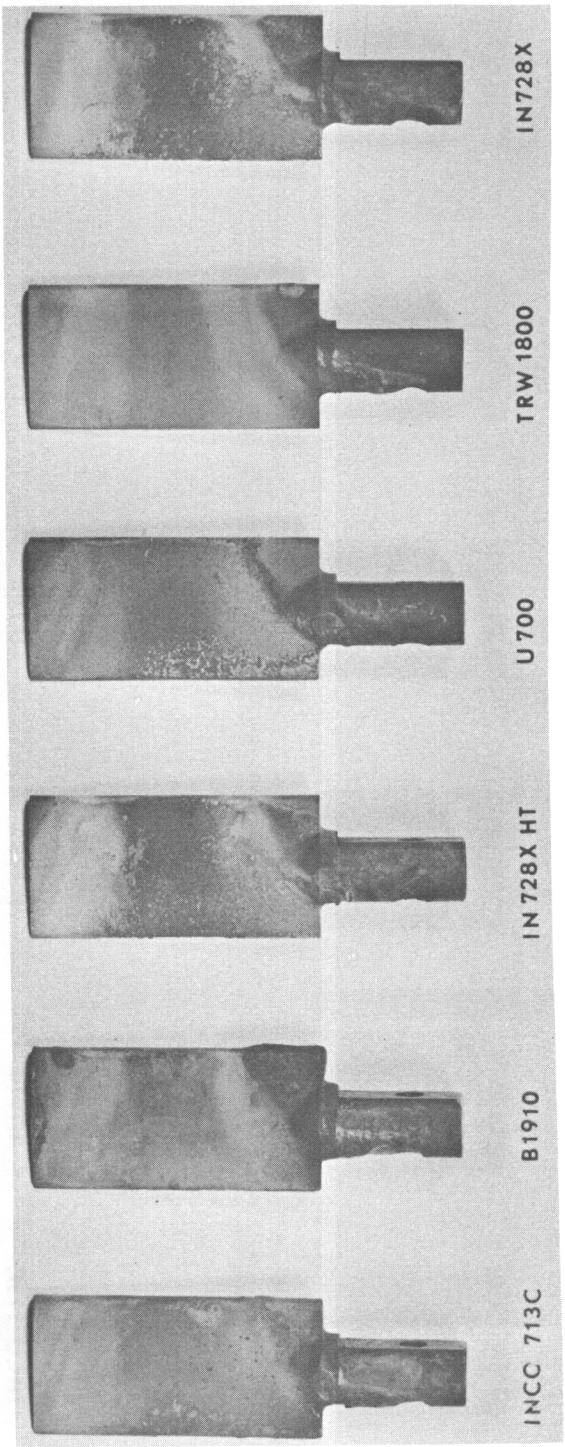

Figure 23. General Appearance of Specimens Tested 360 Hours at 1750°F (Peak) Using JP-4 Fuel and a Salt/Air Ratio of 4 ppm (Test S551).

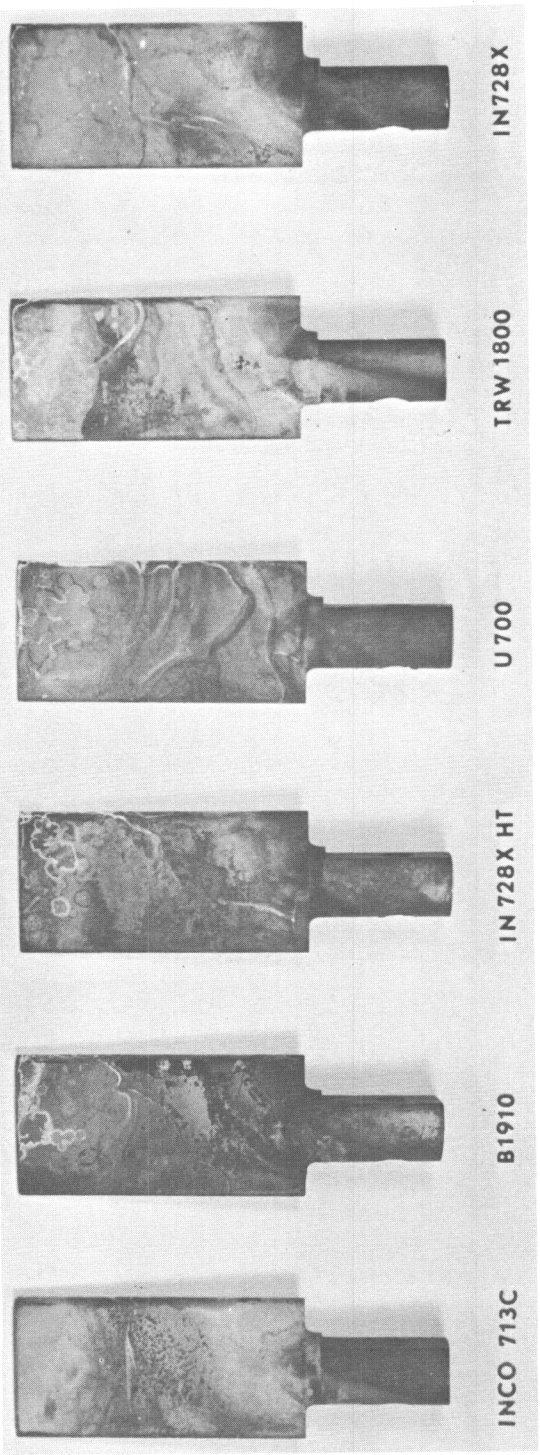

Figure 24. General Appearance of Specimens Tested 120 Hours at 1600°F (Peak) Using JP-4 Fuel and a Salt/Air Ratio of 4 ppm (Test S550).

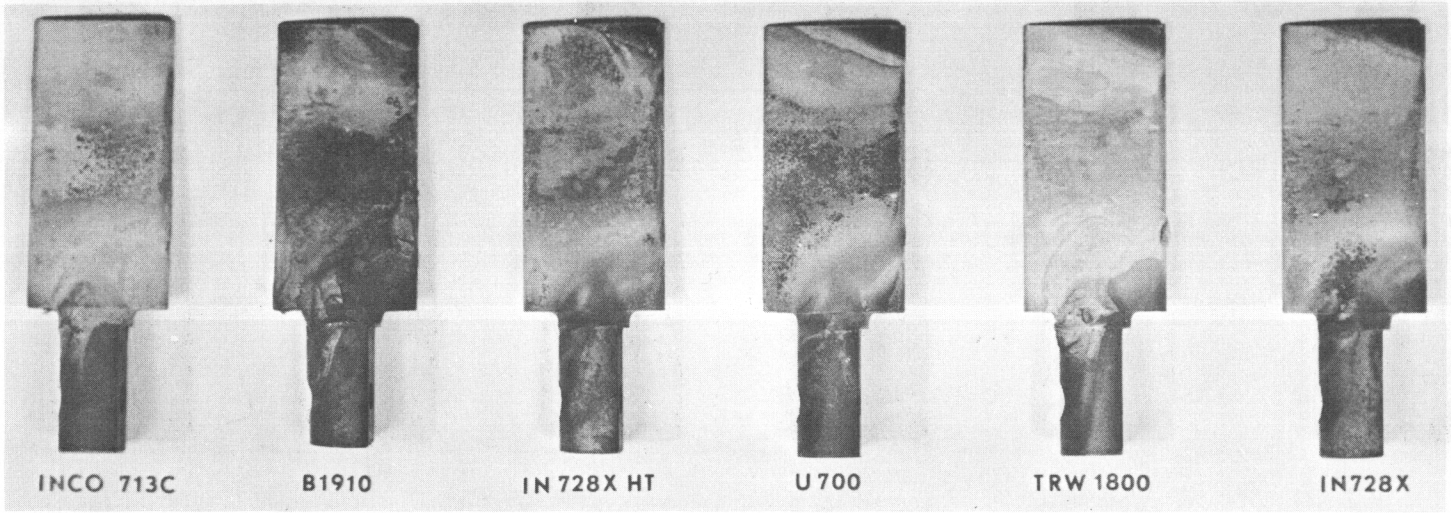

Figure 25. General Appearance of Specimens Tested 240 Hours at 1600°F (Peak) Using JP-4 Fuel and a Salt/Air Ratio of 4 ppm (Test S550).

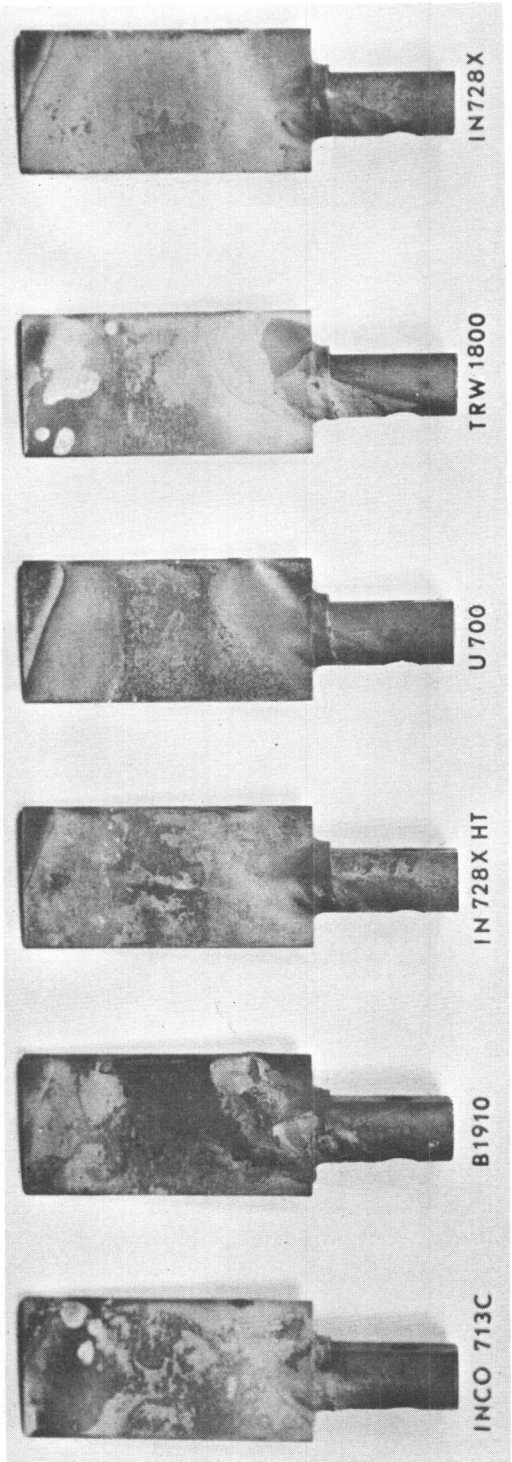

Figure 26. General Appearance of Specimens Tested 360 Hours at 1600°F (Peak) Using JP-4 Fuel and a Salt/Air Ratio of 4 ppm (Test 550).

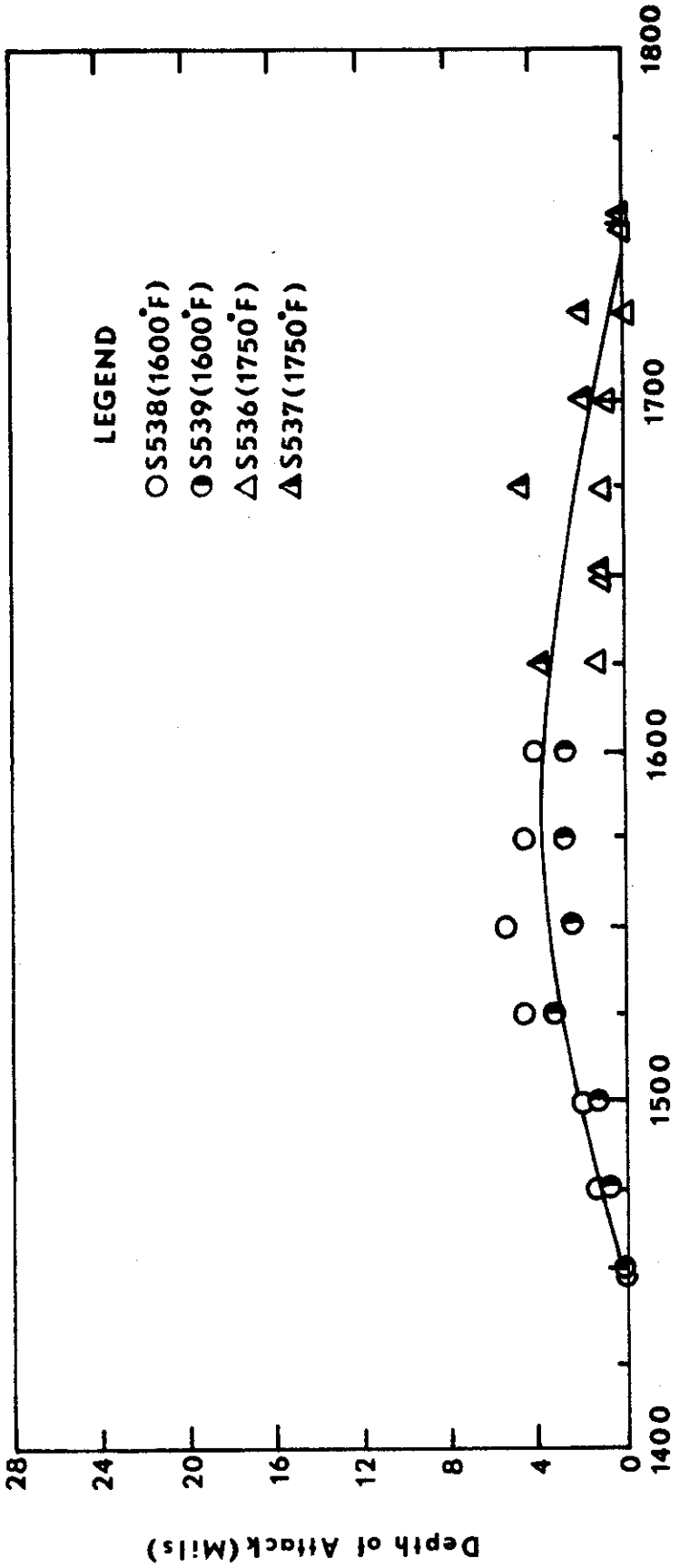

Figure 27. Corrosion as a Function of Temperature for Inco 713C Tested Using JP-4 Fuel with a Salt/Air Ratio of 8 ppm.

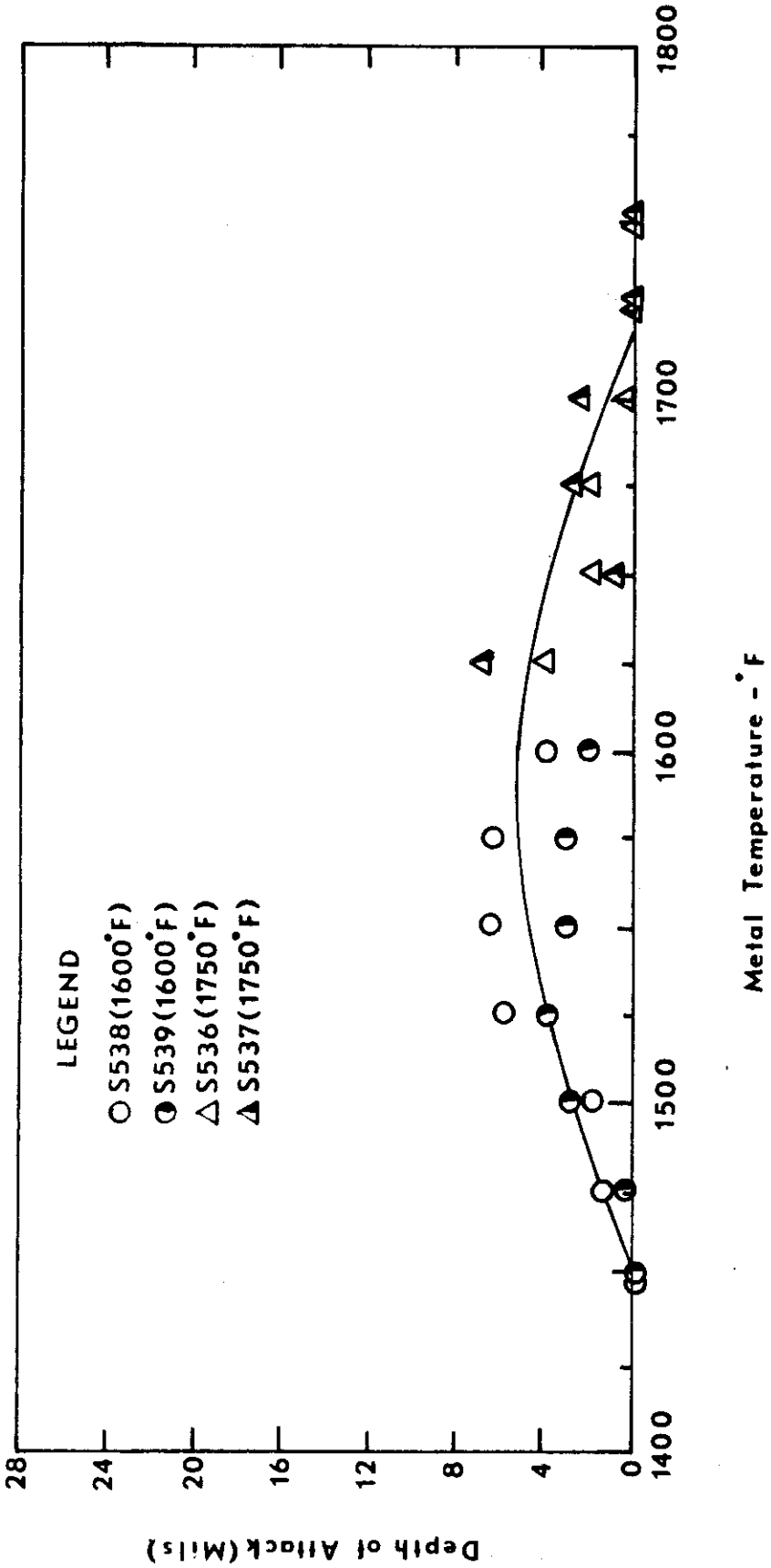

Figure 28. Corrosion as a Function of Temperature for Inco 713LC Tested Using JP-4 Fuel with a Salt/Air Ratio of 8 ppm.

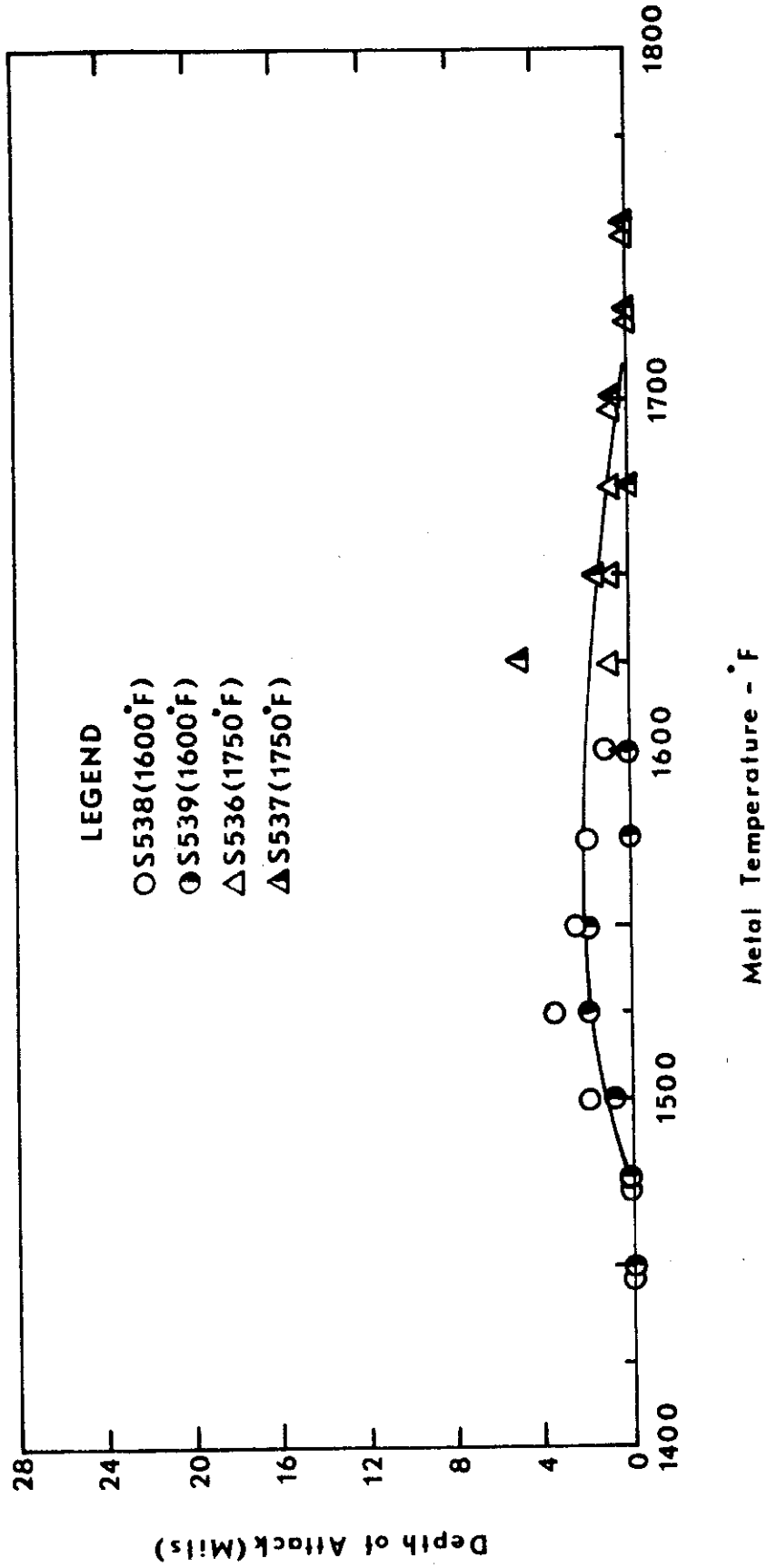

Figure 29. Corrosion as a Function of Temperature for TRW 1800 Tested Using JP-4 Fuel with a Salt/Air Ratio of 8 ppm.

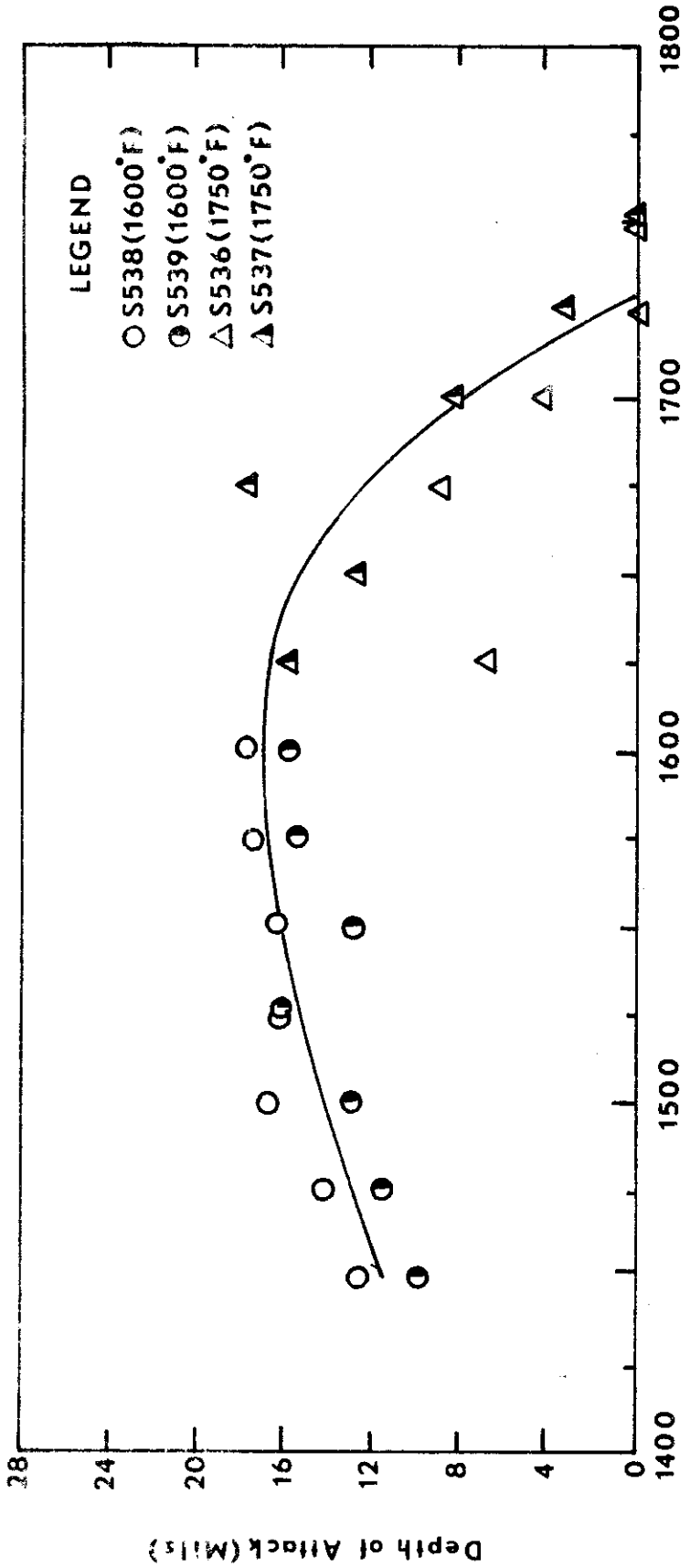

Figure 30. Corrosion as a Function of Temperature for B1900 Tested Using JP-4 Fuel with a Salt/Air Ratio of 8 ppm.

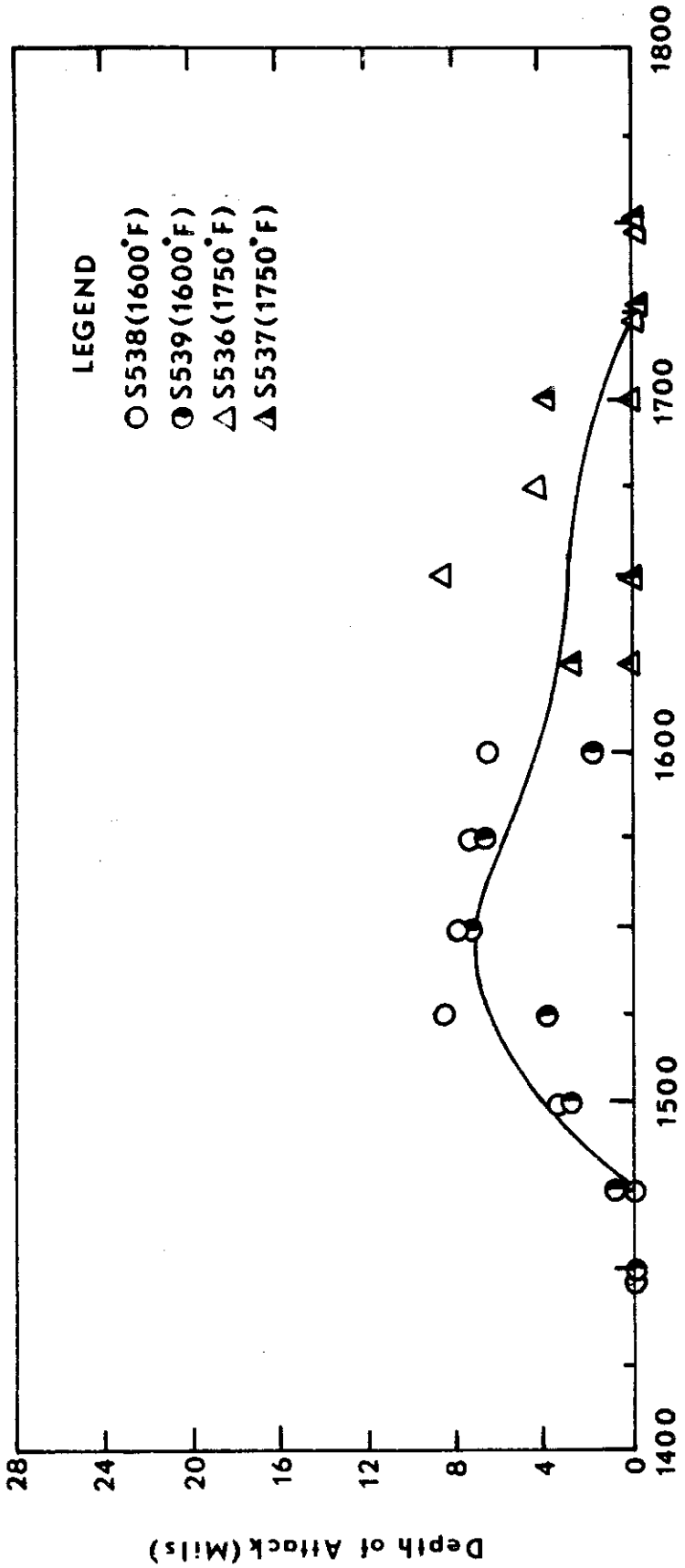

Figure 31. Corrosion as a Function of Temperature for B1910 Tested Using JP-4 Fuel with a Salt/Air Ratio of 8 ppm.

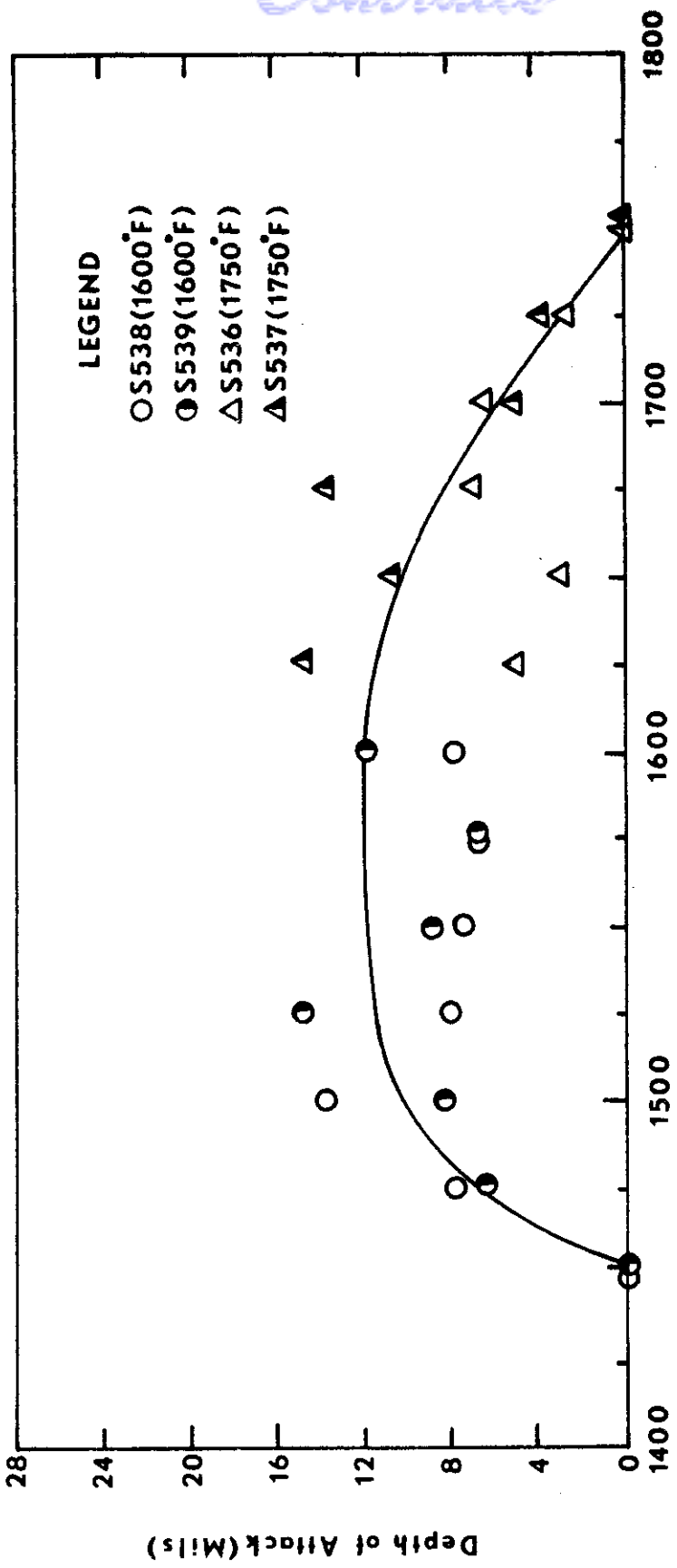

Figure 32. Corrosion as a Function of Temperature for MAR-M-200 Tested Using JP-4 Fuel with a Salt/Air Ratio of 8 ppm.

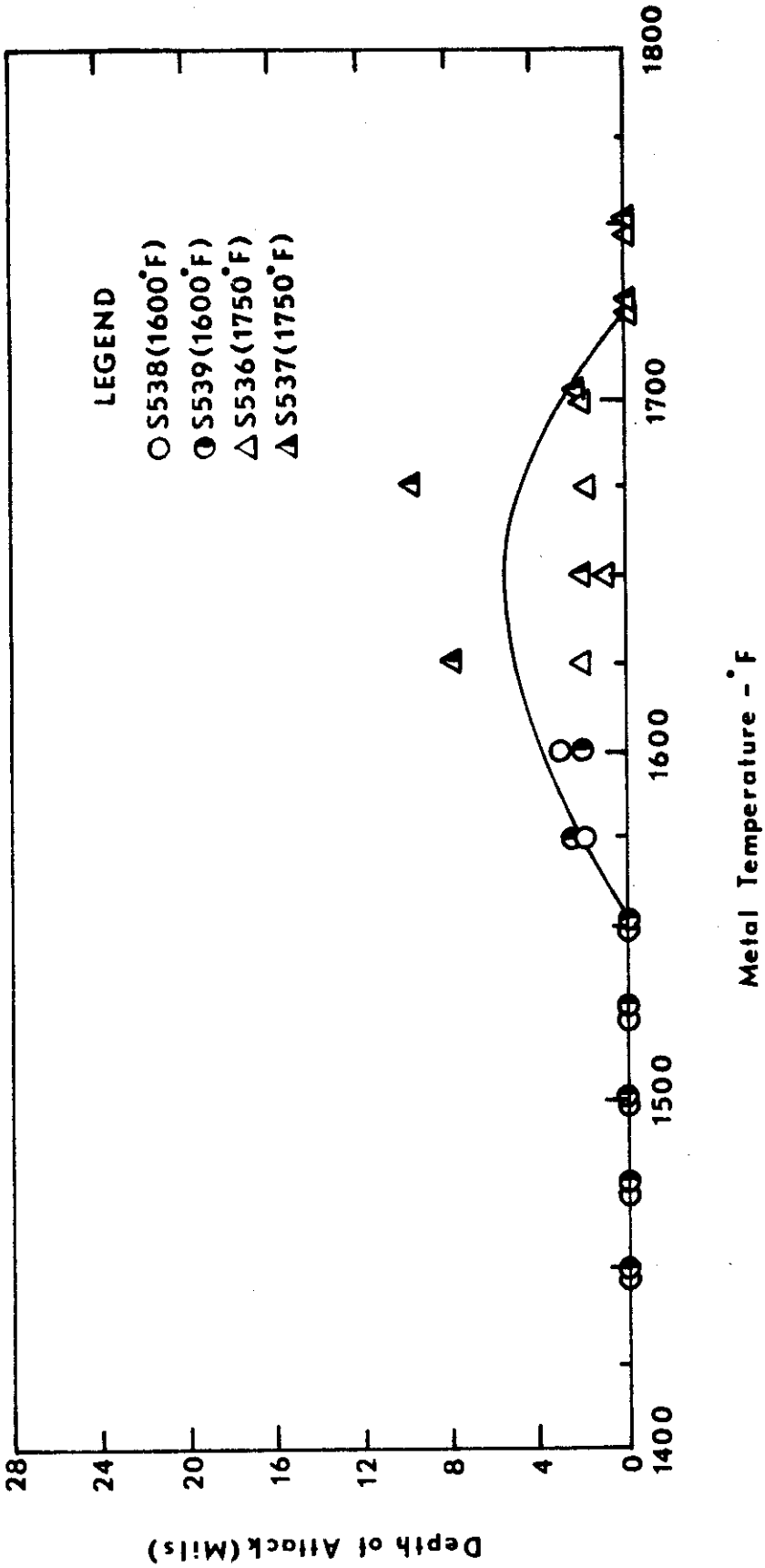

Figure 33. Corrosion as a Function of Temperature for PDRL 161 Tested Using JP-4 Fuel with a Salt/Air Ratio of 8 ppm.

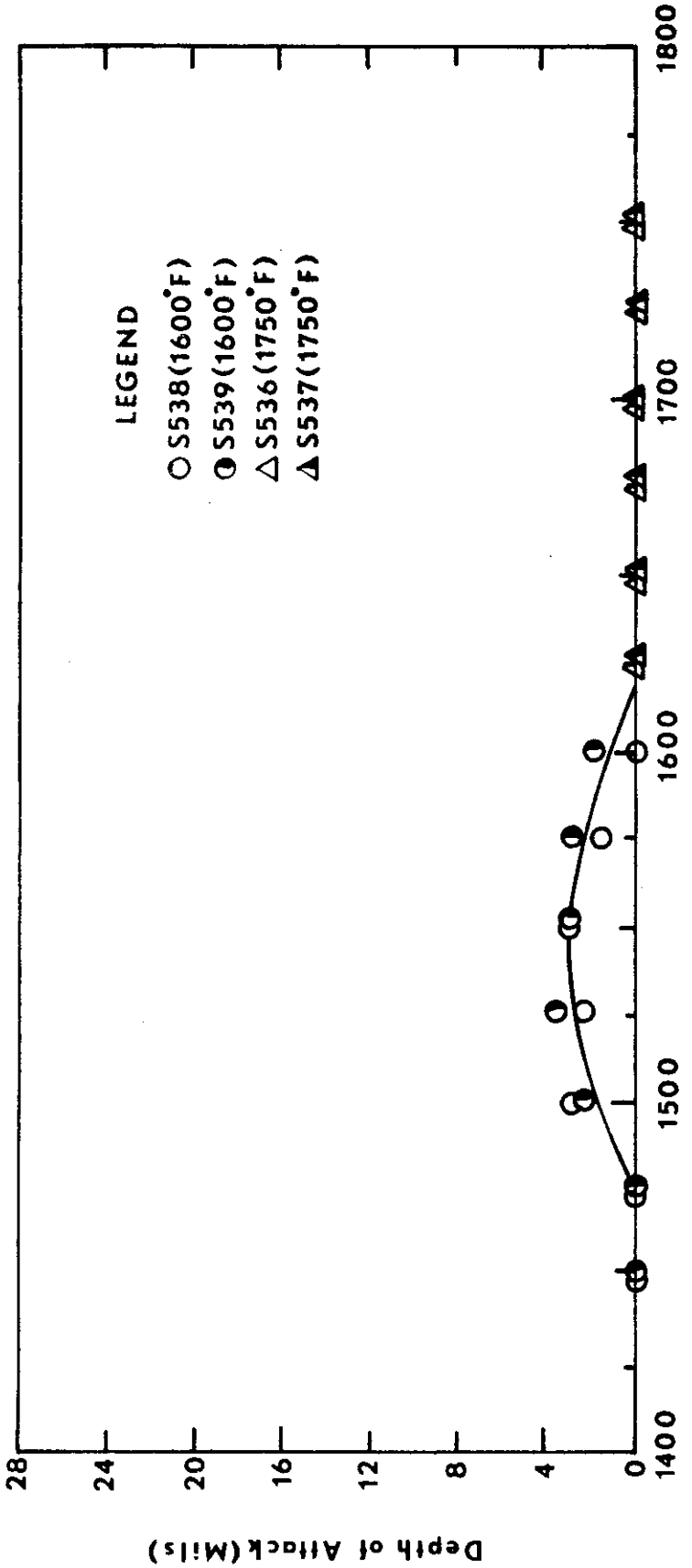

Figure 34. Corrosion as a Function of Temperature for PDRL 162 Tested Using JP-4 Fuel with a Salt/Air Ratio of 8 ppm.

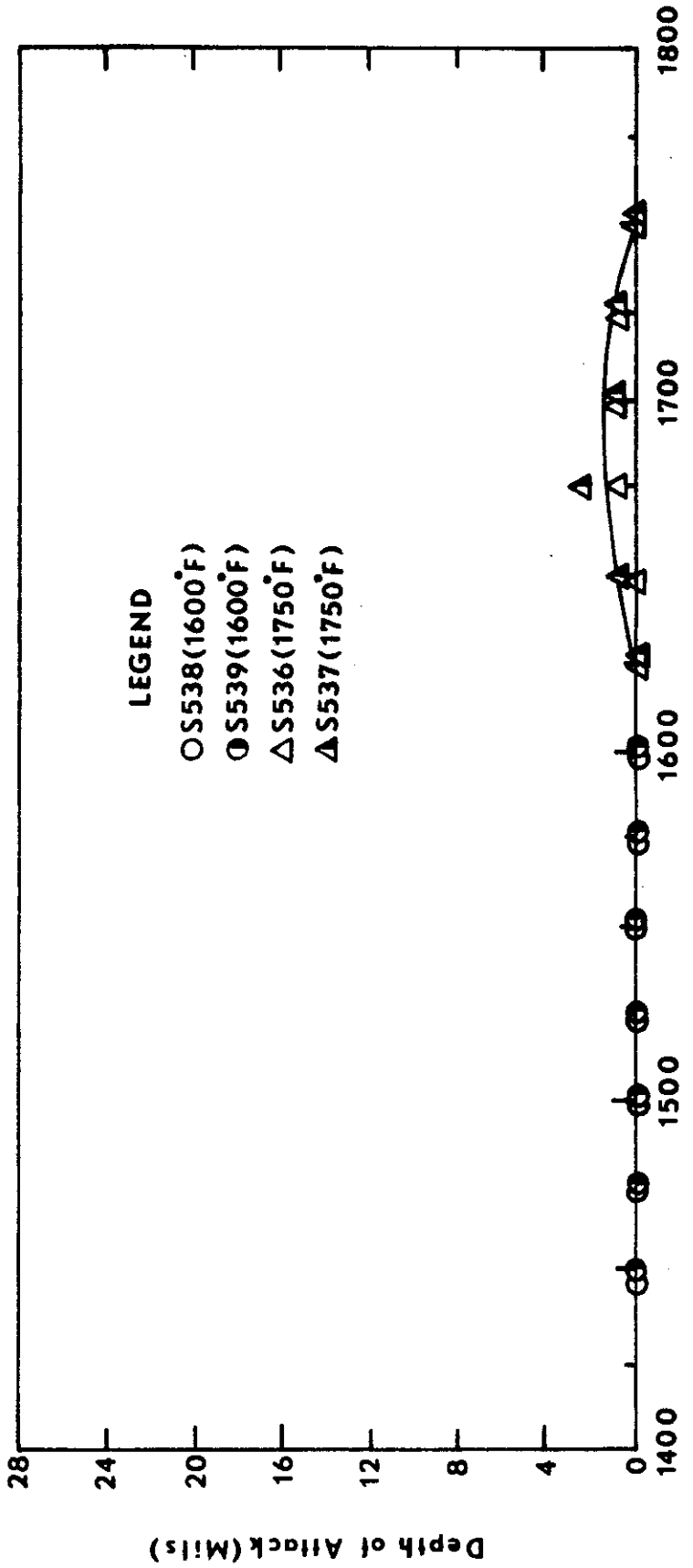

Figure 35. Corrosion as a Function of Temperature for IN728X Tested Using JP-4 Fuel with a Salt/Air Ratio of 8 ppm.

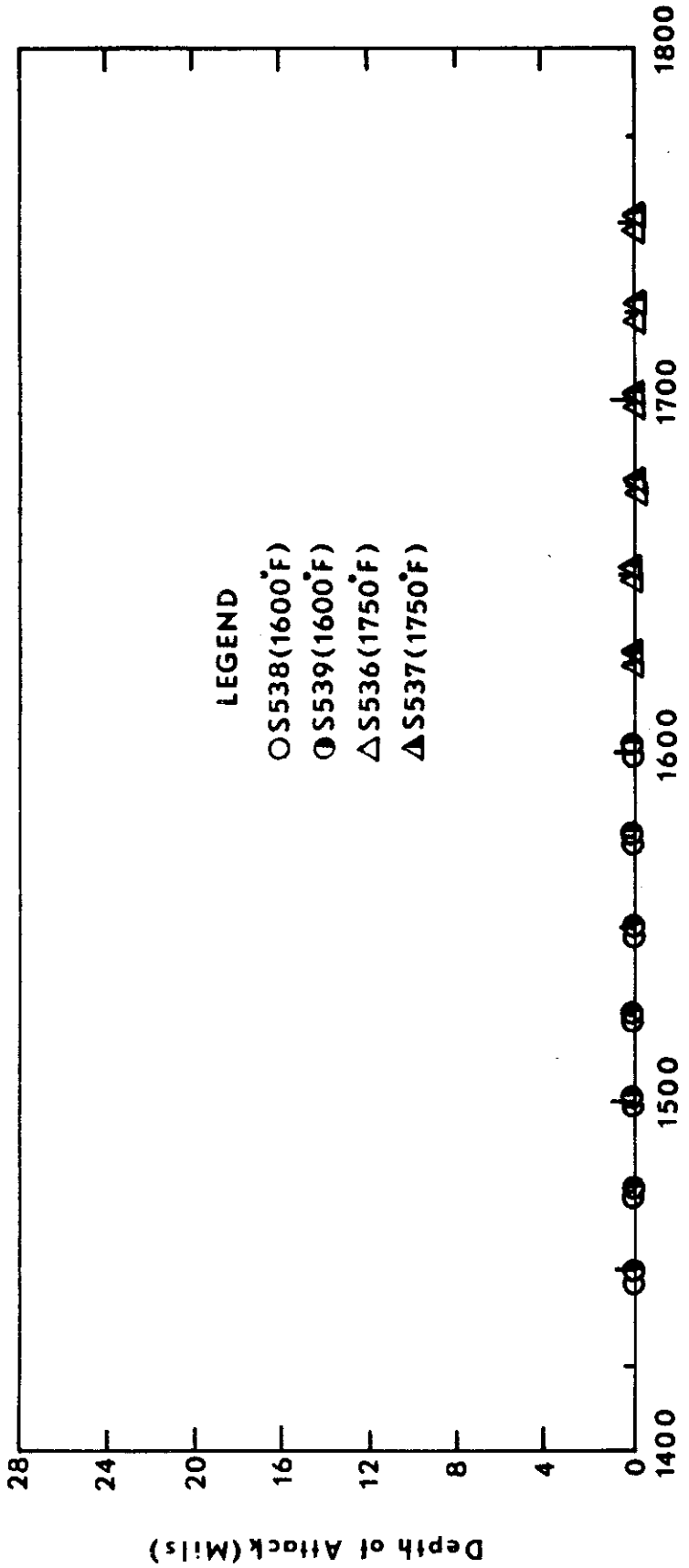

Figure 36. Corrosion as a Function of Temperature for X40 Tested Using JP-4 Fuel with a Salt/Air Ratio of 8 ppm.

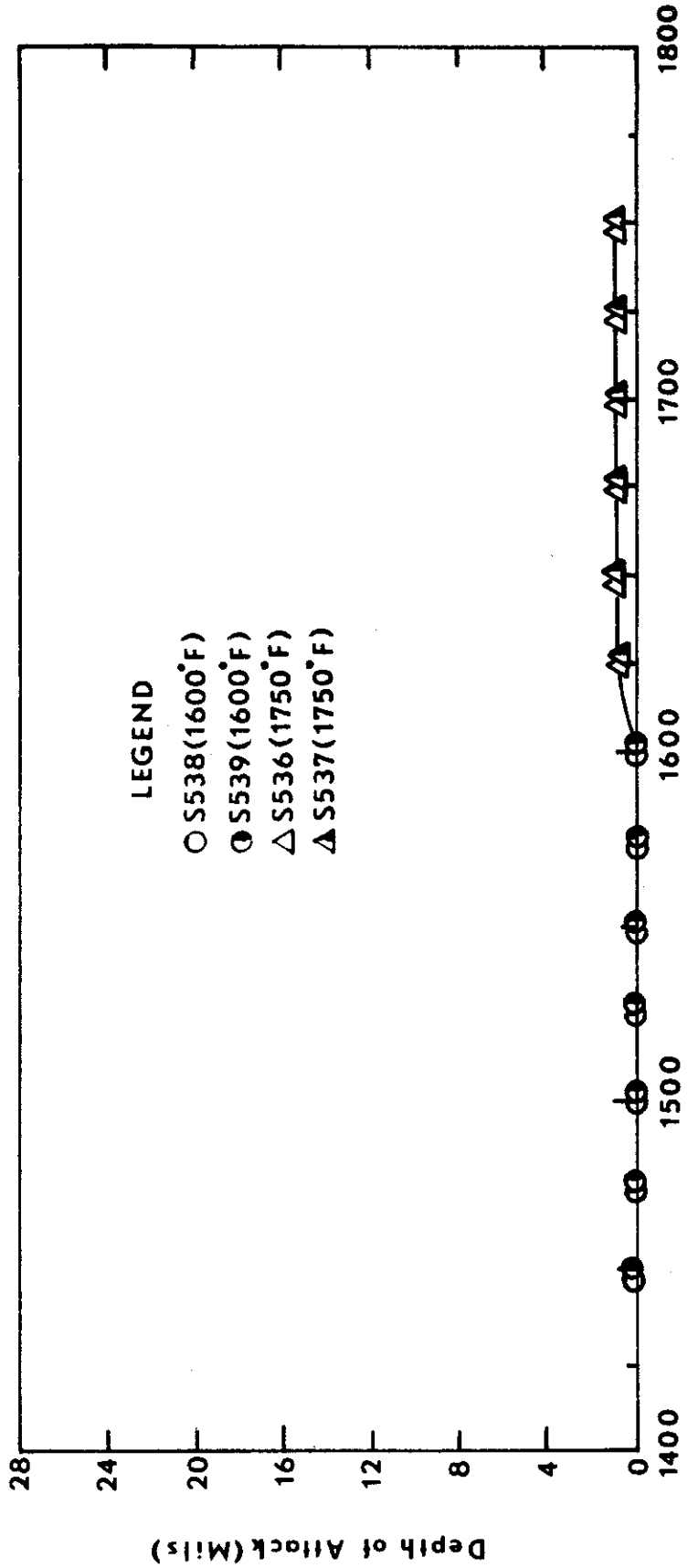

Figure 37. Corrosion as a Function of Temperature for U700 Tested Using JP-4 Fuel with a Salt/Air Ratio of 8 ppm.

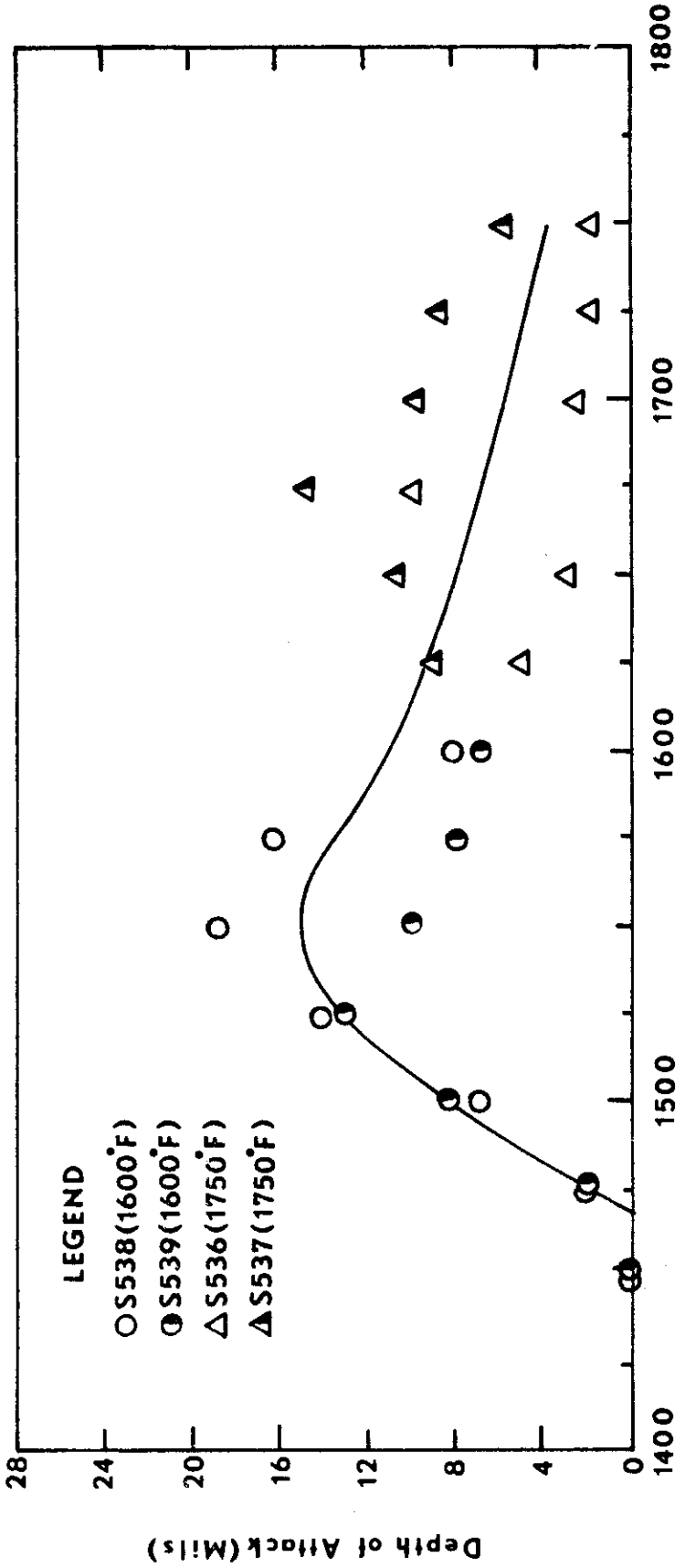

Figure 38. Corrosion as a Function of Temperature for IN100 Tested Using JP-4 Fuel with a Salt/Air Ratio of 8 ppm.

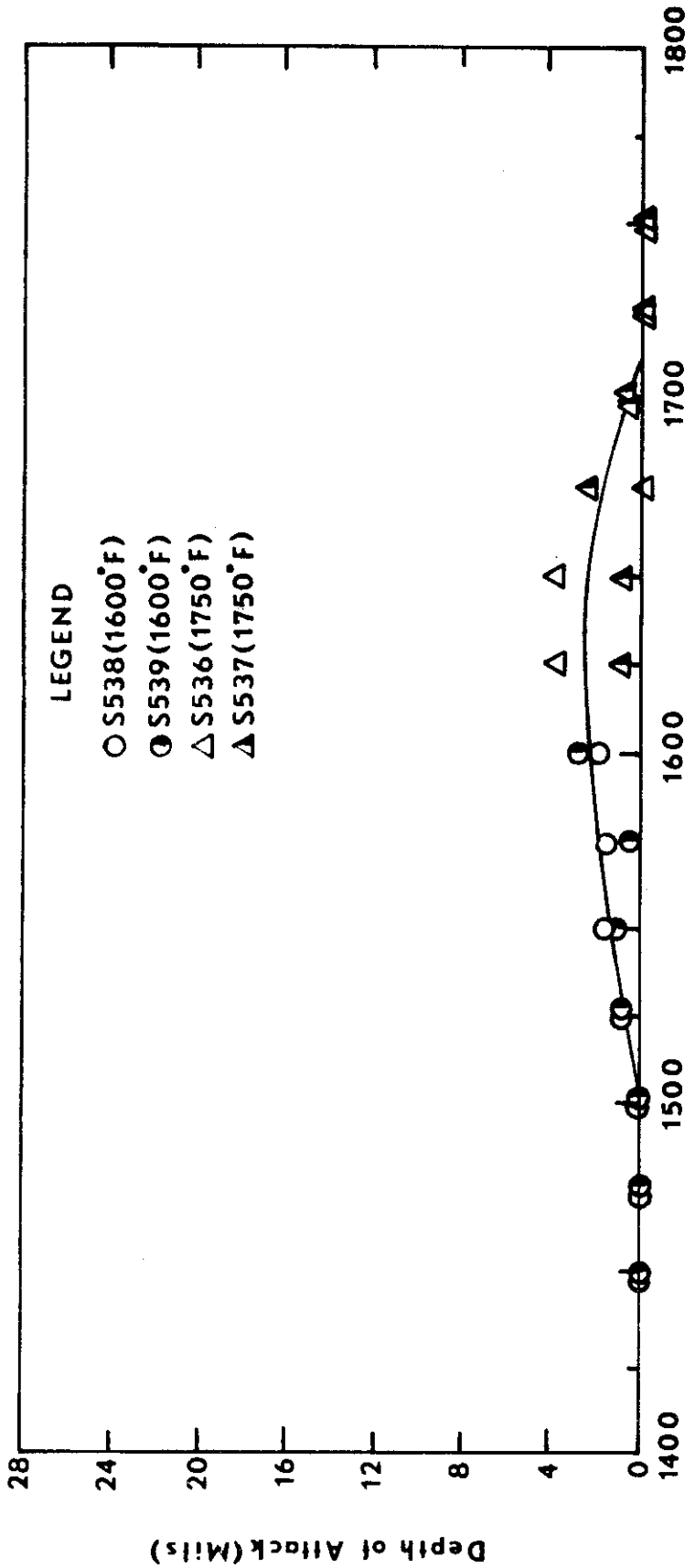

Figure 39. Corrosion as a Function of Temperature for Inco 713C Tested Using JP-4 Fuel with a Salt/Air Ratio of 4 ppm.

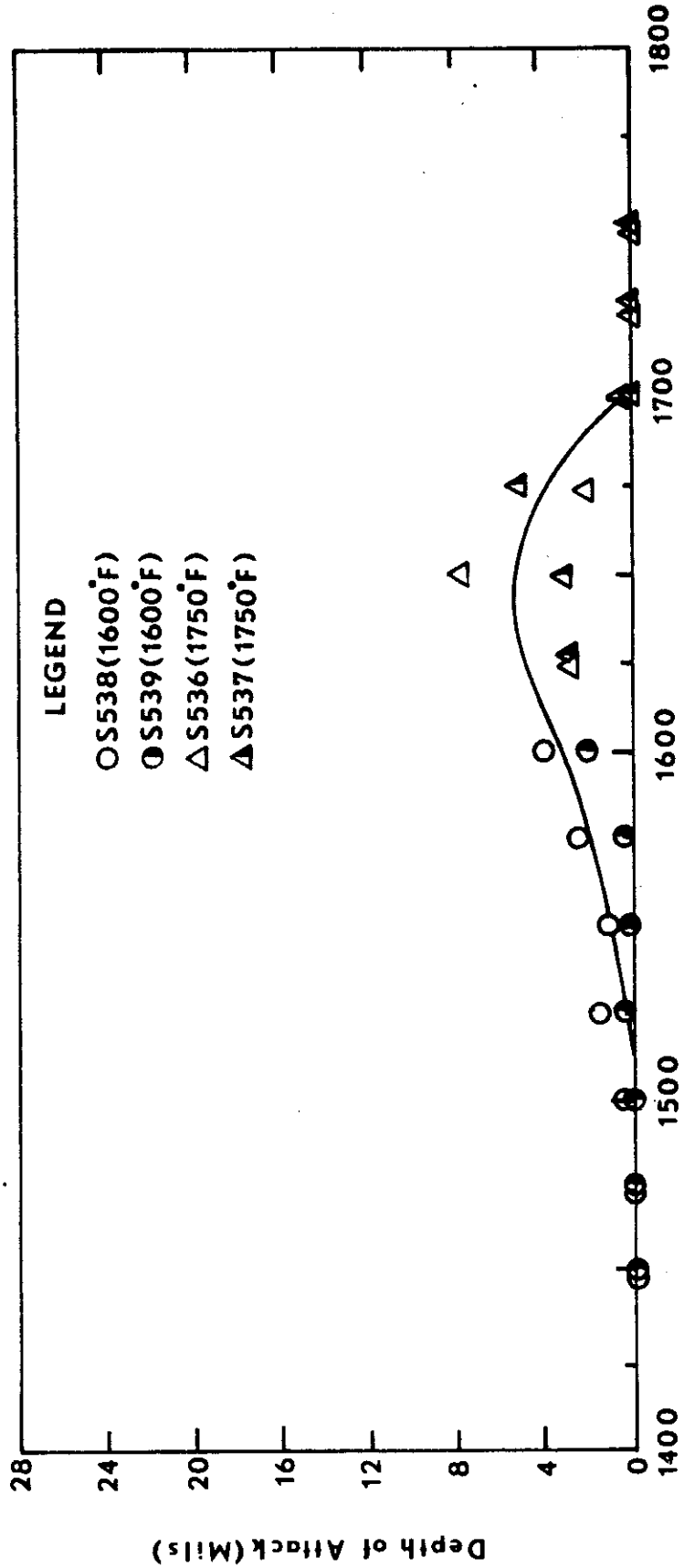

Figure 40. Corrosion as a Function of Temperature for Inco 713LC Tested Using JP-4 Fuel with a Salt/Air Ratio of 4 ppm.

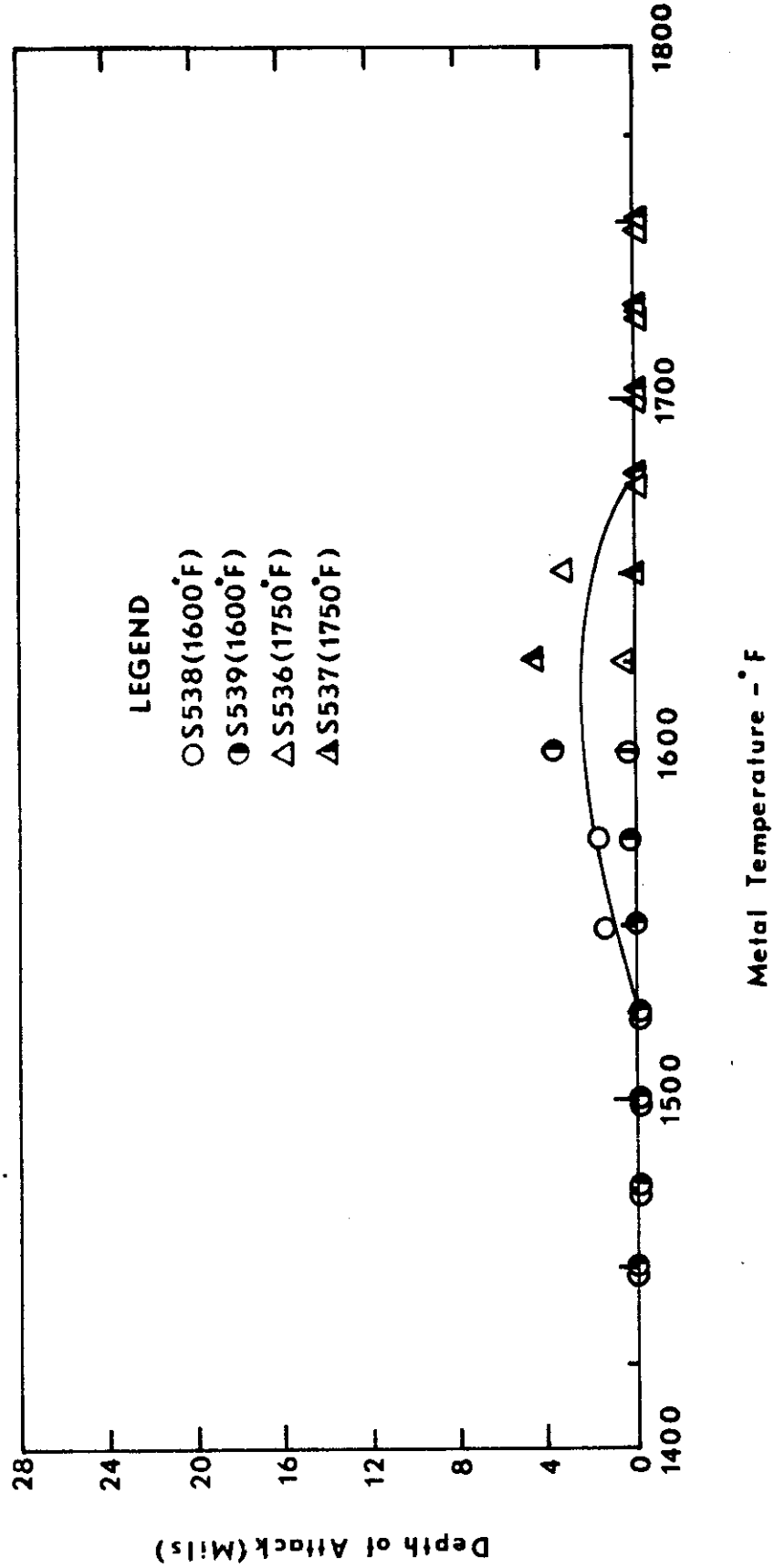

Figure 41. Corrosion as a Function of Temperature for TRW 1800 Tested Using JP-4 Fuel with a Salt/Air Ratio of 4 ppm.

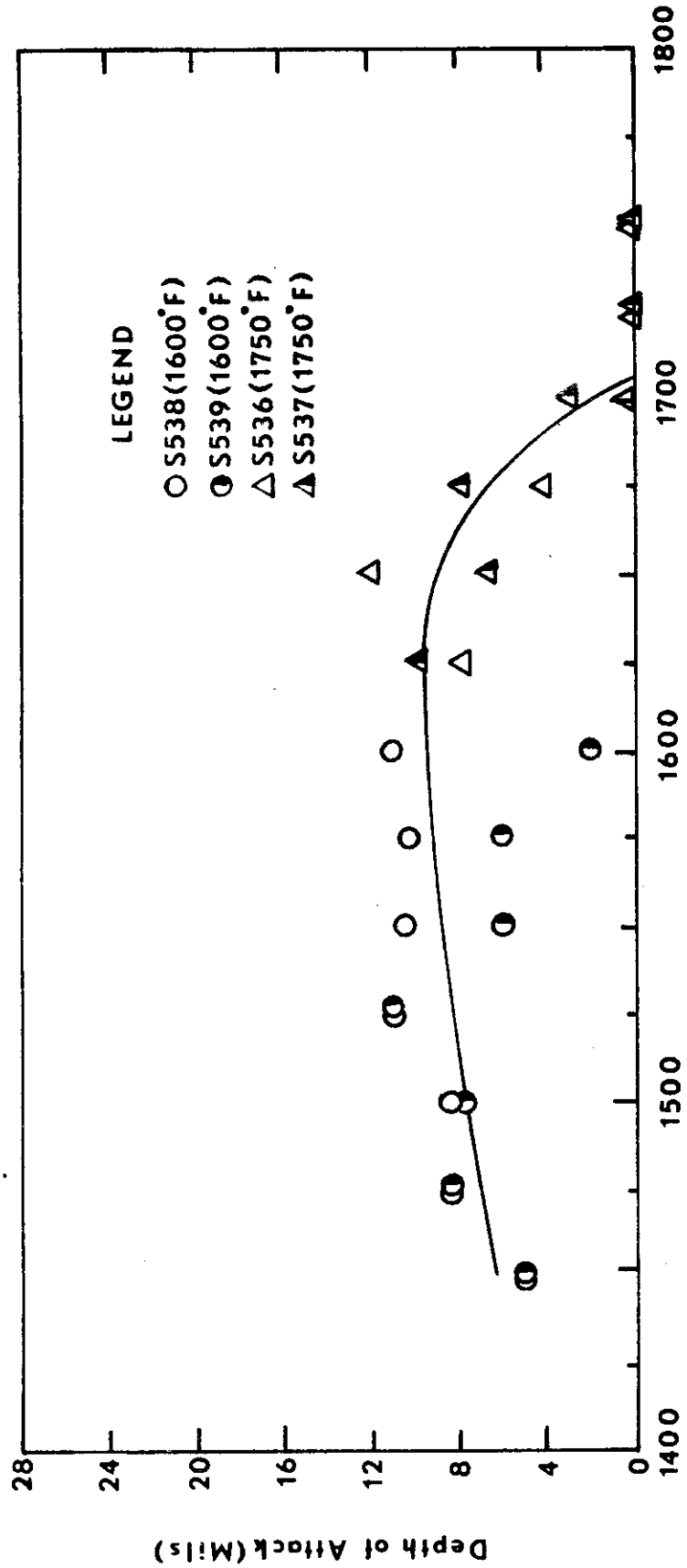

Figure 42. Corrosion as a Function of Temperature for B1900 Tested Using JP-4 Fuel with a Salt/Air Ratio of 4 ppm.

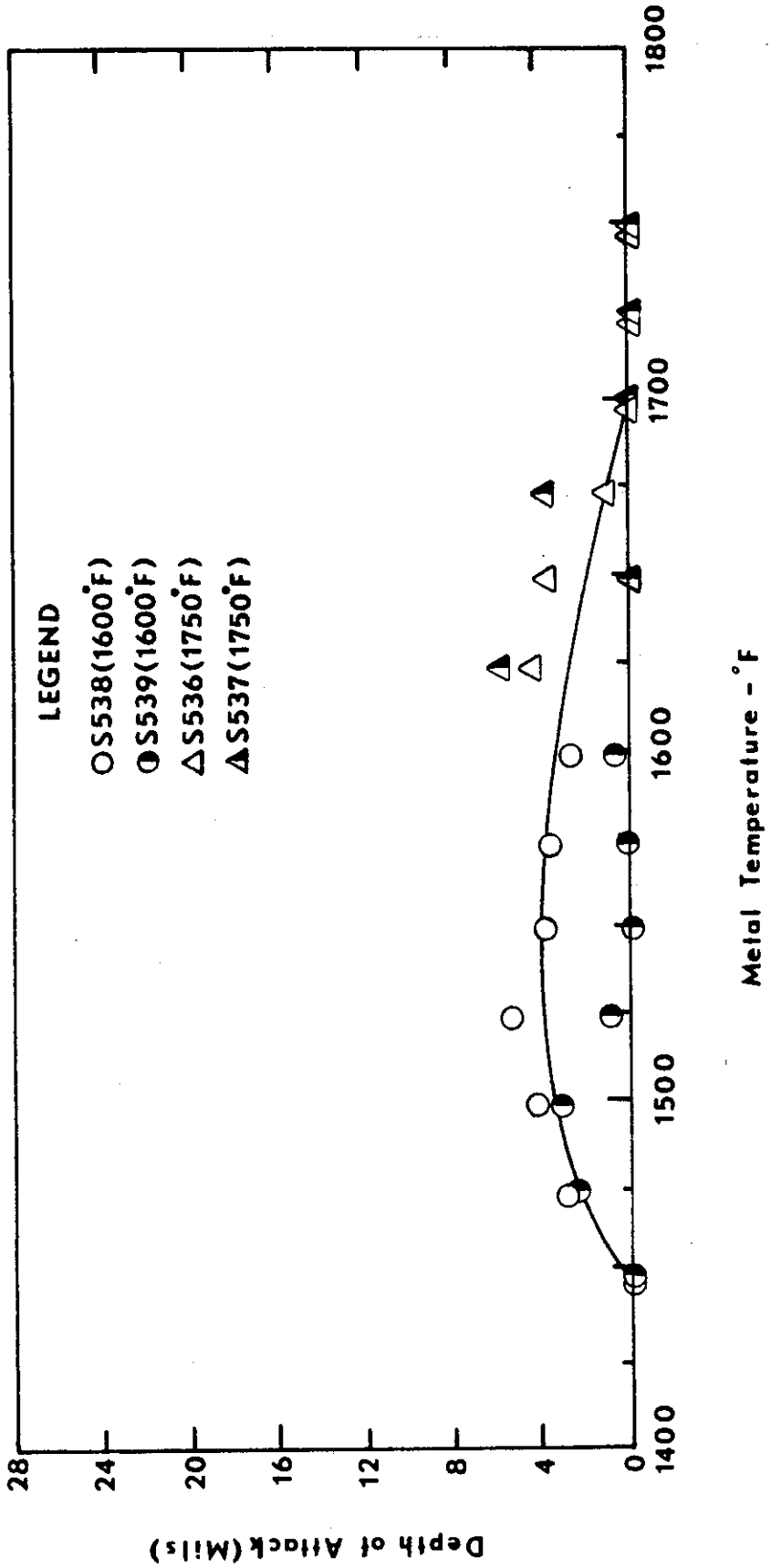

Figure 43. Corrosion as a Function of Temperature for B1910 Tested Using JP-4 Fuel with a Salt/Air Ratio of 4 ppm.

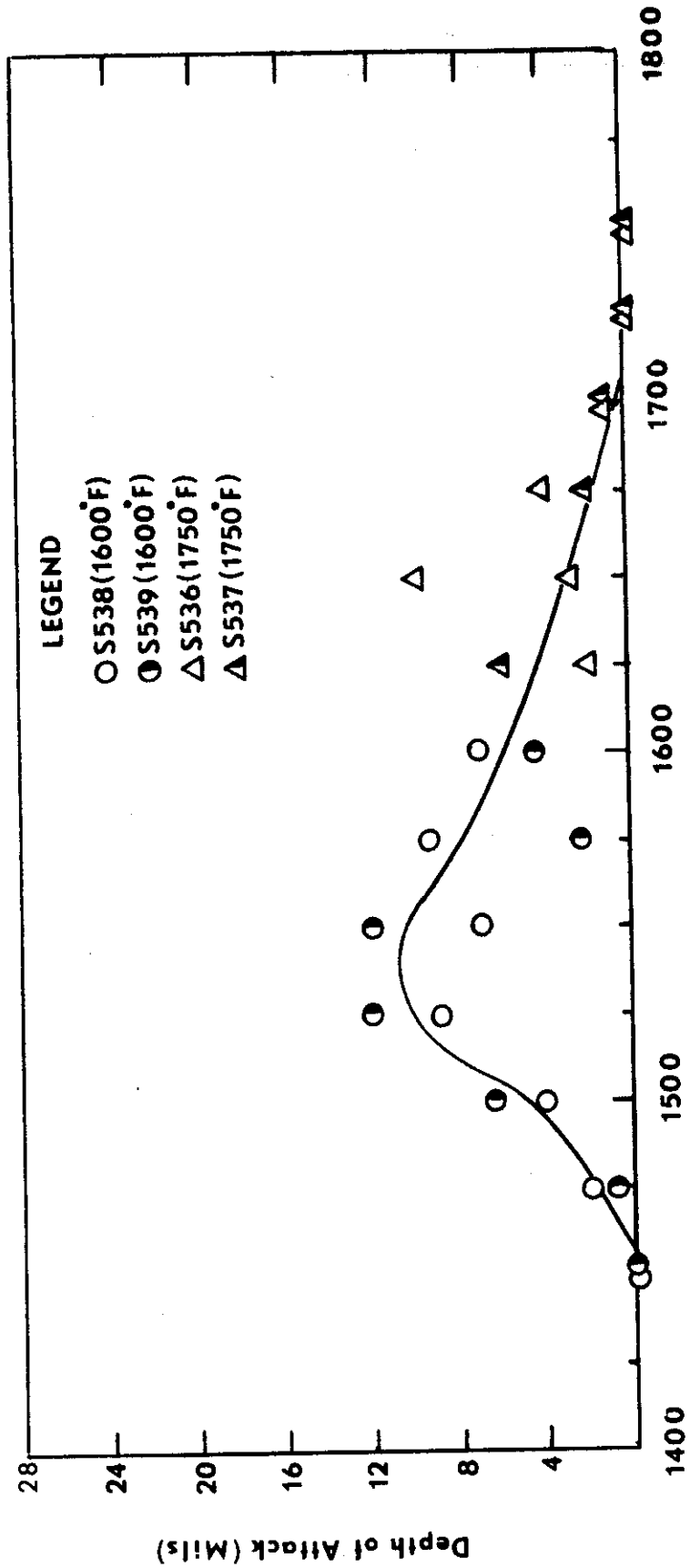

Figure 44. Corrosion as a Function of Temperature for MAR-M-200 Tested Using JP-4 Fuel with a Salt/Air Ratio of 4 ppm.

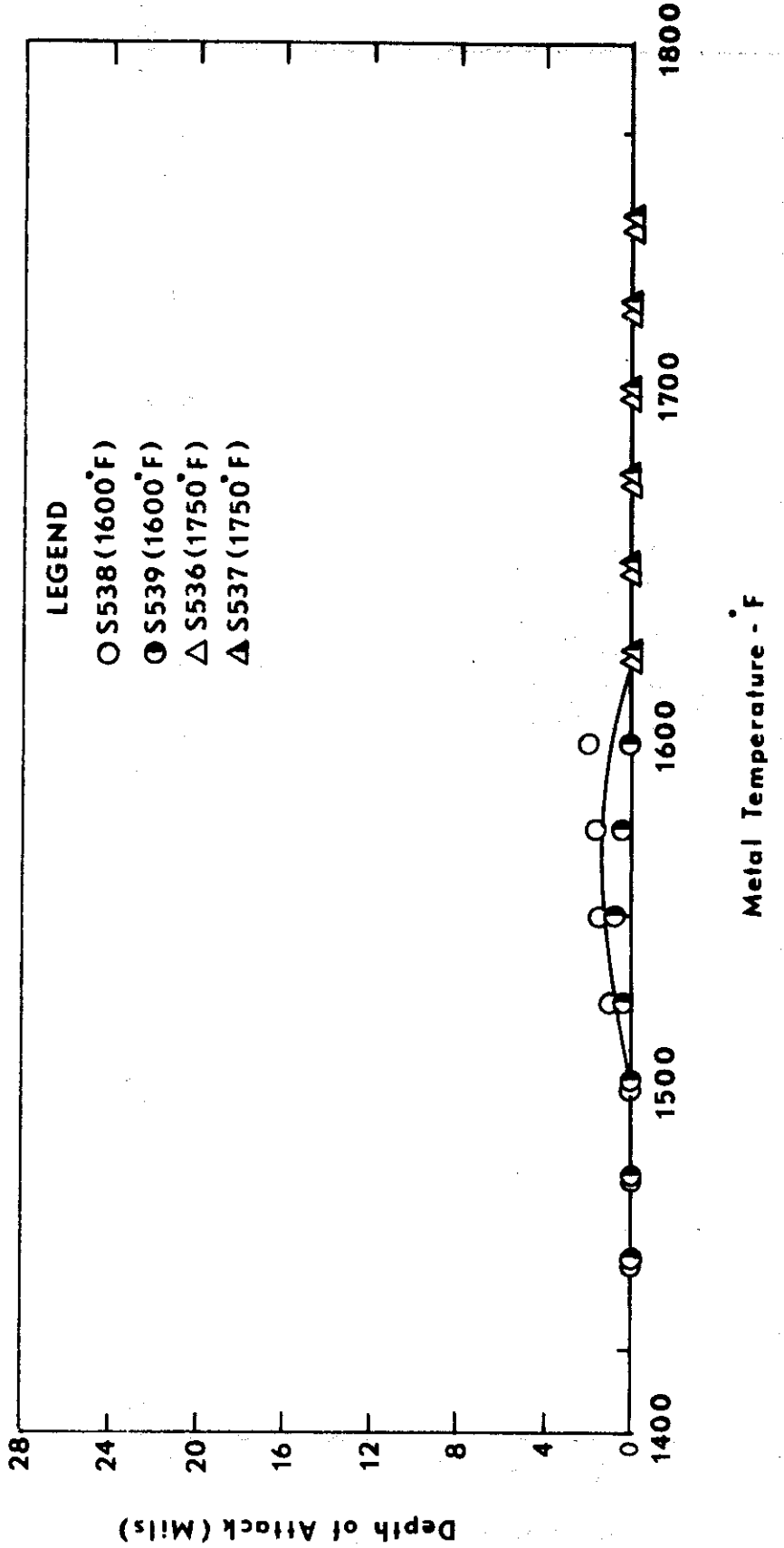

Figure 45. Corrosion as a Function of Temperature for PDRL 161 Tested Using JP-4 Fuel with Salt/Air Ratio of 4 ppm.

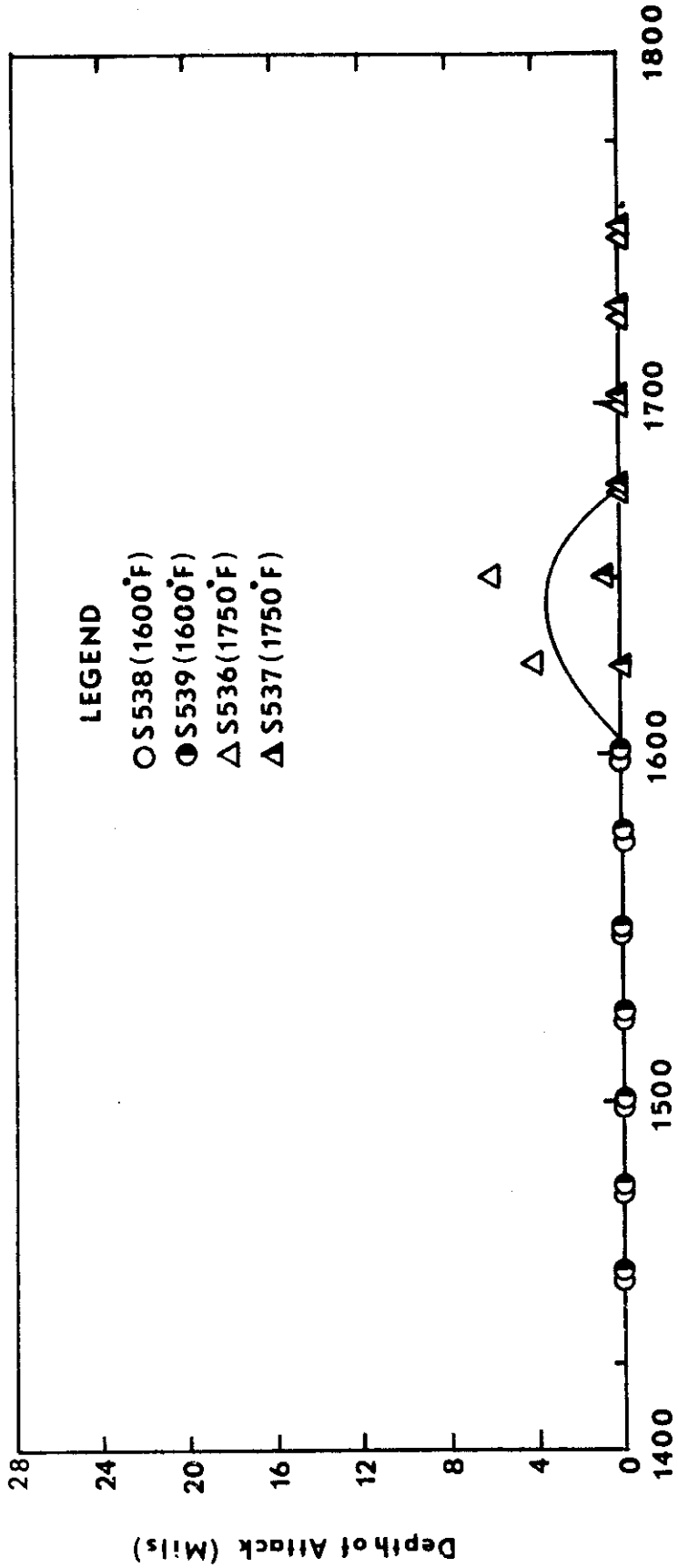

Figure 46. Corrosion as a Function of Temperature for PDRL 162 Tested Using JP-4 Fuel with a Salt/Air Ratio of 4 ppm.

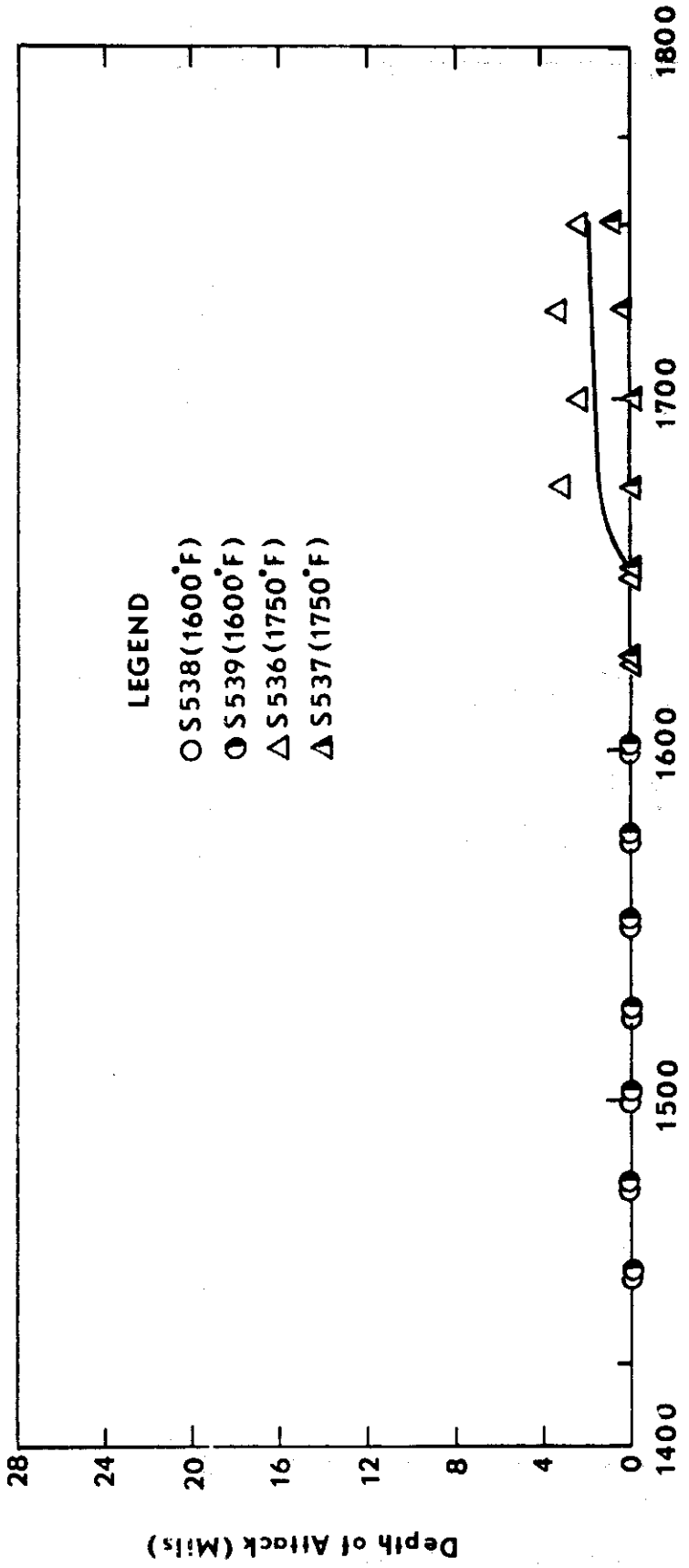

Figure 47. Corrosion as a Function of Temperature for IN728X Tested Using JP-4 Fuel with a Salt/Air Ratio of 4 ppm.

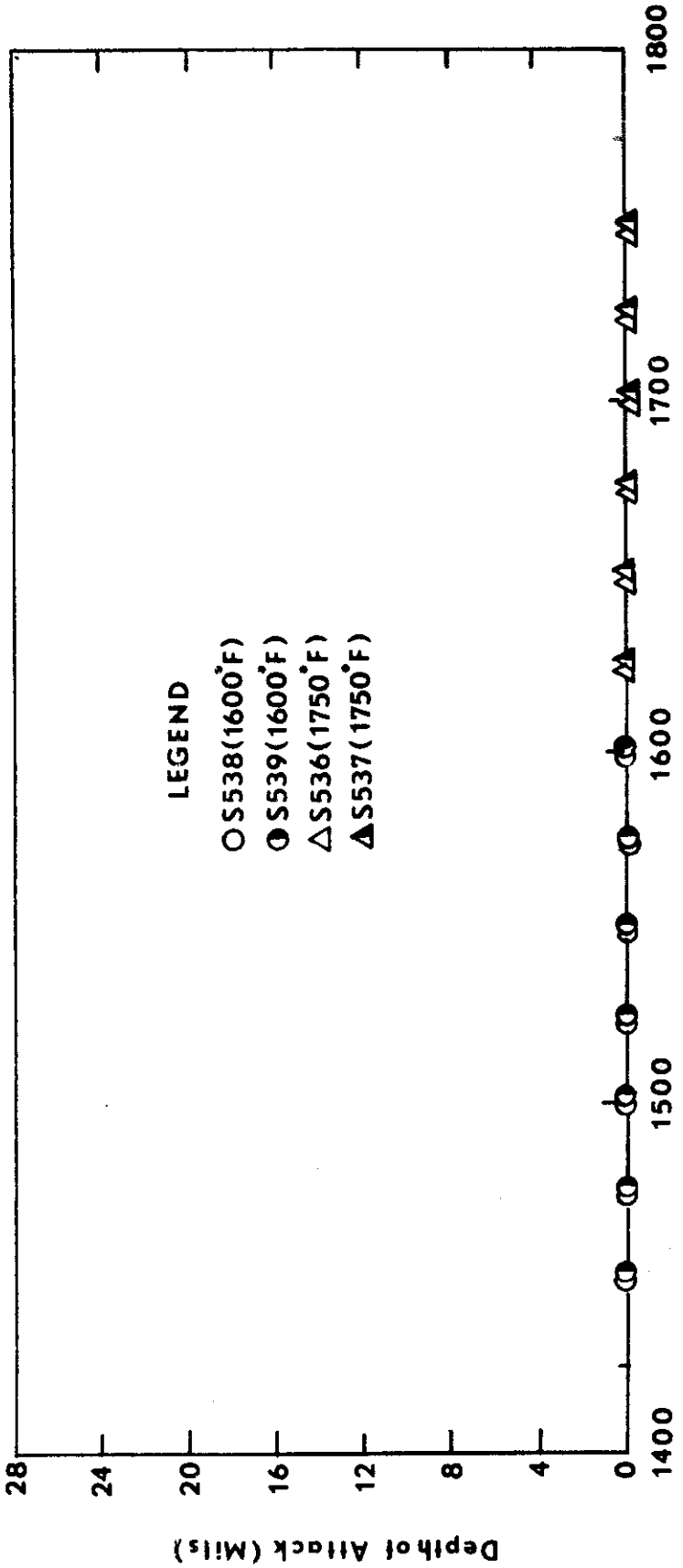

Figure 48. Corrosion as a Function of Temperature for X40 Tested Using JP-4 Fuel with a Salt/Air Ratio of 4 ppm.

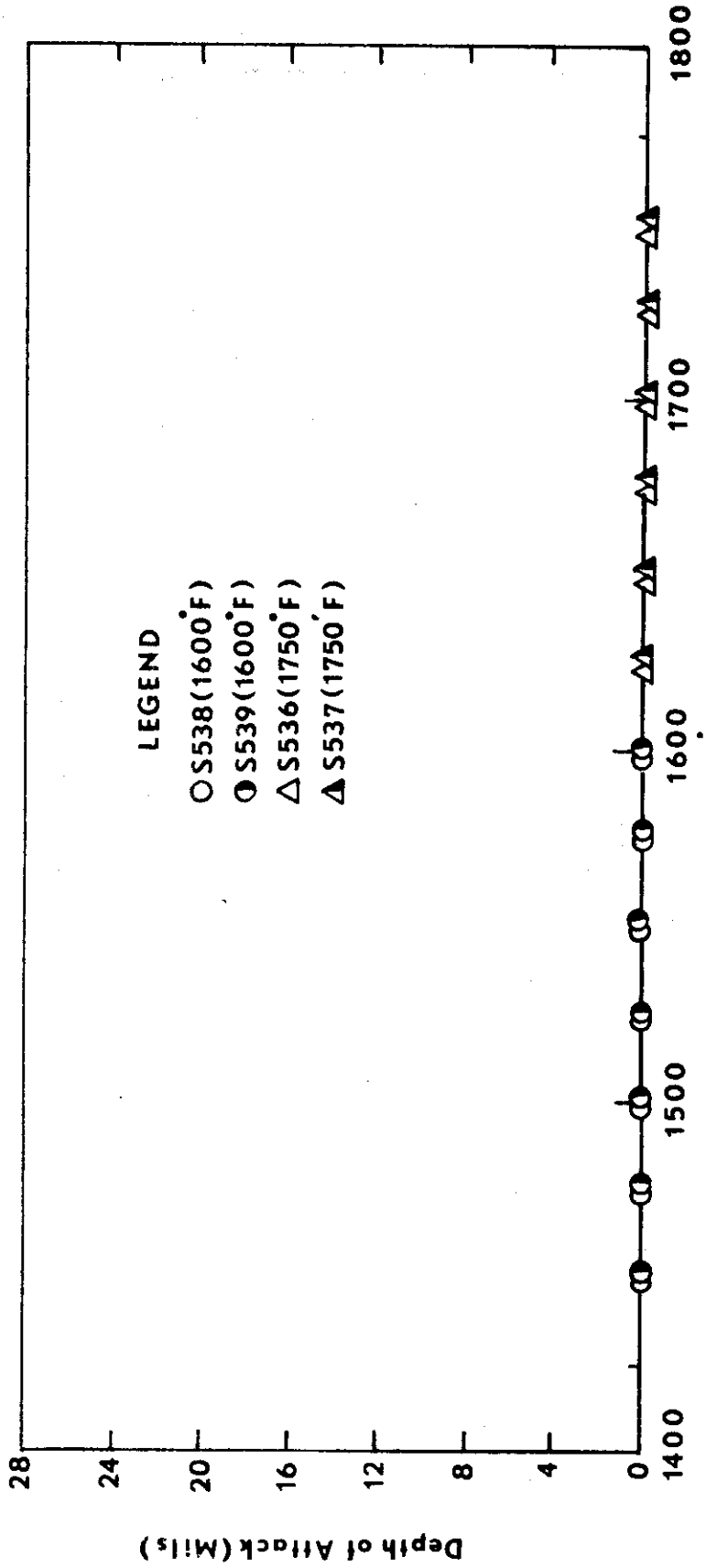

Figure 49. Corrosion as a Function of Temperature for U700 Tested Using JP-4 Fuel with a Salt/Air Ratio of 4 ppm.

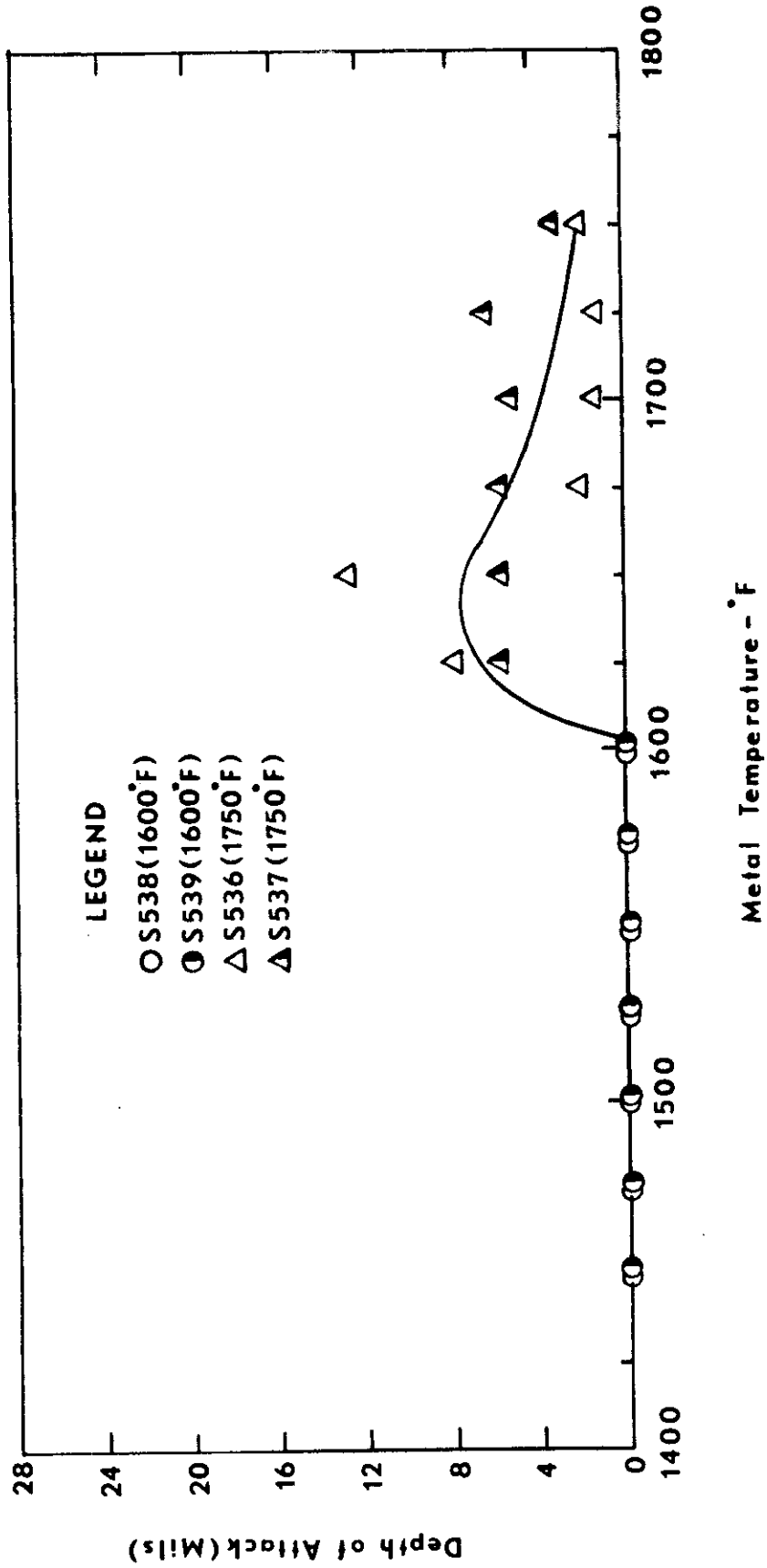

Figure 50. Corrosion as a Function of Temperature for IN100 Tested Using JP-4 Fuel with a Salt/Air Ratio of 4 ppm.

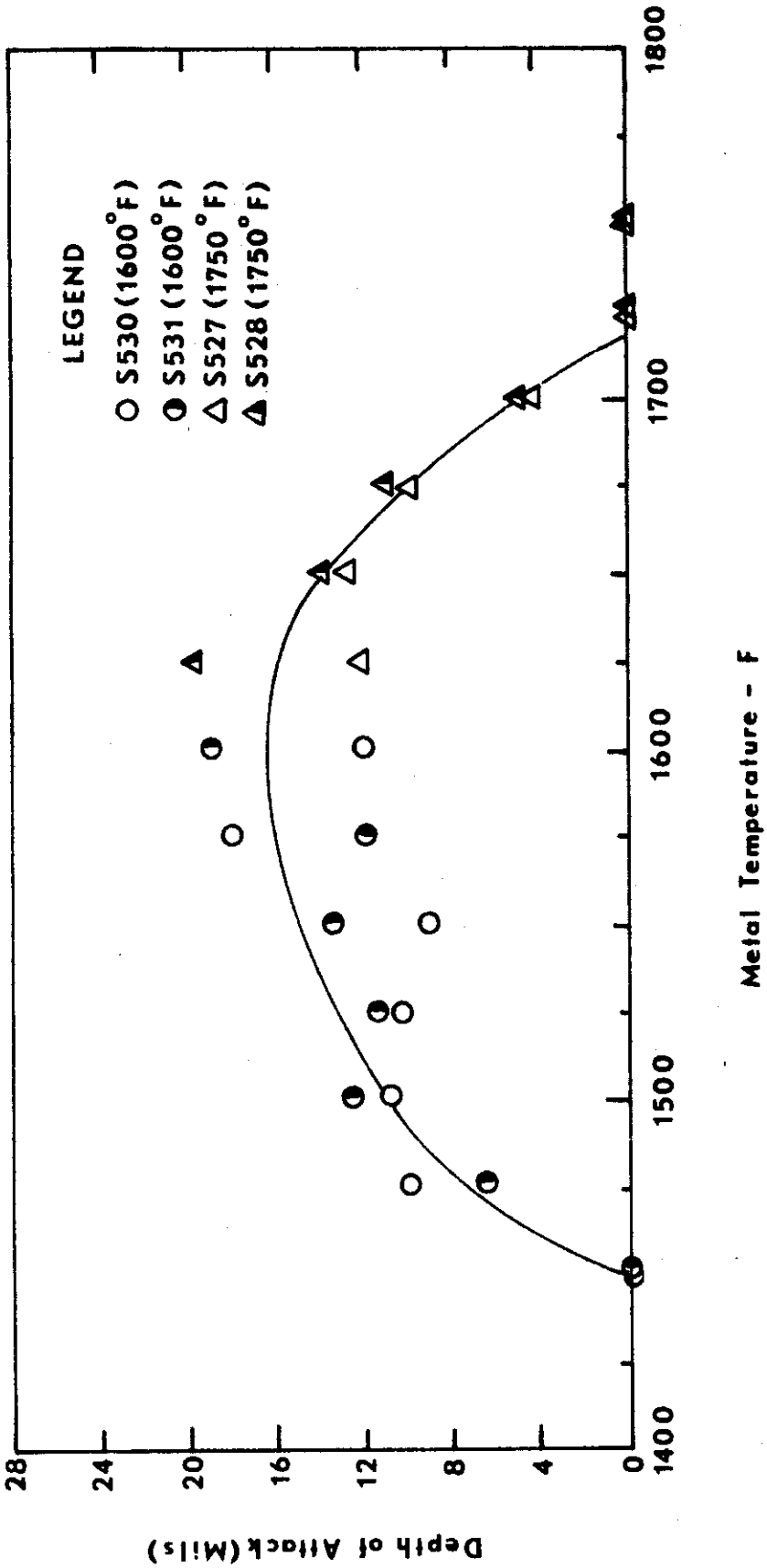

Figure 51. Corrosion as a Function of Temperature for Inco 713C Using JP-4R Fuel with a Salt/Air Ratio of 8 ppm.

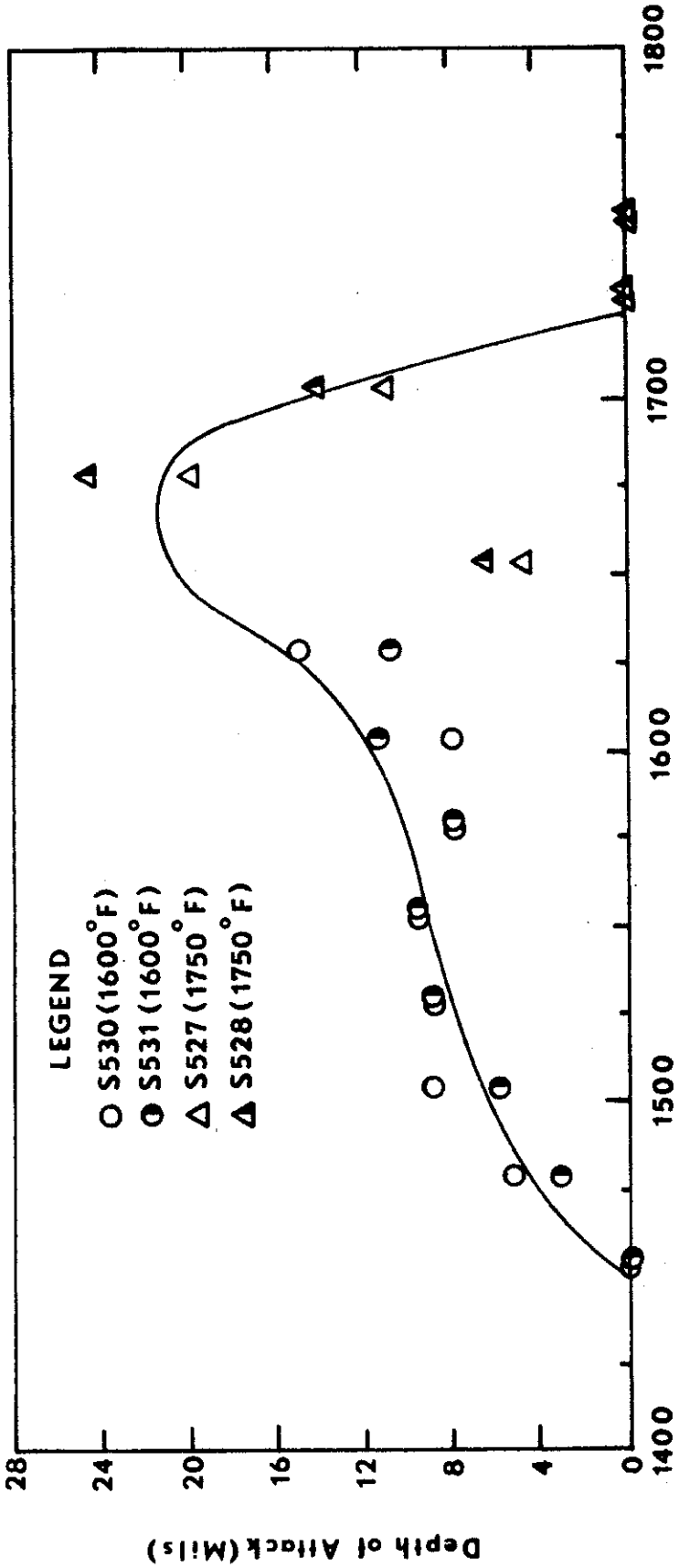

Figure 52. Corrosion as a Function of Temperature for Inco 713LC Using JP-4R Fuel with a Salt/Air Ratio of 8 ppm.

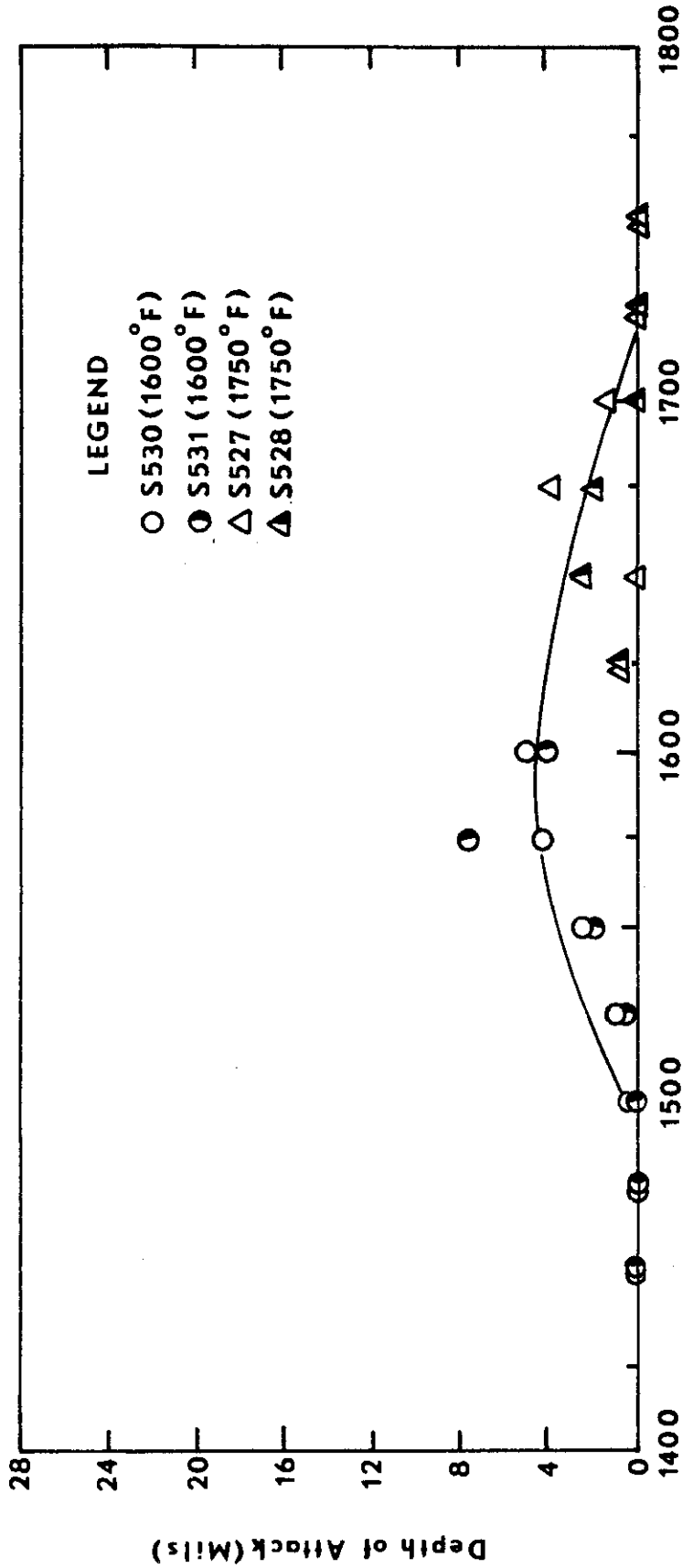

Figure 53. Corrosion as a Function of Temperature for TRW 1800 Using JP-4R Fuel with a Salt/Air Ratio of 8 ppm.

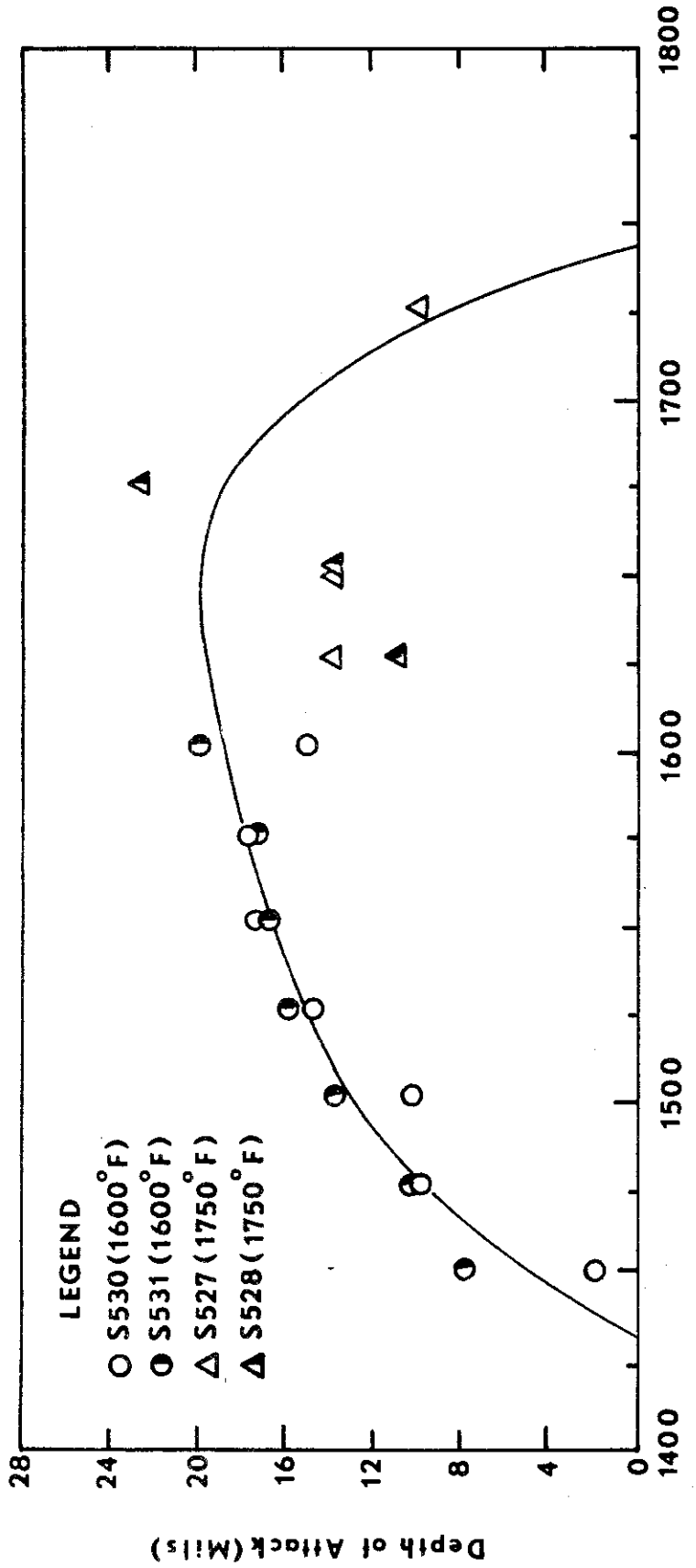

Figure 54. Corrosion as a Function of Temperature for B1900 Using JP-4R Fuel with a Salt/Air Ratio of 8 ppm.

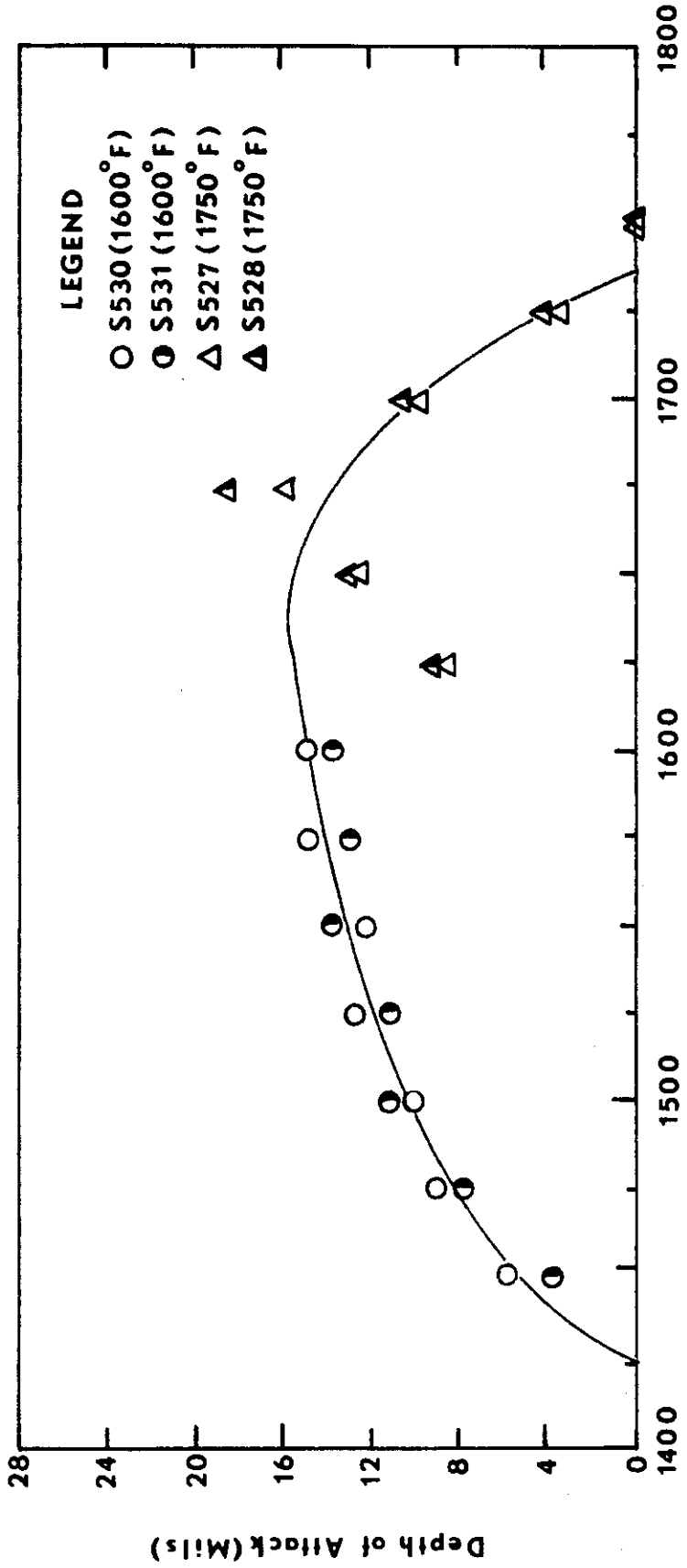

Figure 55. Corrosion as a Function of Temperature for B1910 Using JP-4R Fuel with a Salt/Air Ratio of 8 ppm.

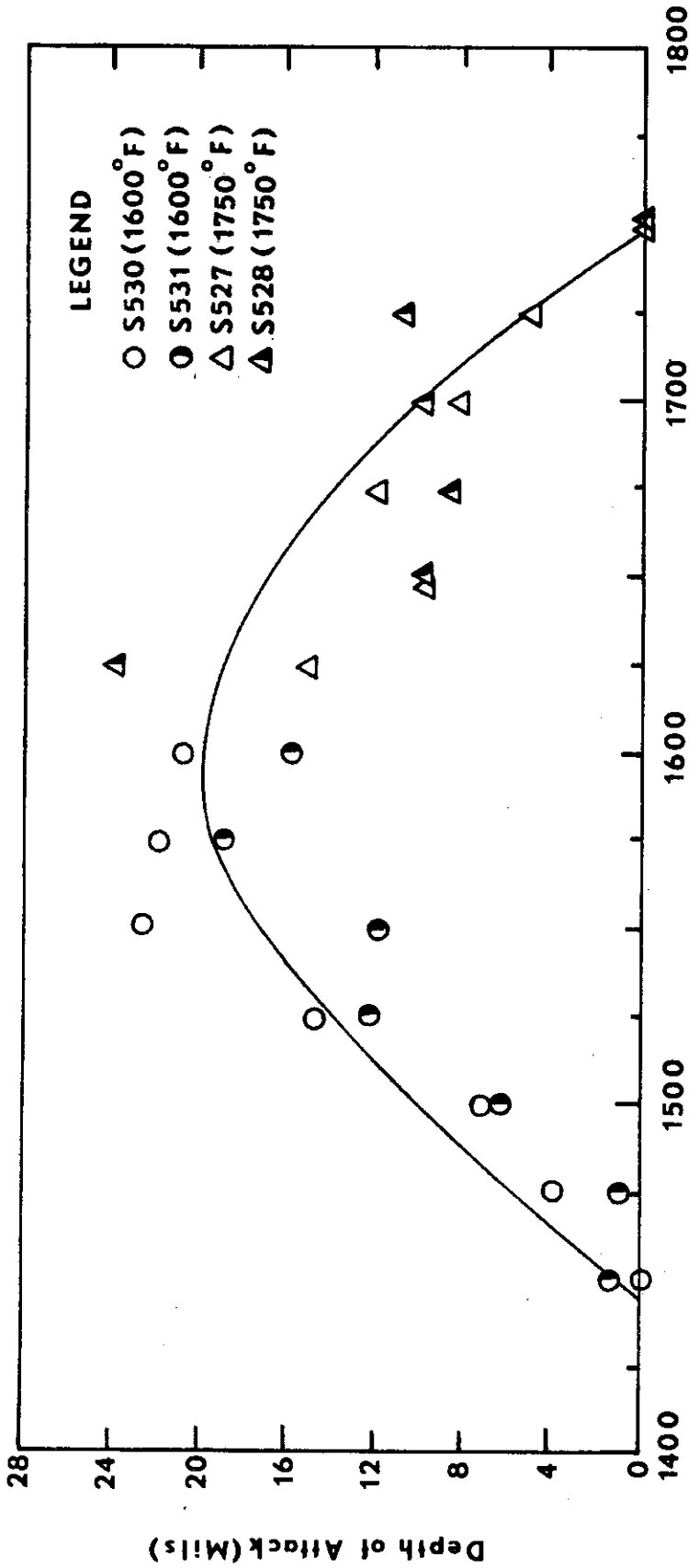

Figure 56. Corrosion as a Function of Temperature for MAR-M-200 Using JP-4R Fuel with a Salt/Air Ratio of 8 ppm.

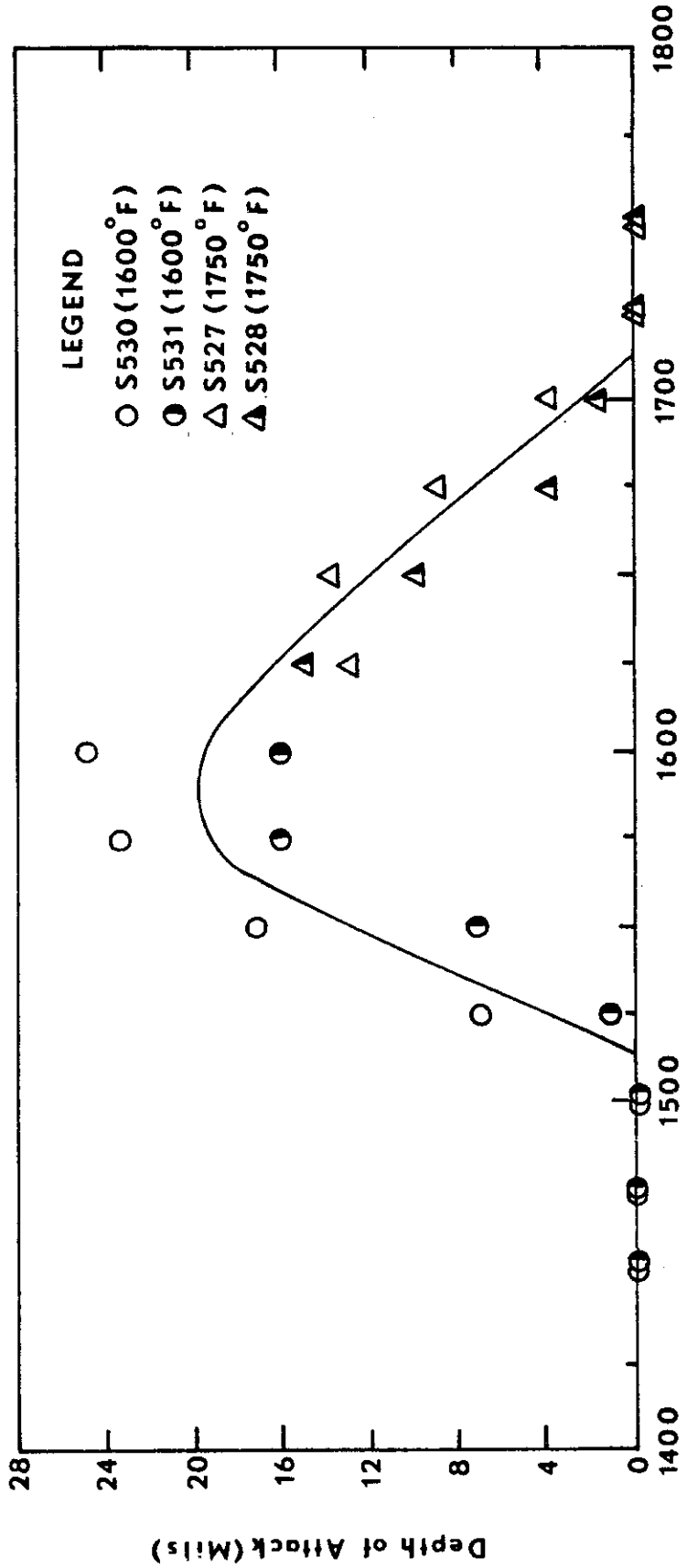

Figure 57. Corrosion as a Function of Temperature for PDRL 161 Using JP-4R Fuel with a Salt/Air Ratio of 8 ppm.

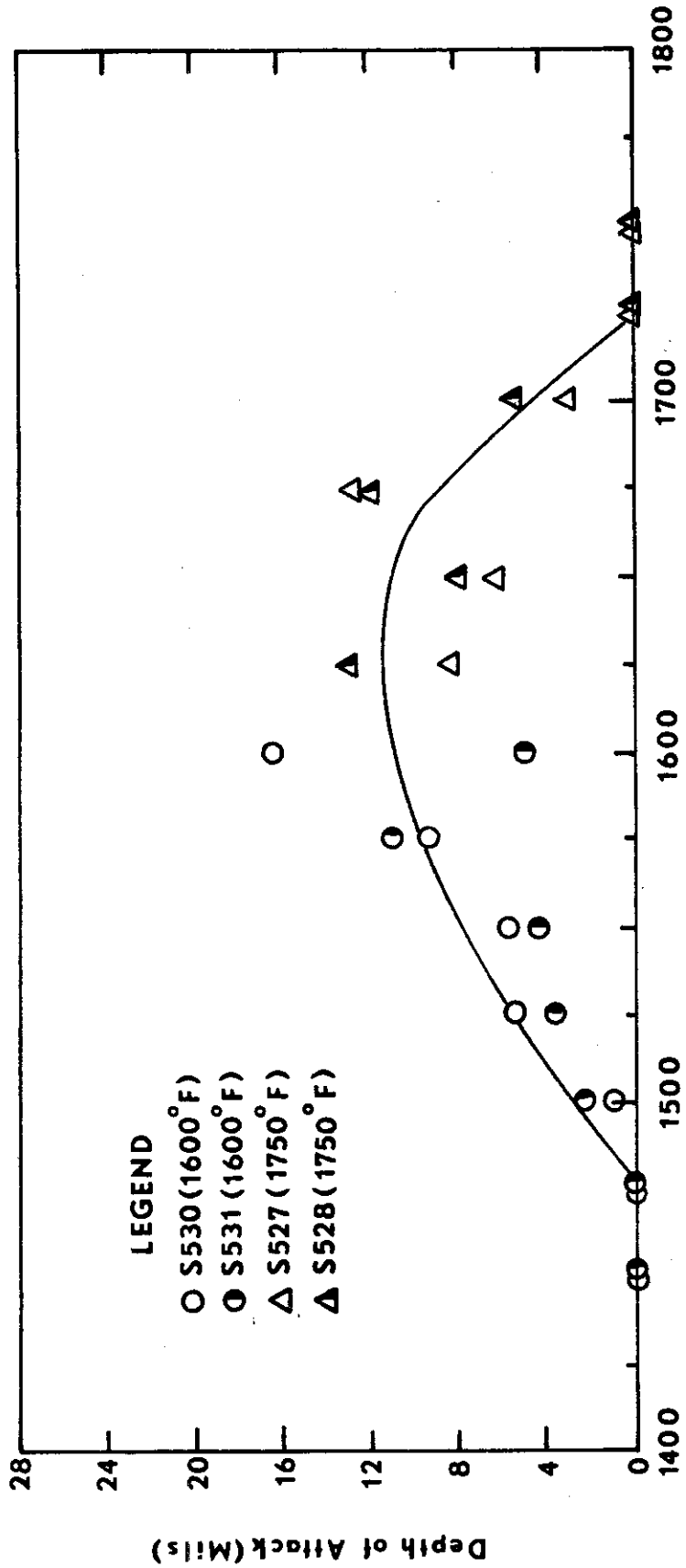

Figure 58. Corrosion as a Function of Temperature for PDRL 162 Using JP-4R Fuel with a Salt/Air Ratio of 8 ppm.

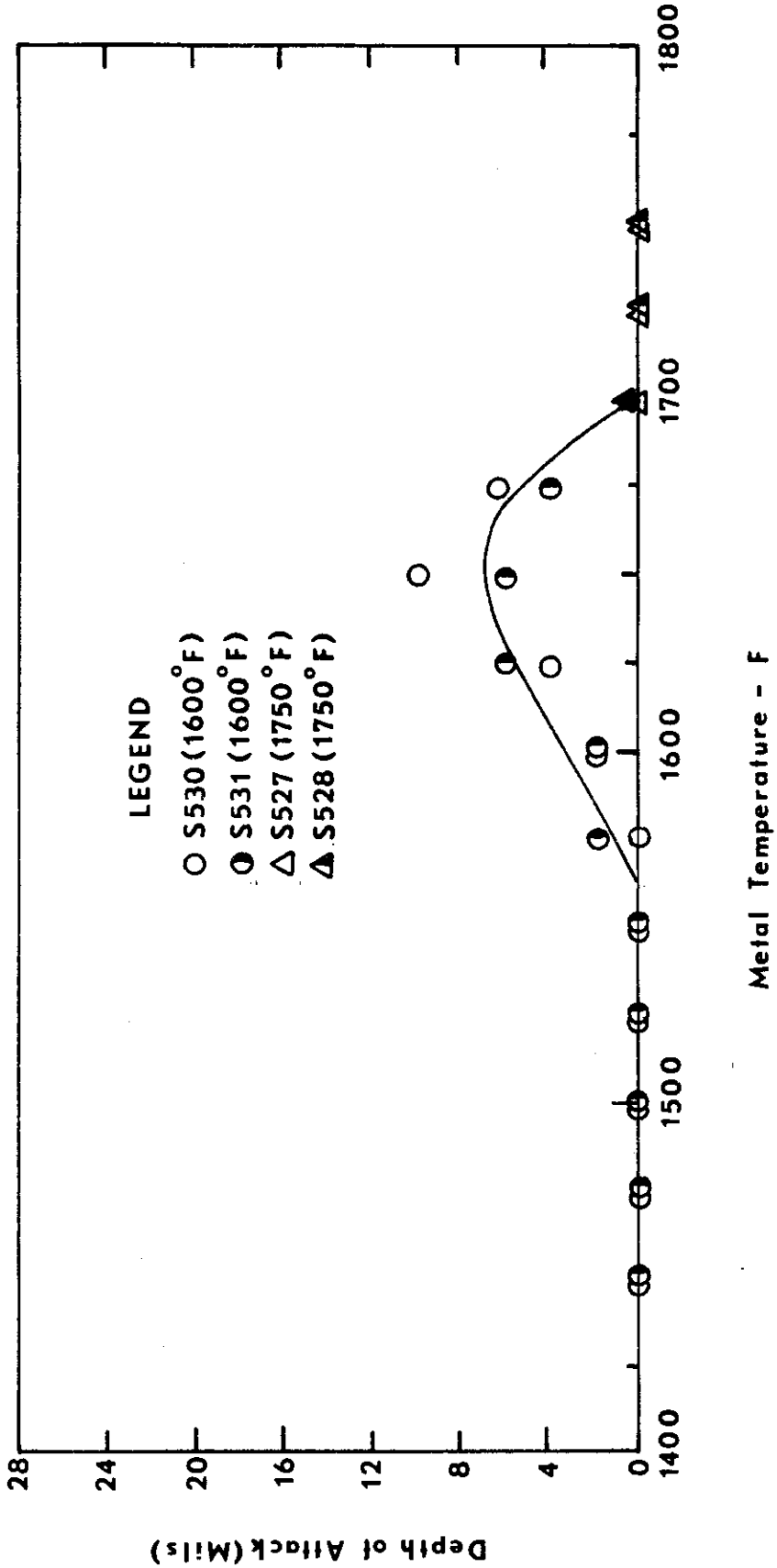

Figure 59. Corrosion as a Function of Temperature for IN728X Using JP-4R Fuel with a Salt/Air Ratio of 8 ppm.

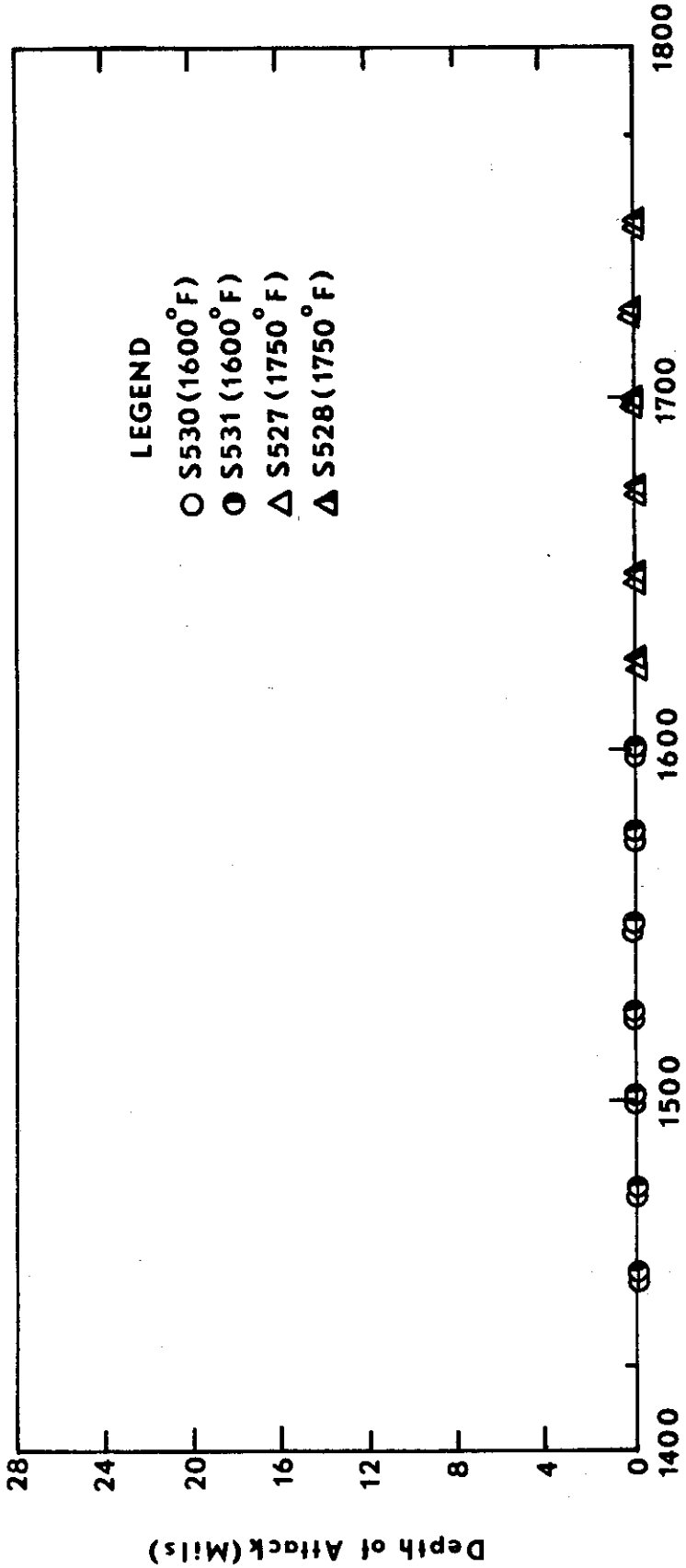

Figure 60. Corrosion as a Function of Temperature for X40 Using JP-4R Fuel with a Salt/Air Ratio of 8 ppm.

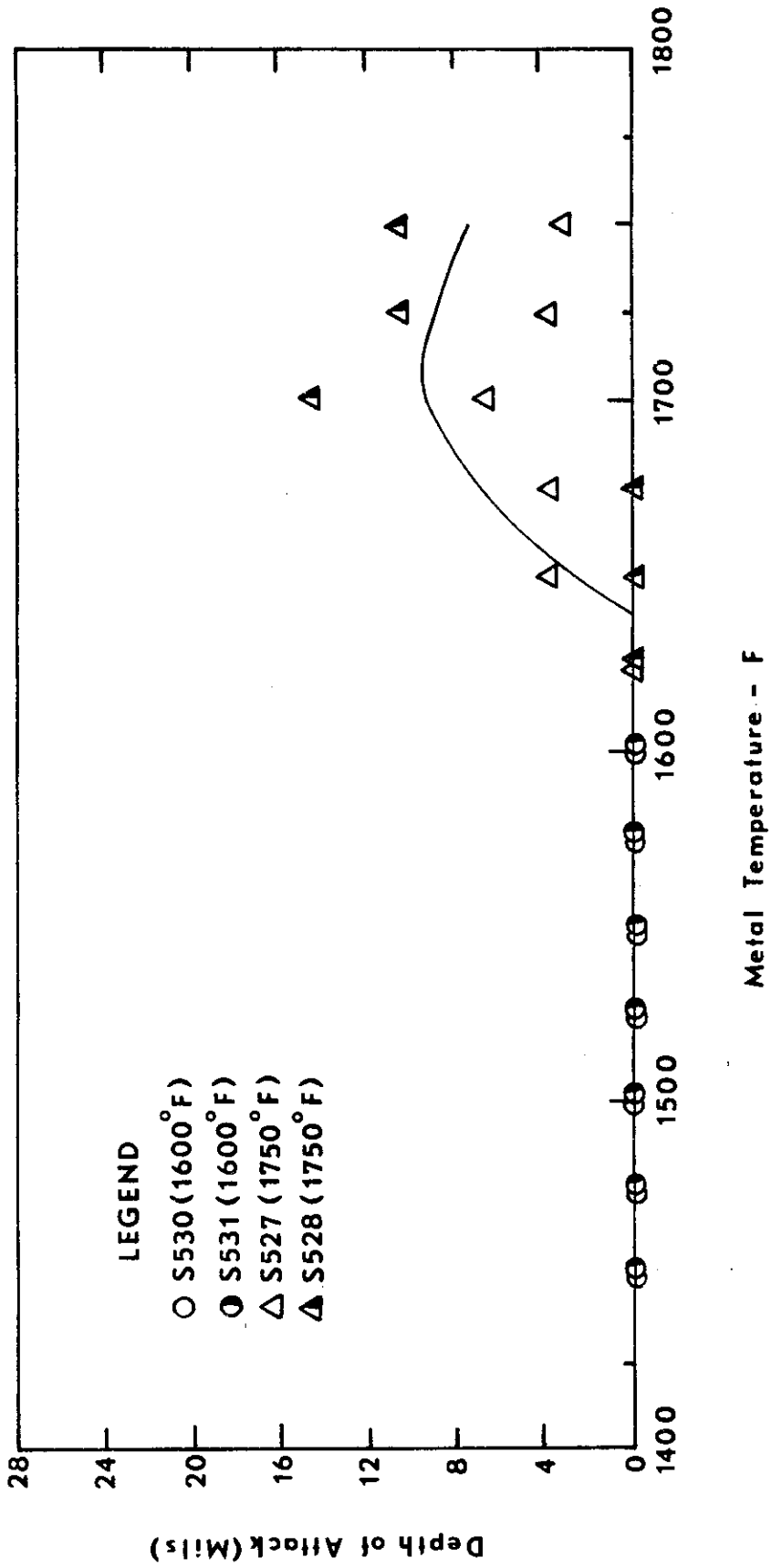

Figure 61. Corrosion as a Function of Temperature for U700 Using a JP-4R Fuel with a Salt/Air Ratio of 8 ppm.

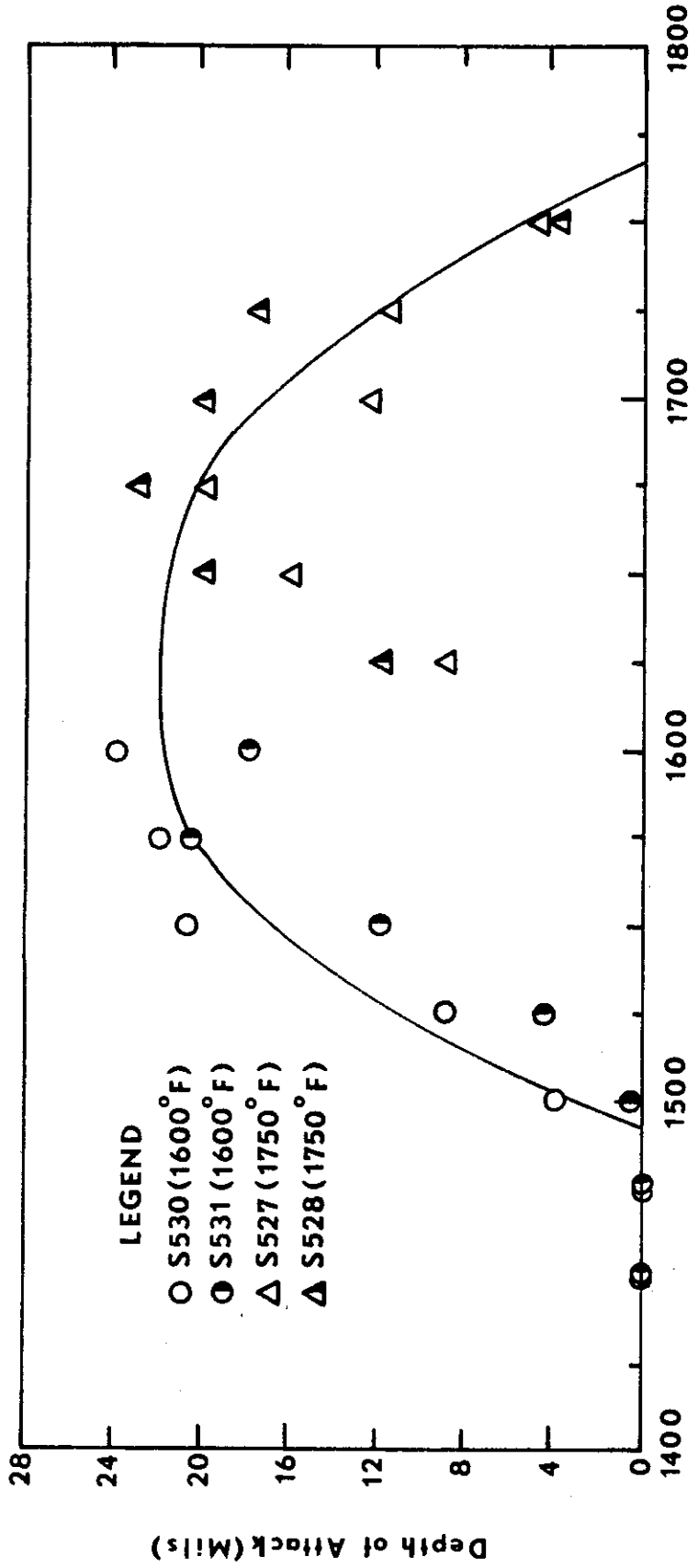

Figure 62. Corrosion as a Function of Temperature for IN100 Using JP-4R Fuel with a Salt/Air Ratio of 8 ppm.

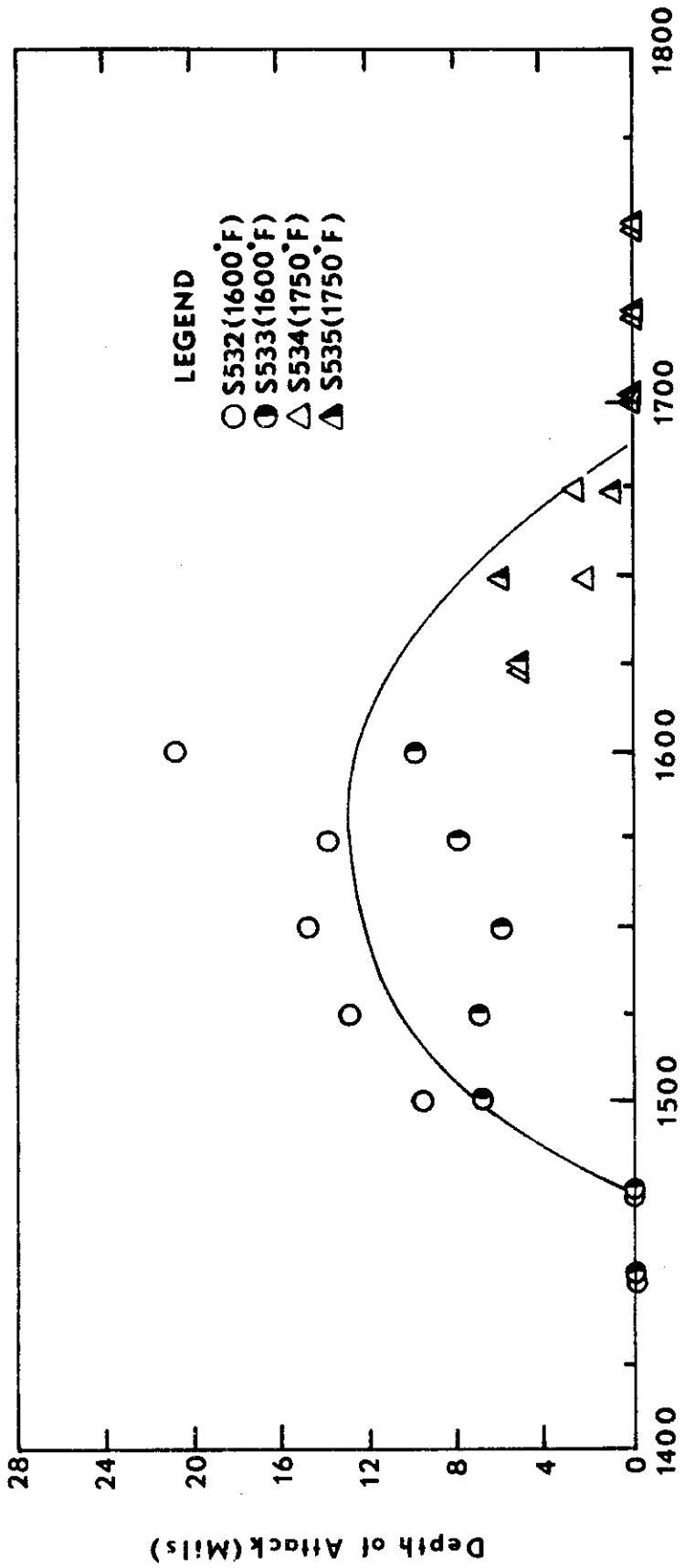

Figure 63. Corrosion as a Function of Temperature for Inco 713C Using JP-4R Fuel with a Salt/Air Ratio of 4 ppm.

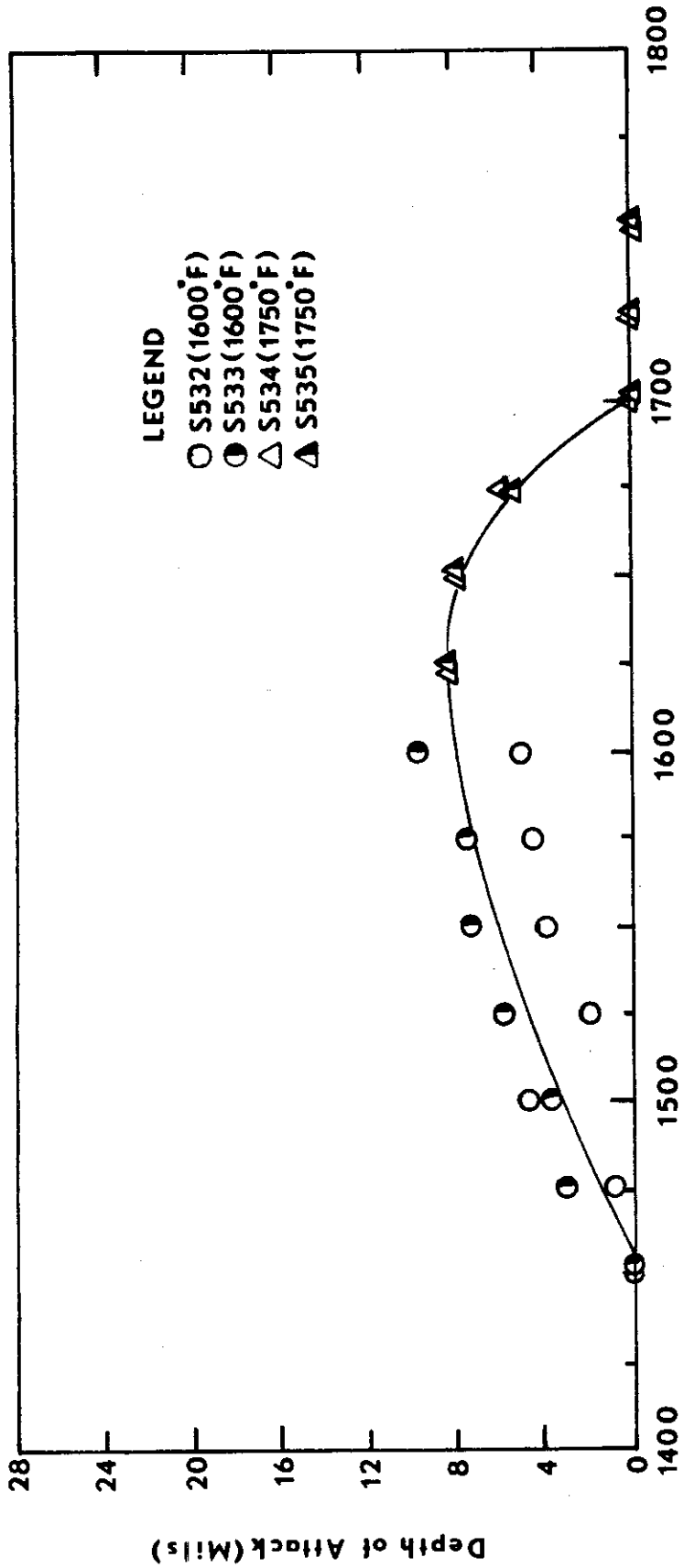

Figure 64. Corrosion as a Function of Temperature for Inco 713LC Using JP-4R Fuel with a Salt/Air Ratio of 4 ppm.

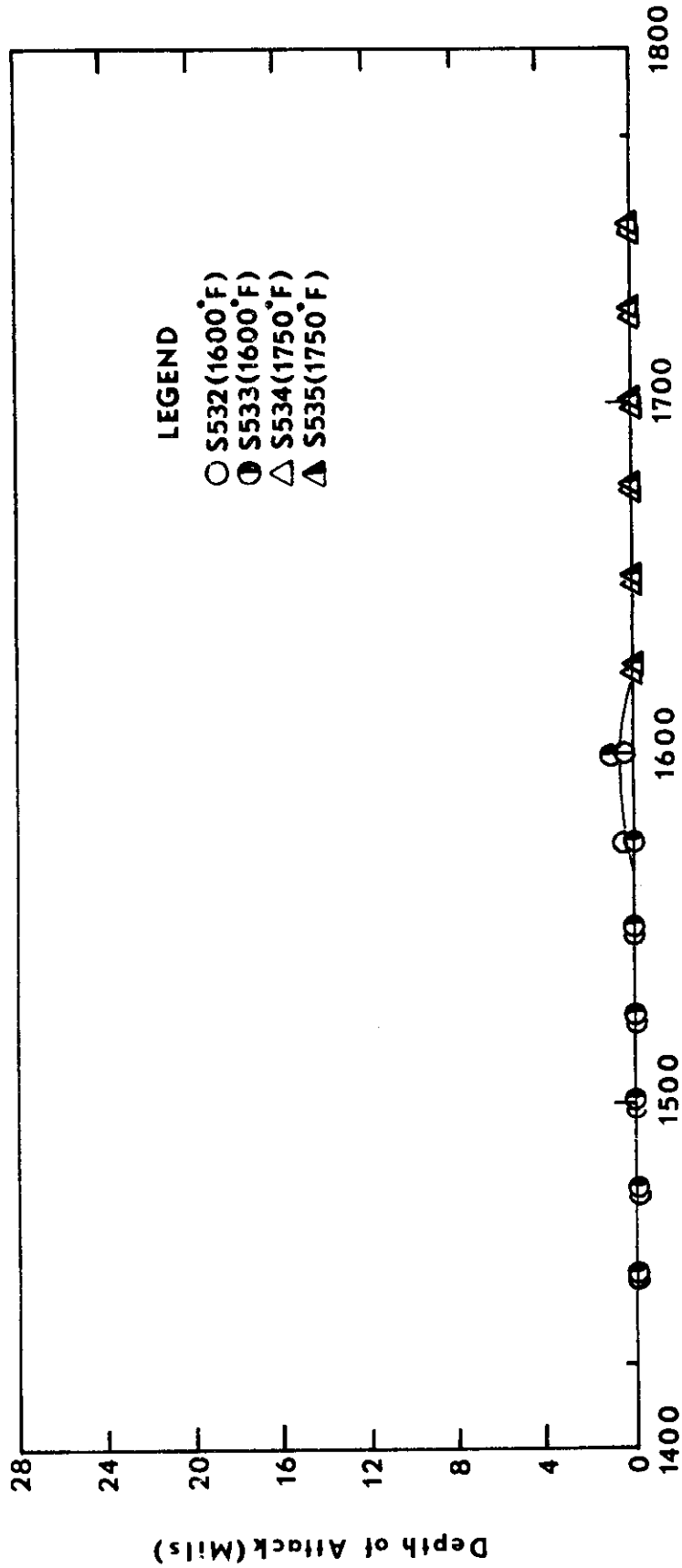

Figure 65. Corrosion as a Function of Temperature for TRW 1800 Using JP-4R Fuel with a Salt/Air Ratio of 4 ppm.

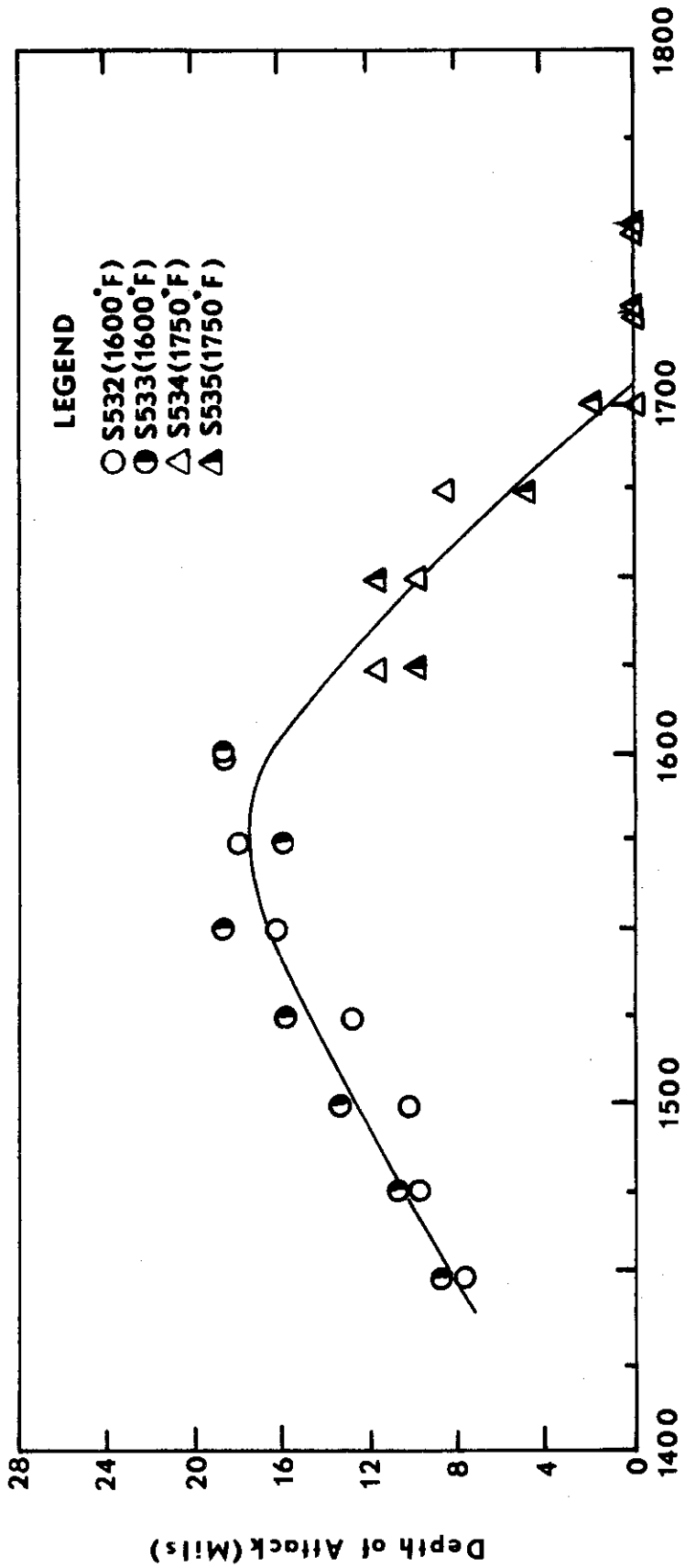

Figure 66. Corrosion as a Function of Temperature for B1900 Using JP-4R Fuel with a Salt/Air Ratio of 4 ppm.

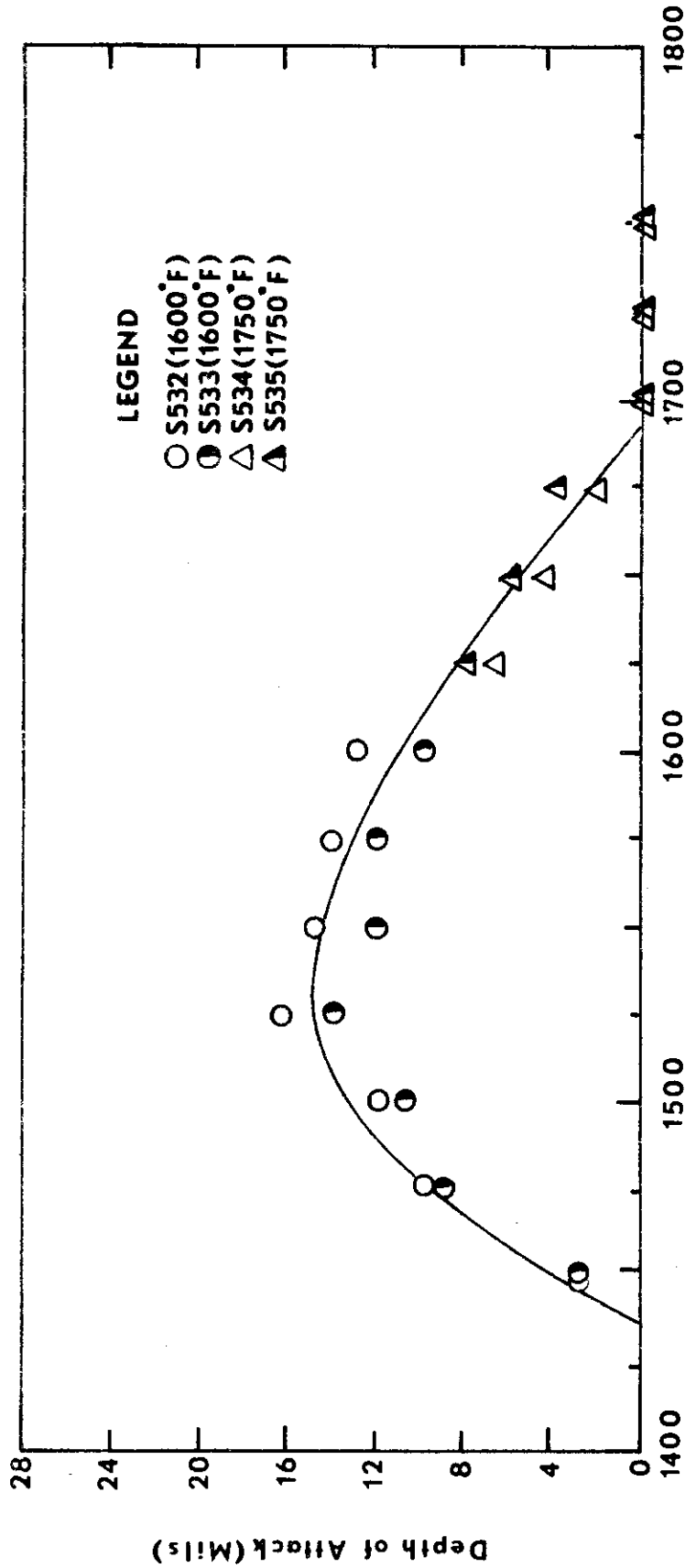

Figure 67. Corrosion as a Function of Temperature for B1910 Using JP-4R Fuel with a Salt/Air Ratio of 4 ppm.

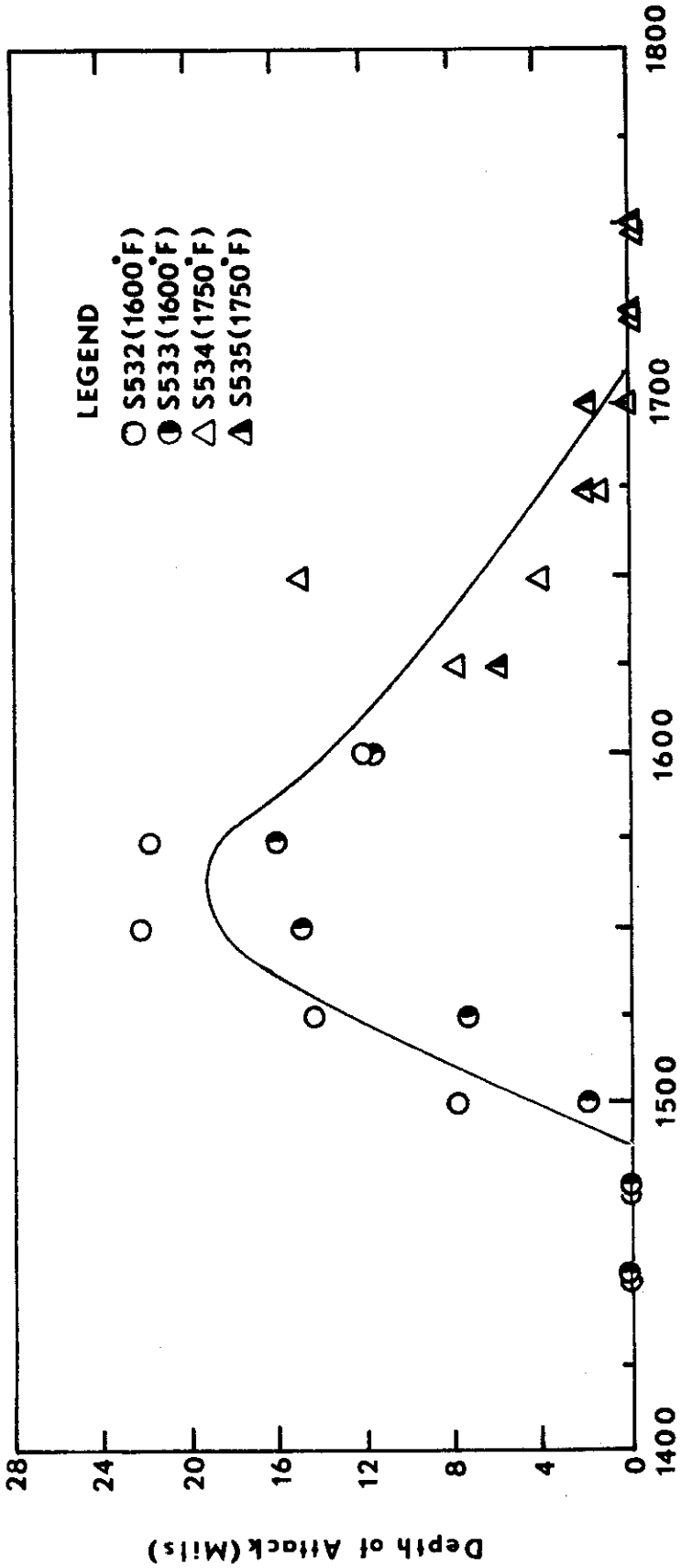

Figure 68. Corrosion as a Function of Temperature for MAR-M-200 Using JP-4R Fuel with a Salt/Air Ratio of 4 ppm.

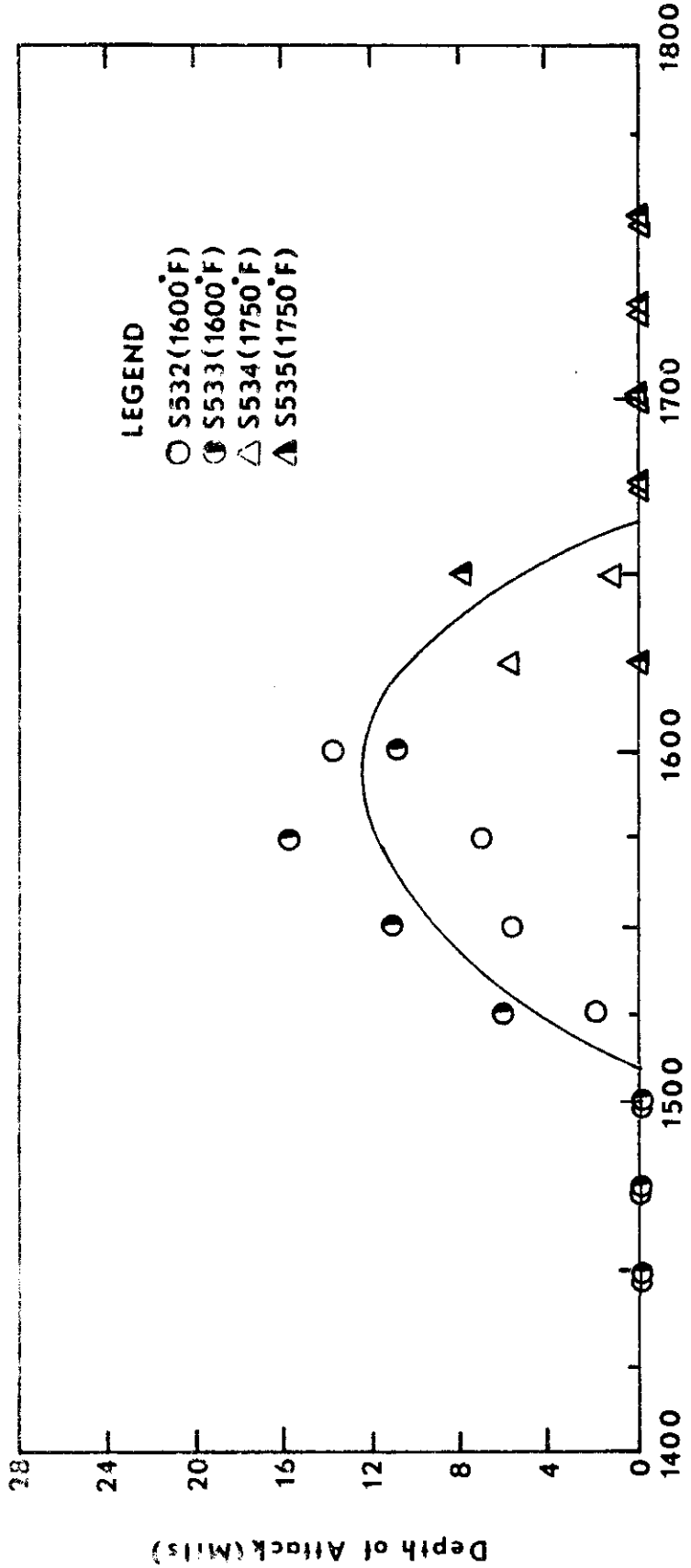

Figure 69. Corrosion as a Function of Temperature for PDRL 161 Using JP-4R Fuel with a Salt/Air Ratio of 4 ppm.

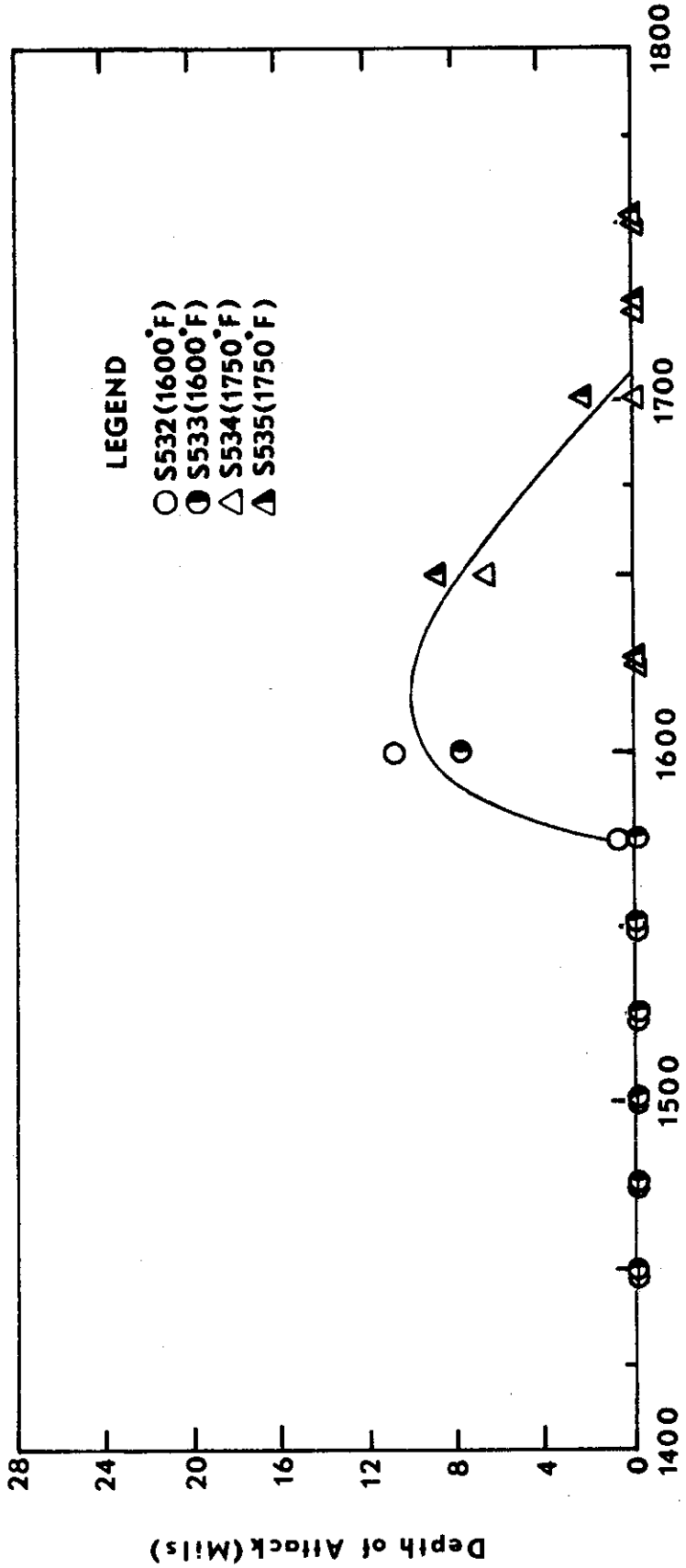

Figure 70. Corrosion as a Function of Temperature for PDRL 162 Using JP-4R Fuel with a Salt/Air Ratio of 4 ppm.

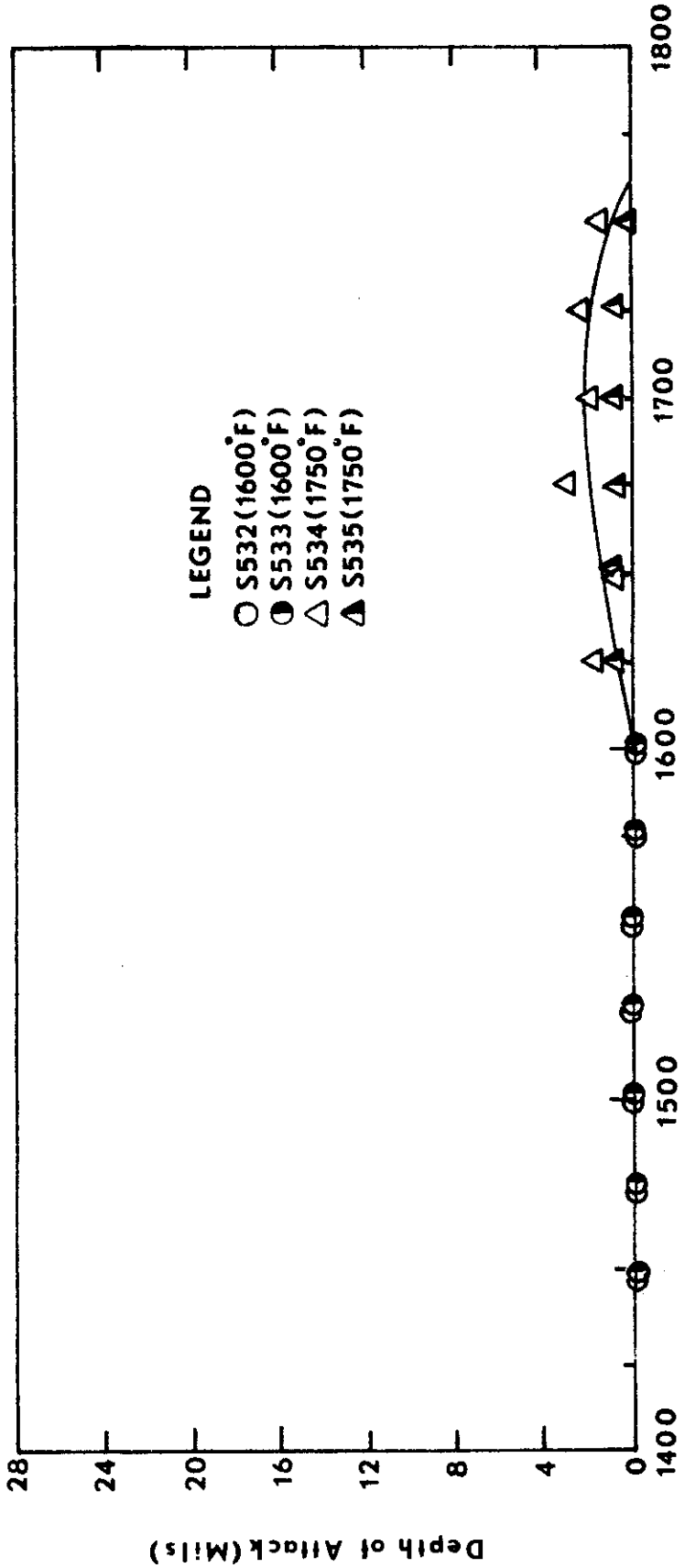

Figure 71. Corrosion as a Function of Temperature for IN728X Using JP-4R Fuel with a Salt/Air Ratio of 4 ppm.

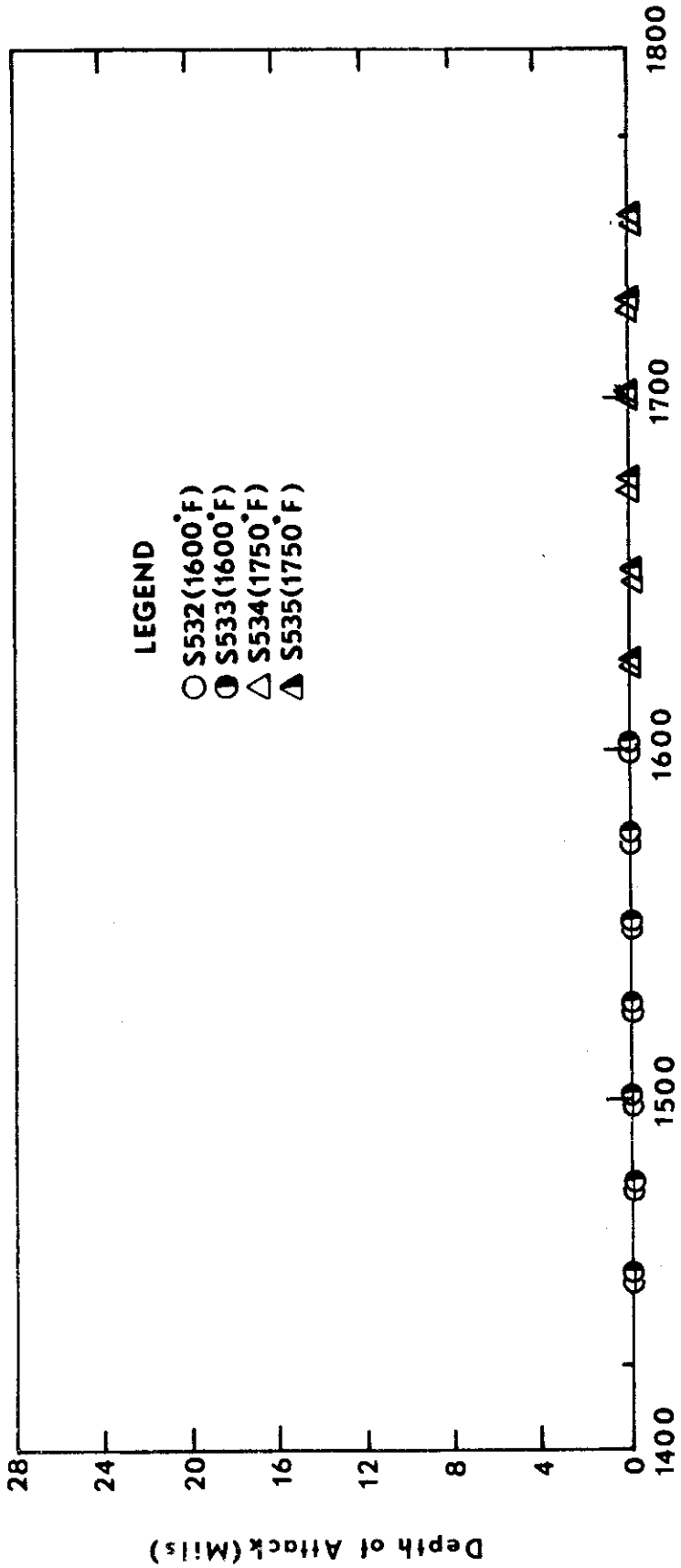

Figure 72. Corrosion as a Function of Temperature for X40 Using JP-4R Fuel with a Salt/Air Ratio of 4 ppm.

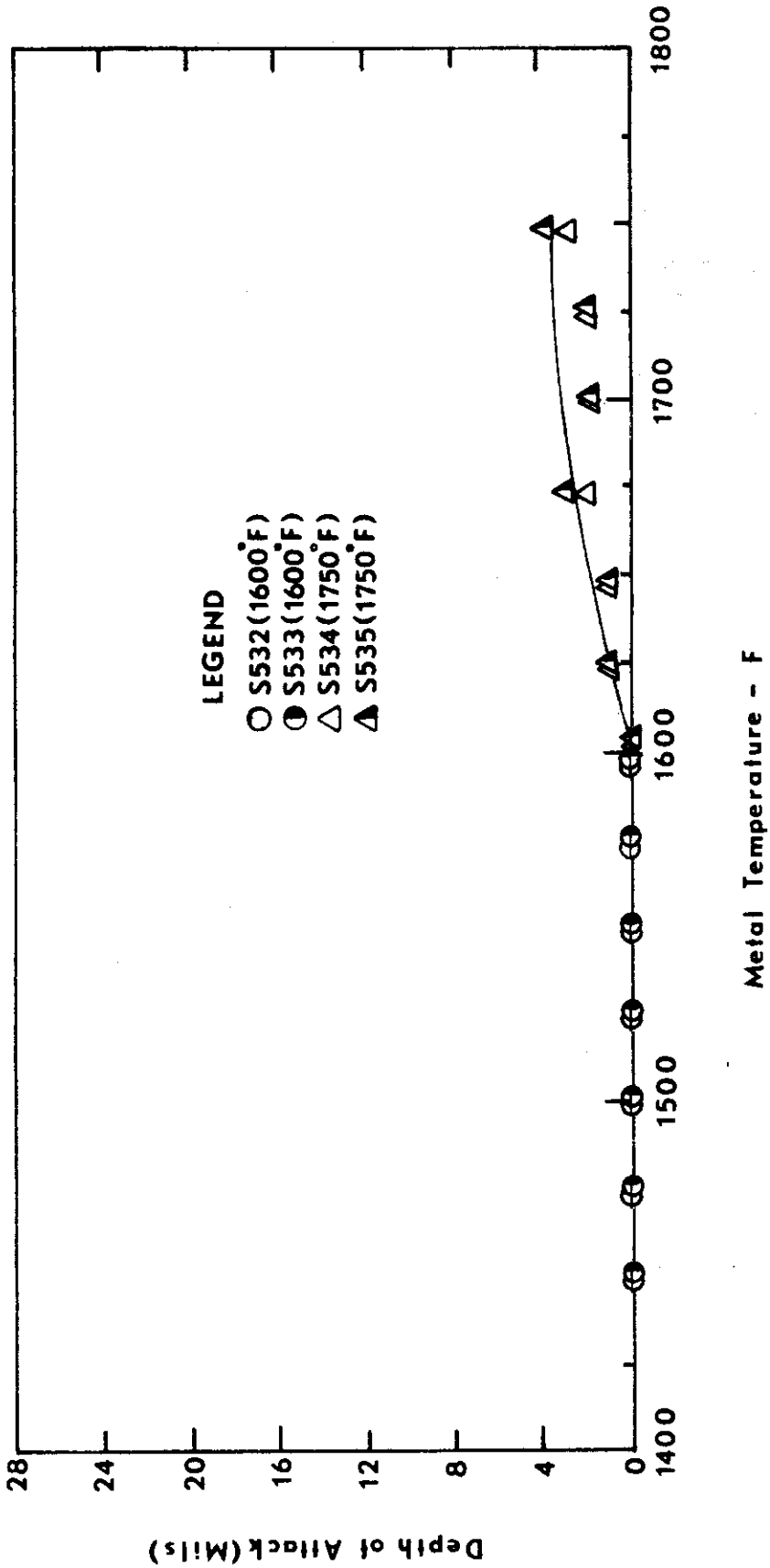

Figure 73. Corrosion as a Function of Temperature for U700 Using JP-4R Fuel with a Salt/Air Ratio of 4 ppm.

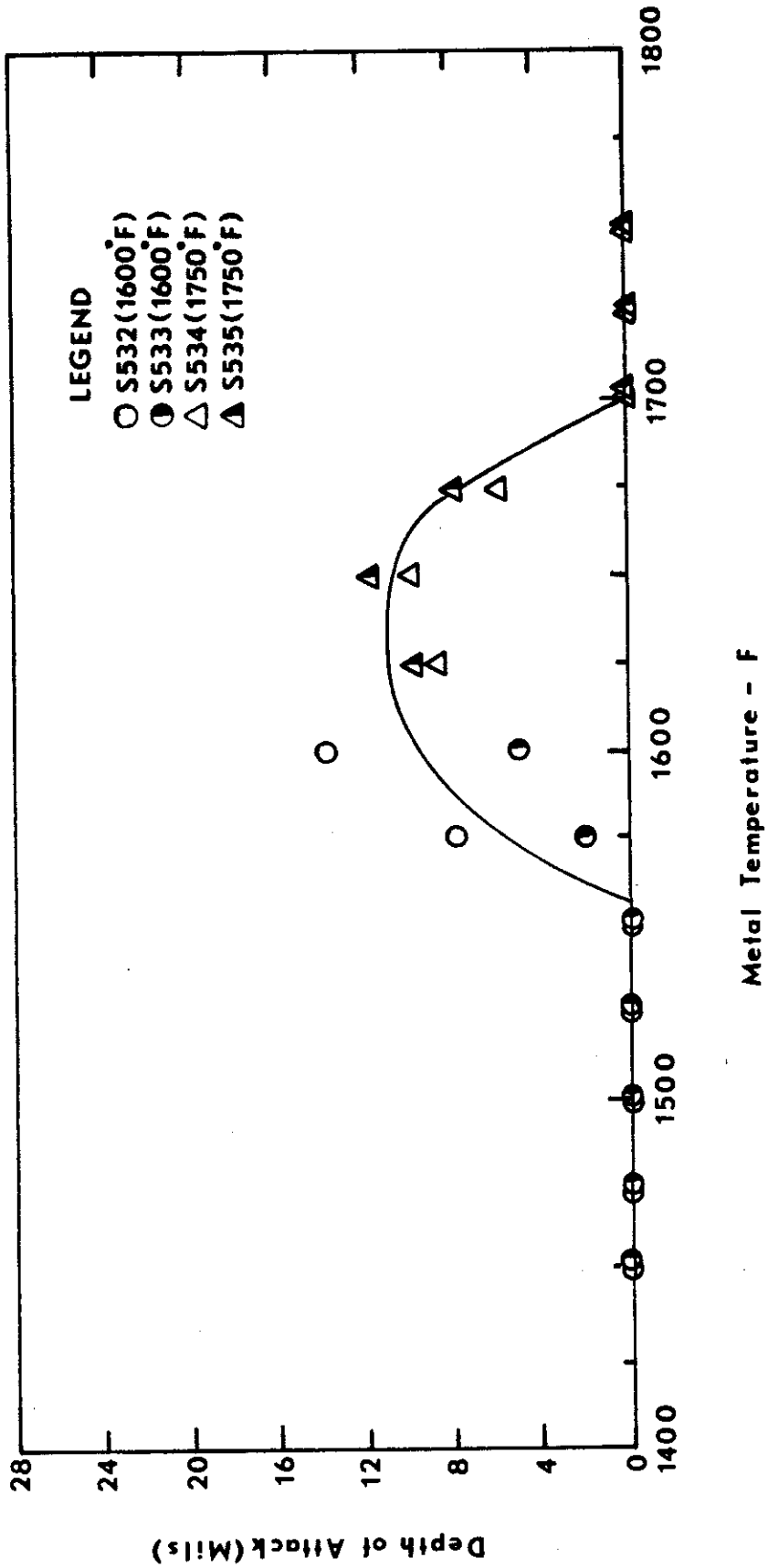

Figure 74. Corrosion as a Function of Temperature for IN100 Using JP-4R Fuel with a Salt/Air Ratio of 4 ppm.

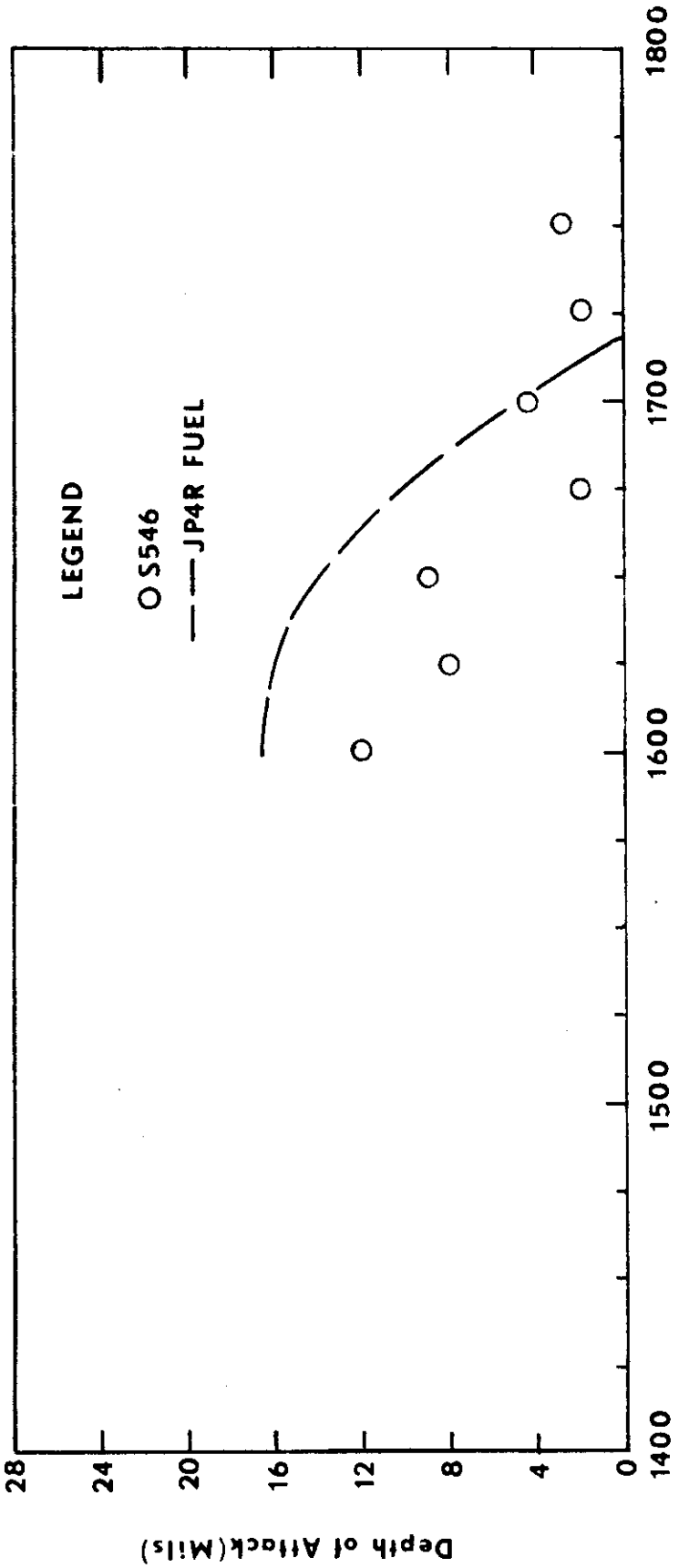

Figure 75. Corrosion as a Function of Temperature for Inco 713C Tested Using JP-5 Fuel (0.16%S) with a Salt/Air Ratio of 8 ppm.

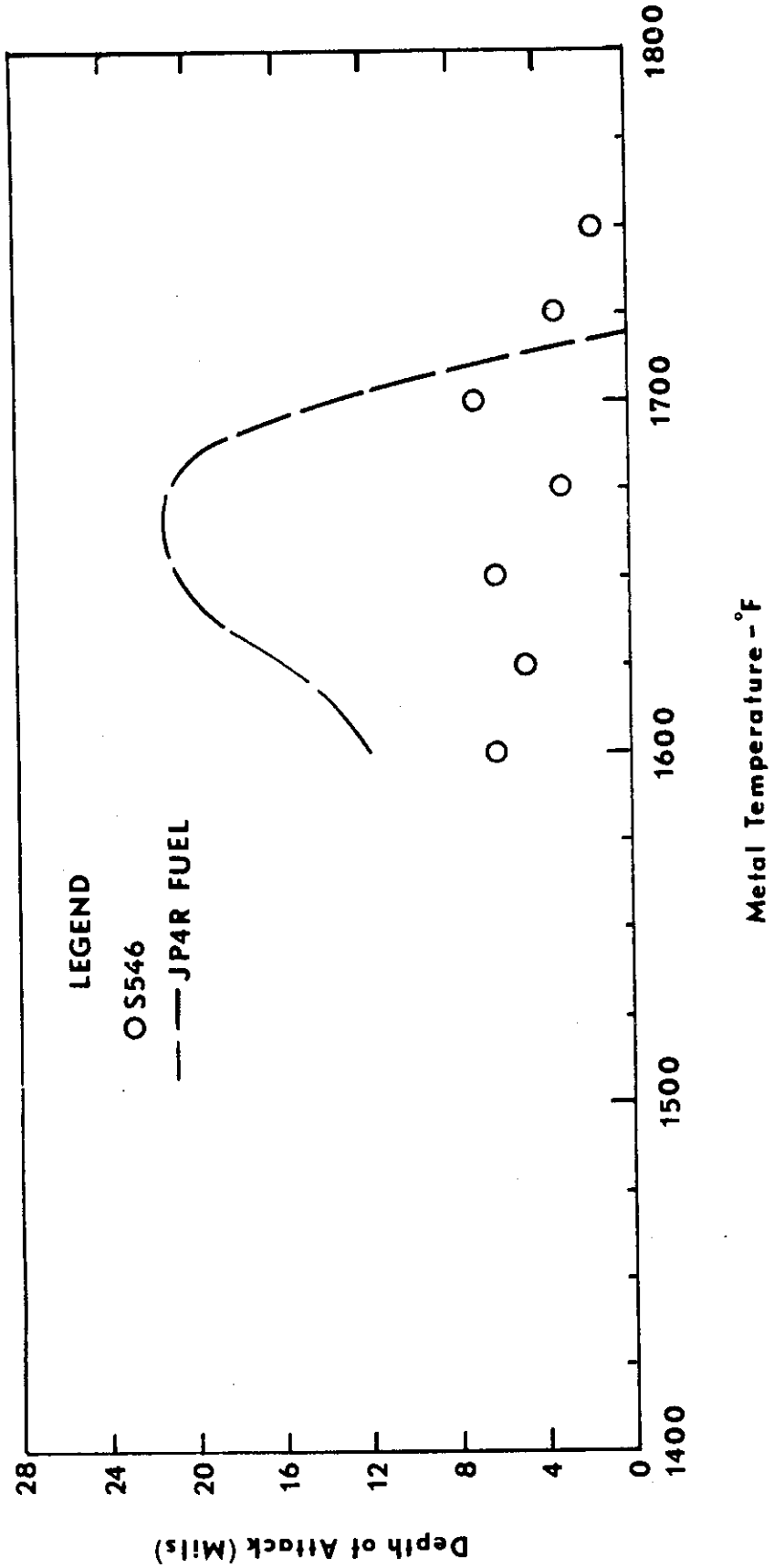

Figure 76. Corrosion as a Function of Temperature for Inco 713LC Tested Using JP-5 Fuel (0.16%S) with a Salt/Air Ratio of 8 ppm.

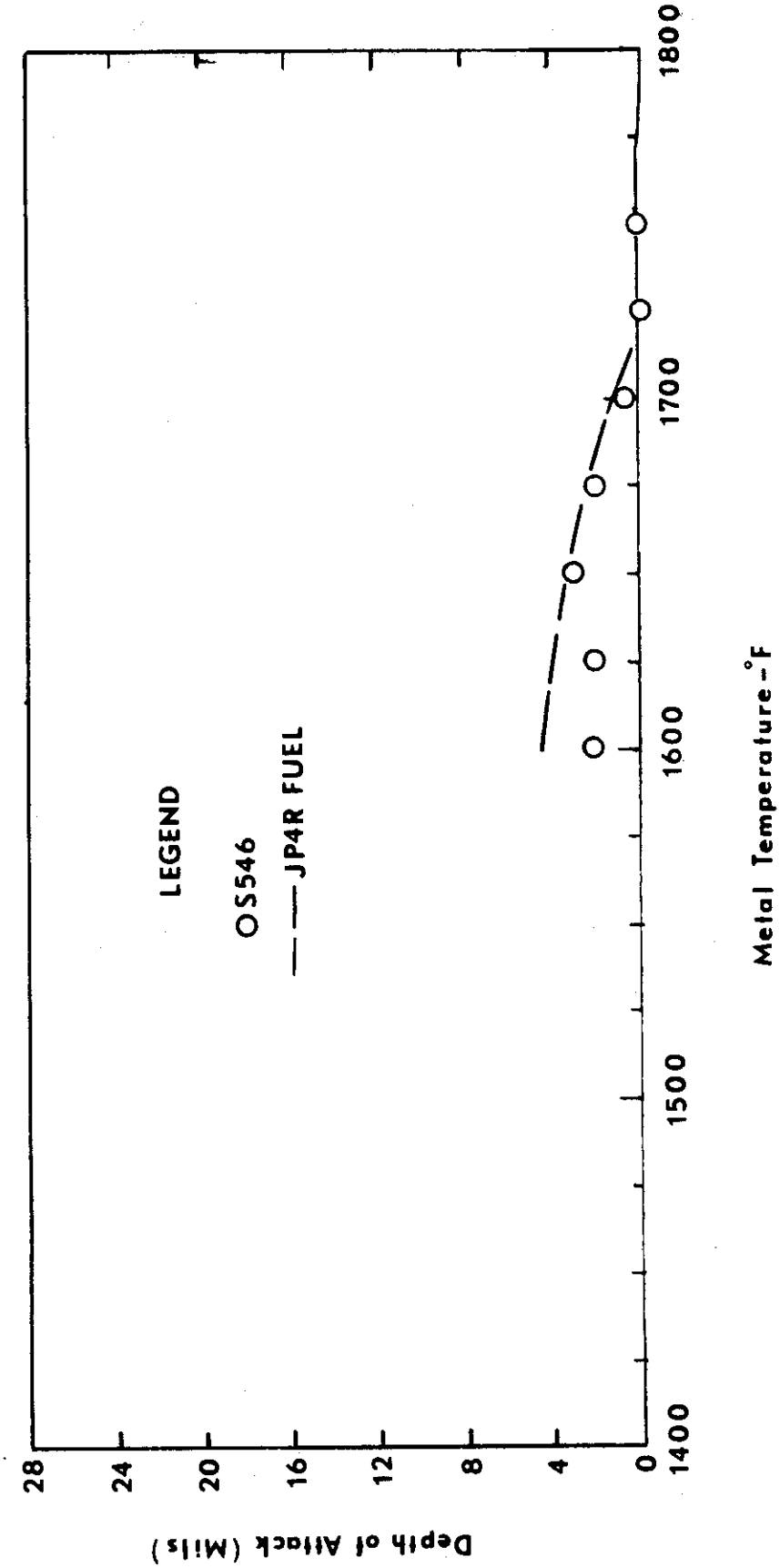

Figure 77. Corrosion as a Function of Temperature for TRW 1800 Tested Using JP-5 Fuel (0.16%S) with a Salt/Air Ratio of 8 ppm.

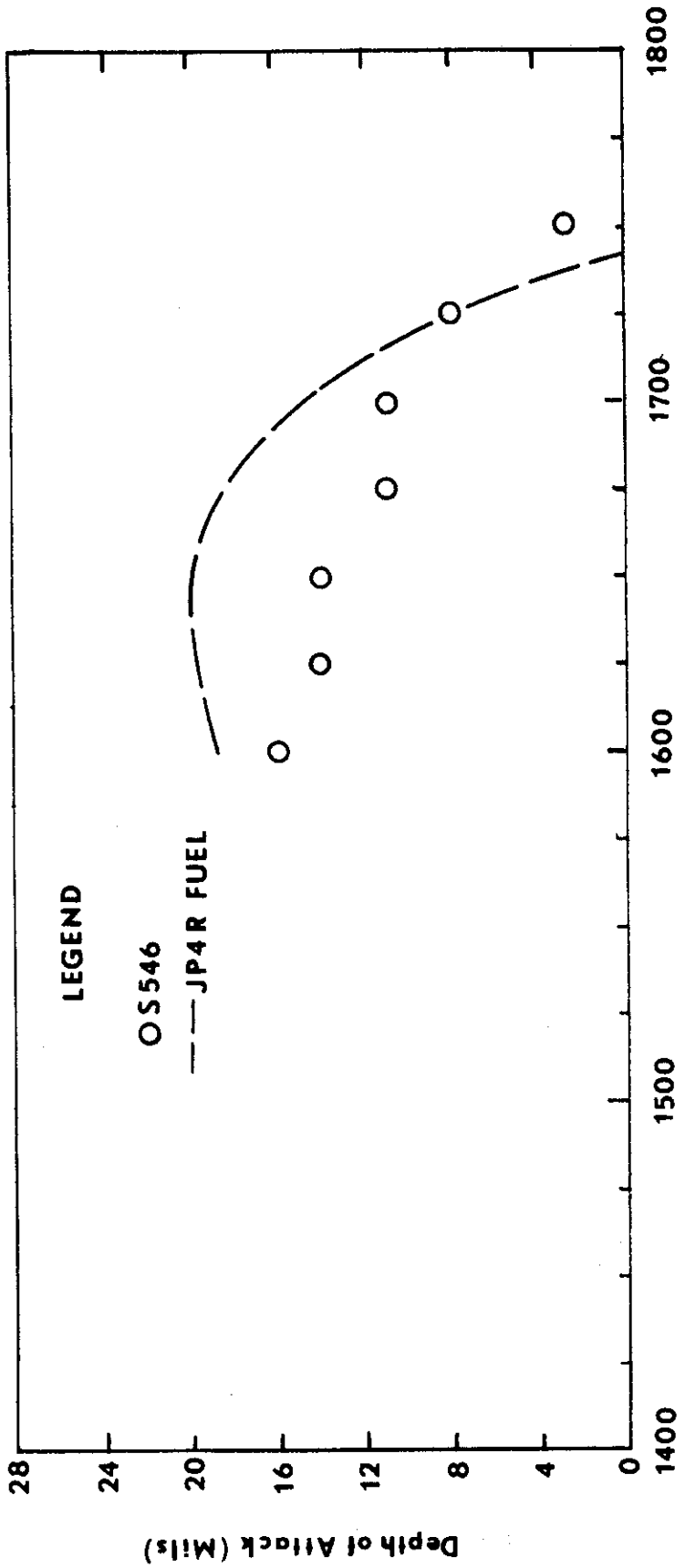

Figure 78. Corrosion as a Function of Temperature for B1900 Tested Using JP-5 Fuel (0.16%S) with a Salt/Air Ratio of 8 ppm.

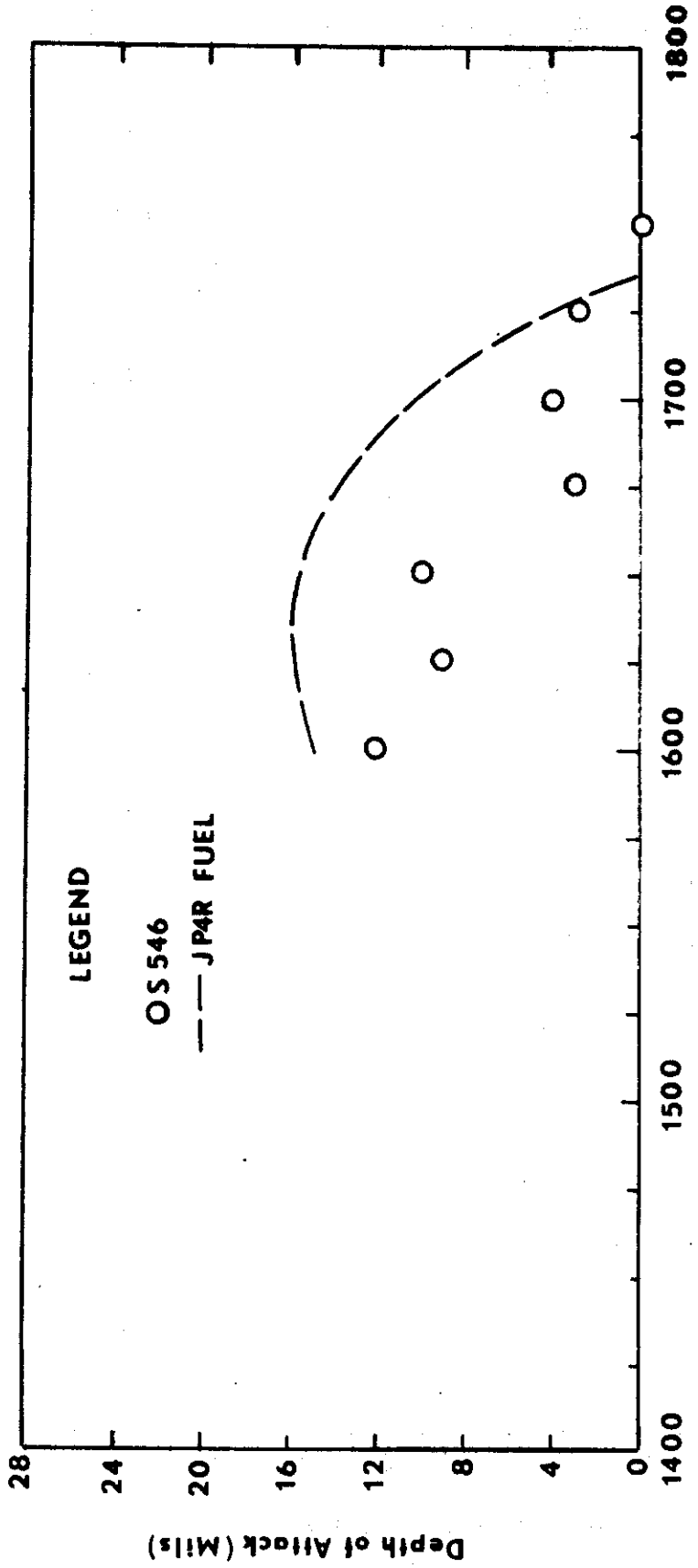

Figure 79. Corrosion as a Function of Temperature for B1910 Tested Using JP-5 Fuel (0.16%S) with a Salt/Air Ratio of 8 ppm.

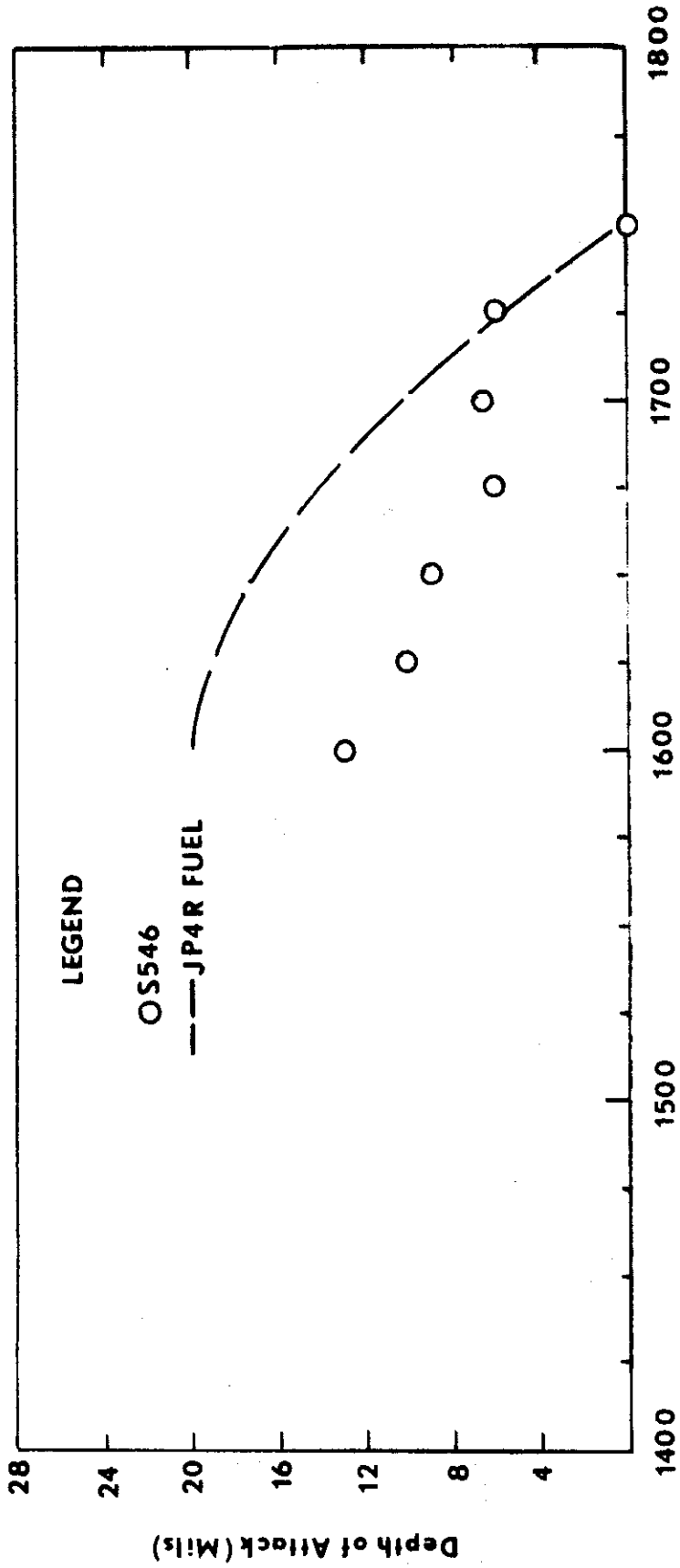

Figure 80. Corrosion as a Function of Temperature for MAR-M-200 Tested Using JP-5 Fuel (0.16%S) with a Salt/Air Ratio of 8 ppm.

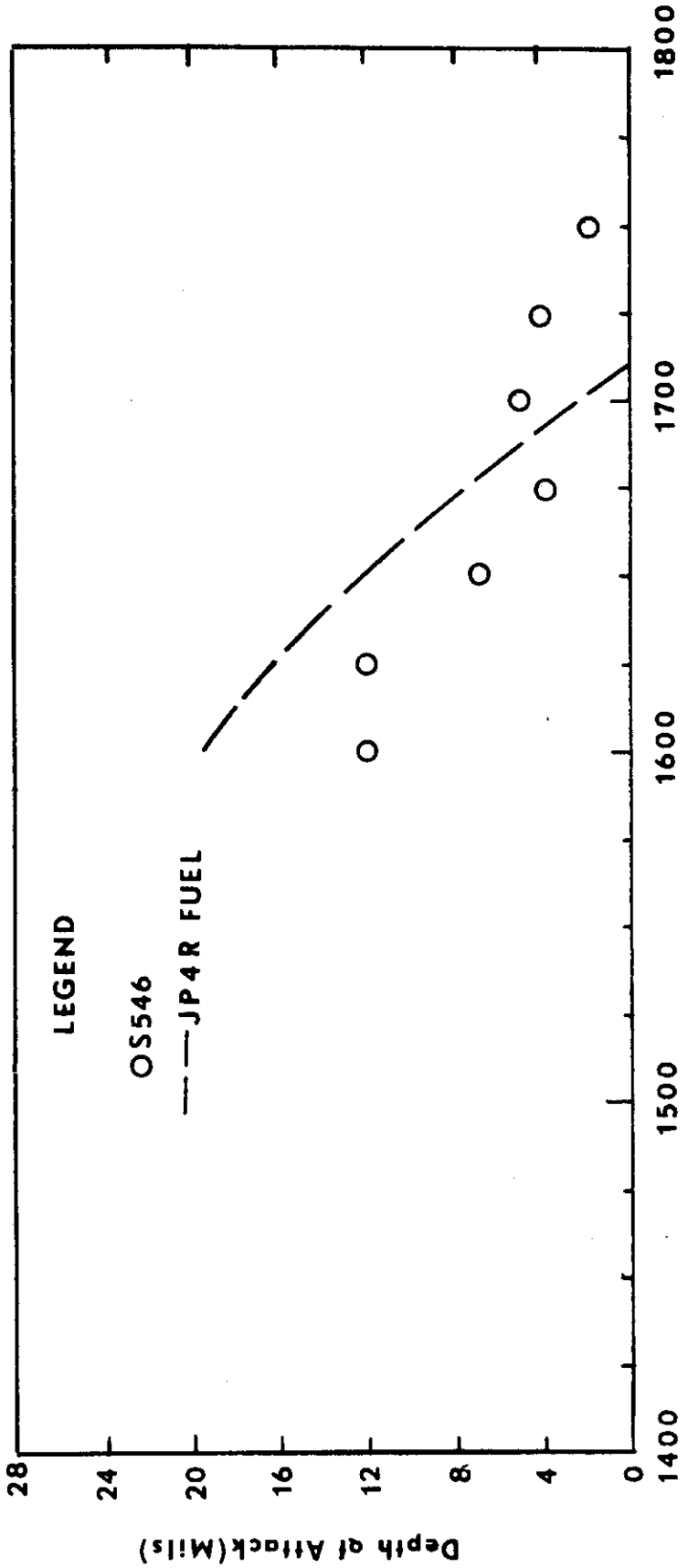

Figure 81. Corrosion as a Function of Temperature for PDRL 161 Tested Using JP-5 Fuel (0.16%S) with a Salt/Air Ratio of 8 ppm.

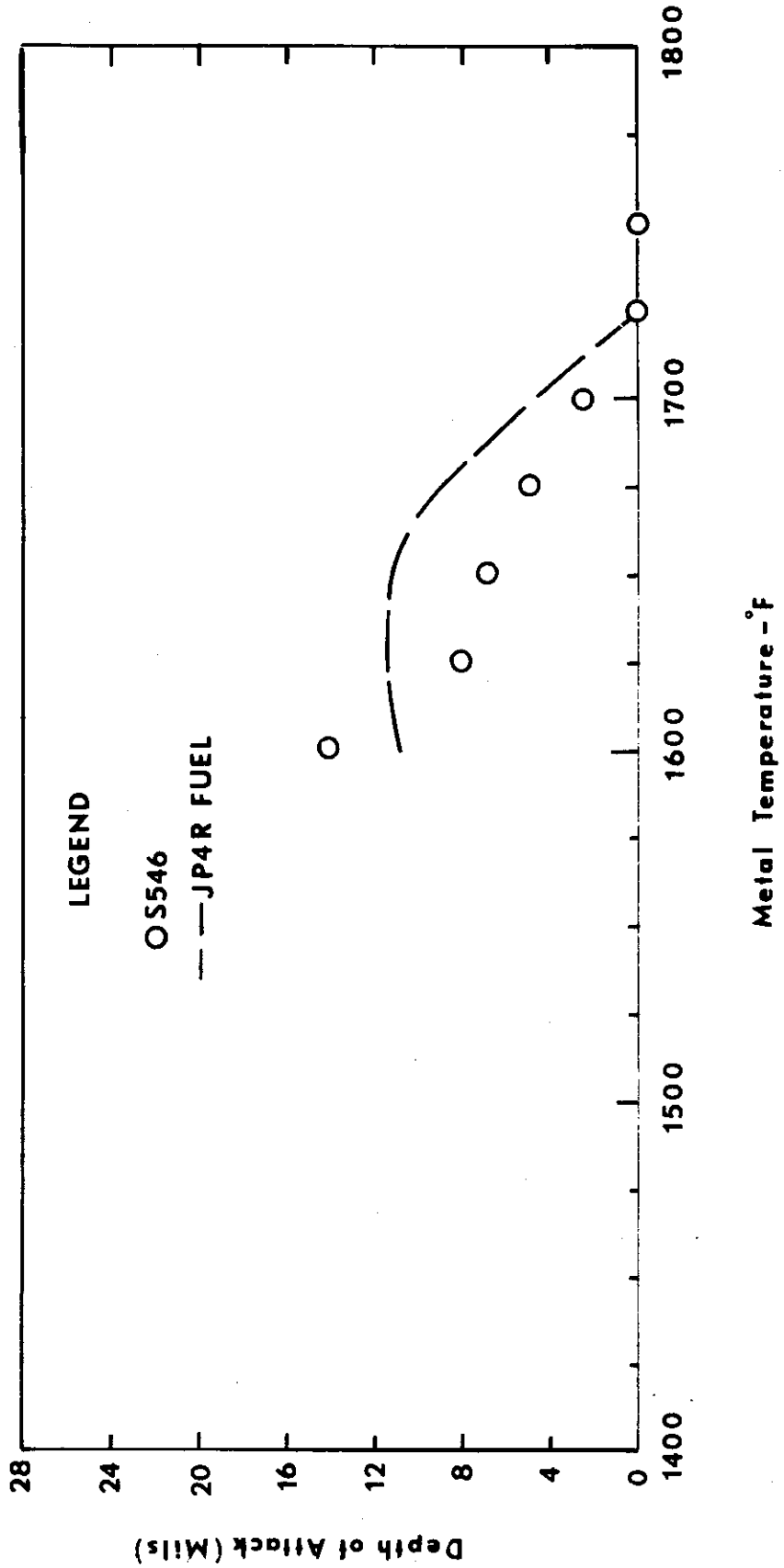

Figure 82. Corrosion as a Function of Temperature for PDRL 162 Tested Using JP-5 Fuel (0.16%S) with a Salt/Air Ratio of 8 ppm.

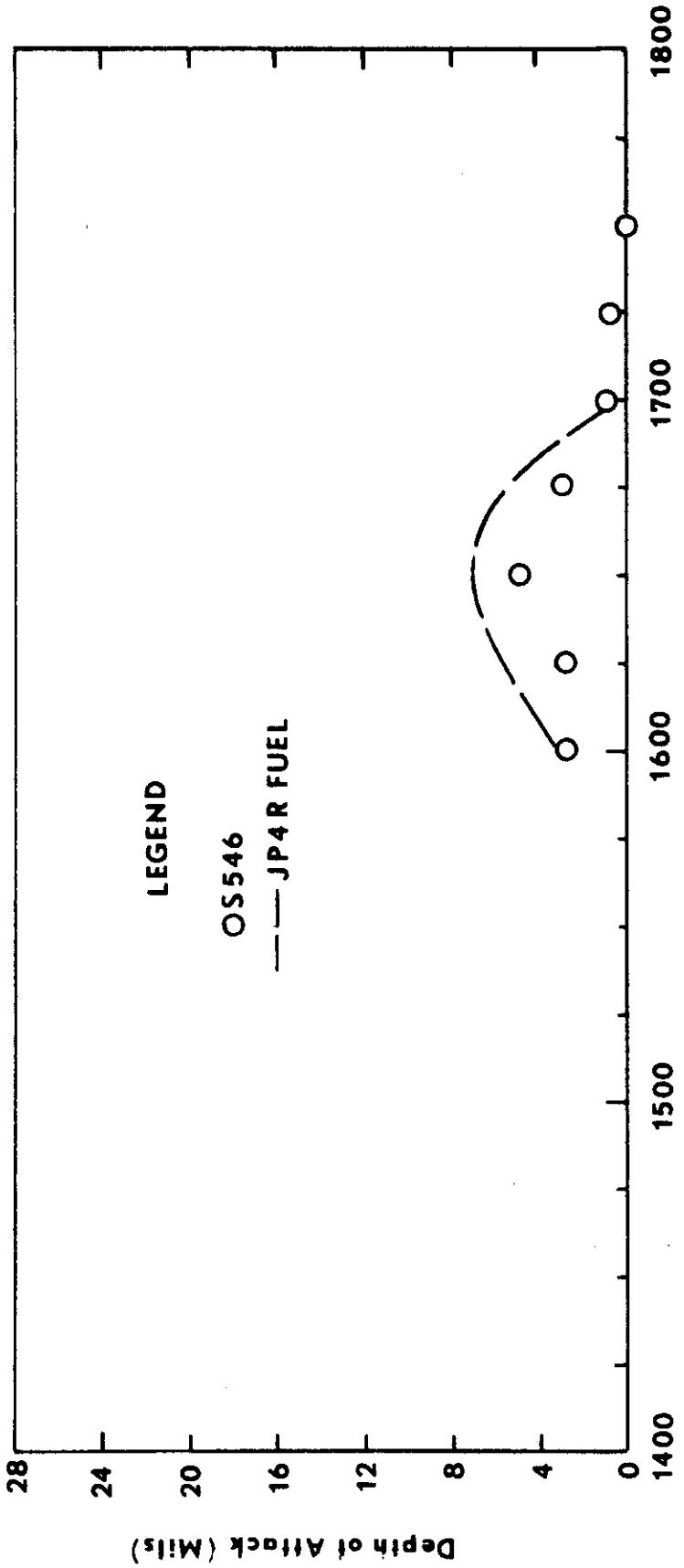

Figure 83. Corrosion as a Function of Temperature for IN728X Tested Using JP-5 Fuel (0.16%S) with a Salt/Air Ratio of 8 ppm.

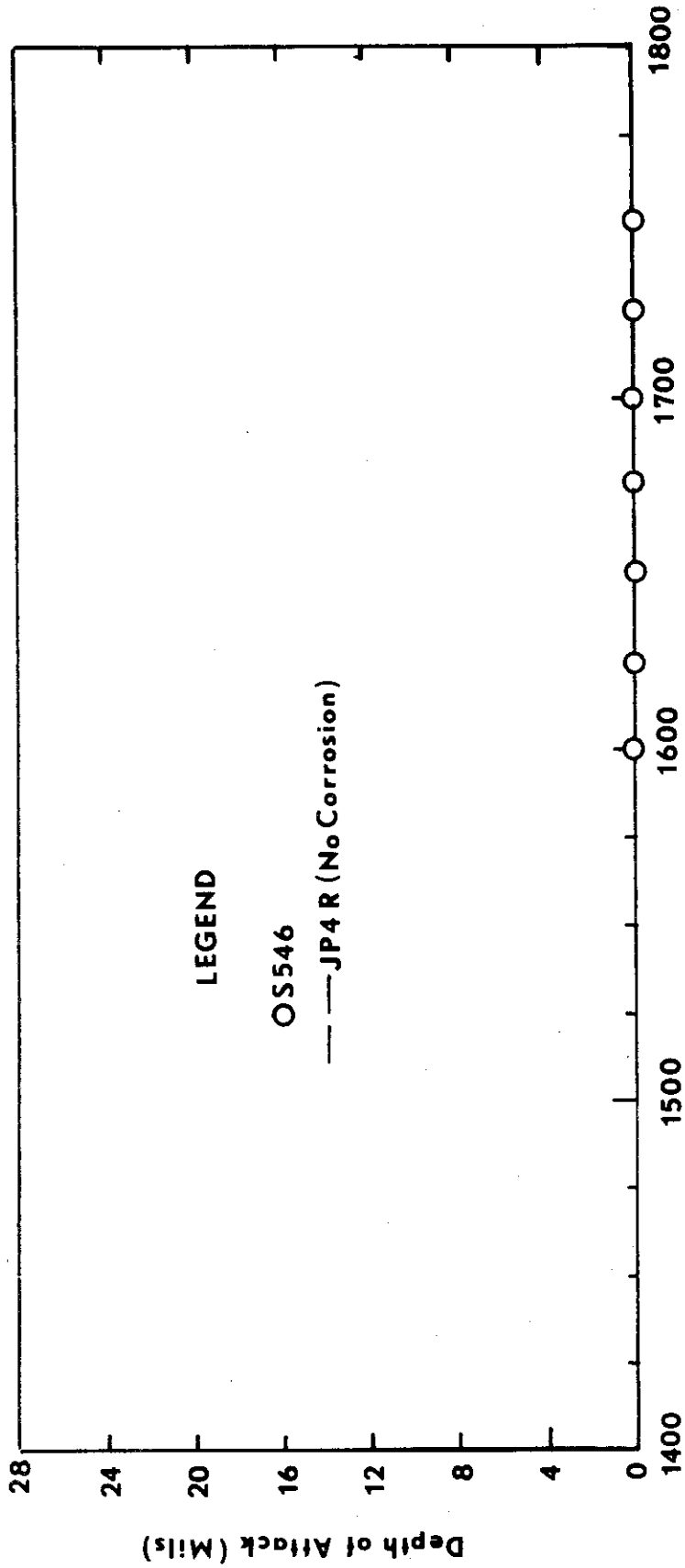

Figure 84. Corrosion as a Function of Temperature for X40 Tested Using JP-5 Fuel (0.16%S) with a Salt/Air Ratio of 8 ppm.

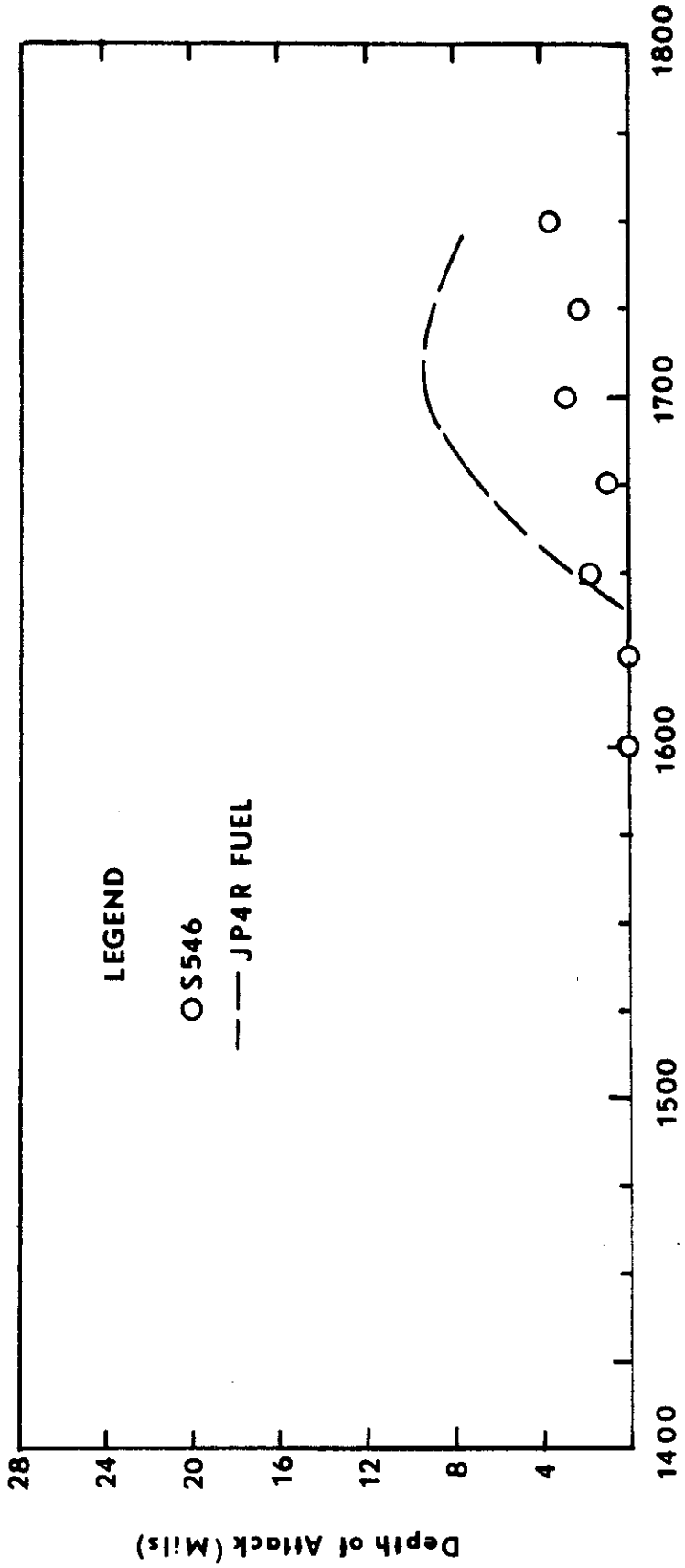

Figure 85. Corrosion as a Function of Temperature for U700 Tested Using JP-5 Fuel (0.16%S) with a Salt/Air Ratio of 8 ppm.

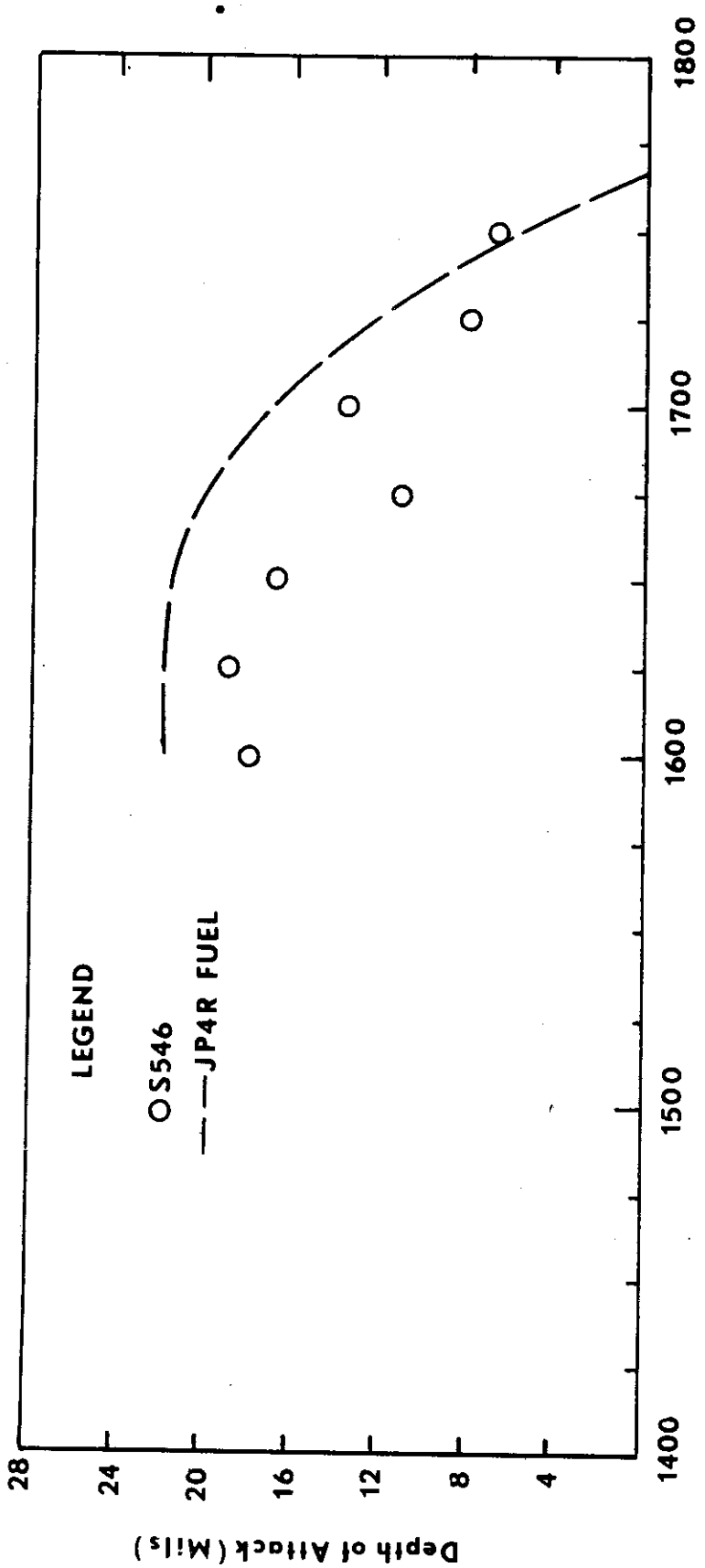

Figure 86. Corrosion as a Function of Temperature for IN100 Tested Using JP-5 Fuel (0.16%S) with a Salt/Air Ratio of 8 ppm.

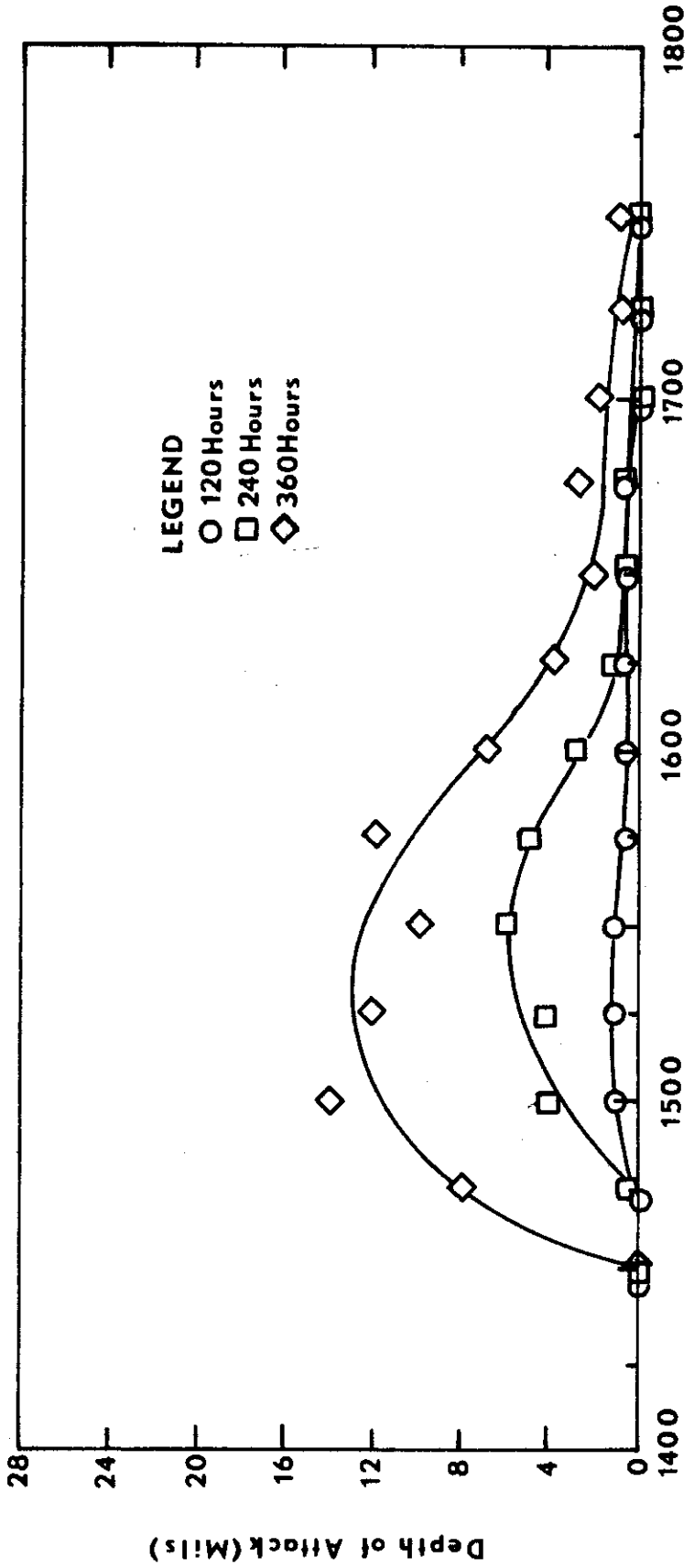

Figure 87. Corrosion as a Function of Temperature for Inco 713C Tested Using JP-4 Fuel with a Salt/Air Ratio of 4 ppm.

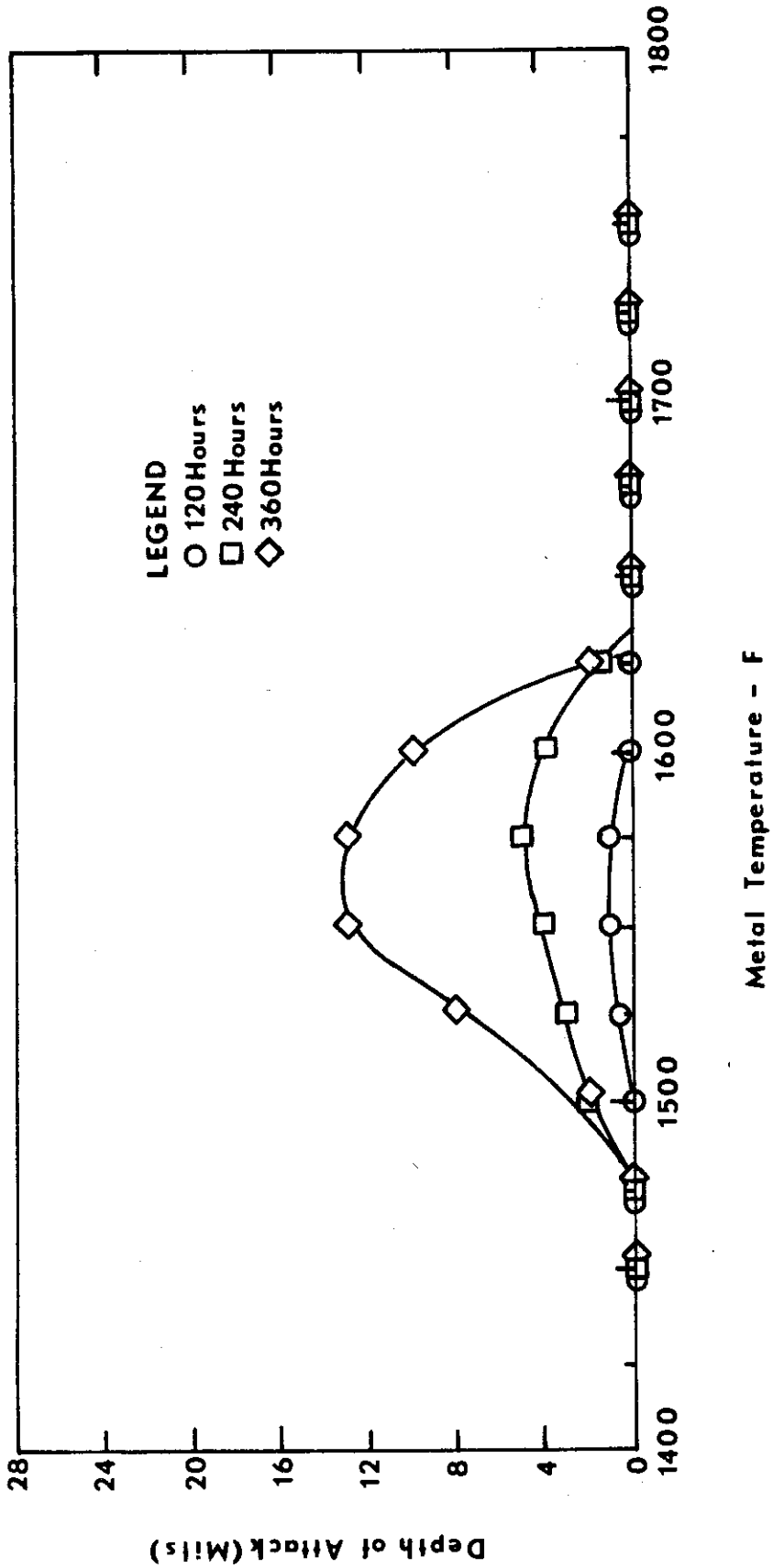

Figure 88. Corrosion as a Function of Temperature for TRW 1800 Tested Using JP-4 Fuel with a Salt/Air Ratio of 4 ppm.

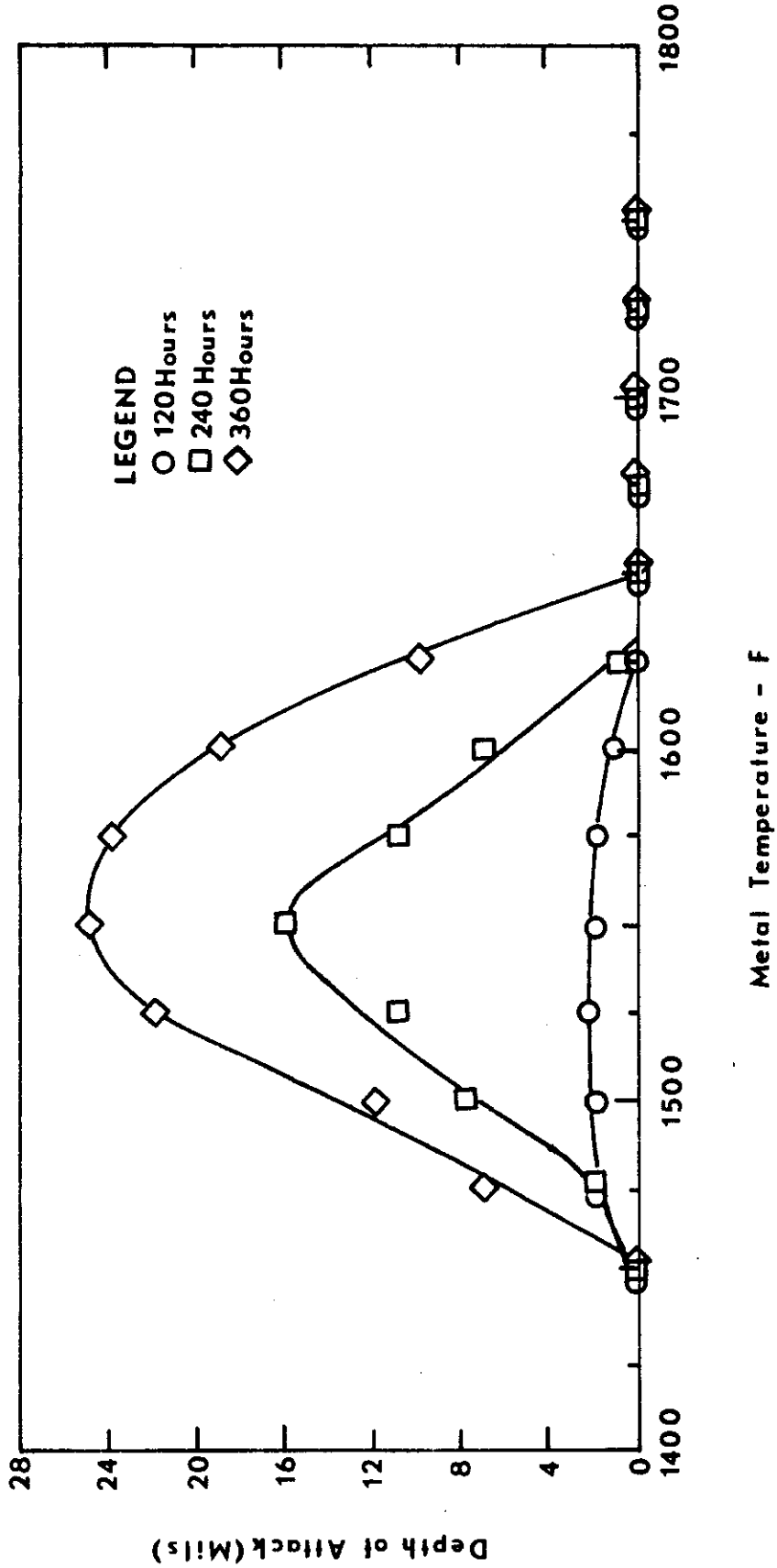

Figure 89. Corrosion as a Function of Temperature for B1910 Tested Using JP-4 Fuel with a Salt/Air Ratio of 4 ppm.

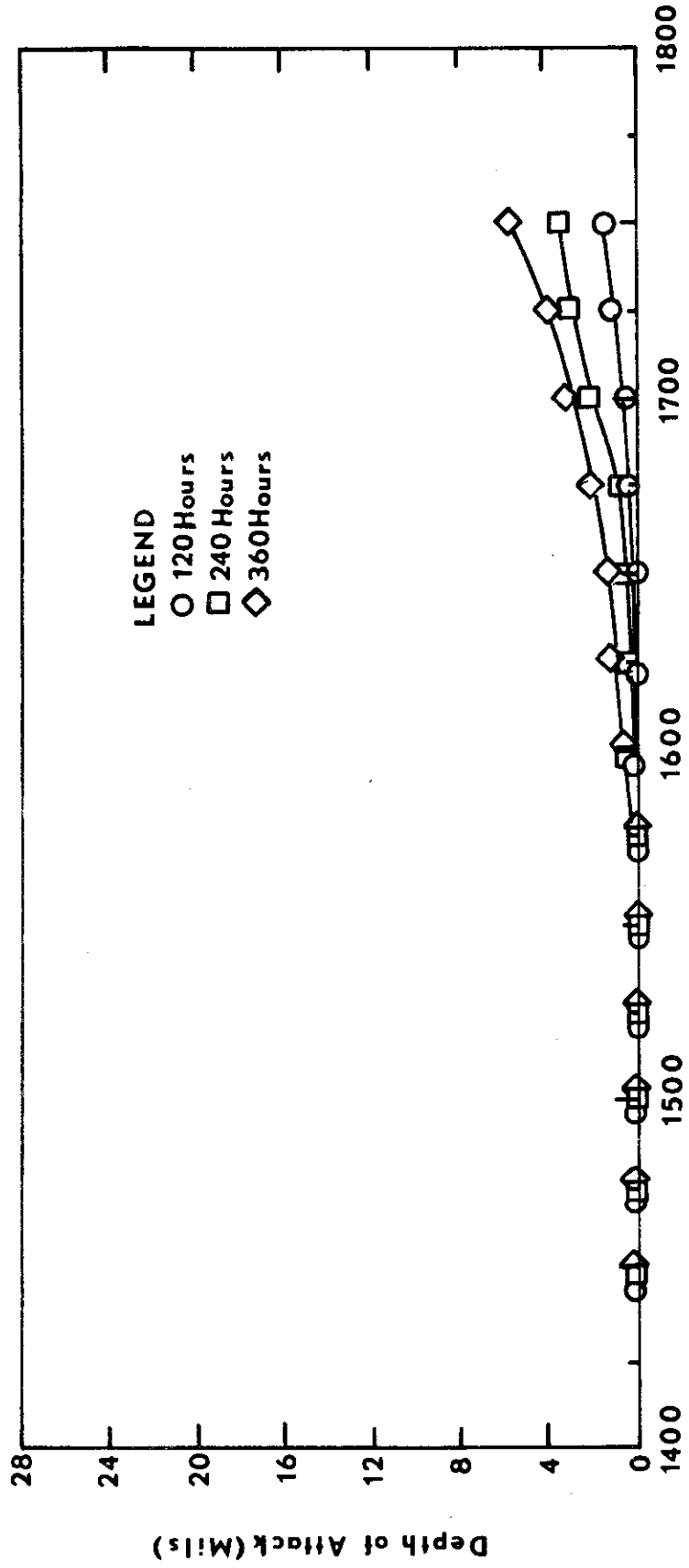

Figure 90. Corrosion as a Function of Temperature for IN728X Tested Using JP-4 Fuel with a Salt/Air Ratio of 4 ppm.

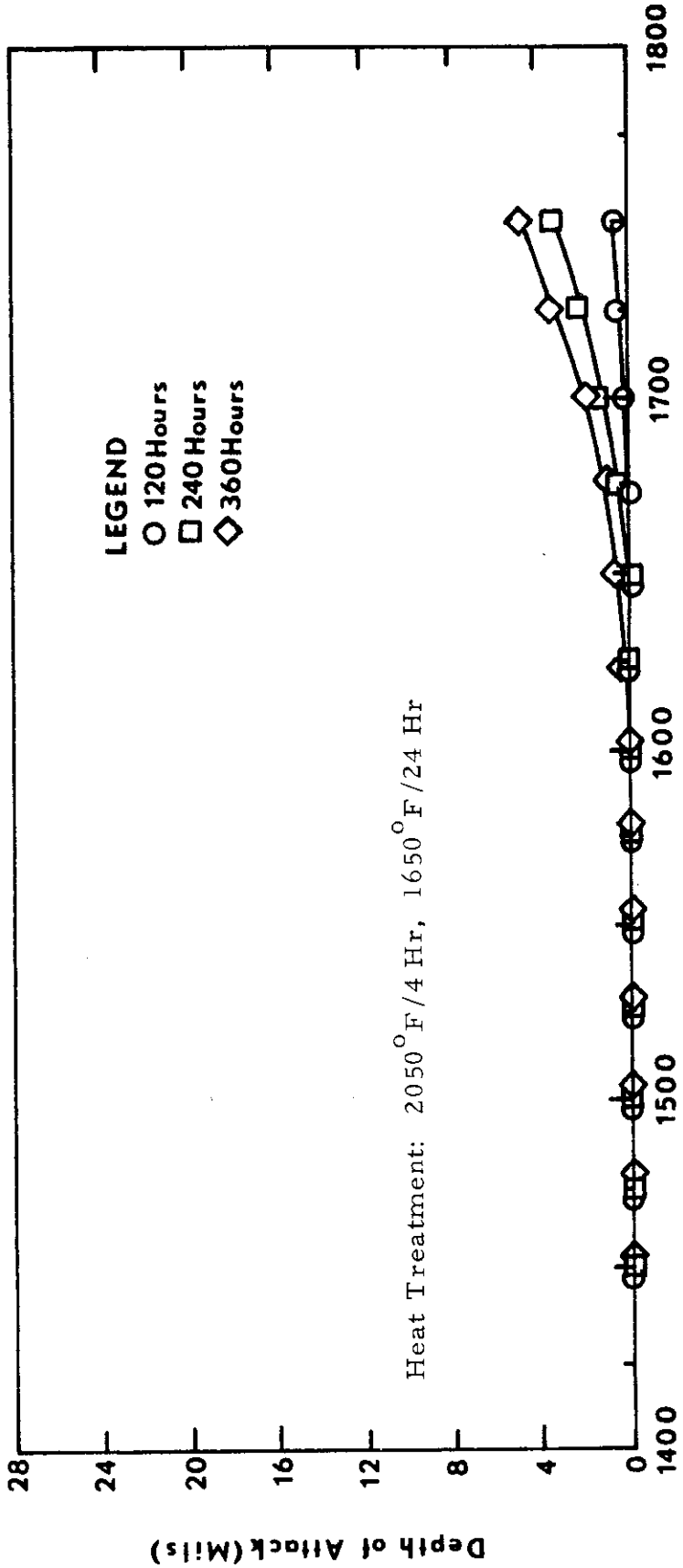

Figure 91. Corrosion as a Function of Temperature for IN728X HT Tested Using JP-4 Fuel with a Salt/Air Ratio of 4 ppm.

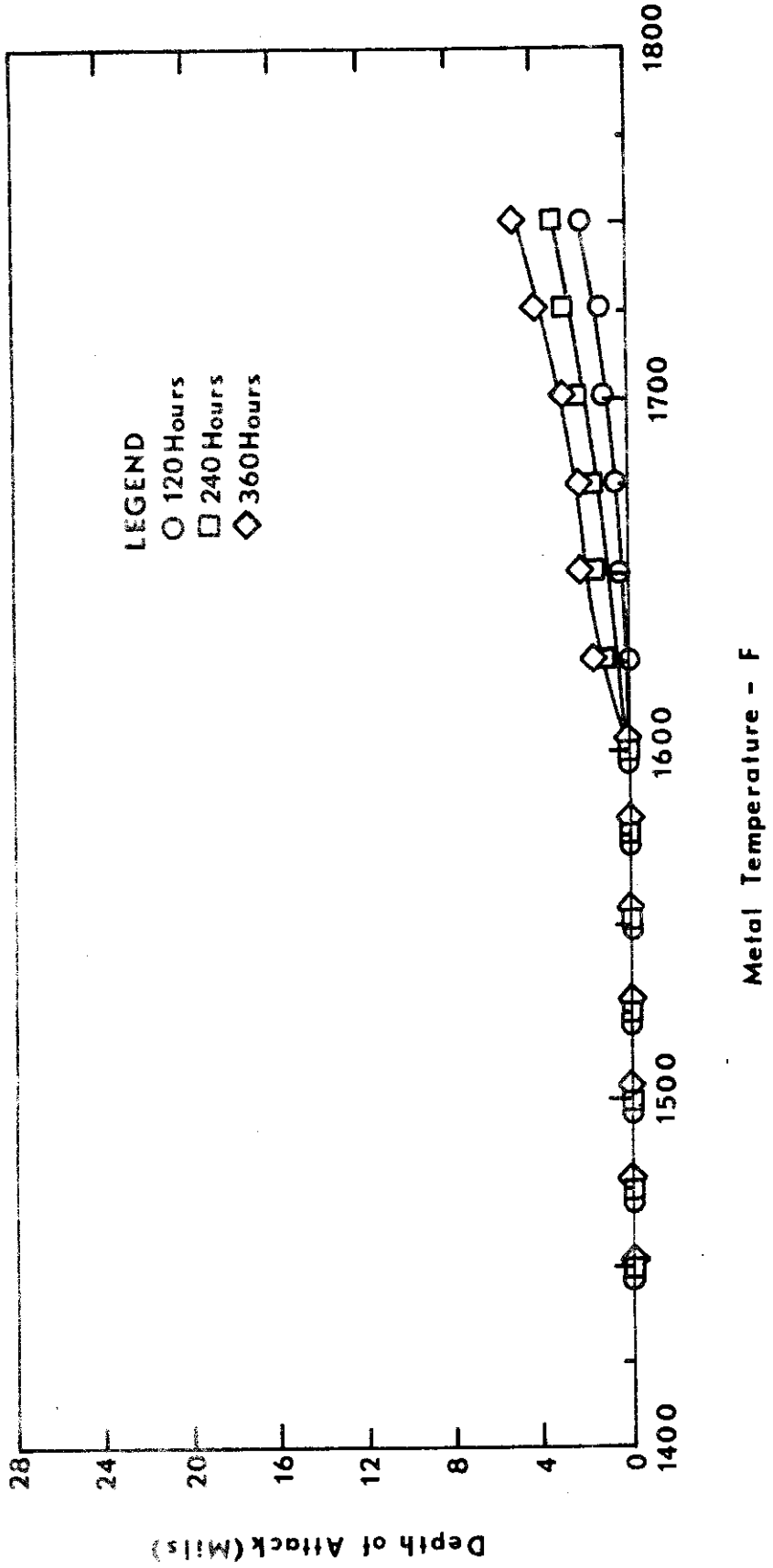

Figure 92. Corrosion as a Function of Temperature for U700 Tested Using JP-4 Fuel with a Salt/Air Ratio of 4 ppm.

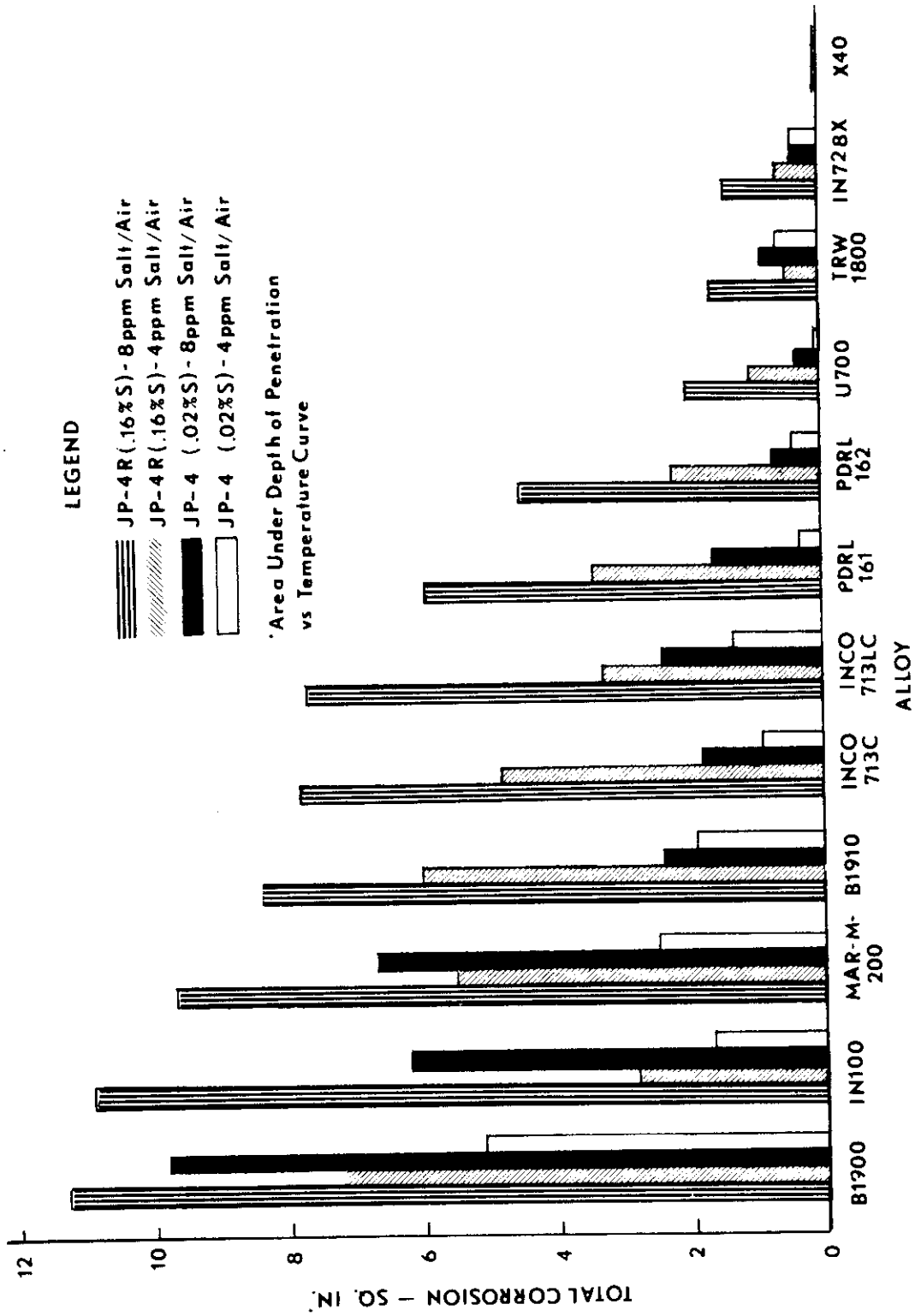

Figure 93. Bar Graph Showing Variation in Total Corrosion of Alloys Tested with JP-4 and JP-4R Fuels Using 4 and 8 ppm Salt/Air Ratios.

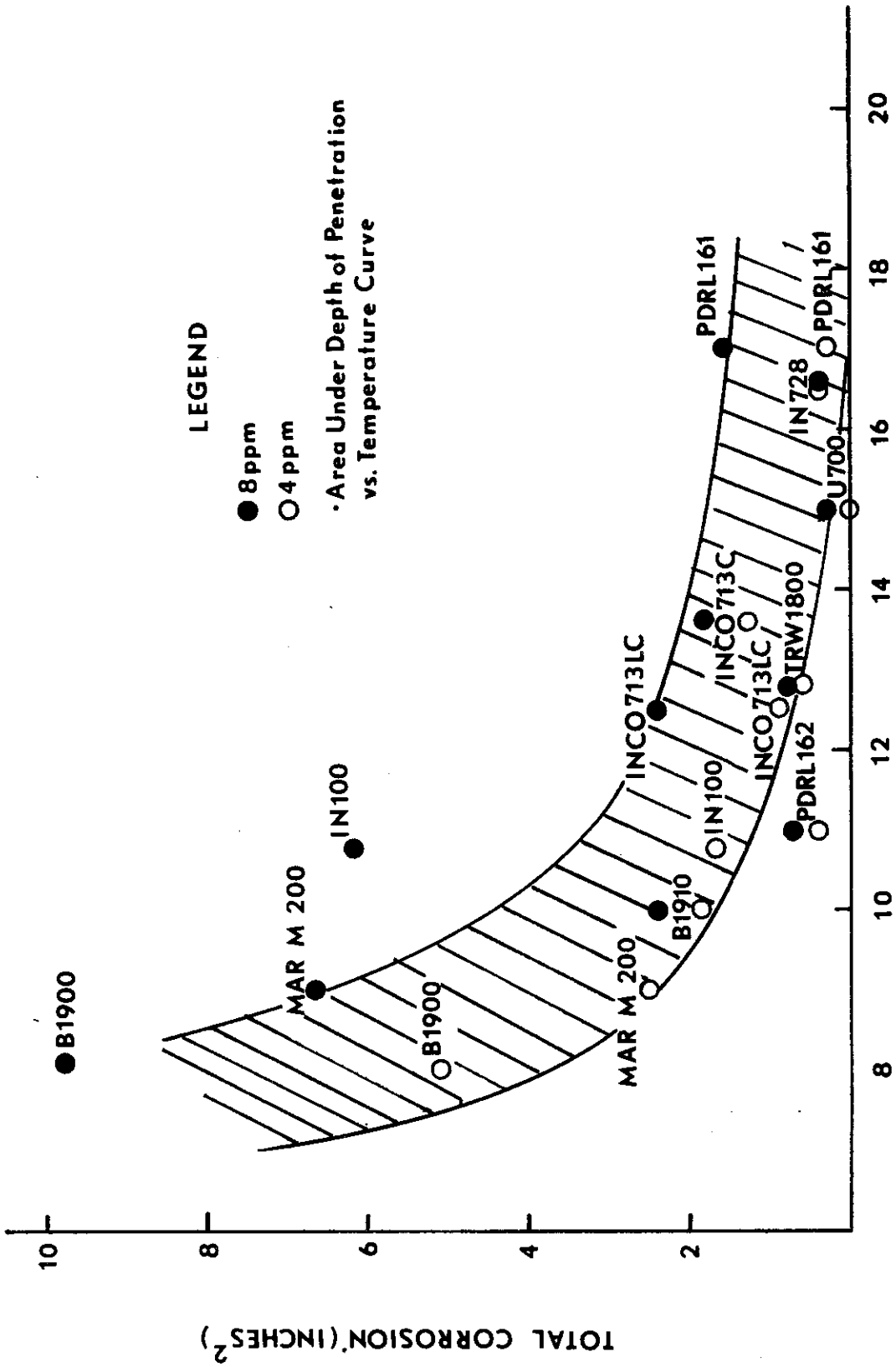

Figure 94. Total Corrosion as a Function of Chromium Content for Alloys Tested Using JP-4R Fuel.

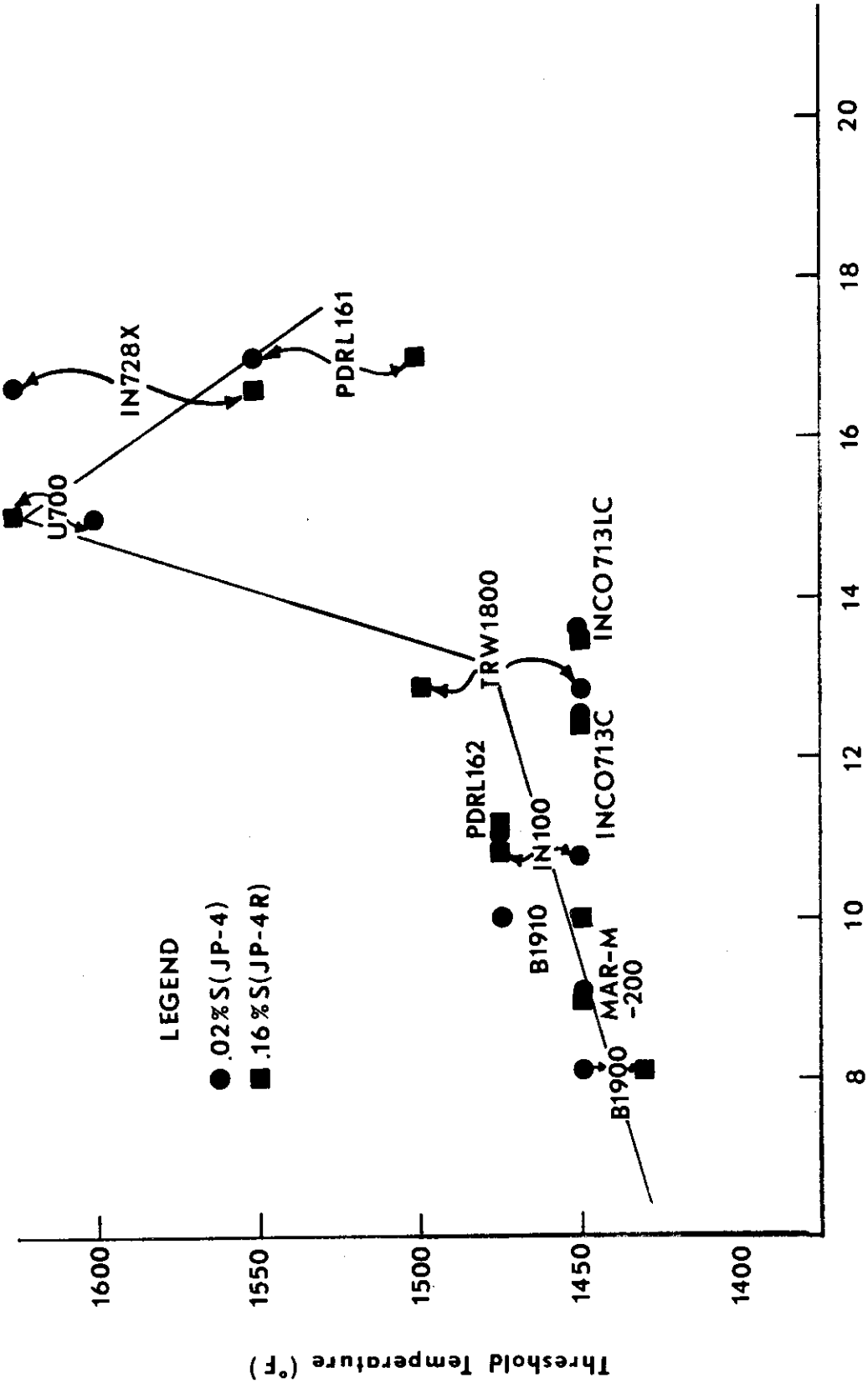

Figure 95. Threshold Temperature as a Function of Chromium Content for Alloys Tested Using a Salt/Air Ratio of 8 ppm.

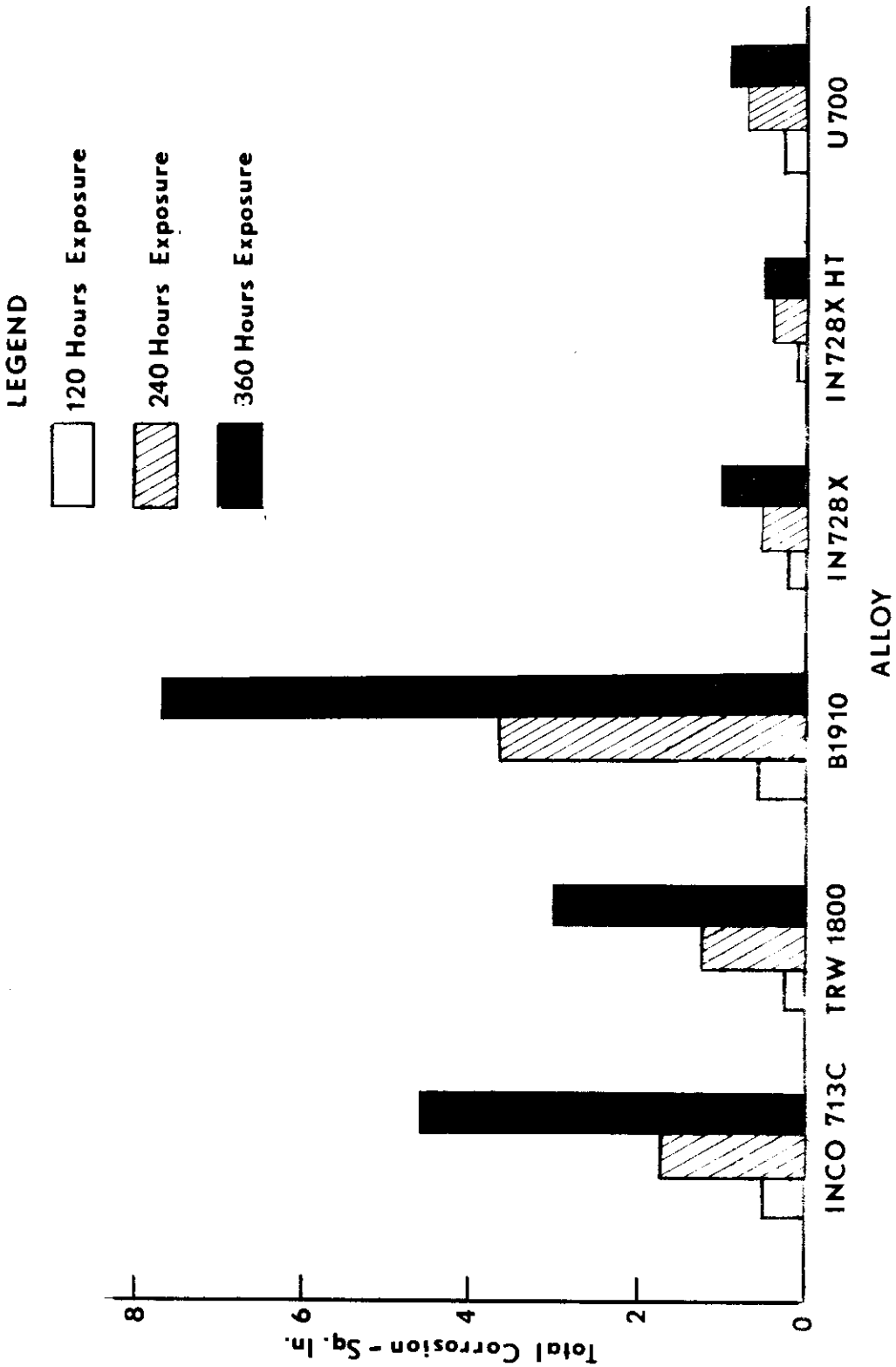

Figure 96. Variation of Total Corrosion with Time for Alloys Tested Using JP-4 Fuel and a Salt/Air Ratio of 4 ppm.

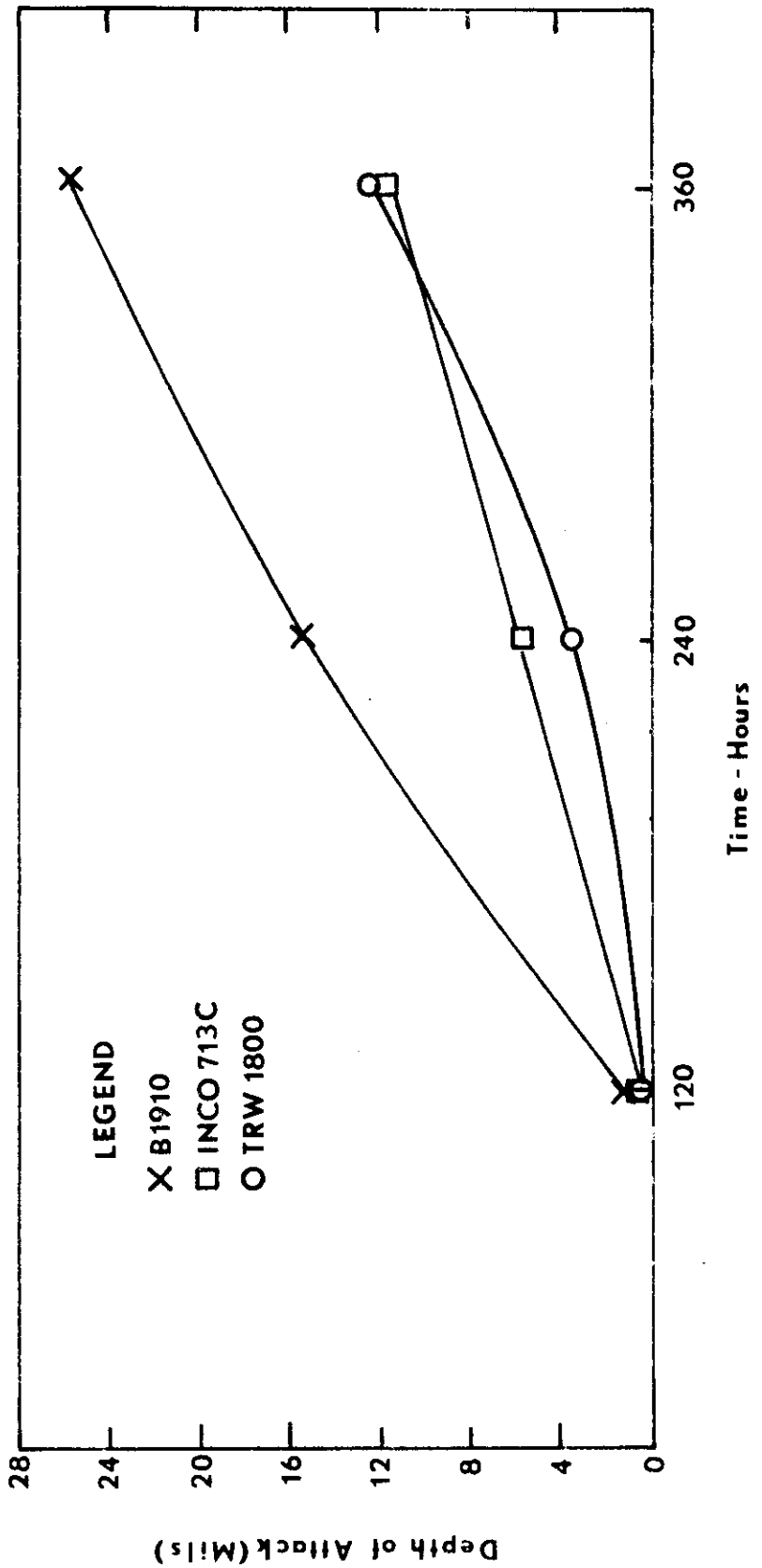

Figure 97. Depth of Attack at 1550°F as a Function of Time of Exposure.

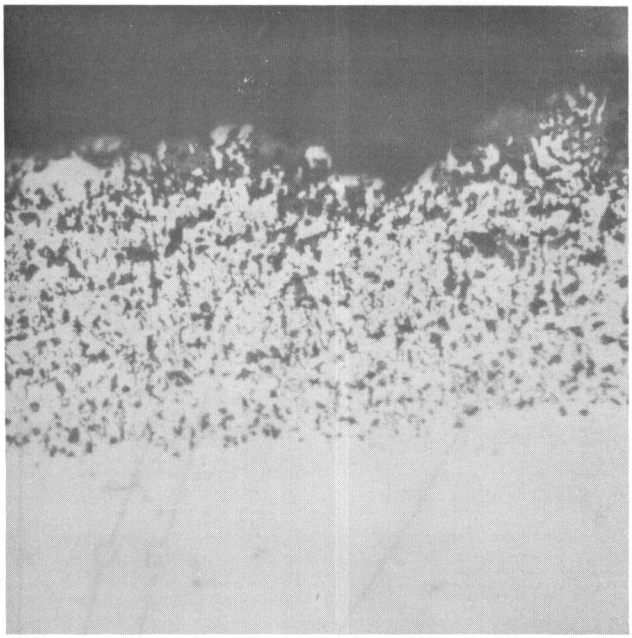

U700 Mag: 400X

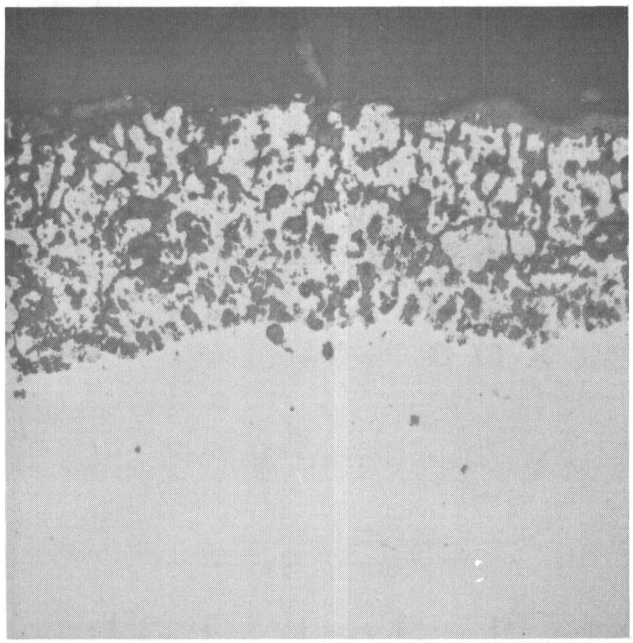

IN728X Mag: 400X

Figure 98. Oxidized Surfaces of U700 and IN728X After 360 Hours of Testing at 1700°F.

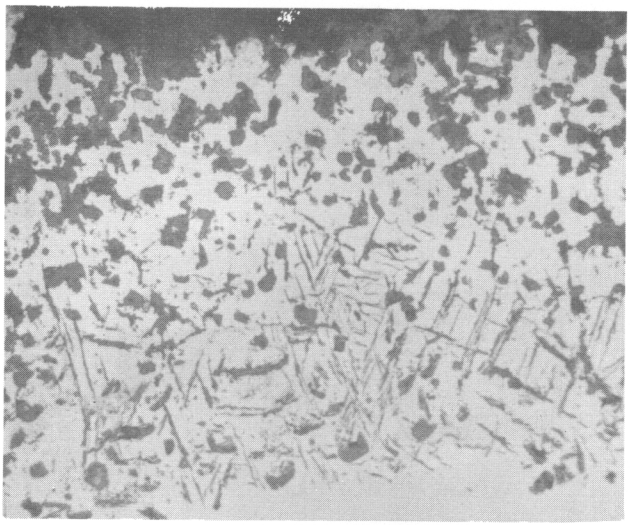

Optical Image

Mag. 400X

Aluminum X-ray Image

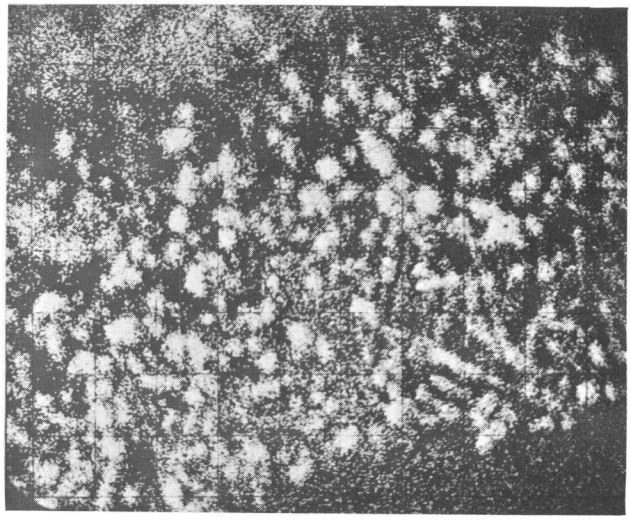

Mag. 400X

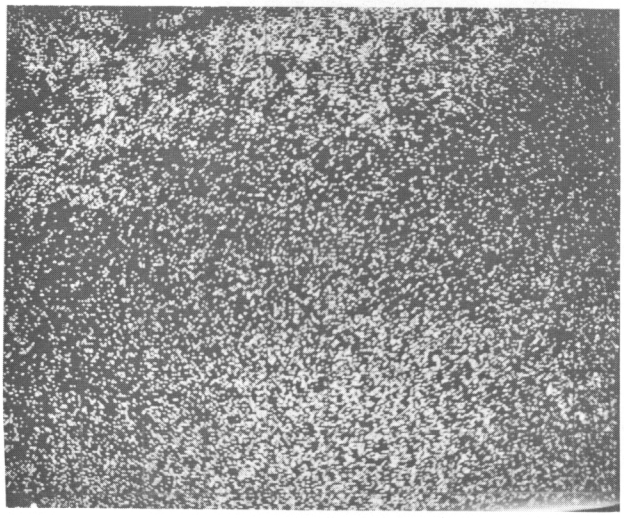

Chromium X-ray Image

Mag. 400X

Figure 99. Optical and Microprobe Images of Needle Phase Surface of IN728X After 360 Hours of Testing at 1750°F.

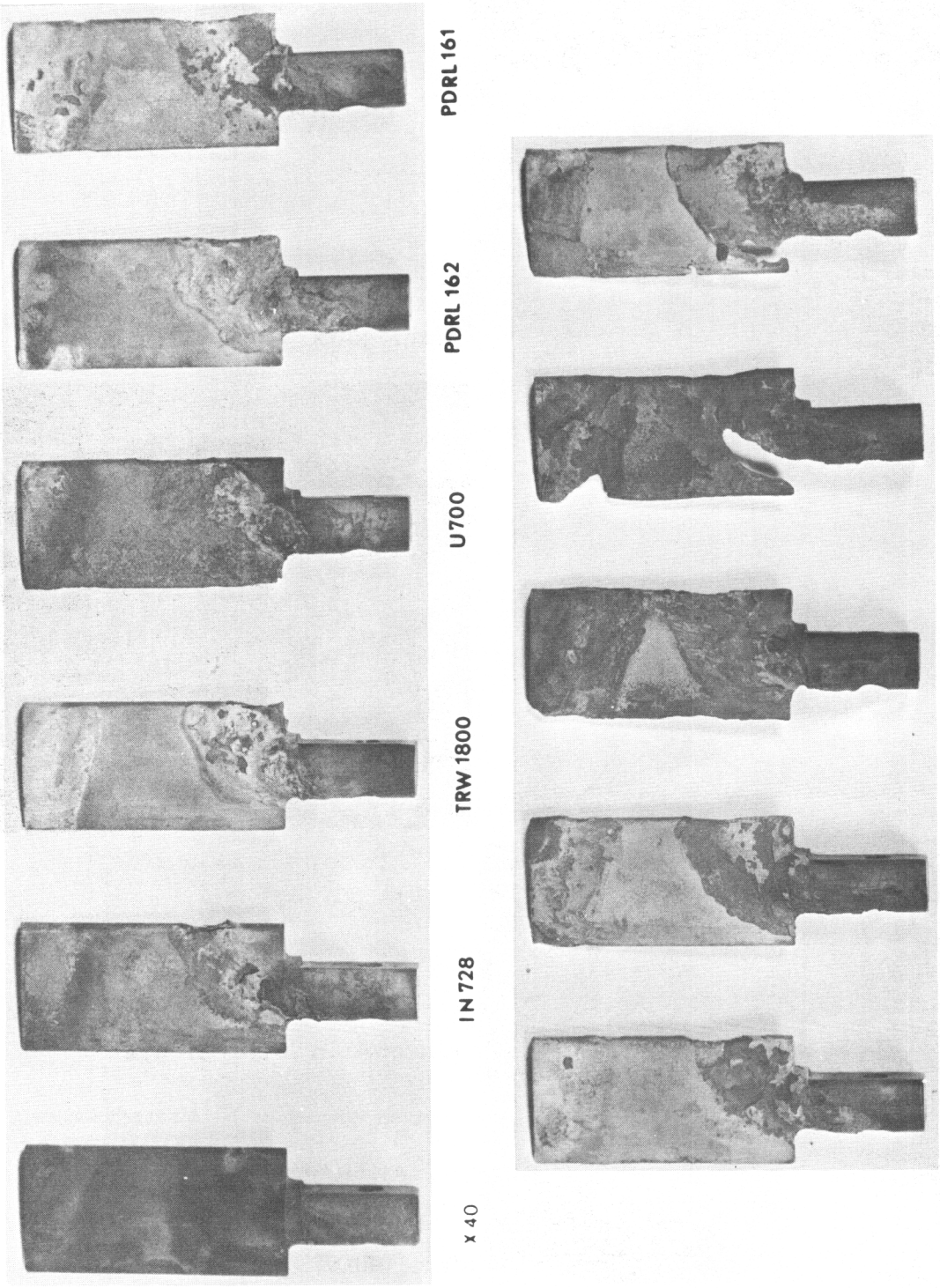

Figure 100. Paddles Used in X-Ray Diffraction Analysis After 120 Hours of Testing at 1750° F Using JP-4R fuel and an 8 ppm Salt/Air Ratio.

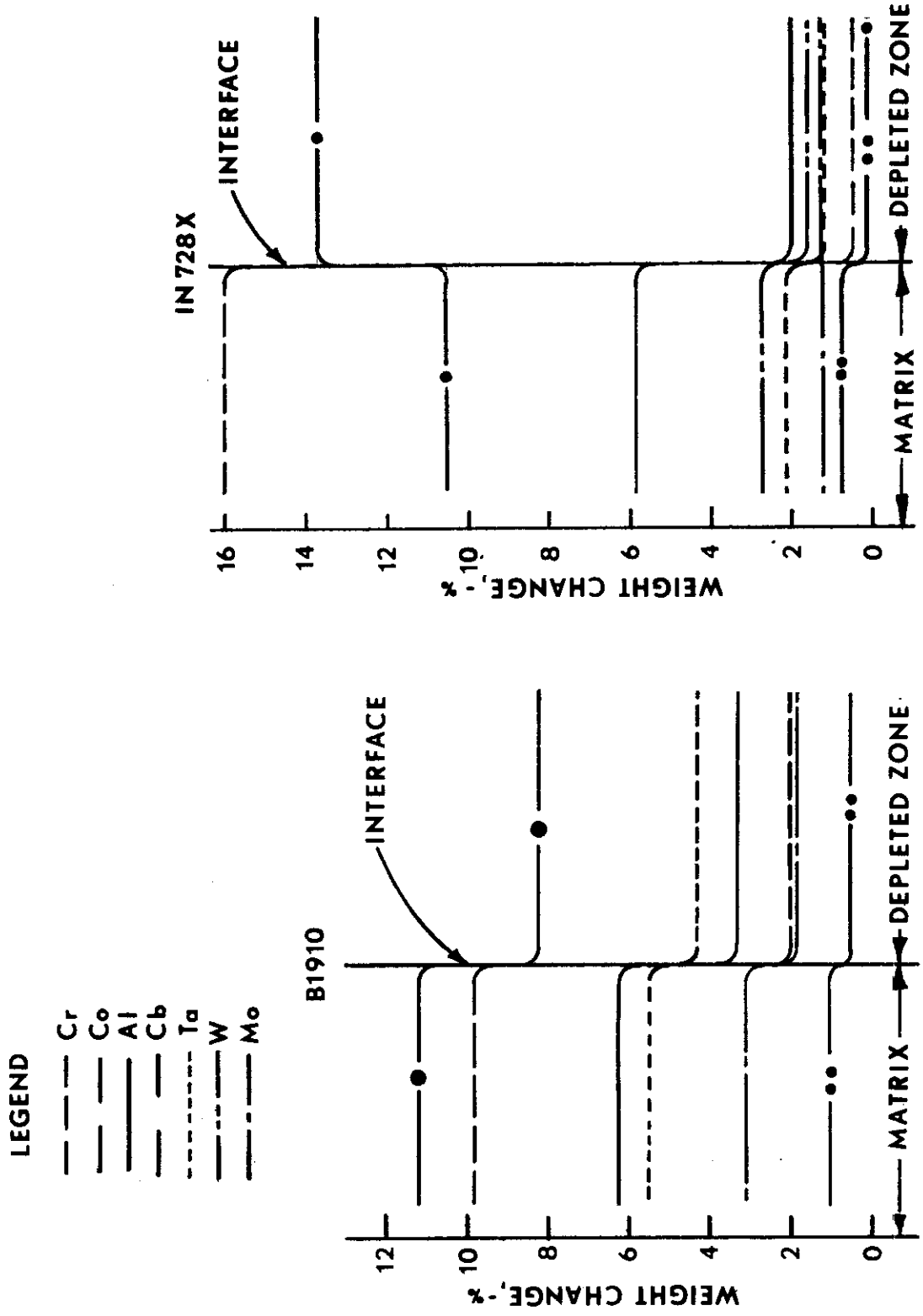

Figure 101. Changes in the Alloy Composition at the Interface Between the Matrix and Depletion Zone for B1910 and IN728X.

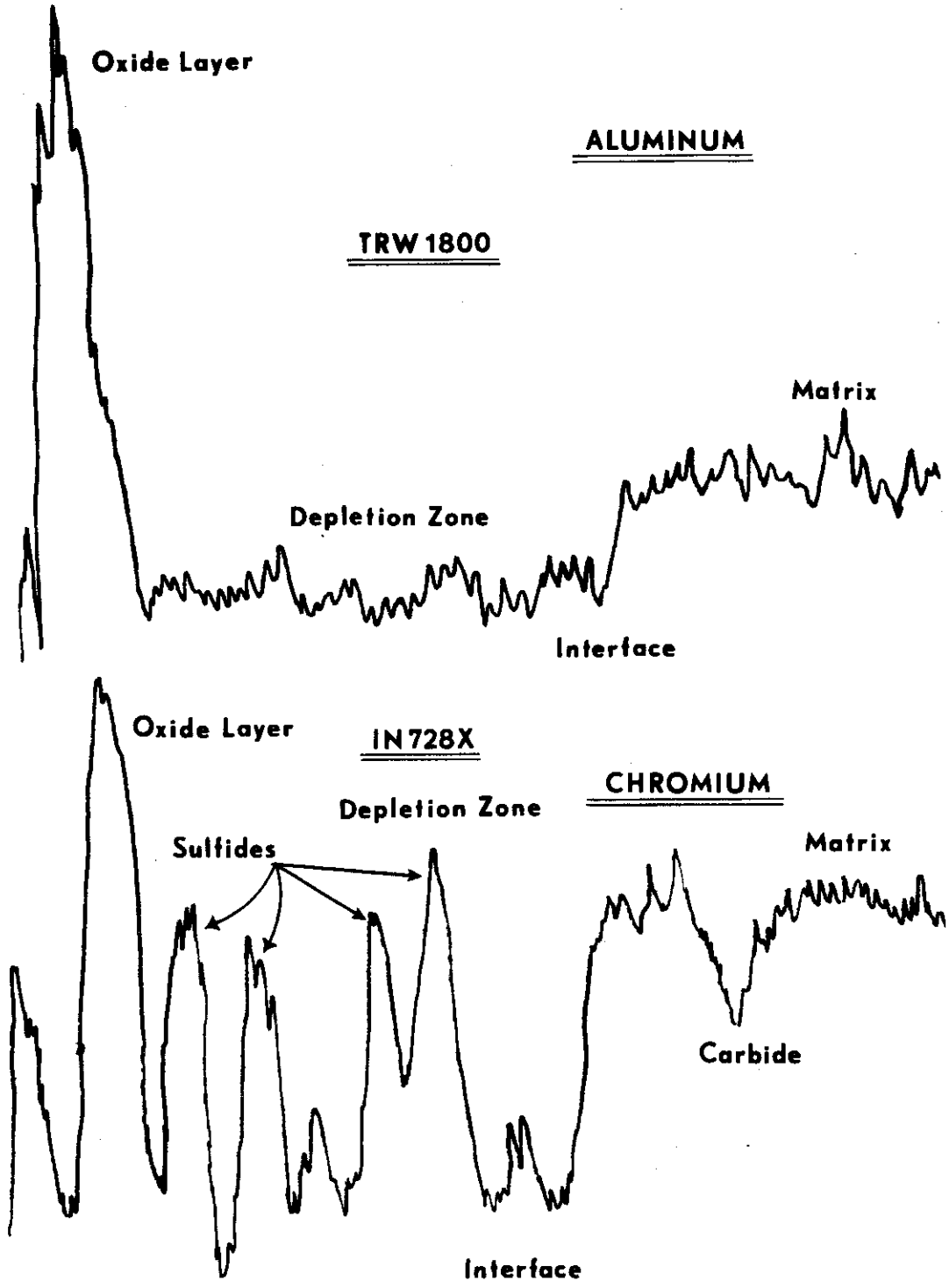

Figure 102. Examples of Microprobe Line Scans for Aluminum and Chromium Near the Surfaces of Corroded Specimens.

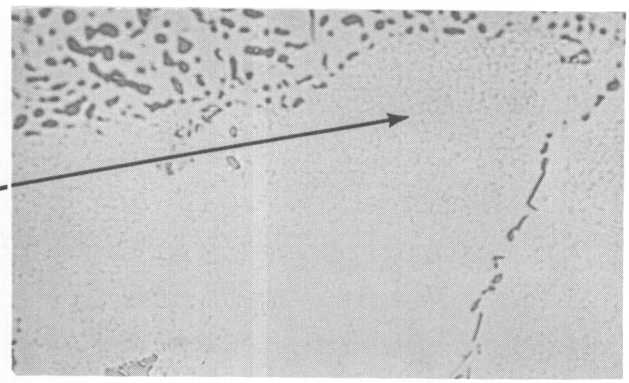

Mag. 1000X

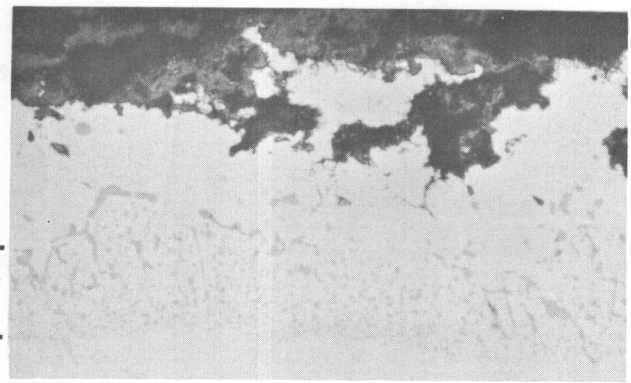

Mag. 500X

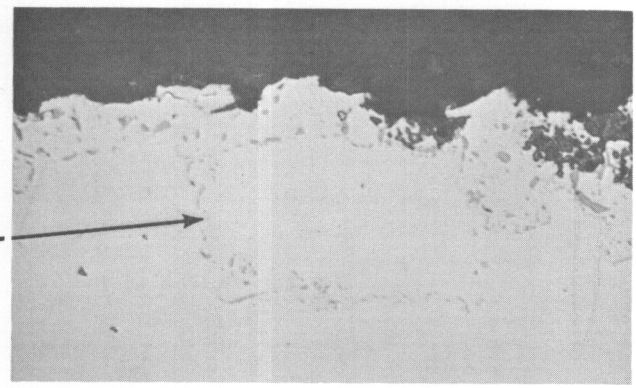

Mag. 500X

Figure 103. Photomicrographs Showing Typical Sulfidation Affected Area in Materials Examined by Microprobe Analysis.

Unclassified

Security Classification

DOCUMENT CONTROL DATA · R&D

(Security classification of title, body of abstract and indexing annotation must be entered when the overall report is classified)

1. ORIGINATING ACTIVITY *(Corporate author)*

AVCO Lycoming Division
J. J. Walters, Project Engineer

2a. REPORT SECURITY CLASSIFICATION
Unclassified

2b. GROUP

3. REPORT TITLE

Study Of Hot Corrosion Of Super Alloys

4. DESCRIPTIVE NOTES *(Type of report and inclusive dates)*

Summary report of investigation during the period 1 July 66 - 30 June 67.

5. AUTHOR(S) *(Last name, first name, initial)*

Walters, J. J.

6. REPORT DATE	7a. TOTAL NO. OF PAGES	7b. NO. OF REFS
September 67	141	

8a. CONTRACT OR GRANT NO.	9a. ORIGINATOR'S REPORT NUMBER(S)
AF33(615)-5212	
b. PROJECT NO. 7381	BPS 66(687381-738107-62405514)
c. Task No. 738107	9b. OTHER REPORT NO(S) *(Any other numbers that may be assigned this report)*
d.	

10. AVAILABILITY/LIMITATION NOTICES This document is subject to special export controls and each transmittal to foreign government or foreign nationals may be made only with prior approval of the Air Force Materials Laboratory (MAAS), Wright-Patterson Air Force Base, Ohio 45433.

11. SUPPLEMENTARY NOTES	12. SPONSORING MILITARY ACTIVITY
	Air Force Materials Laboratory Wright-Patterson AFB, Ohio 45433

13. ABSTRACT

The effect of operating environment and alloy composition on the nature and extent of oxidation-sulfidation attack was studied with the aid of the Lycoming environmental test rig, which operates at one atmosphere pressure.

Sulfidation attack was produced by burning JP-4, JP-4R, and JP-5 fuels (sulfur contents of .02, .16, and .16 weight percent respectively) while ingesting synthetic sea water at controlled rates to yield salt/air ratios of 4ppm and 8ppm. Specimens of 11 nickel base and one cobalt base alloy were subjected to cyclic temperatures, holding at peak temperatures of 1600°F or 1750°F for ten minutes per cycle.

The temperature range over which sulfidation occurred and the depth of attack increased with increasing salt-to-air ratios and with time of exposure. Good resistance to attack was generally associated with higher chromium content but high chromium alone did not guarantee good resistance to attack. Microprobe and x-ray investigations indicated that chromium-rich surface oxides provide good resistance to sulfidation and that high aluminum-titanium ratios provide good oxidation resistance.

DD FORM 1 JAN 64 1473

Unclassified

Security Classification

14. KEY WORDS	LINK A		LINK B		LINK C	
	ROLE	WT	ROLE	WT	ROLE	WT

INSTRUCTIONS

1. ORIGINATING ACTIVITY: Enter the name and address of the contractor, subcontractor, grantee, Department of Defense activity or other organization *(corporate author)* issuing the report.

2*a*. REPORT SECURITY CLASSIFICATION: Enter the overall security classification of the report. Indicate whether "Restricted Data" is included. Marking is to be in accordance with appropriate security regulations.

2*b*. GROUP: Automatic downgrading is specified in DoD Directive 5200.10 and Armed Forces Industrial Manual. Enter the group number. Also, when applicable, show that optional markings have been used for Group 3 and Group 4 as authorized.

3. REPORT TITLE: Enter the complete report title in all capital letters. Titles in all cases should be unclassified. If a meaningful title cannot be selected without classification, show title classification in all capitals in parenthesis immediately following the title.

4. DESCRIPTIVE NOTES: If appropriate, enter the type of report, e.g., interim, progress, summary, annual, or final. Give the inclusive dates when a specific reporting period is covered.

5. AUTHOR(S): Enter the name(s) of author(s) as shown on or in the report. Enter last name, first name, middle initial. If military, show rank and branch of service. The name of the principal author is an absolute minimum requirement.

6. REPORT DATE: Enter the date of the report as day, month, year; or month, year. If more than one date appears on the report, use date of publication.

7*a*. TOTAL NUMBER OF PAGES: The total page count should follow normal pagination procedures, i.e., enter the number of pages containing information.

7*b*. NUMBER OF REFERENCES: Enter the total number of references cited in the report.

8*a*. CONTRACT OR GRANT NUMBER: If appropriate, enter the applicable number of the contract or grant under which the report was written.

8*b*, 8*c*, & 8*d*. PROJECT NUMBER: Enter the appropriate military department identification, such as project number, subproject number, system numbers, task number, etc.

9*a*. ORIGINATOR'S REPORT NUMBER(S): Enter the official report number by which the document will be identified and controlled by the originating activity. This number must be unique to this report.

9*b*. OTHER REPORT NUMBER(S): If the report has been assigned any other report numbers *(either by the originator or by the sponsor)*, also enter this number(s).

10. AVAILABILITY/LIMITATION NOTICES: Enter any limitations on further dissemination of the report, other than those imposed by security classification, using standard statements such as:

(1) "Qualified requesters may obtain copies of this report from DDC."

(2) "Foreign announcement and dissemination of this report by DDC is not authorized."

(3) "U. S. Government agencies may obtain copies of this report directly from DDC. Other qualified DDC users shall request through _____."

(4) "U. S. military agencies may obtain copies of this report directly from DDC. Other qualified users shall request through _____."

(5) "All distribution of this report is controlled. Qualified DDC users shall request through _____."

If the report has been furnished to the Office of Technical Services, Department of Commerce, for sale to the public, indicate this fact and enter the price, if known.

11. SUPPLEMENTARY NOTES: Use for additional explanatory notes.

12. SPONSORING MILITARY ACTIVITY: Enter the name of the departmental project office or laboratory sponsoring *(paying for)* the research and development. Include address.

13. ABSTRACT: Enter an abstract giving a brief and factual summary of the document indicative of the report, even though it may also appear elsewhere in the body of the technical report. If additional space is required, a continuation sheet shall be attached.

It is highly desirable that the abstract of classified reports be unclassified. Each paragraph of the abstract shall end with an indication of the military security classification of the information in the paragraph, represented as *(TS)*, *(S)*, *(C)*, or *(U)*.

There is no limitation on the length of the abstract. However, the suggested length is from 150 to 225 words.

14. KEY WORDS: Key words are technically meaningful terms or short phrases that characterize a report and may be used as index entries for cataloging the report. Key words must be selected so that no security classification is required. Identifiers, such as equipment model designation, trade name, military project code name, geographic location, may be used as key words but will be followed by an indication of technical context. The assignment of links, rules, and weights is optional.